FACULTY OF SCIENCE
DEPARTMENT OF CHEMISTRY
MOLECULAR DESIGN AND SYNTHESIS
Celestijnlaan 200F box 2404
B-3001 HEVERLEE, BELGIUM
tel. + 32 16 32 79 09
david.dupont@chem.kuleuven.be
www.chem.kuleuven.be

David Dupont

Rare Earth and Critical Metal Recycling using ionic liquid technology

April 2016

KU LEUVEN

ARENBERG DOCTORAL SCHOOL
FACULTY OF SCIENCE

Rare Earth and Critical Metal Recycling Using Ionic Liquid Technology

David Dupont

Supervisor:
Prof. K. Binnemans

Dissertation presented in partial fulfilment of the requirements for the degree of Doctor in Science

April 2016

Rare Earth and Critical Metal Recycling Using Ionic Liquid Technology

David DUPONT

Supervisor:
Prof. Koen Binnemans

Members of the Examination Committee:
Prof. Tatjana Parac-Vogt
Prof. Tom Van Gerven
Prof. Thierry Verbiest
Prof. Bart Blanpain
Dr. Ir. Peter Tom Jones
Dr. Peter Nockemann

Dissertation presented in partial fulfilment of the requirements for the degree of Doctor in Science

April 2016

Acknowledgments

I would like to seize this opportunity to thank everyone that contributed to this thesis and my time as a PhD student in Leuven.

My family

I want to thank all my family, but you *mom and dad* in particular, for your unconditional support all these years. You prepared me for life and allowed me to grow up in the best possible environment. Without you, I would not be where I am today. Secondly, I also want to thank my girlfriend *Γεωργία* for making these years so great and full of new experiences.

My promotor

I want to thank *Koen Binnemans,* for accepting to be my promoter during this PhD. You have given me many opportunities and the freedom and trust to explore everything I wanted, supporting me along the way. We had a very fruitful collaboration and accomplished a lot during these years. I greatly appreciate that I could always count on you for advice and to exchange new ideas. I also thank the FWO for financial support.

Colleagues

Last but not least, I want to thank all my colleagues and friends at the university. During my PhD, I witnessed the rapid growth of our group, welcoming new colleagues from all over the world. It has been a joy to work in our large, lively and international group these last years. I also thank my master students and internship students for their hard work. Many thanks also to our supporting staff *Dirk, Paul and Rita* who make sure that everything runs smoothly, every day.

Abstract

Ionic liquids (ILs) are of high interest as alternative solvents in solvent extraction applications and metal processing. Their negligible vapor pressure and low flammability make them safer and more convenient to handle than volatile organic solvents. Furthermore, their structure can be modified and functionalized to incorporate metal extracting groups and to tune their physical properties.

This PhD thesis shows how smart ionic liquid design can provide new innovative solutions to the recycling of critical metals from end-of-life products. Recycling of critical metals is important to guarantee a sustainable long-term supply, diminish the impact on the environment and to reduce the geopolitical dependence on certain countries. An important advantage of recycling is the fact that these metals are already present in the correct ratios in consumer products, but innovative recycling technologies must be developed to recover these metals efficiently without the creation of additional waste. The development of *green(er) and more selective* metal processing techniques is therefore at the core of this PhD thesis.

New IL-based recycling processes were developed for lamp phosphor waste and NdFeB permanent magnets. These consumer products have the highest recycling potential when it comes to the recovery of (heavy) rare earths. Using the unique properties of ionic liquids, new processes were developed which are more efficient, use less chemicals and produce less waste than classic hydrometallurgical processes. New classes of ionic liquids were also designed, with strongly acidic extractants incorporated in their structure, in order to dissolve inorganic metal-containing compounds and to extract metal ions. The ionic liquids and processes that were developed in this PhD thesis can be used as part of a toolbox to tackle issues found in classic hydrometallurgy or solvent extraction. It is important to understand the underlying fundamentals which explain the often unexpected behavior of metals in ionic liquids. A general theory was therefore introduced to explain and predict the effect of metal salts and acids on the (thermomorphic) behavior and mutual solubility of biphasic IL/water systems. This prediction model, based on the principles of the Hofmeister series, can be used for the rational synthesis of ionic liquids as well as for the design of IL-based solvent extraction systems.

Finally, as a side project, we also worked on functionalized magnetic nanoparticles as a way to recover rare earths from diluted waste streams. This complements the field of solvent extraction, which is more suited for concentrated metal solutions. The concept of sterical surface crowding of ligands was introduced as a way to increase the selectivity of the surface ligands towards certain metal ions.

Dutch Abstract

Ionische vloeistoffen zijn erg interessante alternatieve solventen voor solvent extractie toepassingen en het oplossen van metalen. Ze zijn niet vluchtig en weinig ontvlambaar waardoor ze veiliger zijn dan de klassieke organische solventen. De structuur van ionische vloeistoffen laat ook toe om functionele groepen in te bouwen en zo hun eigenschappen te modificeren of specifieke functies toe te voegen zoals metaal extractanten.

In deze PhD thesis werden door middel van het slim ontwerp van ionische vloeistoffen nieuwe innovatieve processen ontwikkeld voor de recyclage van kritieke metalen uit afgedankte producten. De recyclage van kritieke metalen is belangrijk om op termijn de toevoer van deze zeldzame elementen te kunnen garanderen en de druk op het milieu te verminderen, maar ook om de geopolitieke afhankelijkheid ten opzichte van sommige landen terug te dringen. Een groot voordeel is dat de kritieke metalen reeds in de juiste verhouding aanwezig zijn in de gerecycleerde producten. Het is echter belangrijk om efficiënte recyclage technologieën te ontwikkelen die deze metalen kunnen herwinnen zonder bijkomend afval te produceren. De ontwikkeling van *duurzamere en selectievere* processen voor metaalrecyclage is daarom het kernidee van deze PhD thesis.

De nieuwe recyclage processen laten toe om zeldzame aarden te herwinnen uit afgedankte spaarlampen en NdFeB magneten die men terugvindt in harde schijven, luidsprekers en elektrische motoren. Deze recyclage processen zijn efficiënter, gebruiken minder chemicaliën en produceren minder afval dan de klassieke hydrometallurgische processen. Er werden ook nieuwe klassen van ionische vloeistoffen gesynthetiseerd met ingebouwde sterk zure groepen die gebruikt kunnen worden voor het oplossen of extraheren van metalen. Deze PhD thesis toont de flexibiliteit van ionische vloeistoffen aan en biedt een reeks nieuwe inzichten die aangewend kunnen worden in toekomstige metallurgische processen. Er ging ook veel aandacht naar het begrijpen van de onderliggende mechanismes die zorgen voor het vaak ongewone gedrag van metalen in ionische vloeistoffen. Een algemene theorie werd uitgewerkt om het effect van zouten en zuren op ionische vloeistoffen te verklaren en zo de eigenschappen te voorspellen van twee-fase systemen bestaande uit een ionische vloeistof en een waterige fase. Deze algemene theorie, gebaseerd op de principes van de Hofmeister serie, helpt bij de synthese van ionische vloeistoffen en bij het optimaliseren van solvent extractie systemen.

Ten slotte werd er ook gewerkt op gefunctionaliseerd magnetische nanodeeltjes voor het herwinnen van zeldzame aarden uit verdunde waterige oplossingen. Hierbij werd sterische hinder op gefunctionaliseerd oppervlakken geïntroduceerd als een nieuwe methode om de selectiviteit van extractanten te verhogen.

Abbreviations

[cation][anion]	Ionic liquid consisting of a cation and anion
$[N_{RRRR}]$	Tetraalkylammonium cation (NR_4^+)
$[P_{RRRR}]$	Tetraalkylphosphonium cation (PR_4^+)
aq	Aqueous phase
bmim	1-Butyl-3-methylimidazolium
D	Distribution ratio
emim	1-Ethyl-3-methylimidazolium
ERECON	European Rare Earths Competency Network
FG	Functional group
Hbet	Betainium
HD	Hydrogen decrepitation
HDDR	Hydrogenation disproportionation desorption and recombination
HLLE	Homogeneous liquid-liquid extraction
HREE	Heavy rare-earth element
IL	Ionic liquid
ITO	Indium tin oxide
K_a	Acid dissociation constant
LCA	Life-cycle assessment
LCST	Lower critical solution temperature
LREE	Light rare-earth element
NdFeB	Neodymium-iron-boron magnets
org	Organic phase
PCB	Printed circuit board
PGM	Platinum group metal
REE	Rare-earth element
S	Separation factor
T_{cp}	Cloud point temperature
Tf_2N^-	Bis(trifluoromethylsulfonyl)imide (= bistriflimide)
TsO^-	Tosylate
TXRF	Total reflection X-ray fluorescence
UCST	Upper critical solution temperature
WEEE	Waste electrical and electronic equipment
X^-	Anion

Table of contents

Outline

This PhD dissertation is a collection of nine first-author papers, published in peer-reviewed journals during the course of this PhD thesis.

Chapter 1 is the introduction and explains the need for the recycling of critical metals such as the rare earths, by analyzing their current production, demand and geopolitical risks. It then analyzes the opportunities and constraints for the recycling of different end-of-life products and gives an overview of the existing recycling technologies. In the second part, ionic liquids (ILs) are proposed as alternative solvents instead of a traditional hydrometallurgical approach. An overview of different classes of ILs is given, with an emphasis on the synthesis of Brønsted acid ILs. Then, the processing of metals in ILs is discussed both for the dissolution and solvent extraction of metal ions.

Chapter 2 discusses the objectives of the PhD thesis.

Chapter 3 contains an overview of the nine first-author publications (peer reviewed), written during the course of this PhD. These papers can be divided in three categories: (1) the papers on critical metal recycling (paper 1−4), (2) the papers on ionic liquid design (paper 5−7), and (3) the papers on the design of functionalized magnetic nanoparticles (paper 8−9). Paper 1 and 2 describe the use of ionic liquid technology for the selective recovery of rare earths from lamp phosphor waste and spent NdFeB magnets, respectively. Paper 3 focusses on the recovery of antimony from lamp phosphor waste using a zero waste approach. A review of antimony recycling was also written, in which different potential waste streams were investigated (paper 4). Paper 5 and 6 describe the design, synthesis and application of new strongly acidic, metal-extracting ILs, functionalized with sulfonic acid and sulfuric acid (hydrogen sulfate) functional groups, respectively. Paper 7 gives a general description of the effect of salts and acids on biphasic IL/water systems, including the impact on the mutual solubility and thermomorphic behavior. Finally, paper 8 and 9 discuss the use of functionalized magnetic nanoparticles as a tool for the recovery of rare earths from dilute waste streams (paper 8−9).[1,2]

Chapter 4 gives an overview of the additional publications that have been written as science outreach, published blog articles or articles written on request.

Chapter 5 contains the conclusion and an outlook for future work.

This dissertation ends with notes about the safety aspects and media coverage of this research and also lists the publications, conferences and trainings.

1 Introduction

1.1 Critical metals

1.1.1 Assessing criticality

Industrial demand and the rapid growth of consumer electronics have caused metal production to soar in recent years. Copper, for example, has been in use at least 10,000 years but more than 97% of all copper ever mined has been extracted after 1900. Metal production continues at an ever-accelerating pace as the world population continues to expand (Figure 1).

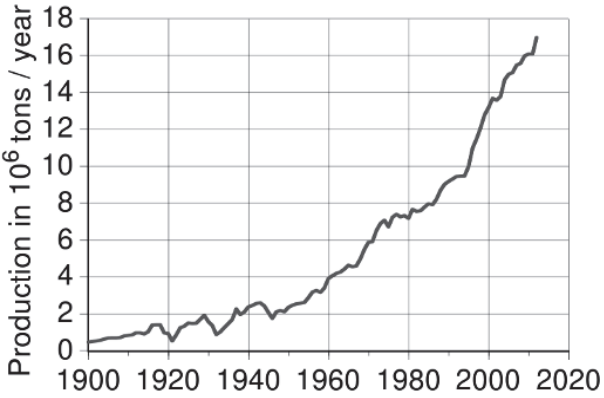

Figure 1. World copper production 1900−2012 (U.S. Geological Survey).

This situation inevitably leads to shortages of certain metals in the long term, as metal reserves on earth are finite. In this context "peak metal" is used to designate the year in which maximal metal production is reached, after which the primary sources are too much exhausted to continue production at this level.[3] Production then inevitably drops as the extraction of metals becomes more difficult. Some have argued that the resulting increase in price makes it economically feasible to exploit additional, less rich deposits, therefore delaying peak production. While this is certainly true in the short term, it does not guarantee long term supply as eventually all deposits will be depleted. Not all metals are equally at risk of supply disruption and the focus is therefore mostly on so-called "critical metals". Critical metals are defined as metals having both a *high supply risk* and a *large economic importance*. The criticality of a metal therefore changes over time, and is also dependent on the country. Metal reserves are not spread evenly across the world and the demand for metals is not always situated close to the producers. The economic and geopolitical implications are obvious and have led to tensions between countries.

In the last decades, certain countries have developed monopoly positions for the production of certain metals. Examples are South Africa and Russia for PGMs, Brasil for niobium, and the USA for beryllium. However, China in particular, has built a prominent role in the production of rare metals and is now the major producer of 14 of the 20 critical raw materials for the EU (Figure 2).[4] It now controls more than 85% of the antimony, magnesium and tungsten production and as much as 99% of the heavy rare earth production.

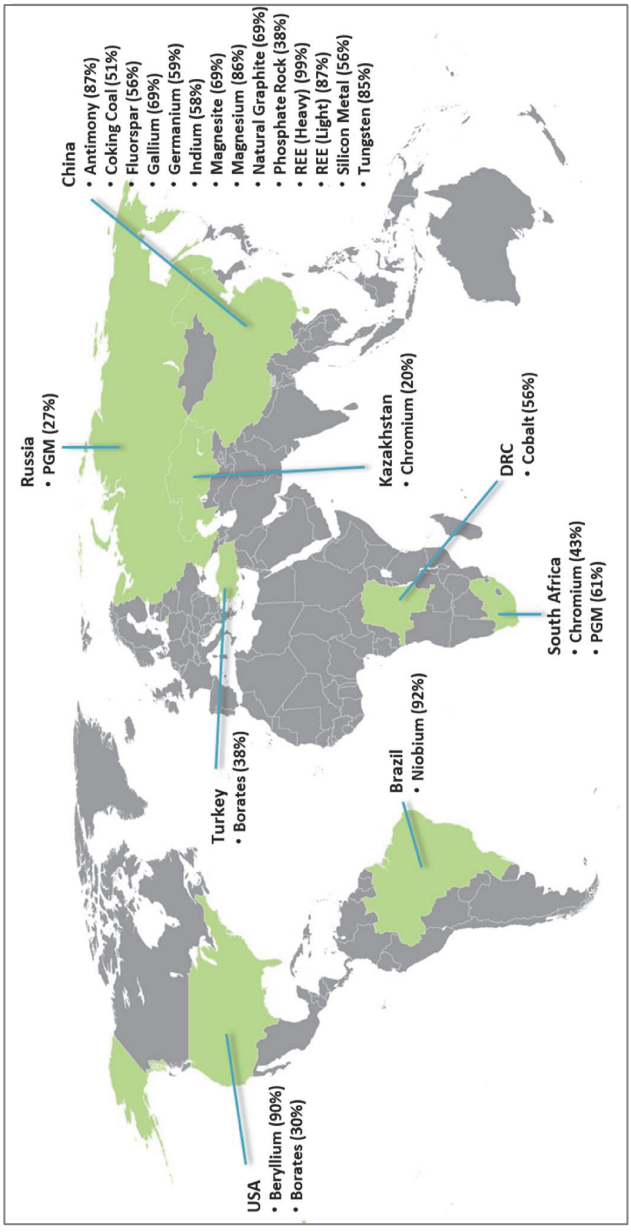

Figure 2. Major supplying countries of the EU critical raw materials.[4]

In general, the **supply risk** is evaluated according to three factors:

1. The substitutability
2. Recycling rates
3. Concentration of production in countries with poor governance

The economic importance (demand) of metals also changes over time due to the economic cycles and technological changes which alter the demand for particular metals. This is especially true for rare metals used in high-tech applications such as semi-conductors, TV screens, solar panels or batteries. These products have seen dramatic changes in composition as their technology evolved over time, often leading to boom-bust scenarios for the price of specific elements. To make things more complicated, specialized scarce metals are often mined as side products of other major metals due to the fact that no concentrated ores exist (Figure 3). The implication is that to satisfy the demand for one rare metal, large amounts of other elements have to be mined as well. This phenomenon, which is referred to as the balance problem makes it very difficult to balance supply and demand in the (rare) metal markets.[5]

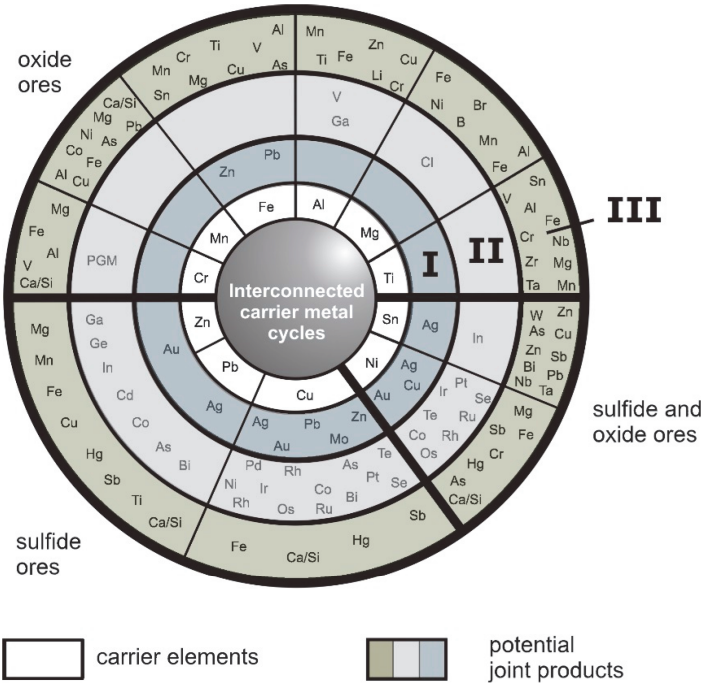

Figure 3.Schematic overview of the general coupling of metal production (PGM: Platinum Group Metals). Reproduced from: The Metrics of Material and Metal Ecology: Harmonizing the resource, technology and environmental cycles by A. M. Reuter.[6]

Comparing reports on critical raw materials from different countries clearly shows the differences in the classification of critical metals but also the different recommendations and strategies to address these risks: focusing more on additional production, recycling or substitution research.[4,7] In this PhD thesis we focus on the situation for Europe when discussing metal supply risks and policy measures.

In 2014, the European Commission released a report on the critical raw materials for the EU. This report showed current and future supply risks and demand trends for the most critical metals.[4] The aim was to convince European policy makers to stimulate the development of alternative European supply sources for the most critical metals through mining, recycling and substitution, therefore diminishing the dependence on foreign supply.[4] This report identified 20 metals and materials as being critical raw materials for the EU, which are shown in the red box in Figure 4. The classification was done by assessing the *economic importance* and *supply risk*.

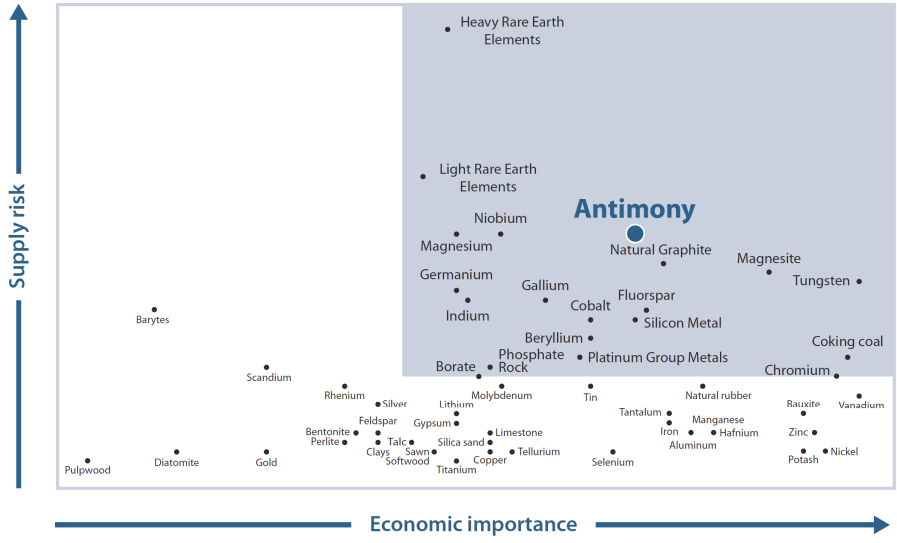

Figure 4. Criticality assessment for the EU, published in 2014 (Redrawn by Paul McGuiness).[4]

1.1.2 Technospheric mining: the key to metal recycling

In order to truly achieve a sustainable long-term supply of metals, the only option is to close the loop between metal production and the end-of-life products through recycling (Figure 5). This requires radical changes in every step of the value chain such as smart product design, better collection and efficient recycling technologies. This is still far from complete, but as metals become scarcer more attention is going to these alternative sources as a way to limit the dependence on primary production.

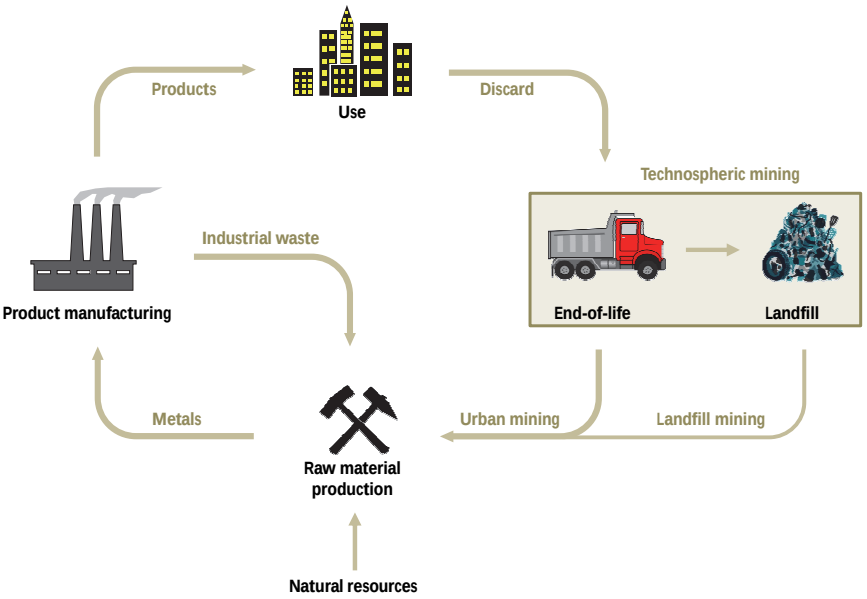

Figure 5. Life cycle of a material and its different stages.

Three different types of recycling can be distinguished:

1. Recycling of industrial waste (alloy, scrap and process residue recycling)
2. Recycling of end-of-life products (urban mining)
3. Recycling of valuable materials from landfills (landfill mining)

The recycling of industrial scrap and process residues is the easiest one to implement and is often already introduced in industrial processes to optimize their efficiency.[8] However, this technology is often not made public, and thus difficult to study and quantify. Recovery of materials and energy through *enhanced landfill mining* also shows potential, especially for monolandfills containing one type of waste.[9,10] *Urban mining* is very interesting for products which are collected efficiently (e.g. electronic waste, fluorescent lights, cars) and easily dismantled. In general, urban mining deals with small volumes with high metal concentrations, while landfill mining is based on high volumes with lower metal concentrations.[9]

Waste electrical and electronic equipment (WEEE) or *e-waste,* is the most rapidly growing type of waste all over the world.[11] In 2012, 14.2 kg of e-waste was discarded on average by every person on earth in the form of cellphones, computers, radios, televisions, fluorescent lamps, etc.[11] Detailed quantitative reports about the metal contents in various electronic products have proven the potential of this type of waste as an alternative resource for scarce elements, because they are concentrates of valuable elements (e.g. gold, palladium, silver, indium, gallium, cobalt, rare-earths, and tantalum). A mobile phone for example, contains about 305 mg of silver and 30 mg of gold which is 40 to 50 times more concentrated than in the ores from primary mining.[11] In addition, the recycling of e-waste also regenerates the required metals in the ratios needed to manufacture these devices again.[5] The volumes of waste are therefore reduced to a minimum compared to primary mining.[5] Several industrial scale urban mining schemes have already been successfully implemented by companies such as Solvay and Umicore.[8,11,12]

As an illustration, Table 1 shows the amount of valuable metals in different electronic items, as compiled by the Öko-Institut report (2012).[11]

Table 1. Content of valuable metals in all flatscreens, notebooks and smartphones sold in Germany in 2010 (Öko-institut report).[11]

Metal	**Flatscreens (kg)**	**Notebooks (kg)**	**Smartphones (kg)**	**Occurrence**
Dysprosium		430		Permanent magnets
Europium	50	<1		Background illumination
Gadolinium	10	5		Background illumination
Gallium	15	10		Semiconductor chip
Gold	1645	740	230	PCBs[1] and contacts
Indium	2365	290		Displays (ITO layer)
Cobalt		461000	48500	Lithium-ion batteries
Neodymium		15160	385	Permanent magnets
Palladium	465	280	85	PCBs[1] and contacts
Platinum		30		Hard disk platters
Praseodymium	<1	1950	80	Permanent magnets
Silver	6090	3100	2350	PCBs[1] and contacts
Tantalum		12065		Capacitors
Terbium	14	<1		Background illumination
Yttrium	680	12		Background illumination

[1]PCB: Printed circuit board

Despite all these incentives for recycling, the recycling rates for most rare metals are still alarmingly low (Figure 6).[13] The main reason is that they are very dispersed, with every item often only containing traces of these elements. Common metals such as iron, nickel, copper, aluminum or zinc show much better recycling rates because they are commonly used in their pure form, making collection and recycling much more straightforward.[13]

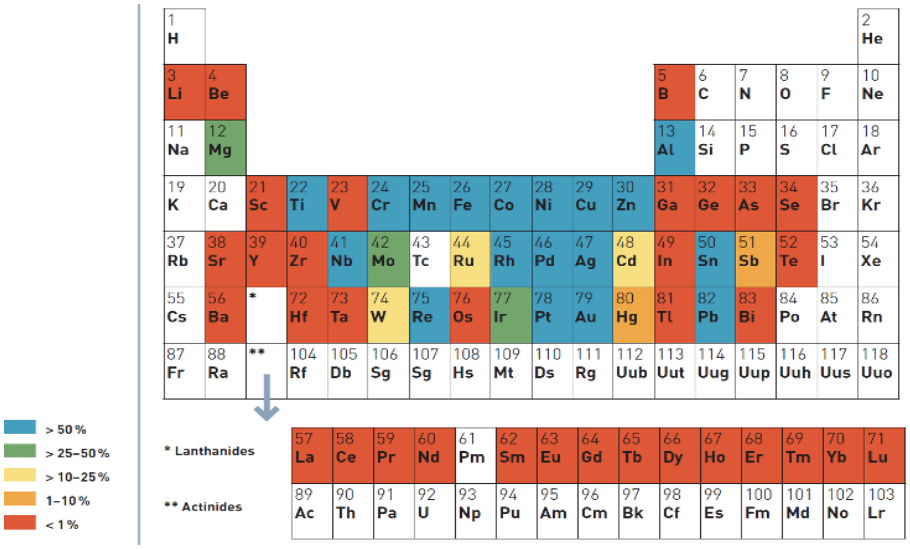

Figure 6.Worldwide end-of-life recycling rates (%) for 60 metals (UNEP report 2011).[13]

The main bottleneck at this moment is the inefficient collection of this waste. Billions of euros worth of electronic equipment is held by households ("hibernating") and it is up to governments and policy makers to organize and stimulate the collection of these end-of-life items. The most successful examples are found for items with a toxicological risk such as fluorescent light bulbs (mercury) and batteries (acids and heavy metals). These items are often collected on a large scale in order to deal with these risks and avoid them ending up in landfills and pollute the environment. Their large availability and valuable metal content makes them ideal starting points for urban mining processes. Urban mining can help Europe to guarantee a secure supply of industrially important elements. In the future, the strategic, technological, ecological and geopolitical advantages of urban mining will continue to stimulate this evolution and contribute to closing the loop of metal production and consumption. A particularly interesting example is the recovery of rare earths from end-of-life consumer products, which is the objective of this PhD thesis.

1.2 The rare-earth elements

The rare earths are a group of 17 elements consisting of the 15 lanthanides plus scandium and yttrium (Figure 7). The rare earths (REEs) are sometimes divided in light rare earths (LREE) and heavy rare earths (HREE). The division between light and heavy REEs is arbitrary, but is often situated around europium.

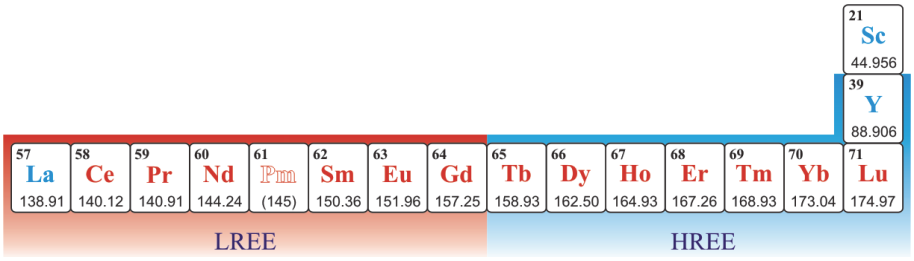

Figure 7. Overview of the rare-earth elements.

The unique properties of REEs have allowed major technological breakthroughs such as color television, compact fluorescent lights and high-strength magnets used in hard-disk drives, wind turbines and electric cars. The major share of the rare-earth market (by value) is taken by the neodymium-iron-boron (NdFeB) permanent magnets (37%) and the fluorescent lamp phosphors (32%). Other markets such as polishing powders and the glass and ceramics industry use larger amounts of rare earths but these are applications with little added value as they use cheap and largely available REEs (e.g. La, Ce). At the end of the last century, China took over most rare-earth production by aggressively cutting costs, thus forcing other major producers such as the U.S. to shut down their operations. Since 2000, China controls more than 90% of the REE market, making REEs highly critical elements as they are crucial for many high-tech and military applications. These tensions culminated in the world wide rare-earth crisis of 2011, when China decided to install strict export quota thus cutting off other countries from a reliable supply of these important elements. This led to soaring prices and a trade war between the U.S., Europe and Japan on the one hand and China on the other hand. This crisis was short-lived and anno 2015 REE prices have dropped back to pre-crisis lows, but this shows nevertheless the fragility of the global supply-demand balance for some of the critical metals. A graph showing the historical price evolution of rare earths (2003−2015) has been included in the text to help visualize this remarkable boom-bust evolution (Figure 8). Since accurate price quotations for rare-earth elements are often difficult to come by we have also chosen to include the raw data so that it can serve as a reference for future use. All data were obtained from the annual commodity reports compiled by the United States Geological Survey (USGS).

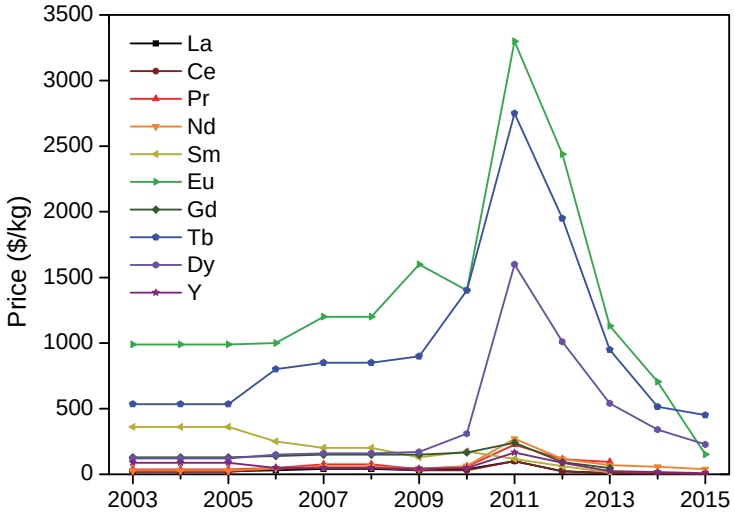

Year	*La*	*Ce*	*Pr*	*Nd*	*Sm*	*Eu*	*Gd*	*Tb*	*Dy*	*Y*
2002	*23*	*19*	*37*	*29*	*360*	*990*	*130*	*535*	*120*	*88*
2003	*23*	*19*	*37*	*29*	*360*	*990*	*130*	*535*	*120*	*88*
2004	*23*	*19*	*37*	*29*	*360*	*990*	*130*	*535*	*120*	*88*
2005	*23*	*19*	*37*	*29*	*360*	*990*	*130*	*535*	*120*	*88*
2006	*30*	*40*	*50*	*45*	*250*	*1000*	*140*	*800*	*150*	*50*
2007	*40*	*50*	*75*	*60*	*200*	*1200*	*150*	*850*	*160*	*50*
2008	*40*	*50*	*75*	*60*	*200*	*1200*	*150*	*850*	*160*	*50*
2009	*30*	*30*	*38*	*42*	*130*	*1600*	*150*	*900*	*170*	*44*
2010	*38*	*30*	*60*	*63*	*175*	*1400*	*165*	*1400*	*310*	*50*
2011	*100*	*100*	*225*	*270*	*117*	*3300*	*239*	*2750*	*1600*	*165*
2012	*23*	*23*	*115*	*117*	*62*	*2440*	*92*	*1950*	*1010*	*88*
2013	*8*	*8*	*94*	*70*	*14*	*1130*	*47*	*949*	*540*	*25*
2014	*5*	*5*		*58*		*705*		*515*	*340*	*16*
2015	*2*	*2*		*40*		*153*		*450*	*228*	*9*

Figure 8. Historical rare-earth prices ($/kg) based on USGS reports.

A direct consequence of the 2011 rare-earth crisis was the determination of policymakers to establish alternative supplies of rare earths.[14] Old deposits were reopened and exploration started for new deposits. A lot of research also started on the recycling of REEs from end-of-life consumer products such as hard-disk drives, fluorescent lamps and NiMH batteries.[14] Another approach is the substitution of REEs in technological applications. Successful examples exist, but some applications have not yet found satisfying solutions despite decades of research.[14] A successful example of substitution can be recognized in Figure 8: the steady drop of samarium prices is a direct result from the substitution of samarium-cobalt magnets by the more powerful neodymium-iron-boron magnets.

1.2.1 Primary mining of rare earths and the balance problem

Rare-earth elements (REEs) are actually not very rare as they have an abundance in the earth's crust which is situated between those of copper and silver.[15] Unfortunately, the absence of concentrated deposits makes their recovery challenging. The rare-earth elements are also present as a mix of elements, due to their very similar chemical properties. This complicates their separation which requires very large solvent extraction set-ups and a lot of chemicals. In the 1980s REE production shifted from the USA (Mountain pass, CA) to China due to environmental concerns and aggressive pricing from the upcoming Chinese miners. Although rare-earth deposits have been found all over the world, today over 90% of the world's production is still concentrated in China because very few of them manage to produce rare earths in a price competitive way (Figure 9). This supremacy poses significant geostrategic risks and has been a source of tension due to the importance of rare earths in many technological and military applications.[8,12,14-17] Following the rare-earth crisis of 2011, junior mining projects surged all over the world, but many of these projects are now dormant or abandoned due the lower prices for rare-earths elements and the high cost and technical difficulties associated with rare-earth processing and separation.

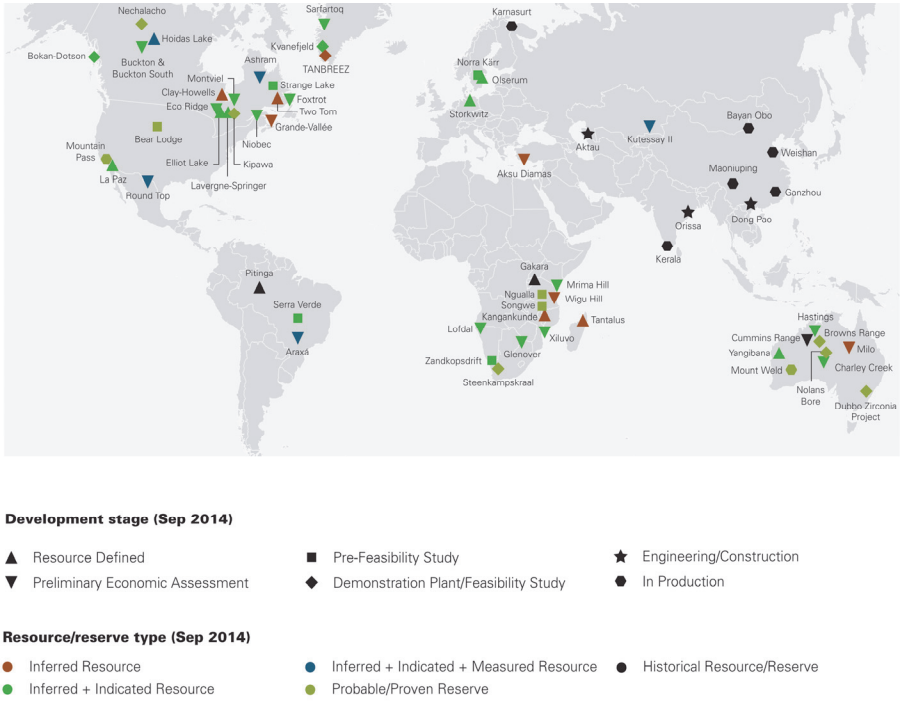

Figure 9. Overview of the different REE mining projects around the world, in different stages of development (June 2013). Many of them have since then become dormant. Reproduced from the ERECON report (2015).[14]

An important drawback of primary mining is that the rare earths are present as a mix in the ores. This means that in order to cover the world's demand for the industrially important REEs such as Nd, Eu, Tb, Dy and Y, an enormous overproduction of La and Ce is required. These elements are far more abundant in most ores (Table 2).[5,8] This mismatch between supply and demand is called the *balance problem* and is one of the main driving forces for the recycling of rare earths from end-of-life products.[5,8] Few ores are enriched in heavy REEs and today most heavy REEs are produced in so-called ion-adsorption clays in China which are weathered deposits. When such clays are situated below rocks that contain rare-earth minerals, they can act as giant chromatography column when the rain weathers the overlying rock. The most soluble, light REEs pass through the clay more easily than the heavy REEs. In this manner, these ion-adsorption clays can be highly enriched in heavy REEs and almost free of radioactive elements.[18] Other REE sources include apatite and hard-rock deposits such as zircon, titanate, niobate, eudialyte and gadolinite.[18]

Table 2. Overview of the main exploited REE-containing minerals and deposits.[14,18]

Mineral	**Structure**	**REE content**	**Exploited deposits**
Monazite	$(La,Ce,Th)PO_4$	Light REEs	Mt. Weld (Australia)
Bastnäsite	$(La,Ce)CO_3F$	Light REEs	Mountain pass (USA) Bayan Obo (China)
Xenotime	YPO_4	Heavy REEs	Lehat (Malaysia)
Laterite[1]	Ion-adsorption clays	Light REEs	Xunwu (China)
		Heavy REEs	Longnan (China)
Loparite	$(La,Ce,Na,Ca)(Ti,Nb)O_3$	Light REEs	Kola peninsula (Russia)

The extraction of rare earths from these different ores is very energy demanding and poses serious environmental challenges due to the presence of radioactive elements, and the use of strong acids.[18] Monazite for example is dissolved in a process called *acid cracking* (H_2SO_4 98%, 150 °C). A more recent process uses *alkaline cracking* (NaOH 73%, 140 °C) which generates less waste and allows the phosphate content to be recovered as trisodium phosphate.[18] Additional separation steps are required to remove the radioactive thorium and isolate the rare earths. Bastnäsite can be roasted in air (620 °C) followed by dissolution in HCl (Molycorp, USA) or bastnäsite can be roasted with H_2SO_4 98% at 500 °C which is preferred in China but is very harmful to the environment due to the release of HF gas.[18] The third important source of rare earths are the ion-adsorption clays. The rare earths are extracted by in-situ leaching (ion-exchange) using dilute solutions of monovalent sulfate or chloride salts at ambient temperature. Their much lower grade (0.05-0.3 wt%) is offset by the easier mining and processing.[18] However, this in-situ leaching is very polluting and often operated illegally on a small scale.

1.2.2 Recycling and urban mining opportunities for rare earths

Rare earths are used in a wide variety of technological applications and consumer items. The high criticality of certain specific rare earths (Nd, Eu, Tb, Dy, Y) is primarily caused by their crucial role in strong permanent magnets and lamp phosphors, which together account for more than 70% of the rare-earth market by value.[8] The successful recycling of rare earths from these objects depends on the ability to efficiently collect and dismantle them, as well as the availability of cost-efficient recycling technologies to recover the rare earths.[8,9,11,12,19-23]

A recent report by European Rare Earths Competency Network (ERECON) (2015) has suggested the following priority list.[14] This list takes into account the criticality of the rare earths used in those products, as well as the potential value of the waste stream, the future demand, the possibility of substitution and the technical feasibility of recycling.[14] Specific consumer products have been identified which have the highest potential for recycling (Table 3).[14]

1. Permanent magnets (Pr, Nd, Sm, Tb, Dy)
2. Phosphors (La, Ce, Eu, Gd, Tb, Y)
3. Batteries (La, Ce, Pr, Nd)
4. Polishing compounds (Ce)
5. Catalysts (La, Ce, Pr, Nd, Y)

Table 3. Priority list for the recycling of rare earths from end-of-life products.[8,14]

Product	REEs[1]	Priority[2]
Permanent magnets		
Hard disk drives, CD players	Pr, Nd	1
Automotive applications	Pr, Nd, Tb, Dy	2
Electric motors (industry)	Pr, Nd, Tb, Dy	3
Loudspeakers	Pr, Nd	4
Mixed electronics, toys and gadgets	Pr, Nd	5
Electric bicycles	Pr, Nd, Tb, Dy	6
Wind turbines and generators	Pr, Nd, Tb, Dy	7
Phosphors		
Fluorescent lamps	Eu, Tb, Y (Ce, Gd, La)	1
LCD screens	Eu, Tb, Y (Ce, Gd, La)	2
Plasma screens	Eu, Tb, Y (Ce, Gd, La)	3
CRT screens	Eu, Y, Sm	4
LED lights	Ce, Lu, Y	5

[1]Uses the data compiled by Binnemans *et al* (2013) and the ERECON report (2015).[8,14]

[2]This priority list takes into account the market size, the elements and the easy of recovery (ERECON).[14]

1.2.3 Recycling of lamp phosphor waste

Fluorescent lamps are already collected on a large scale in order to safely dispose the mercury inside the light bulbs. The metal, glass and plastic fraction of the lamps could in principle also be recycled but this is often not done due to practical limitations. The remaining fraction (≈ 3 wt%) is the so-called lamp phosphor waste powder which is coated on the inside of the glass (Figure 10).

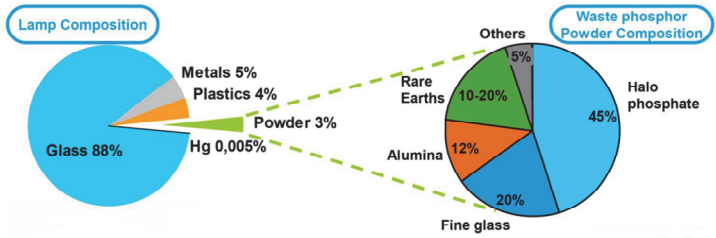

Figure 10. Fluorescent lamp composition (Source: Solvay).

The lamp phosphor waste powder consists mainly of luminescent compounds (phosphors) that are responsible for the emission of visible light, but also contains silica (glass) and alumina (binder) as well as traces of mercury. This lamp phosphor waste powder is therefore a complex but valuable product, containing several different fractions (Figure 11).

Overview of the approximate lamp phosphor waste composition

	Formula	Role	Content (wt%)
HALO	$(Sr,Ca)_{10}(PO_4)_6(Cl,F)_2:Sb^{3+},Mn^{2+}$	White phosphor	50
YOX	$Y_2O_3:Eu^{3+}$	Red phosphor	20
BAM	$BaMgAl_{10}O_{17}:Eu^{2+}$	Blue phosphor	5
LAP	$LaPO_4:Ce^{3+},Tb^{3+}$	Green phosphor	5−10
CAT	$CeMgAl_{11}O_{19}:Tb^{3+}$	Green phosphor	
Silica/alumina	SiO_2/Al_2O_3	Glass/Binder	10−20
Mercury	Hg	Emission of UV	Traces

Figure 11. Schematic overview of the composition of lamp phosphor waste with the four highlighted critical elements: yttrium, terbium, europium and antimony.[24-26]

The interest in these powders is mainly derived from the relatively high rare-earth content, in particular the highly-critical europium, terbium and yttrium, but also antimony has been in focus.[24,25] Before attempting the recovery of valuable metals from the lamp phosphor waste powder, it can be sieved in order to remove most of the glass, as the glass particles are much larger than the phosphor powder particles (≈ 3-6 µm). The mercury can be removed in advance using a high-temperature mercury distillation or it can be removed during the recycling process using sorbents.[26-29] Recently, Tunsu *et al.* (2015) also proposed a wet decontamination

method using I_2/KI solutions to solubilize the mercury, followed by the removal of the mercury using anion exchange sorbents, solvent extraction or reducing agents.[30] Many different recycling methods have been proposed to dissolve, recover and separate the different phosphors, but their economic recycling remains challenging.[8,19,31] A general scheme for the recovery of rare earths from lamp phosphor waste and the position in the life cycle of fluorescent lamps is shown in Figure 12.

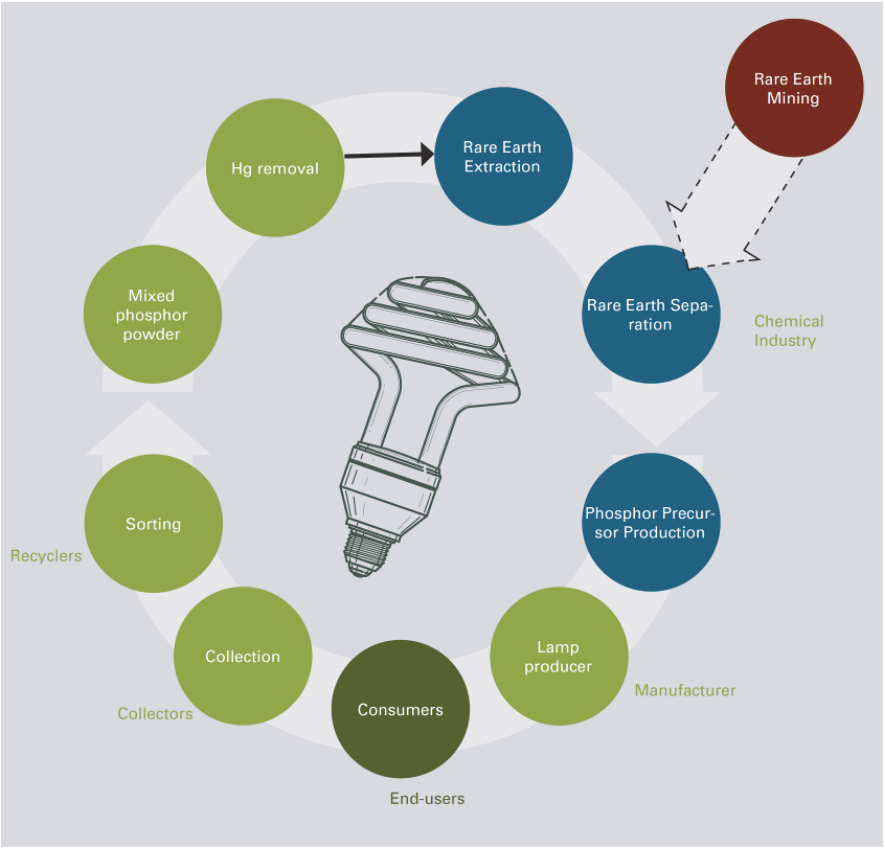

Figure 12. Schematic overview of the life cycle of fluorescent lamps. Reproduced from ERECON report (2015).[14]

Current recycling technologies can be divided in two main groups: the *physicochemical methods* and the *chemical dissolution methods*.[8,19] The physicochemical methods focus on the separation of the phosphors and their direct reuse using methods such as dense-medium centrifugation, froth flotation, two-liquid flotation or pneumatic separation in an air stream.[8,19,23,32-36] The major drawback of these physicochemical methods is that the phosphors are degraded during their lifetime, meaning that separation and direct reuse results in an inferior

product compared to freshly produced phosphors.[8] Chemical methods are usually based on the (selective) dissolution of the phosphors, followed by solvent extraction to extract and separate the different elements (Table 4).[8,19,23-25,31,37-40] These methods contain many steps and consume a lot of chemicals (acids, bases, organic solvents) due to the different elements present in the powders.[8,19,31] However, this approach is usually preferred since it produces pure elements which can be used in the production of new lamp phosphors. In 2012, a recycling process was implemented on industrial scale by Solvay in La Rochelle (France).[41] There, up to 3000 tons/year of waste phosphor powder can be treated in order to recover the rare earths and valorize the rest of the waste. However, more selective methods continue to be developed in order to improve the efficiency and facilitate the recovery of rare earths. In this PhD thesis, a new ionic liquid process was developed which allows the (previously impossible) selective dissolution and revalorization of the red phosphor YOX.[24]

Table 4. A selection of processes to recover yttrium from lamp phosphor waste.[31]

Main process steps	**Author**	**Ref**
Dissolution in H_2SO_4 / HNO_3 Thiocyanate conversion KSCN Solvent extraction (NR_4^+ extractant)	Rabah *et al*. (2008)	42
Dissolution in H_2SO_4 Precipitation with oxalic acid	De Michelis *et al*. (2011)	43
Step-wise dissolution: HCl, H_2SO_4 and NaOH Solvent extraction	Osram patent (2012)	39
Step-wise dissolution: HCl, alkaline fusion and HNO_3 Solvent extraction	Solvay patent (2012)	41
Dissolution in H_2SO_4 / H_2O_2 Purification with Na_2S / NaOH Precipitation with oxalic acid	Innocenzi *et al*. (2013)	44
Dissolution in H_2SO_4 / HNO_3 Solvent extraction (DODGAA extractant)	Yang *et al*. (2013)	37
Dual hydrochloric acid dissolution and alkaline fusion	Liu *et al*. (2014)	45
Dissolution in HNO_3 or HCl (ultrasound-assisted) Solvent extraction (e.g. Cyanex® 923)	Tunsu *et al.* (2014)	29
Selective dissolution in [Hbet][Tf_2N] Precipitation with oxalic acid	**Dupont *et al.* (2015)[1]**	24

[1]This process was developed within the framework of this PhD thesis.[24]

1.2.4 Recycling of NdFeB magnets

NdFeB magnets are the strongest permanent magnets known today and have allowed the miniaturization of many high-tech products such as hard disk drives, speakers, electric motors, etc.[8,14] The demand for neodymium and dysprosium is expected to grow by 700% and 2600%, respectively, over the next 25 years as the NdFeB market expands rapidly.[46] It is also estimated that by 2020 over 200,000 tonnes of REEs will be held in NdFeB magnets worldwide. A schematic overview of the value chain and lifecycle of NdFeB magnet is given in Figure 13.[14]

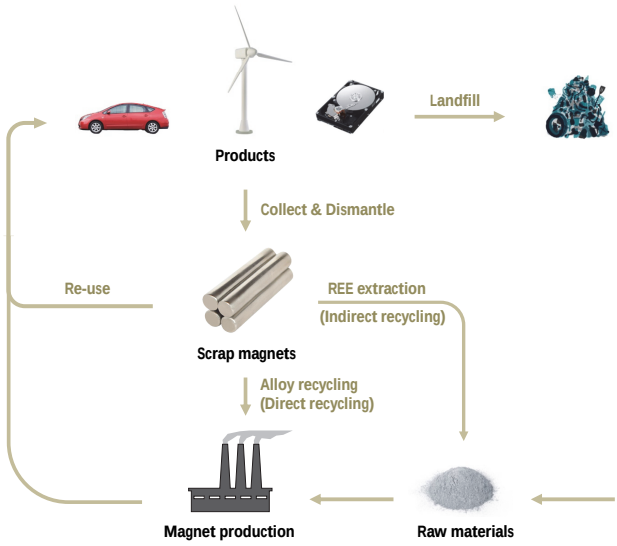

Figure 13. Overview of the life cycle and recycling opportunities of NdFeB magnets.

The magnets consist primarily of a Nd−Fe−B alloy (e.g. $Nd_2F_{14}B$) but they also contain additives to improve their magnetic properties and durability (Figure 14).[38,39]

Overview of the approximate NdFeB magnet composition[(a)]

Name	Role	Content (wt%)
Fe	Main element	72
Nd	Main element	27
B	Main element	1
Additives/substitutes:		
Dy / Tb	High temperature performances	0−8
Pr	Cheaper replacement for Nd	0-8
Co	Increase Curie temperature	0-5
Al/Nb/Ga	Increase coercivity	< 1
Cu	Reduce processing temperature	< 0.1
Mo / V	Corrosion resistance	< 0.1
Zr/Si	Improve magnetic properties	< 0.1

[(a)] Some magnets are also coated with a polymer or a metal coating (e.g. Ni, Zn, Al, TiN,)

Figure 14. Schematic overview of the composition of NdFeB magnets.

By recycling the magnets in cars, wind turbines, e-bikes and consumer electronics, a more sustainable production could be guaranteed. In certain cases, this can be achieved by direct re-use of the magnets, but often the re-processing of alloys (*direct recycling*), or extraction of the rare earths (*indirect recycling*) is more desirable (Figure 13). Direct recycling is less costly and more energy- and material-efficient, but requires standardized product designs and controlled collection systems in order to allow the reuse of the magnets. Reprocessing of the existing alloy is more energy-demanding and less material-efficient but is more flexible as the alloys can be recast to produce different types of magnets. Two methods can be employed: the first is the melting of the scrap magnets down to a master alloy which can be used to produce bonded magnets or hot-deformed magnets.[14] The second is the use of hydrogen-based routes such as hydrogen decrepitation (HD) or hydrogenation disproportionation desorption and recombination (HDDR), which can be used to obtain sintered and bonded magnets.[14,47,48] The problem with alloy reprocessing is that it is highly dependent on the input material and oxygen contamination. There are still challenges to overcome in order to produce magnets with sufficiently good magnetic properties.[48] Finally, extraction of REEs from the magnets is also being considered. It has a higher cost but is able to produce the raw materials required for the production of new magnets (Figure 15).[8]

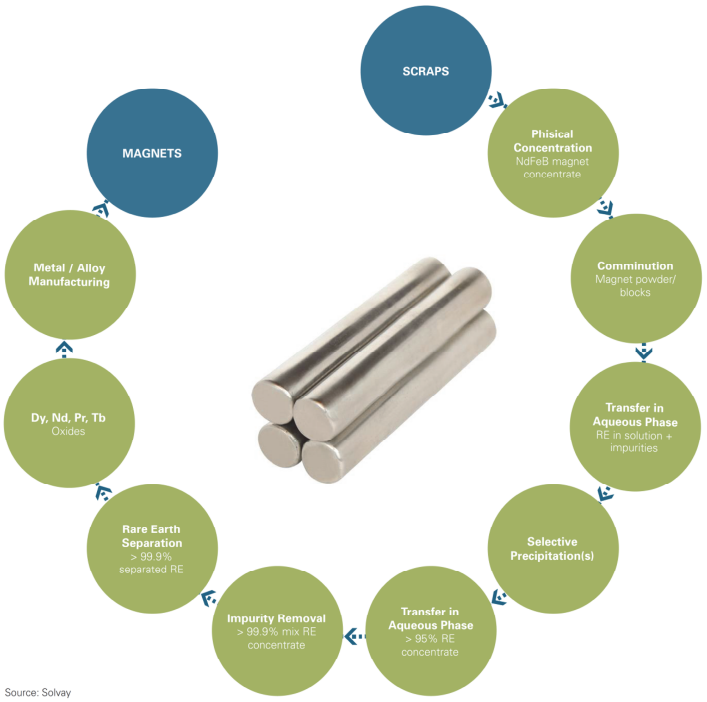

Figure 15. Schematic overview of a possible hydrometallurgical REE recovery scheme from recycled NdFeB magnets. Reproduced from ERECON report(2015). Source: Solvay.[14]

Various processes have been developed recently which use acids to dissolve the (oxidized) magnets and then extract/isolate the rare earths (Table 5).[8,22,49-54] The magnets are usually first milled and grinded to facilitate the oxidation and accelerate the reaction. The recycling methods also have to deal with the many trace elements and impurities present in the magnet which makes some form of solvent extraction unavoidable in order to obtain highly pure rare-earth oxides. Ionic liquids have been proposed as alternative solvents for liquid-liquid extraction and as extractants.[8,50,51,55,56] In this PhD thesis, a new ionic liquid process was developed which combines leaching and extraction in the same ionic liquid due to the fact that this ionic liquid, [Hbet][Tf_2N], has both acidic and thermomorphic properties (explained later on in this introduction).[57] This novel process also introduced microwave-assisted roasting of the magnets as an energy-efficient method for magnet oxidation.[57]

Table 5. Selection of hydrometallurgical processes to recover REEs from NdFeB magnets.[8,22]

Main process steps	**Author**	**Ref**
Dissolution in H_2SO_4 (2 M) Precipitate double sulfate with NaOH / KOH / NH_4OH	U.S. Bureau of Mines Patent (1992)	58
Dissolution in HCl (3 M) Precipitation with oxalic acid	Itakura *et al*. (2006)	52
Dissolution in HCl (0.02 M) with autoclave (180 °C) Precipitation of the rare earths	Koyama *et al*. (2009)	54
Dissolution in H_2SO_4 Precipitation with NaOH	Lee *et al*. (2013)	53
Dissolution in HCl (4 M) Step-wise precipitation with NH_4OH and oxalic acid	Lai *et al*. (2014)	49
Roasting of the magnet Dissolution in HCl / NH_4Cl Solvent extraction (PR_4^+ extractant) Precipitation with oxalic acid	Vander Hoogerstraete *et al*. (2014)	51
Roasting of the magnet Dissolution in HNO_3 / NH_4NO_3 Solvent extraction (PR_4^+ extractant) Solvent extraction (EDTA extractant) Precipitation with oxalic acid	Riano *et al*. (2015)	50
Roasting of the magnet Dissolution in [Hbet][Tf_2N] Precipitation with oxalic acid	**Dupont *et al*. (2015)**[1]	57

[1]This process was developed within the framework of this PhD thesis.[57]

1.2.5 General notes on recycling and green chemistry

The large R&D efforts in industry and academia have demonstrated that the recycling of rare earths from end-of-life products such as fluorescent lamps and NdFeB magnets (e.g. hard disk drives) is technically feasible.[8,14] However, their implementation and industrial upscaling is still hampered by several factors which will have to be resolved before their recycling becomes widespread:

1. Insufficient and non-selective collection of the waste
2. Dissipative use
3. Presence of contaminants
4. Price volatility for the raw materials and products
5. Transportation of the (hazardous) waste
6. Price competition with low-cost primary production

Base metals such as iron, copper and aluminum are used in large quantities and often in their pure form. On the other hand, rare earths and other critical metals are usually present in very small quantities in their end products. Their collection is further complicated by the fact that dismantling is required as a pre-treatment step. Smart product design is therefore crucial to facilitate and automate product dismantling in a later stage. Smart product design and selective collection can provide homogeneous waste streams, but even then, the presence of contaminants is unavoidable. Sophisticated separation processes have to be designed which can cope with the presence of such contaminants in order to avoid them ending up in the products. Finally, one of the major challenges is the (uncontrollable) price evolution of raw materials and products which can pose a big threat to recycling efforts.

Nevertheless, it is clear that critical metal recycling is crucial as the world needs to move to a more circular and sustainable economy. A greener future will require access to these critical metals used in hybrid cars, e-bikes, windmills and energy-effective lighting solutions. Industry, universities and policymakers have to work together to create a framework in which recycling technologies can be developed, tested and implemented regardless of short-term price fluctuations. As the unique properties of certain metals make them difficult to substitute, the best long term solution is to close the life cycle of these metals in order to halt their dissipation.

These notes of caution are important and it is becoming increasingly clear that sustainable innovation has to consider the whole life cycle of a product. During this thesis we often use the word **"green chemistry"**. However, the inherent ambiguity of the word green chemistry makes it important to dedicate a paragraph to define this concept in general and in the context of this thesis.

Green Chemistry

The broadest definition is that Green chemistry is an area of chemistry focused on the design of products and processes that minimize the use and generation of hazardous substances.[59] The difference between green chemistry and environmental chemistry is that green chemistry focusses more on the development of technology to prevent pollution and reduce consumption of nonrenewable resources, whereas environmental chemistry focuses on the effects of polluting chemicals on nature.

In 1998, Paul Anastas and John C. Warner published a set of twelve principles to guide the practice of green chemistry.[59] These principles help define whether or not a process merits the label green but also offers guidelines on how to reduce the environmental and health impacts of chemical production,.

1. It is better to prevent waste than to treat or clean up waste after it is formed.
2. Synthetic methods should be designed to maximize the incorporation of all materials used in the process into the final product.
3. Wherever practicable, synthetic methodologies should be designed to use and generate substances that possess little or no toxicity to human health and the environment.
4. Chemical products should be designed to preserve efficacy of function while reducing toxicity.
5. The use of auxiliary substances (solvents, separation agents,...) should be made unnecessary wherever possible and innocuous when used.
6. Energy requirements should be recognized for their environmental and economic impacts and should be minimized. Synthetic methods should be conducted at ambient temperature and pressure.
7. A raw material or feedstock should be renewable rather than depleting wherever technically and economically practicable.
8. Reduce derivatives: unnecessary derivatization (blocking group, protection/deprotection, temporary modification) should be avoided whenever possible.
9. Catalytic reagents (as selective as possible) are superior to stoichiometric reagents.
10. Chemical products should be designed so that at the end of their function they do not persist in the environment and break down into innocuous degradation products.
11. Analytical methods need to be further developed to allow for real-time, in-process monitoring and control prior to the formation of hazardous substances.
12. Substances and the form of a substance used in a chemical process should be chosen to minimize potential for chemical accidents, including releases, explosions, and fires.

The study of green and sustainable processes has evolved tremendously over the years.[60,61] Important tools have been developed to assess the environmental impact of a process or product, in particular life-cycle analysis (LCA). This type of analysis takes into account all stages of a product life cycle from production until disposal or recycling and assesses the impact on different relevant categories such as toxicity, fossil fuel depletion, climate change, etc. (Figure 16). This tool allows a systematic study of the environmental impact of a process and makes it possible to compare different processes.

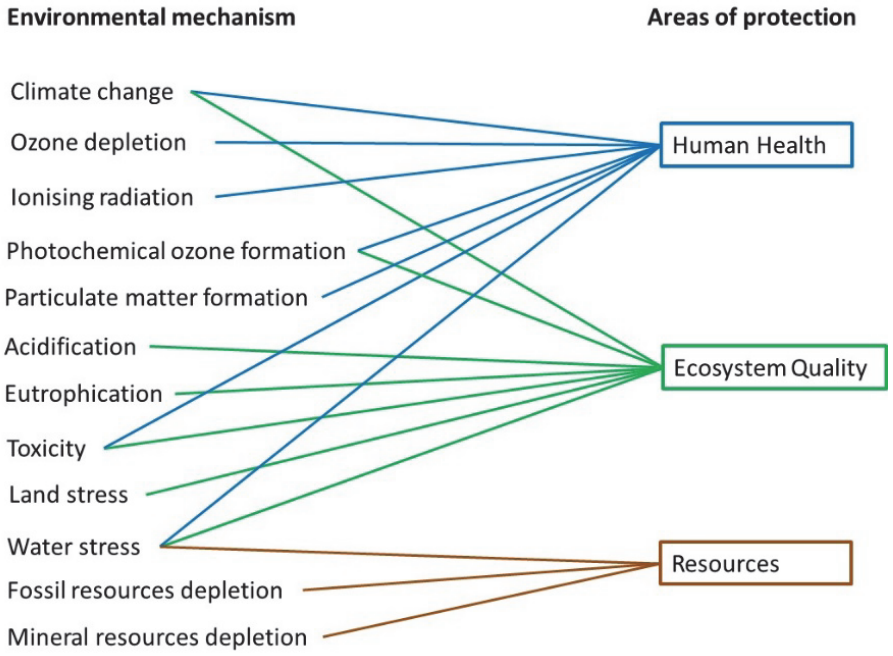

Figure 16. Overview of the most important impact categories used in life-cycle assessments.

During this PhD thesis we focused our efforts on the development of new recycling technologies which would limit the consumption of chemicals and energy. We also tried to apply the principles of *zero-waste valorization* which dictates that no waste should be created during the valorization of a residue or spent product. This means that all compounds formed during the process should be non-toxic (e.g. water) or usable as new feedstock. During the design of our processes we were assisted by a colleague working full time on life-cycle analysis. This allowed us to study the impact of our processes and to compare them to the current state-of-the-art technologies. Overall, we believe this PhD thesis demonstrates that in certain circumstances, ionic liquids can contribute to the design of more sustainable metal recycling processes compared to classic hydro- or pyrometallurgical processes.

1.3 Ionic liquids as designer solvents

1.3.1 Introduction

Ionic liquids (ILs) are traditionally defined as salts which are liquid below 100 °C. Most ionic liquids consist of bulky organic cations and organic or inorganic anions (Figure 17). The structure of an ionic liquid can be abbreviated as [Cation][Anion]. Millions of different simple ionic liquids can be prepared by combining different cations and anions.[62]

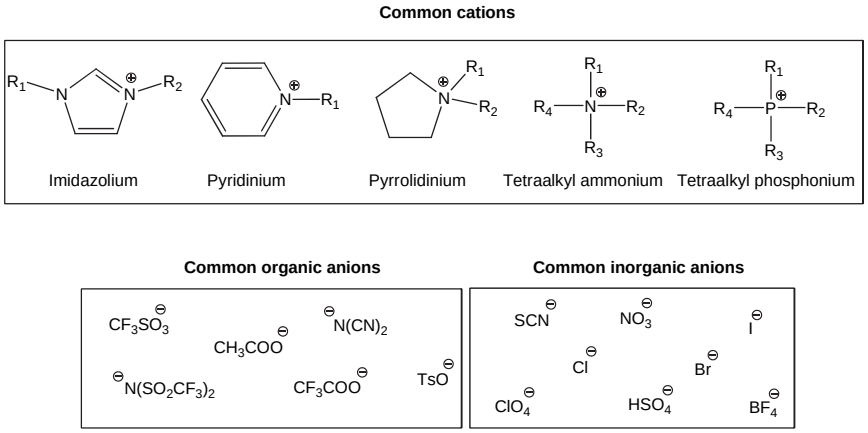

Figure 17. Overview of some common ionic liquid cations and anions.

Ionic liquids find applications in a wide variety of fields including catalysis, organic synthesis, electrodeposition, biomass and polymer processing, drug delivery, microwave chemistry, metal processing, solvent extraction and compound purification.[62,63] Ionic liquids have several physical properties which make them particularly attractive solvents. The first is their negligible vapor pressure due to the fact that they consist entirely of ions. This means that no noxious fumes are formed, even upon heating since ionic liquids will degrade before evaporating. Ionic liquids also have a low flammability, further improving their safety. This is in stark contrast to common organic solvents (e.g. toluene, kerosene, ethanol, acetone) which are all quite volatile and very flammable since solvent fires can start with the smallest sparks or electrical discharges. Another advantage is their ability to solvate a wide range of organic, polymeric and inorganic materials. A typical example is the dissolution of cellulose in ionic liquids.[64] The excellent temperature stability and large liquidus range permits reaction conditions which are not accessible in water or organic solvents. Ionic liquids have also gathered a lot of interest for electrochemical applications due to their broad electrochemical window and good conductivity which allows the electrodeposition of metals such as Al, Li, Ti, V and W, that cannot be deposited from aqueous solution.[65]

The main disadvantage of ionic liquids is their high viscosity at room temperature, but at higher temperatures or when water-saturated (i.e. in biphasic solvent extraction system) their viscosity drops significantly. There are also large differences between individual ionic liquids, with viscosities ranging from 10 cP to above 10000 cP depending on the nature of their ions. Other physical properties such as the miscibility with water, the density and the melting point are also greatly affected by the anion and cation choice.[66] This offers the opportunity to tune the properties of a given ionic liquid for a specific application. Therefore, ionic liquids are often called *designer solvents*.

The main synthesis routes for ionic liquids are summarized in Scheme 1. In a first step (**A**), an amine base (e.g. trialkylamine, imidazole, pyridine, pyrrolidine) is quaternized by reacting it with an alkyl chloride (or bromide), thus obtaining the corresponding chloride (or bromide) ionic liquid $[N_{RRRR}][Cl]$.[67] The same scheme also applies to trialkylphosphines for the synthesis of phosphonium ionic liquids.[68]

The chloride anion can be exchanged (**B**) for another anion X^- if X^- has a higher affinity for the ionic liquid (Scheme 1).[69] For water-miscible ionic liquids this must be done using an anion exchange resin, loaded with the desired anion X^-.[70] For water-immiscible ionic liquids, the anion exchange is best carried out by contacting the ionic liquid with a aqueous phase containing the desired anion in the form of a salt NaX.[69] The anion can also be introduced using its corresponding acid HX, but this is limited to strong acids (full dissociation).

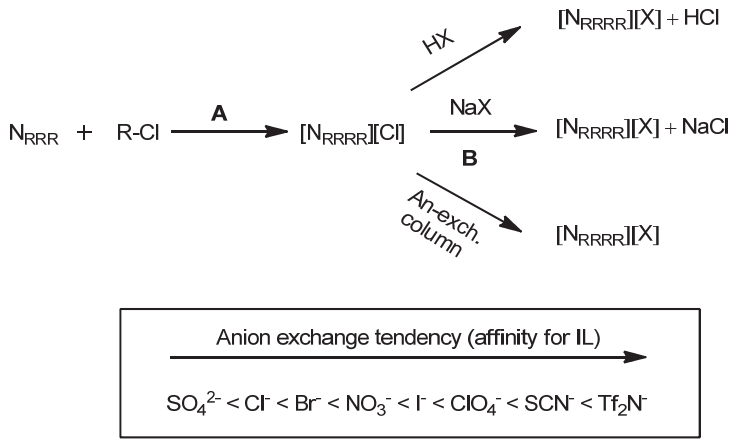

*Scheme 1. Main synthesis pathway for ionic liquids consisting of a quaterization reaction (**A**) and an anion exchange step (**B**) to introduce the desired anion X^-. The relative tendency of an anion to replace chloride in the ionic liquid is shown below.*

1.3.2 Functionalized (acidic) ionic liquids

Using these standard ionic liquid building blocks (Figure 17), a wide variety of functionalized ionic liquids can be designed.[71,72] Common functional groups (FGs) include: carboxyl groups, sulfonic acid groups, alcohols, (poly)ethers, esters and chiral groups, but also metal-containing ionic liquids belong to this group.[62,64,65,71-74] The functional groups are usually introduced during the quaternization reaction, using a substitution reaction (**C**), addition reaction (**D**) or ring-opening reaction (**E**), depending on the chosen functional group (Scheme 2).[75] The same applies for trialkylphosphines for the synthesis of phosphonium ionic liquids.

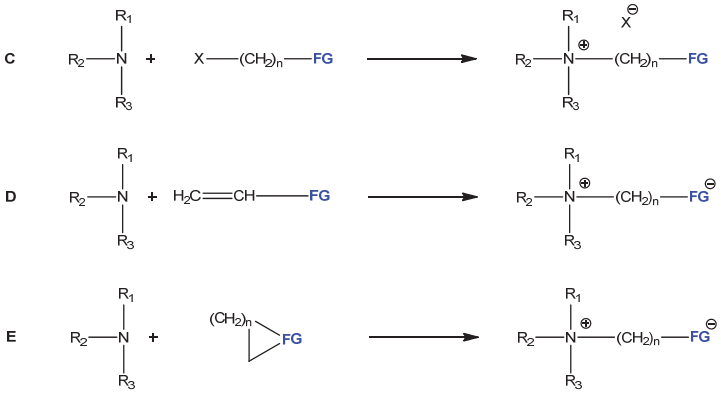

*Scheme 2. Three important synthetic pathways (**C**, **D**, **E**) for the introduction of functional groups in ionic liquids during the quaternization reaction (X = Cl, Br).*

The most versatile method is the alkylation by a substitution reaction (**C**), but this may require the use of protective groups on the functional group in some cases.[75] A Michael-type addition reaction (**D**) has been reported but is only possible for strongly electron-withdrawing functional groups such as –COOR, $–SO_3H$ or –CN.[76,77] Ring-opening alkylation (**E**) is very effective, but only applicable for certain functional groups such as sulfonate, carboxylate, alcohol and phosphate groups, amongst others (Figure 18). The length of the carbon linker is also fixed due to the limited amount of (sufficiently reactive) rings.

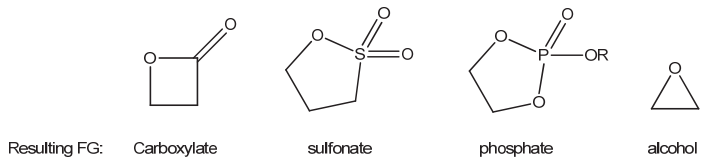

Figure 18. Common ring molecules used to introduce functional groups.

Once a functional group is introduced in the ionic liquid it can of course be further modified using chemical reactions and reduction/oxidation reactions. The advantage of functionalized ionic liquids is that they can act as a solvent and as an active compound (e.g. extractant, acid, catalyst, ligand), which is why they are also known as *task-specific* ionic liquids.[71] The exact definition of task-specific ionic liquids has been debated, but is used here to designate any ionic liquid which derives its efficacy for a certain application from its structure and not simply from the fact that it is an ionic liquid. This means that for solvent extraction applications, simple tetraalkylammonium ionic liquids could also be regarded as task-specific ionic liquids, since their specific chemical structure is key to their efficacy as extractant.[56,78] Task-specific ionic liquids have found many uses as reusable catalysts in organic synthesis, but also in polymer processing and metal processing or even as ingredients in pharmaceuticals and cosmetics.[62-65,71,72,74,79,80] Ionic liquid applications continue to evolve as more and more ionic liquid classes emerge and new properties are discovered.[63,80-83] In this PhD thesis we focussed on the synthesis and applications of ILs with acidic functional groups, ILs with thermomorphic behavior and ILs relevant to the dissolution and solvent extraction of metals.

Some have questioned the "green" label attributed to ionic liquids, by pointing at the low biodegradability of some IL cations and anions.[84] It is true that ionic liquids as a group are not inherently green, just like all organic solvents are not per definition toxic. However, the unique properties of certain ionic liquids can make a process much greener by replacing toxic chemicals and solvents. An interesting evolution is the move towards greener, biodegradable ILs based on biomolecules such as sugars, amino acids, terpenes, choline or betaine.[85-94] These ionic liquids are synthesized from widely available bio feedstock and result in biodegradable ionic liquids, therefore significantly reducing their environmental impact. Such ionic liquids are interesting replacements for toxic solvents in organic synthesis, and a wide array of other materials. More biocompatible ionic liquids would also permit their use in pharmaceutical production or even as active pharmaceutical ingredients.[80,90] Some examples of bio-based ionic liquid cations are shown in Figure 19. Biodegradable anions include compounds like acetate, maleate, fumarate, aspartate, prolinate, etc.

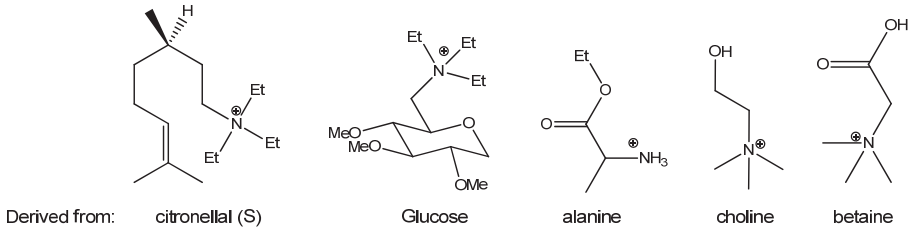

Figure 19. Some examples of biodegradable ionic liquid cations.

Brønsted acidic ionic liquids are an interesting class of functionalized ionic liquids. They find applications as reusable homogeneous catalysts in organic reactions,[71,95-97] and they are also known to dissolve metal oxides.[73,74,98] The two main classes of Brønsted acidic ionic liquids are the carboxyl-functionalized ionic liquids and the sulfonic acid functionalized ionic liquids.

Carboxyl functionalized ionic liquids

Carboxyl groups are best introduced using ester-functionalized alkyl chlorides (**F**) or bromides such as methyl chloroacetate or methyl chlorobutyrate, resulting in a C_1 and C_3 linker respectively.[99] The methyl group of the ester is then removed with a strong acid (e.g. HCl) to obtain the carboxyl-functionalized ionic liquid. Direct reaction of the amine base with carboxyl-functionalized alkyl chlorides (**G**) such as 3-bromopropionic acid has been reported, but may lead to considerable protonation of the nitrogen atom instead of alkylation.[99,100] Halogen-free synthesis routes are less common, but examples have been reported such as the ring-opening reaction with *β*-propiolactone (**H**),[101] or the Michael-type addition to *α,β*-unsaturated esters.[76,77] The different synthesis routes are shown in Scheme 3. The same scheme applies to pyridinium, pyrrolidinium, ammonium and phosphonium ionic liquids.

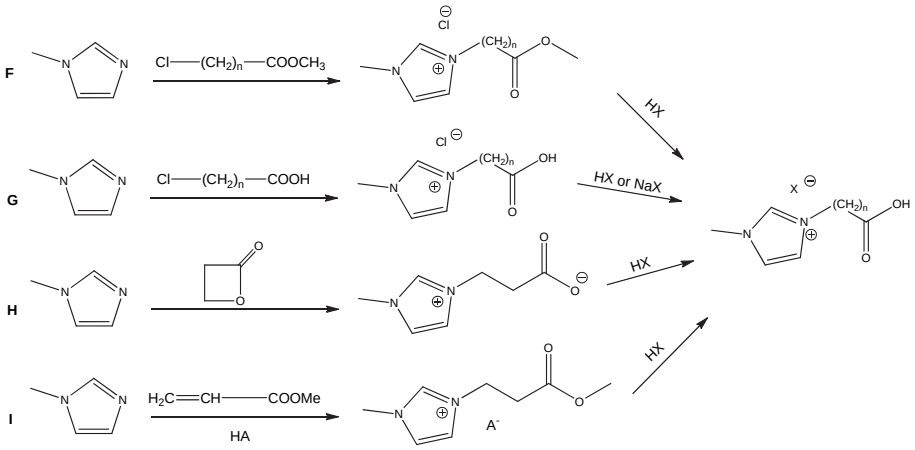

*Scheme 3. Synthesis routes for carboxyl-functionalized ionic liquids (**F**, **G**, **H**, **I**). In reaction **I**, HA must be strong acid (e.g. TsOH, $MeSO_3H$, HBF_4) in the case of imidazolium, or AcOH in the case of tertiary amines.[76,77] HX must be a stronger acid than the carboxylic acid group.*

Carboxyl-functionalized ionic liquids are weak acids with pK_a's in the range of 1.3 to 4.5, depending on their structure, the size of the carbon linker and the anion.[99] An interesting carboxyl-functionalized ionic liquid is betaine bistriflimide ([Hbet][Tf_2N]), due to its thermomorphic behavior and ability to dissolve metal oxides.[73,74]

Sulfonic acid ionic liquids

Sulfonic acids ($pK_a \approx -2$) are stronger acids than carboxylic acids.[95] This functional group is usually introduced by a ring-opening reaction (**J**) using sultones such as 1,3-propane sultone (5-membered ring) or 1,4-butane sultone (6-membered ring), resulting in a C_3 and C_4 linker, respectively (Scheme 4).[95]

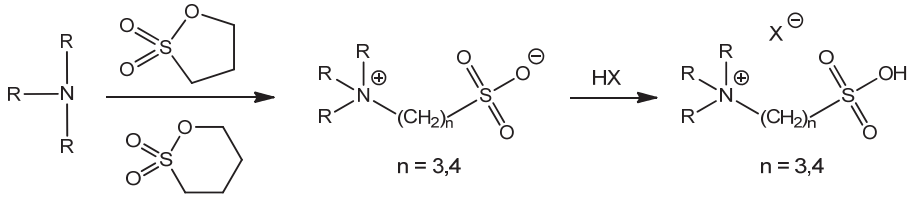

*Scheme 4. Synthesis route for sulfonic acid functionalized ionic liquids (**J**). The acid HX much be a stronger acid than the sulfonic acid group in order to ensure complete protonation.*

A large variety of sulfonic acid ionic liquids have been prepared with ammonium, imidazolium and phosphonium cations.[95,98,102] These sulfonic acid ionic liquids have been used as reusable dual-phase catalysts for Fischer esterifications, condensation reactions, dehydration reactions, etc.[95,97,102-104] These compounds have also been used in their zwitterion form as electrolytes and liquid crystalline phase.[105,106]

Other acidic ionic liquids

A way to further increase the acidity of the sulfonic acid group is by fluorinating the carbon chain close to the functional group. However, such fluorinated hydrocarbons are poorly degradable and therefore avoided in green chemistry. Another approach is to replace the C-sulfonation, by N-sulfonation or O-sulfonation, which results in the more strongly acidic sulfamic acid and alkylsulfuric acid functional groups, respectively (Figure 20). So far, very few examples exist of such ionic liquids, but these reactions have been used successfully to prepare similar molecules, salts, zwitterions, and functionalized polymer resins.[107-109] Sulfamic acid is used as strongly acidic catalysts and as cleaning solution for metal surfaces.[107,110-112] Alkylsulfuric acids are used as acidifiers, alkylating agents and detergents.[113,114]

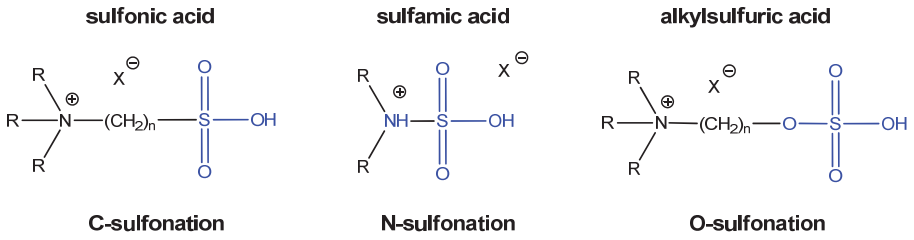

Figure 20. Three types of sulfonated ionic liquid classes: sulfonic acids (C-sulfonation), sulfamic acids (N-sulfonation) and alkylsulfuric acid (O-sulfonation).

N-sulfonation is the result of a reaction between chlorosulfonic acid and a primary or secondary amine (**K**).[107,108] The intermediary zwitterion has a pK_a between 1 and 2, depending on the substituents. Protonating the zwitterion requires very strong acids such as bistriflimic acid (HTf_2N). These protonated sulfamic acids could be considered super acids since it has been shown that they cannot be fully protonated by perchloric acid ($HClO_4$) ($pK_a \approx -10$).[107] Note that these compounds are slowly decomposed in water to form H_2SO_4 and the corresponding ammonium salt.[107]

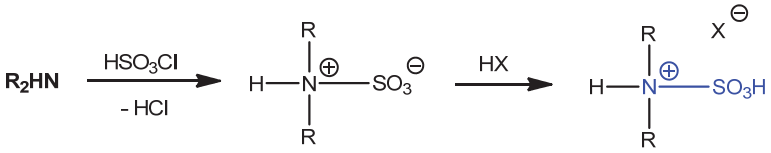

*Scheme 5. N-sulfonation reaction between a secondary amine and chlorosulfonic acid (**K**). HX must be a very strong acid (e.g. HTf_2N), capable of protonating the sulfamic acid group.*

This reaction does not work with tertiary amines (trialkylamine, pyridine,…) since these will form stable (non-acidic) adducts with SO_3 (e.g. $Me_3N{\cdot}SO_3$).[108] These adducts can be isolated and are excellent sulfonating agents for molecules that are not compatible with acidic conditions.[107] The lower reactivity compared to chlorosulfonic acid also allows selective N-sulfonation over O-sulfonation which can be very useful to sulfonate functionalized alkylamines or biopolymers such as chitosan which contains amine and hydroxyl groups on their functional units.[107,115]

Functionalization with a hydrogen sulfate group can be achieved with two different methods (Scheme 6). The first is the O-sulfonation of a hydroxyl group with chlorosulfonic acid, which yields the hydrogen sulfate group in good yield (**L**).[108] The second is the reaction between an alkene and sulfuric acid (**M**).[113]

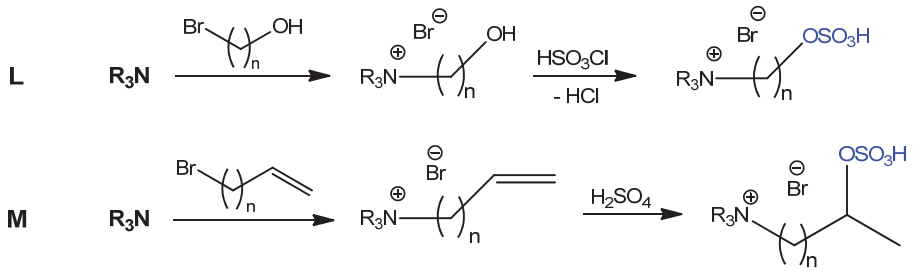

*Scheme 6. Two pathways to obtain hydrogen sulfate functionalized ionic liquids (**L**, **M**).*

The resulting alkylsulfuric acid compounds ($pK_a \approx -3.5$) are considered to be stable, non-toxic and biodegradable.[114,116] Alkylsulfates are used as detergents (e.g. lauryl sulfate) since they are fully deprotonated in water.

1.3.3 Metal processing and solvent extraction with ionic liquids

The processing of metals and metal oxides in ionic liquids is a promising research topic.[65,117-120] The advantages of ILs include their large temperature range, wide electrochemical window and excellent reusability which can eliminate aqueous waste streams in hydrometallurgical processes.[120] The use of ionic liquids and deep eutectic solvents as solvents for the processing, extraction and electrodeposition of metals was reviewed by Abbott and coworkers.[65,120] The solubility of metal salts in ionic liquids is often quite limited compared to aqueous solutions, due to the absence of an efficient solvating mechanism. The solubility of metal salts can be increased by incorporating functional groups in so-called task-specific ionic liquids.[73,74,120]

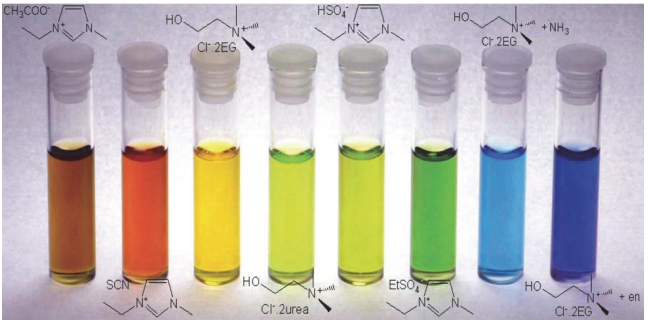

Figure 21. Solutions of $CuCl_2 \cdot 2H_2O$ in eight different ionic liquids (Abbott et al.).[120]

Another approach is to incorporate the metal ions in the cation (e.g. [Ag(py-O)$_3$][Tf_2N]) or anion (e.g. [emim][Al_2Cl_7] or [bmim][$FeCl_4$]) of the ionic liquid, resulting in ionic liquids with very high metal loadings.[65,120,121] For electrodeposition, ionic liquids with metal-containing cations are preferred since the metal-containing cations are attracted to the negatively charged cathode. Such liquid metal salts have been prepared for copper, zinc, manganese and silver amongst others.[121,122] Ionic liquids with metal-containing anions have been prepared for the halides of the metals Al, Fe, Co, Ni, Mn, Cu, Sn, In, Pt, Ir, Pd and Au, using the reaction between a chloride ionic liquid and the metal chloride salt (eq 1).[123] Furthermore, REE-containing room-temperature ILs have been prepared using thiocyanate complexes (e.g. [Bmim]$_5$]La(NCS)$_8$]),[124] and carbonyl complexes have been reported for Mn, Co, Fe and Rh (e.g. [bmim][$Mn(CO)_5$]).[71]

$$[emim][Cl] + x\ MCl_n \rightarrow [emim][M_xCl_{nx+1}] \qquad (1)$$

Some of these ionic liquids have very interesting properties. Aluminate ionic liquids for example are Lewis acids and have been used as catalyst in Friedel-Crafts alkylation reactions.[71] Ionic liquids with Dy(III)- and Fe(III)-containing anions show strong paramagnetic behavior and can be guided by a magnet.[125,126]

An important class of ionic liquids for metal processing, are the acidic ionic liquids. These ionic liquids contain acidic cations or anions and can dissolve metal oxides.[73,74,120] Ionic liquids with acidic anions such as [bmim][HSO_4] and [bmim][HCO_3] have been used for the dissolution of metal oxides in brass ash (Cu, Zn) and sulphidic ores containing Au and Ag.[127-129] However, ionic liquids with acidic cations are more convenient, since deprotonation of the acidic group results in the formation of zwitterions which can then coordinate the metal ions. Carboxylic acid ionic liquids ([R-COOH][X]) and sulfonic acid ionic liquids ([R-SO_3H][X]) can therefore efficiently dissolve metal oxides (M_zO_y) (eq 2−3).[73,74,98,120]

$$2y\ [\text{R-COOH}][\text{X}] + M_zO_y \rightarrow z\ [(\text{R-COO})_{(2y/z)}\text{M}][\text{X}]_{(2y/z)} + y\ H_2O \qquad (2)$$

$$2y\ [\text{R-SO}_3\text{H}][\text{X}] + M_zO_y \rightarrow z\ [(\text{R-SO}_3)_{(2y/z)}\text{M}][\text{X}]_{(2y/z)} + y\ H_2O \qquad (3)$$

It has been demonstrated that the carboxyl-functionalized ionic liquid betainium bistriflimide [Hbet][Tf_2N] (Figure 22) can dissolve stoichiometric amounts of Sc_2O_3, Y_2O_3, La_2O_3, Pr_6O_{11}, Nd_2O_3, Sm_2O_3, Eu_2O_3, Gd_2O_3, Tb_4O_7, Dy_2O_3, Ho_2O_3, Er_2O_3, Yb_2O_3, Lu_2O_3, UO_3, PbO, ZnO, CdO, HgO, CuO, Ag_2O, NiO, PdO, and MnO.[73,74]

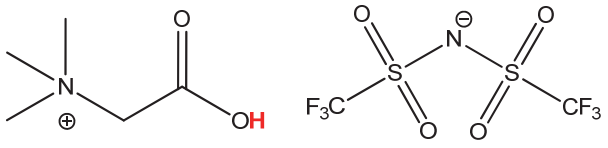

Figure 22. Structure of the betainium bistriflimide ionic liquid, [Hbet][Tf_2N].

The metal ions are coordinated effectively by the deprotonated carboxylate zwitterions.[130] The strength of the metal complexes varies for different metal ions and this can be used in solvent extraction to separate metal ions. The affinity of these acidic extractants for metal ions is mainly governed by electrostatic interactions, which means that the strength of the complex increases as the charge density of the metal ions increases, but deviations from this trend occur when the ligand-metal bond has a significant covalent character.

The solubility of metal salts in the pure acidic ionic liquids is very low due to inefficient solvation of anions.[24,73,74] These ionic liquids can therefore be used to selectively dissolve metal oxides (or hydroxides) which do not form anions when dissolved in the ionic liquid (eq 2-3).[24,73,74] This selectivity is very useful because it is opposite to the behavior observed in aqueous solutions, where the metal oxide is usually more difficult to dissolve than the corresponding metal chloride.[24] This selectivity was used in this PhD thesis to recover valuable metals from waste products.[24,57]

Solvent extraction or liquid-liquid extraction is based on the distribution of a solute between two immiscible liquid phases.[131,132] The preferential distribution of a compound amongst two phases can be modified by the addition of other compounds such as ligands and extractants.[133]

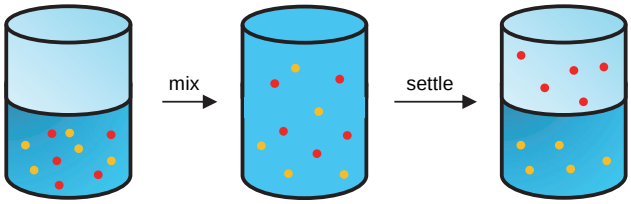

Figure 23. Solvent extraction is the preferential distribution of compounds amongst two phases, sometimes helped by the addition of ligands or extractants.

Solvent extraction is used for the purification of organic molecules and proteins, but also for the separation of metal ions, which is the focus of this work.[69,70] Solvent extraction of metal ions is one of the cornerstones of hydrometallurgy and has been extensively researched and implemented in industrial processes.[134] Important industrial examples include the separation of cobalt and nickel, the separation of rare earths and the PUREX process for nuclear reprocessing.[134] Specific extractants can be designed to optimize the selectivity for a certain metal ion, making this a very flexible separation technique.[135] Extractants are generally classified into three main groups, representing different extraction mechanisms.[133,135]

1. **Acidic extractants (cation exchange mechanism)**
   - Carboxylic acids (e.g. Versatic® 10 acid)
   - Sulfonic acids (e.g. DNNSA)
   - Acidic organophosphorus extractants (e.g. DEHPA, Cyanex® 272)
   - Thioacids (e.g. Cyanex® 302)
   - Chelating acids (e.g. β-diketonates)

2. **Neutral extractants (solvating mechanism)**
   - Neutral compounds (e.g. TBP, TOPO, MBT, Cyanex® 923)
   - Acidic extractants used as neutral extractants

3. **Basic extractants (anion exchange mechanism)**
   - Protonated mono-, di- or trialkyl amines and phosphines
   - Quaternary ammonium salts (e.g. Aliquat® 336)
   - Quaternary phosphonium salts (e.g. Cyphos® IL 101)
   - Tertiary sulfonium salts

The extraction mechanism for a metal salt (MX_n) depends on the type of extractant:

Acidic extractant HA: $n\ HA + \mathbf{M}X_{n(aq)} \leftrightarrows n\ HX + \mathbf{M}A_{n(org)}$

Neutral extractant L: $z\ L + \mathbf{M}X_{n(aq)} \leftrightarrows \mathbf{M}L_zX_{n(org)}$

Basic extractant [Cat][X]: $z\ [Cat][X] + \mathbf{M}X_{n(aq)} \leftrightarrows [Cat]_z[\mathbf{M}X_{n+z}]_{(org)}$

Solvent extraction is usually carried out by dissolving extractants in an organic solvent such as kerosene or toluene and contacting it with the metal-containing aqueous phase.[131] These extraction systems are very efficient but the volatility and flammability of the organic solvents pose serious safety and environmental threats. Therefore, ionic liquids have been proposed as alternative solvents for solvent extraction.[136-138] Ionic liquids have a negligible vapor pressure and are non-flammable, making them safer and greener than most organic solvents.[136-138] An important additional benefit of ionic liquids is the possibility to functionalize them and design them specifically for a certain application.[136] This structural flexibility is not present for normal organic solvents, making the use of extractants mandatory. In ionic liquids, the extractant can be built into the ionic liquid, which can then act both as the solvent and as the extractant.[139] Many examples have been reported of water-immiscible ionic liquids that can be used as acidic, neutral or basic extractants in solvent extraction experiments (Figure 24).[25,56,78,79,98,140-144]

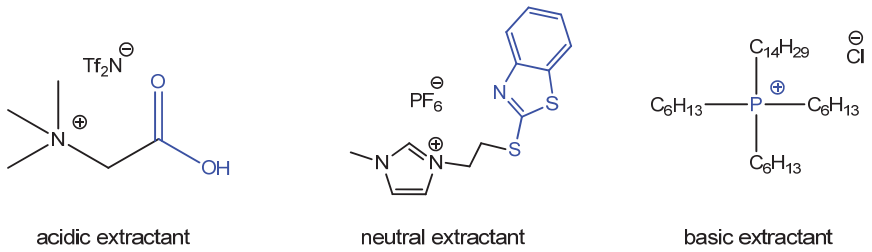

Figure 24. Examples of ionic liquids used for the solvent extraction of metal ions.

In some cases, the high viscosity of certain ionic liquids may require them to be diluted in an organic solvent, but most ionic liquids can be used as organic phase in their pure (undiluted) form.[25,56,78,79,98,140-144] This significantly simplifies the design of the solvent extraction set-up and also opens up the possibility of new extraction systems. For example, in the past some extractants such as alkylsulfates and alkylsulfonates, were rarely used due to their strong detergent properties and their tendency to form micelles in organic solvents.[139,145] However, by incorporating these groups in an ionic liquid, detergent behavior can be avoided and these promising extractants can be used to extract metal ions from water.[98,139]

In contrast to other separation techniques such as ion-chromatography, solvent extraction can be easily scaled up using mixer-settlers in which the phases are first mixed together, followed by a settling stage that allows the phases to separate by gravity (Figure 25).[131,133,134] This type of continuous extraction processes were also demonstrated for ionic liquids.[146]

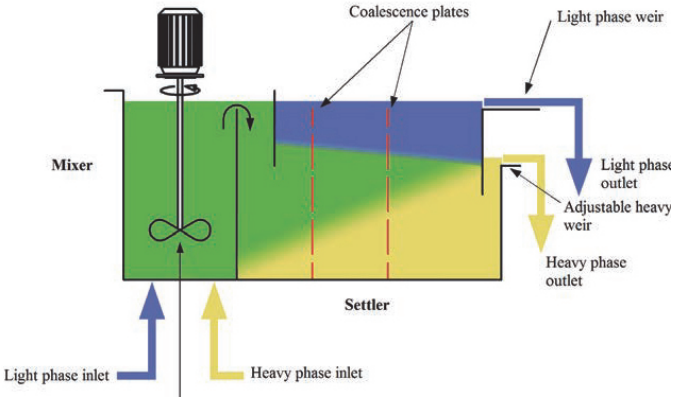

Figure 25.Mixer-settler set-up for large scale solvent extraction (image credit: Wikipedia).

Consecutive mixer settlers can be used to improve the separation, preferably in a counter-current process.[147] In counter-current extraction, multiple mixer settlers are connected so that the aqueous outlet feeds the next mixer-settler, while the organic outlet moves in the opposite direction (Figure 26).[147] This way, the efficiency of the overall process is significantly increased. A well-known example is the separation of lanthanides, which requires more than a 1000 mixer-settlers to separate all the elements due to the small separation factors between the lanthanides.[18,148,149]

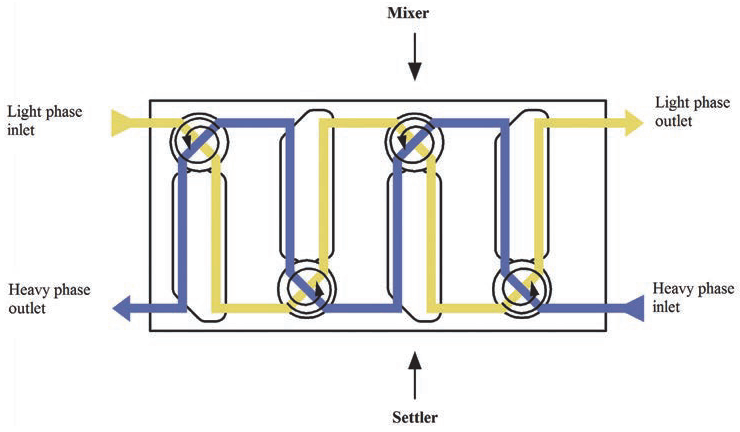

Figure 26. Schematic representation of a counter-current solvent extraction process (image credit: Wikipedia).

1.3.4 Thermomorphic ionic liquids

Some two-component systems (e.g. liquid-liquid extraction systems) show thermomorphic behavior, meaning that at a certain temperature a transition is observed between a homogeneous system and a two-phase system.[150-153] The temperature at which this occurs is called the cloud point temperature (T_{cp}).[150-153] Two different types of thermomorphic systems have been observed: systems with an upper critical solution temperature (UCST) and systems with a lower critical solution temperature (LCST).[150-153] UCST systems go from a two-phase system to a homogeneous system when the temperature is increased above the cloud point temperature, while LCST systems go from a homogeneous state to a two-phase system when the temperature is increased above the cloud point temperature (Figure 27).

Figure 27. Schematic overview of thermomorphic systems with an upper critical solution temperature (UCST) and lower critical solution temperature (LCST).

The cloud point temperature of such two-component systems is also dependent on the phase ratio and can be visualized in a phase diagram (Figure 28).

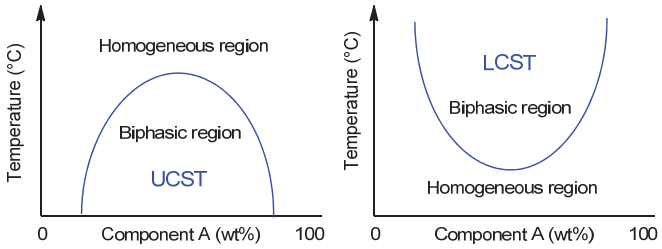

Figure 28. Phase diagrams for UCST and LCST thermomorphic systems.

Thermodynamically, mixing of two components A and B occurs when the Gibbs free energy of mixing (ΔG_{mix}) is negative (eq 4). For thermomorphic systems this means that UCST behavior is observed when the entropy of mixing (ΔS_{mix}) is positive, and LCST behavior when ΔS_{mix} is negative.[151,152] When $\Delta G_{mix} = 0$, phase transition is observed because it is energetically equally favorable for component A to be dissolved in component B than for separate A-A and B-B phases to occur.

$$\Delta G_{mix} = \Delta H_{mix} - T\Delta S_{mix} \quad (4)$$

To find useful thermomorphic IL/solvent systems, one must therefore look for two-component systems with $\Delta G_{mix} = 0$ preferably around 20-75 °C, since this is where the phase transition will occur. In other words, the ionic liquids must have a medium affinity for the solvent. If an ionic liquid is too soluble a homogeneous mixture is obtained, and if it is completely immiscible a two-phase mixture can be expected. In the fine range between fully miscible and fully immiscible lie the thermomorphic IL/solvent systems.[150-152] Luckily, the structure of ionic liquids can be tuned very easily to meet these demands, either by varying the anion or cation of the ionic liquid. Most new thermomorphic IL/solvent systems are still discovered using this trial-and-error approach.[150-152] In recent work we have proposed a prediction model for UCST and LCST behavior based on the choice of IL anion and solvent.[69] This method does not predict the occurrence of thermomorphic behavior, but it does accurately predict whether a thermomorphic ionic liquid will have UCST ($\Delta S_{mix} > 0$) or LCST behavior ($\Delta S_{mix} < 0$), based on the affinity of the anion for the solvent.[69]

Thermomorphic ionic liquid systems have been investigated extensively and many ionic liquids with UCST and LCST behavior have been identified. A selection of literature examples is shown here in Table 6.[69,150-152,154-156]

Table 6. Thermomorphic behavior of some known ionic liquid / solvent systems.

Ionic liquid	Solvent	Phase behaviour	T_{cp} (°C)	Molar ratio (solvent: IL)	Ref.
$[C_4mim][BF_4]$	Water	UCST	5	13:1	[157]
$[Hbet][Tf_2N]$	Water	UCST	56	20:1	[74]
$[Hbetmim][Tf_2N]$	Water	UCST	64	23:1	[73]
$[HbetmMor][Tf_2N]$	Water	UCST	52	24:1	[73]
$[Chol][Tf_2N]$	Water	UCST	72	21:1	[158]
$[L\text{-}Car][Tf_2N]$	Water	UCST	8	25:1	[73]
$[P_{4444}][Fum]$	Water	UCST	62	50:1	[154]
$[P_{66614}][Cl]$	Heptane	UCST	22	43:1	[159]
$[P_{66614}][Br]$	Heptane	UCST	69	40:1	[159]
$[C_{12}mim][Cl]$	Benzene	UCST	24	31:1	[159]
$[C_{12}mim][Cl]$	Toluene	UCST	65	31:1	[159]
$[P_{4444}][Mal]$	Water	LCST	22	20:1	[154]
$[P_{4444}][CF_3COO]$	Water	LCST	29	37:1	[150]
$[P_{4444}][TsO]$	Water	LCST	53	44:1	[150]
$[P_{4448}][Br]$	Water	LCST	24	14:1	[150]
$[P_{6666}][(EtO)HPO_2]$	Water	LCST	33	50:1	[156]
$[P_{444}E_1][DEHP]$	Water	LCST	34	15:1	[160]
$[N_{4444}][Br]$	Toluene	LCST	25	36:1	[161]

An interesting application of thermomorphic ionic liquid / water systems is *homogeneous liquid-liquid extraction* (HLLE).[79,158,160,162] The advantage of HLLE is that there is no diffusion limitation since the interphase disappears in the homogeneous state (Figure 29). Therefore, no stirring is required and a fast and efficient extraction can be obtained. UCST systems must be heated above the cloud temperature to become homogeneous, while for LCST systems the temperature must be lowered to become homogeneous.

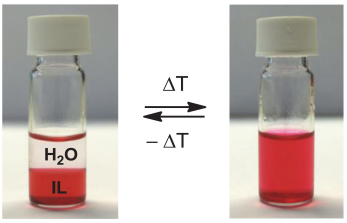

Figure 29. Reversible transition between a homogeneous system and a two-phase system for a mixture of [Hbet][Tf$_2$N]:H$_2$O (1:1 wt/wt), colored with methyl red sodium salt. The cloud point temperature of this UCST system is 56 °C.[24]

The extraction of metal ions in such a HLLE systems was first described by Vander Hoogerstraete *et al*. for the carboxyl-functionalized ionic liquid [Hbet][Tf$_2$N] (Figure 30).[79]

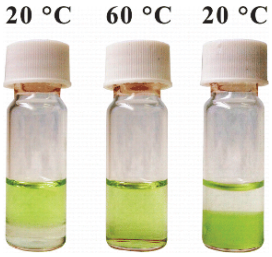

Figure 30. Homogeneous liquid−liquid extraction of Pr(III) ions (green color) from an aqueous solution (upper layer), using the [Hbet][Tf$_2$N]−water (1:1 wt/wt) system.[79]

This UCST system has found applications in metal recycling processes due to its ability to dissolve and extract a variety of different metals ions: U(VI), Rh(III), Ru(III), REE(III), Ga(III), In(III), Fe(III), Pd(II), Mn(II), Cu(II), Ni(II), and Zn(II), amongst others.[24,57,79,140-142,162] Another example of a UCST system for HLLE is the alcohol-functionalized [Chol][Tf$_2$N]:H$_2$O system with choline hexafluoroacetylacetonate as extractant for the extraction of Nd(III) ions.[158] Recently, LCST systems for HLLE have also been demonstrated for the extraction of transition metal ions using different non-fluorinated bis(2-ethylhexyl)phosphate phosphonium ionic liquids.[160]

1.3.5 The Hofmeister series

The Hofmeister series has important implications for ionic liquid systems and its effects were used throughout this PhD study. A short introduction into this concept is therefore provided in this chapter. In 1888, Franz Hofmeister first described the effect of salt cations and anions on the stability and solubility of ovalbumin in solution by ranking these ions in the so-called Hofmeister series (Figure 31).[163] He observed that some ions caused faster aggregation of this protein (*salting-out effect*) while other ions stabilized the protein in solution (*salting-in effect*).[164]

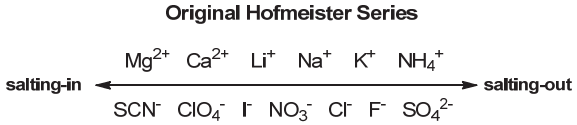

Figure 31. Original Hofmeister series showing the effect of various anions and cations on the salting-in/out of the protein ovalbumin. [163]

It was later demonstrated that this specific series was only applicable to negatively charged, hydrophobic proteins such as ovalbumin.[165,166] Changing the surface charge or the hydrophobicity of the protein caused a reversal in the salting-out series.[167,168] However, while the direction of the sequence can change, the sequence itself remains the same since this is simply a ranking by charge density. This was rationalized by Schwiertz *et al.* in a model which describes the direction of the Hofmeister series depending on the surface charge and the hydrophobicity of a protein or colloidal surface.[167,168] These insights have also been transposed to explain the effect of salts on the solubility and behavior of other proteins, colloidal surfaces, polymers, and organic compounds.[164,167-174] Despite the apparent simplicity of this theory, the exact origin still continues to puzzle scientists to this day.[175,176]

IL/water mixtures are also greatly affected by the addition of salts. Many papers have been written, describing the effect of salts on the mutual solubility and the consequent effect on the cloud point temperature of thermomorphic systems.[177-181] Strong salting-in (increased miscibility) and salting-out (decreased miscibility) effects are observed depending on the type of salt that is added to the system. The salting-out sequence for ILs is given in Figure 32. Note that the cation salting-out series is in the opposite direction with respect to the original Hofmeister series. The cause of this phenomenon was thoroughly investigated and described in our paper.[69]

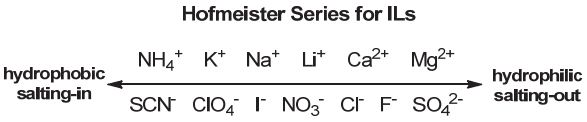

Figure 32. Salting-in/out effect for ionic liquid – water systems.

An important phenomenon observed in IL/water/salt systems is the possibility of anion exchange.[70,182] This does not occur in protein/water/salt or solvent/water/salt systems and is therefore often overlooked. Since ionic liquids consist entirely of ions, there is the possibility that the ionic liquid anions are exchanged with the salt anions in the aqueous phase.[70,182] For cations this is not observed since large organic cations are usually used, which do not exchange for small inorganic cations. On the other hand, ionic liquid anions are often small inorganic anions (e.g. Cl^-, $MeSO_3^-$), which are easily exchangeable. We showed that the tendency of an anion to be exchanged can be rationalized by the Hofmeister series, which is shown schematically in Figure 33. Anions with a high charge density are strongly hydrated (hydrophilic) and tend to remain in the aqueous phase, while anions with a low charge density are more hydrophobic and have an increased affinity for the ionic liquid phase.

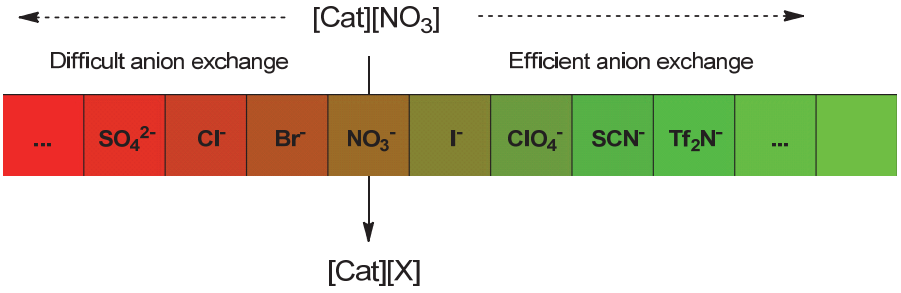

Figure 33. Schematic representation of the anion exchange tendency when a water-immiscible ionic liquid [Cat][An] is contacted with an aqueous solutions of a salt NaX.

This scheme can be used to synthesize hydrophobic ionic liquids through a simple anion exchange step. For example, $[P_{66614}][Tf_2N]$ can be synthesized in one step starting from $[P_{66614}][Cl]$ and contacting it with an aqueous $LiTf_2N$ solution, while the synthesis of $[P_{66614}][NO_3]$ from the same precursor requires a large excess of nitrate salt and several contacts to obtain sufficient anion exchange.[55,183] The anion exchange tendency is also important to design stable IL/water solvent extraction systems. For example, Onghena et al. have demonstrated the extraction of metal ions from chloride and nitrate aqueous solutions with ionic liquid $[Hbet][Tf_2N]$ and confirmed the absence of anion exchange.[140] However, other extraction systems such as the extraction of metal ions from an aqueous phase with the ionic liquid $[P_{66614}][Cl]$ must be done from chloride solutions in order to avoid anion exchange and contamination of the ionic liquid.[56] Recently, Larsson and Binnemans optimized the use of split-anion extraction systems for the separation of rare-earth elements.[183] The success of this extraction system is also based on the very high anion concentration in the ionic liquid (organic phase). This is a very important parameter for basic extractants and cannot be achieved without the use of ionic liquids.

2 Objectives

The previous section has demonstrated the importance of critical metal recycling from end-of-life products and the importance of developing new technologies to achieve this in the most efficient and sustainable way. Ionic liquids were proposed as alternative solvents for solvent extraction and metal leaching. Especially functionalized ionic liquids show a lot of promise since they can be modified to meet the requirements of a certain application (e.g. acidity, hydrophobicity, viscosity, metal ion affinity, etc).

In this PhD thesis, new and innovative processes were designed using the unique properties of ionic liquids. Both existing and newly-designed ionic liquids were used to achieve a better selectivity, efficacy or reusability in the effort to recover the rare earths from end-of-life waste. We focused on two items: the lamp phosphor waste powders and the NdFeB magnets because these two products were highlighted previously as the most promising secondary sources for rare earths.

The goal was therefore to develop a toolbox for critical metal recovery based on ionic liquid technology. This includes the design of recycling processes, but also the synthesis of new designer ionic liquids and a fundamental study of the effect of metal salts and mineral acids on IL/water extraction systems. The primary target here was to find systems that outperformed classic hydrometallurgical methods due to the inherent properties of ionic liquids and to understand the underlying reasons. These insights are essential for the rational design of future IL-based processes.

Particular attention was given to the green and sustainable character of the developed technologies. During this PhD thesis I cooperated with a colleague working full-time on life cycle assessment (LCA). This allowed us to compare the environmental impact of our processes with the current state-of-the art hydro- or pyrometallurgical processes. LCA also helped to identify key impact categories (e.g. climate change, fossil fuel depletion, toxicity) that are affected by a process, giving us the opportunity to improve specific aspects of the process. In recycling processes, it is important not to create more waste or consume more energy than it would require producing raw materials through primary mining. Therefore, the development of all these processes was driven by the desire to avoid toxic compounds, minimize the use of chemicals and energy and limit the amount of waste. This principle of sustainable metallurgy runs throughout this PhD thesis as it aims to find new innovative solutions to the most challenging rare-earth recovery processes.

3 Publications

This section contains an overview (not chronological) of the nine first-author publications produced throughout this PhD study. All papers are reprinted with permission from the authors and the publisher. The supplementary information of these papers is not included due to size constraints, but is available on pubs.rsc.org (RSC journals) or pubs.acs.org (ACS journals).

These are the themes which are discussed in the nine papers of this chapter:

Critical metal recycling

- Paper 1: Recycling of rare earths from lamp phosphor waste
- Paper 2: Recycling of rare earths from NdFeB magnets
- Paper 3: Recycling of antimony from lamp phosphor waste
- Paper 4: A critical review of secondary antimony sources

Ionic liquid design

- Paper 5: Design of sulfonic acidic ionic liquids for metal processing
- Paper 6: Design of new alkylsulfuric acid ionic liquids
- Paper 7: Effect of salts on biphasic IL/water systems

Functionalized magnetic nanoparticles

- Paper 8: Functionalized magnetic nanoparticles for REE separation
- Paper 9: Functionalized core-shell nanoparticles for REE separation

Paper 1: Recycling of rare earths from lamp phosphor waste

Title:

Rare-earth Recycling Using a Functionalized Ionic Liquid for the Selective Dissolution and Revalorization of $Y_2O_3:Eu^{3+}$ from Lamp Phosphor Waste

Type: Full paper + Front cover
Journal: Green Chemistry (IF 8.02)
Publisher: Royal Society of Chemistry (RSC)
Publication date: 28/11/2014

Reprint with permission from:
D. Dupont and K. Binnemans, *Green Chem*., **2015**, 17, 856-868.

Electronic Supplementary Information (ESI) available: http://pubs.rsc.org.

Graphical abstract

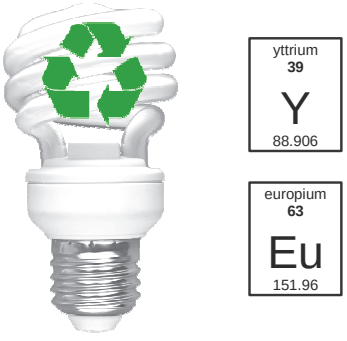

An innovative and green recycling process for lamp phosphor waste was developed based on the selective dissolution and revalorization of the valuable red lamp phosphor $Y_2O_3:Eu^{3+}$ in the functionalized ionic liquid [Hbet][Tf_2N].

Volume 17 | Number 2 | February 2015 | Pages 621–1320

Green Chemistry

Cutting-edge research for a greener sustainable future

www.rsc.org/greenchem

ISSN 1463-9262

ROYAL SOCIETY OF CHEMISTRY

PAPER

David Dupont and Koen Binnemans

Rare-earth recycling using a functionalized ionic liquid for the selective dissolution and revalorization of Y_2O_3:Eu^{3+} from lamp phosphor waste

Green Chemistry

PAPER

View Article Online
View Journal | View Issue

Cite this: *Green Chem.*, 2015, **17**, 856

Rare-earth recycling using a functionalized ionic liquid for the selective dissolution and revalorization of Y_2O_3:Eu^{3+} from lamp phosphor waste†

David Dupont and Koen Binnemans*

The supply risk for certain rare-earth elements (REEs) has sparked the development of recycling schemes for end-of-life products like fluorescent lamps. In this paper a new recycling process for lamp phosphor waste is proposed based on the use of the functionalized ionic liquid betainium bis(trifluoromethylsulfonyl)imide, [Hbet][Tf_2N]. This innovative method allows the selective dissolution of the valuable red phosphor Y_2O_3:Eu^{3+} (YOX) without leaching the other constituents of the waste powder (other phosphors, glass particles and alumina). A selective dissolution of YOX is useful because this phosphor contains 80 wt% of the REEs although it only represents 20 wt% of the lamp phosphor waste. The proposed recycling process is a major improvement compared to currently used hydrometallurgical processes where the non-valuable halophosphate (HALO) phosphor $(Sr,Ca)_{10}(PO_4)_6(Cl,F)_2$:$Sb^{3+}$,$Mn^{2+}$ is inevitably leached when attempting to dissolve YOX. Since the HALO phosphor can make up as much as 50 wt% of the lamp phosphor waste powder, this consumes significant amounts of acid and complicates the further processing steps (*e.g.* solvent extraction). The dissolved yttrium and europium can be recovered by a single stripping step using a stoichiometric amount of solid oxalic acid or by contacting the ionic liquid with a hydrochloric acid solution. Both approaches regenerate the ionic liquid, but precipitation stripping with oxalic acid has the additional advantage that there is no loss of ionic liquid to the water phase and that the yttrium/europium oxalate can be calcined as such to reform the red Y_2O_3:Eu^{3+} phosphor (purity >99.9 wt%), effectively closing the loop after only three process steps. The red phosphor prepared from the recycled yttrium and europium showed excellent luminescent properties. The resulting recycling process for lamp phosphor waste consumes only oxalic acid and features a selective leaching, a fast stripping and an immediate revalorization step. Combined with the mild conditions, the reusability of the ionic liquid and the fact that no additional waste water is generated, this process is a very green and efficient alternative to traditional mineral acid leaching.

Received 29th October 2014,
Accepted 25th November 2014

DOI: 10.1039/c4gc02107j

www.rsc.org/greenchem

Introduction

Rare-earth elements (REEs) include the 15 lanthanides plus yttrium and scandium. They are used in many high-tech applications, including wind turbines, electric vehicles, NiMH batteries, hard disk drives and fluorescent lamps.[1] The demand for these elements is expected to grow by more than 8% per year until 2020.[2] China dominates the REE supply from primary mining (>90% of the global production in 2013), and the worldwide recycling rate is still very low (<1%).[2] Since the tightening of the Chinese export quota for rare earths in 2010, rare-earth elements have been labeled as critical raw materials by the European Commission and the U.S. Department of Energy.[1–4] Opening or reopening mines outside China requires time and large financial investments. Therefore recycling of REEs from end-user products like magnets and fluorescent lamps, which together represent over 70% of the rare-earth market in terms of value (38% for magnets; 32% for lamp phosphors), could help to secure the supply of these critical elements.[3] Efficient recycling of these elements could help to create a closed-loop system and to solve the balance problem that is caused by the unwanted co-production of other rare-earth elements during primary mining.[3,5] This unwanted co-production has led to the accumulation of large stocks of certain elements (La, Ce) while facing shortages of others (Y, Eu, Tb, Nd, Dy).[3–7] New recycling technologies are becoming

KU Leuven, Department of Chemistry, Celestijnenlaan 200F – P.O. Box 2404, B-3001 Heverlee, Belgium. E-mail: Koen.Binnemans@chem.kuleuven.be

†Electronic supplementary information (ESI) available: Characterization of the synthesized Y_2O_3:Eu^{3+} phosphor, including SEM images, XRD diffractograms and luminescence decay curves. See DOI: 10.1039/c4gc02107j

Table 1 Overview of the lamp phosphors considered in this work and the approximate content found in lamp phosphor waste[3]

Name	Formula	Waste fraction[a] (wt%)	Value
HALO	$(Sr,Ca)_{10}(PO_4)_6(Cl,F)_2:Sb^{3+},Mn^{2+}$	40–50	Low
YOX	$Y_2O_3:Eu^{3+}$	20	High
BAM	$BaMgAl_{10}O_{17}:Eu^{2+}$	5	Low
LAP	$LaPO_4:Ce^{3+},Tb^{3+}$	6–7	High

[a] Approximate fraction found in lamp phosphor waste; the remaining consists of SiO_2 (as fine glass particles), Al_2O_3, and small quantities of other phosphors like CAT which behaves similarly to BAM, and CBT.

increasingly selective, efficient and sustainable and they are opening up new possibilities for urban mining and rare-earth waste revalorization.[1,3,6–13]

Originally, the collection of used fluorescent light lamps was put in operation to ensure the safe disposal of the mercury contained in the lamps; however, the lamp phosphors were discarded or stockpiled. It is estimated that by 2020 the stockpiled lamp phosphor waste will contain around 25 000 tons of rare earths.[3] In recent years, the recovery of the REEs contained in these powders has received a lot of attention due to the increasing supply risk for some of these elements.[3,9] Lamp phosphor waste powder contains around 20 wt% of REEs including critical (Y, Eu, Tb) and less critical (La, Ce, Gd) REEs.[3,5,14] These powders are used in fluorescent light lamps to convert ultraviolet radiation into visible light. They consist of fine particles (1–10 μm) coated on the interior surface of the glass. A blend of red $Y_2O_3:Eu^{3+}$ (YOX), blue $BaMgAl_{10}O_{17}:Eu^{2+}$ (BAM) and green $LaPO_4:Ce^{3+}$, Tb^{3+} (LAP), $(Ce,Tb)MgAl_{11}O_{19}$ (CAT) or $(Gd,Mg)B_5O_{10}$: Ce^{3+}, Tb^{3+} (CBT) phosphors is used to obtain the desired color rendering index (Table 1). In addition to rare-earth phosphors, lamp phosphor waste also often contains large amounts (40–50 wt%) of non-valuable halophosphate (HALO), which emits cold white light and does not contain any REEs.[3] The recycling value of the different phosphor components varies greatly. The phosphor with the highest economic value is the red $Y_2O_3:Eu^{3+}$ (YOX) phosphor. This phosphor consists almost entirely of the two critical rare earths yttrium and europium as opposed to the other phosphors, which are only doped with small amounts of critical REEs. This explains why YOX holds 80 wt% of the rare earths present in the lamp phosphor waste powder even though YOX only accounts for 20 wt% of the lamp phosphor waste (Table 1).[3,14]

Many approaches have been proposed for the recycling of lamp phosphors. Physical separation methods like magnetic separation, flotation and centrifugation could allow the direct reuse of the phosphors, but so far they are not used industrially due to the high purity requirements and the deterioration of the phosphor powders during their lifetimes.[3,15–17] Chemical methods can be used to dissolve the phosphors completely or selectively based on the increasing difficulty to dissolve some of the phosphors: HALO < YOX ≪ LAP/BAM/CAT.[3,9,14,18–21] The halophosphate (HALO) phosphor is easily dissolved in dilute hydrochloric acid solutions at room temperature. The dissolution of $Y_2O_3:Eu^{3+}$ (YOX) requires more acidic conditions (*e.g.* 1 M HCl, 60–90 °C).[3,22] LAP requires the use of very strong acidic conditions (*e.g.* 18 M H_2SO_4, 120–230 °C),[3,22] while the aluminate phosphors BAM and CAT are best dissolved under strongly alkaline conditions (35 wt% NaOH, 150 °C) in an autoclave or by molten alkali (*e.g.* Na_2CO_3, 1000 °C).[3,14] Ionic liquids have been proposed for the selective extraction of previously dissolved rare earths, but so far they have not been used as a tool for the dissolution of phosphors.[22,23] New recycling schemes often focus on the recovery of yttrium and europium from the red phosphor $Y_2O_3:Eu^{3+}$ (YOX), because of its high value and the relative ease of dissolving this phosphor compared to BAM, CAT and LAP.[18,19,22–24] The main problem with these processes is that the halophosphate phosphor (HALO) is often ignored as they focus mostly on the so-called tri-band phosphors which all contain rare earths (YOX, BAM, LAP, CAT). However, real lamp phosphor waste contains up to 50 wt% of HALO and therefore has to be considered when trying to develop an industrially applicable recycling method.[3,9,14,25] Unfortunately, halophosphate $(Sr,Ca)_{10}(PO_4)_6(Cl,F)_2:Sb^{3+},Mn^{2+}$ (HALO) is very easily dissolved in dilute acids even at room temperature.[3] HALO contains no rare earths and has a very low intrinsic value; therefore dissolving this phosphor leads to considerable pollution of the leachate and introduces a large amount of unwanted exogens (Sr, Ca, F, Sb, Mn, Cl) in the waste water, greatly complicating the further processing (eqn (1)).[3]

$$(Sr,Ca)_{10}(PO_4)_6(Cl,F)_2:Sb^{3+},Mn^{2+} + 18H^+ \rightarrow 10(Sr,Ca)^{2+} + 6H_3PO_4 + 2(Cl,F)^- + Sb^{3+} + Mn^{2+} \quad (1)$$

The dissolution of HALO also consumes considerable amounts of acid (18 protons per formula unit of HALO) and leads to the formation of large amounts of H_3PO_4 (6 molecules per formula unit of HALO) which forms very insoluble YPO_4 and $EuPO_4$ precipitates with the dissolved Y^{3+} and Eu^{3+} ions from the YOX. The design of a selective dissolution method for YOX without dissolving HALO would therefore greatly increase the efficiency and profitability of a recycling process for lamp phosphor waste, but, to the best of our knowledge, such a process has not been described so far.

At present, only one example is known of an industrially applied recycling process for lamp phosphor waste. This process was successfully implemented by Solvay in 2012 and treats more than 2000 tons of phosphor waste powder per year.[8] According to the patent literature, multiple consecutive acidic (HCl, HNO_3) and alkaline (NaOH) attacks are required, including an alkaline fusion with Na_2CO_3 at 1000 °C, to fully disintegrate all the phosphors. The individual rare earths are then separated and recovered using solvent extraction, in order to manufacture new phosphors.[14] The main drawbacks of this process are the large consumption of chemicals, the large production of waste water and the large number of process steps required to fully recycle the lamp phosphor waste.[3]

The process described in this paper aims to solve all these issues by proposing a functionalized ionic liquid as an alternative to selectively dissolve and regenerate the valuable red phosphor Y_2O_3:Eu^{3+} (YOX). This three-step process (no need for solvent extraction) is very efficient, consumes only oxalic acid and generates zero additional waste (except CO_2). The ionic liquid is also automatically regenerated during the stripping step and can be reused. This type of leaching system can be described as ionometallurgy, which is the analogue of hydrometallurgy in ionic liquids and has shown an interesting new behavior in various cases.[26–30] Depending on the application, ionic liquids are considered to be green solvents because of their negligible vapor pressure, low flammability and reduced toxicity compared to organic solvents and have led to several important improvements in various fields such as metallurgy, extraction, electrochemistry, organic synthesis and catalysis.[10,12,30–35] Here, the functionalized ionic liquid betainium bis(trifluoromethylsulfonyl)imide, [Hbet][Tf_2N], is proposed for the selective dissolution of Y_2O_3:Eu^{3+} without dissolving the other components in the lamp phosphor waste (HALO, BAM, LAP, CAT, SiO_2, Al_2O_3). [Hbet][Tf_2N] is a Brønsted acidic functionalized ionic liquid which has the ability to dissolve rare-earth oxides and many transition metal oxides (Fig. 1).[36,37] The dissolution of metal oxides in this ionic liquid has been studied extensively by Nockemann *et al.*[36–38] Silica and alumina cannot be dissolved in [Hbet][Tf_2N] which is highly relevant to the recycling of lamp phosphor waste since these powders can contain significant amounts of silica (as fine glass particles) and alumina.[3,9] The dissolution is driven by the reactivity of the carboxylic acid group located on the cation of the ionic liquid. In the resulting complex the rare-earth ions are coordinated by the betaine ligands, which are zwitterionic compounds when deprotonated.[38] The anions in [Hbet][Tf_2N] simply act as spectator anions and do not participate in the complex formation. However, the Tf_2N^- anion is required to obtain a hydrophobic ionic liquid ([Hbet]Cl is a water-soluble salt). The Tf_2N^- anion is also very stable and well-suited for high-temperature applications.[39]

A blend of YOX, LAP, BAM and HALO was used to simulate the composition of the lamp phosphor waste and to study the selective dissolution of YOX in [Hbet][Tf_2N]. The dissolution of CAT was not investigated in this work because this aluminate phosphor behaves similarly to BAM, meaning that it will not dissolve in the ionic liquid and thus ends up in the same remaining fraction as BAM and LAP.

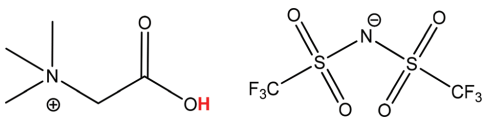

Fig. 1 Structure of the ionic liquid betainium bis(trifluoromethylsulfonyl)imide, [Hbet][Tf_2N]. The acidic proton of the betaine group is highlighted in red.

Experimental

Chemicals

The phosphors $BaMgAl_{10}O_{17}$:Eu^{2+} (BAM), Y_2O_3:Eu^{3+} (YOX), $LaPO_4$:Ce^{3+},Tb^{3+} (LAP), and $(Sr,Ca)_{10}(PO_4)_6(Cl,F)_2$:$Sb^{3+}$,$Mn^{2+}$ (HALO) were purchased from Nichia (Japan) with 99% purity. Betaine chloride (HbetCl) (99%), methyl red sodium salt (pure) and 1,4-dioxane (99.9%) were obtained from Acros Organics (Geel, Belgium). Lithium bis(trifluoromethylsulfonyl)-imide ($LiTf_2N$) (99%) was obtained from IoLiTec (Germany) and oxalic acid dihydrate (>99.5%) from J.T. Baker. Heavy water (D_2O) (99.9 atom% D) was purchased from Sigma–Aldrich (Belgium). Absolute ethanol and hydrogen chloride (HCl) were obtained from VWR (Belgium). The silicone solution in isopropanol was purchased from SERVA Electrophoresis GmbH (Germany) and the gallium standard solution (1000 ppm) from Merck (Belgium). All chemicals were used as received without further purification.

Equipment and characterization

^1H NMR and ^{13}C NMR spectra were recorded on a Bruker Avance 300 spectrometer, operating at a frequency of 300 MHz for ^1H and 75 MHz for ^{13}C, respectively. The samples were prepared by dissolving a small amount of product in heavy water (D_2O). An elemental analysis (carbon, hydrogen, nitrogen) was performed on a CE Instruments EA-1110 element analyzer. A thermogravimetric analysis (TGA) was done on a TA Instruments T500 thermogravimeter (heating rate: 2 °C min^{-1} from room temperature to 350 °C, under a nitrogen atmosphere). The viscosity of the ionic liquid was measured using an automatic Brookfield plate cone viscometer, Model LVDV-II CP (Brookfield Engineering Laboratories, USA). Photoluminescence spectra and luminescence lifetime measurements were recorded on an Edinburgh Instruments FS920 spectrofluorimeter. This instrument is equipped with a xenon arc lamp (450 W), a microsecond xenon flash lamp (60 W) and a red-sensitive photomultiplier (Hamamatsu R-2658). The morphology and the size distribution were determined by scanning electron microscopy (SEM) using a Philips XL 30 FEG device. Powder X-ray diffraction (XRD) was carried out on an Agilent SuperNova X-ray diffractometer, using Mo Kα radiation (λ = 0.71073 Å) and a CCD detector. ICP-MS measurements were carried out on a Thermo X-Series PlasmaQuad (PQ) 2 device. Microwave irradiation experiments were carried out on a CEM Discover monomode microwave apparatus (2.45 GHz, 100 W) with an integrated IR sensor, using 10 mL glass tube containers, sealed with snap caps. A Heraeus Megafuge 1.0 centrifuge was used to separate the undissolved phosphor particles from the ionic liquid after the leaching experiments. Total reflection X-ray fluorescence spectroscopy (TXRF) was performed with a Bruker S2 Picofox TXRF spectrometer equipped with a molybdenum source. For the sample preparation, plastic microtubes were filled with a small amount of ionic liquid sample (200 mg), ethanol (700 µL) and 100 µL of a gallium standard solution (1000 ppm). Gallium was chosen because this element has a high sensitivity and does not interfere with the

lanthanide signals. The microtubes were then vigorously shaken on a vibrating plate (IKA MS 3 basic). Finally, a 1 μL drop of this solution was put on a quartz plate, previously treated with a silicone/isopropanol solution (Serva®) to avoid spreading of the sample droplet on the quartz plate. The quartz plates were then dried for 30 min at 60 °C prior to analysis. Each sample was measured for 10 min.

Synthesis of [Hbet][Tf_2N]

The ionic liquid [Hbet][Tf_2N] was synthesized according to a literature method.[36] HbetCl (0.390 mol, 59.91 g) and $LiTf_2N$ (0.390 mol, 111.97 g) were dissolved in water (50 mL) and stirred for 2 h at room temperature. The mixture was then allowed to phase-separate and the water phase containing LiCl was removed. [Hbet][Tf_2N] was then washed several times with ice water (10 mL) to remove chloride impurities until the $AgNO_3$ test was negative in the water phase after the washing step. The remaining water was removed using a rotary evaporator under reduced pressure. The yield was 79% (0.310 mol, 123.47 g) with a chloride content below detection limit for the TXRF analysis (0.1–0.2 ppm).[40] NMR characterization with chemical shifts (δ) given in ppm and J values given in Hz resulted in δ_H (300 MHz; DMSO; Me_4Si) 3.22 (9 H, s, 3 × Me) 4.30 (2 H, s, CH_2) and δ_C (75 MHz; DMSO; Me_4Si) 166.34 (s, COO) 119.45 (q, 2 × CF3, J = 312.75), 62.60 (s, N-CH_2), 52.88 (3 × CH_3). A CHN elemental analysis found (%): C, 21.17; H, 3.96; N, 6.76. Calc. (%) for $C_7H_{12}N_2O_6F_6S_2$: C, 21.11; H, 3.04; N, 7.03.

Leaching experiments

Small glass vials (4 mL) were filled with a fixed amount of [Hbet][Tf_2N] (2 g), a 10 mg sample of each of the four phosphors per g of ionic liquid (4 × 10 mg g^{-1}) and also a small amount of water during some experiments (1–5 wt%). Note that all the quantities are expressed per gram of ionic liquid (mg g^{-1}). A magnetic stirring bar was then added to each of the vials and they were closed using a plastic screw cap. The dissolution experiments were carried out using a heating plate with a silicone oil bath, an integrated magnetic stirrer and a temperature sensor. The vials were placed in the silicone oil bath at the appropriate temperature and stirred for a certain amount of time. The vials were then placed in a centrifuge (5300 rpm, 20 min) to precipitate the undissolved phosphor powders and to obtain a clear ionic liquid. The metal content dissolved in the ionic liquid was determined using total reflection X-ray fluorescence spectroscopy (TXRF).

Stripping experiments

Two different stripping methods were investigated. Method 1 involved the use of an aqueous HCl phase to extract the rare-earth ions from the ionic liquid to the water phase, method 2 consisted of adding pure (solid) oxalic acid directly to the ionic liquid to precipitate the rare-earth ions as rare-earth oxalates. For every stripping experiment, Y_2O_3:Eu^{3+} (10 mg g^{-1}) was first fully dissolved in a large batch of ionic liquid (5 wt% H_2O). Small glass vials (5 mL) were then filled with a fixed amount of this REE-containing ionic liquid (1 g). For method 1, an HCl solution (1 g) was then added to the rare-earth containing ionic liquid. This lowly viscous biphasic mixture was shaken (1500 rpm) using a mechanical shaker at a set temperature (25, 70 and 80 °C). The samples were then centrifuged (1 min, 5300 rpm) to speed up phase separation, and analyzed by TXRF to determine the remaining metal content in the ionic liquid phase. For method 2, pure (solid) oxalic acid was added directly to the ionic liquid phase. These samples were more viscous and consisted of only one phase, so they were stirred using a magnetic stirring bar and a stirring plate/oil bath set-up to control the temperature (25, 50 and 70 °C). The samples were then centrifuged (5300 rpm, 20 min) to remove the oxalate precipitate and the ionic liquid phase was analyzed with TXRF to determine the remaining metal content.

Optimized full recycling process

The retained recycling process consisted of three steps. First a synthetic mixture of HALO, YOX, BAM and LAP phosphors was added to the ionic liquid [Hbet][Tf_2N] containing 5 wt% of water. The system was optimized for 10 mg of YOX per g of ionic liquid, which corresponds to approximately 40–50 mg of real lamp phosphor waste. A stirring bar was added and the samples were stirred for 24–48 h at 90 °C to obtain a selective and 100% leaching of YOX. The remaining solid lamp phosphor waste was separated from the ionic liquid by centrifugation (5300 rpm, 20 min). A stoichiometric amount of pure oxalic acid was then added to the ionic liquid loaded with yttrium and europium to precipitate the rare-earth ions as oxalates and regenerate the ionic liquid. The samples were stirred for 10 min at 70 °C to obtain 100% stripping. The oxalate precipitate was separated from the ionic liquid by filtration and washed with water (lowers the viscosity). The water can be removed by evaporation later on. An alternative could be to filter at 70 °C at which point the viscosity of the [Hbet][Tf_2N] (5 wt% H_2O) becomes very low. The mixed (yttrium, europium) oxalate was dried in a vacuum oven at 50 °C and then calcined at 950 °C (5 h) in an oven to obtain new Y_2O_3:Eu^{3+} (YOX) with a purity >99.9 wt%.

Results and discussion

Selective dissolution of YOX in [Hbet][Tf_2N]

The protonated functionalized ionic liquid betainium bis(trifluoromethylsulfonyl)imide, [Hbet][Tf_2N], has the ability to dissolve certain metal oxides, including rare-earth oxides like Y_2O_3 and Eu_2O_3.[36,37] Different parameters (water content, temperature, *etc.*) were investigated to find which leaching conditions were required to selectively dissolve the red Y_2O_3:Eu^{3+} (YOX) phosphor within a reasonable period of time.

In the first experiments, the influence of water addition was investigated. Water-free ionic liquid was used and increasing amounts of water were then added (0, 1, 2.5 and 5 wt%). Care was taken never to exceed the solubility of water in the ionic liquid (13 wt%), because it was important to maintain one

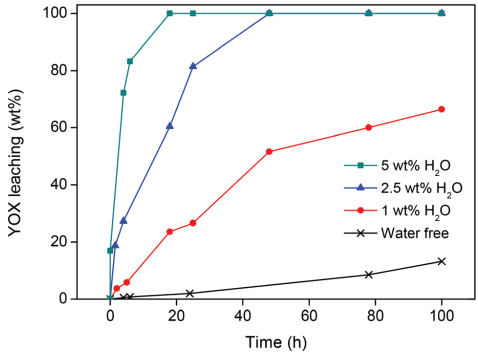

Fig. 2 Dissolution of YOX (wt%) in [Hbet][Tf_2N] at 90 °C with varying amounts of water in the ionic liquid (0, 1, 2.5 and 5 wt%). The solutions were stirred at 600 rpm. No dissolution of BAM and LAP was observed.

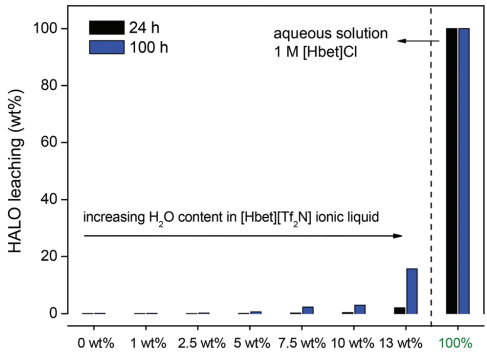

Fig. 3 Leaching (wt%) of HALO by [Hbet][Tf_2N] at 90 °C (600 rpm) after 24 h and 100 h with increasing amounts of water in the ionic liquid: 0, 1, 2.5, 5, 7.5, 10 and 13 wt% (= water-saturated). Leaching is also shown in an aqueous solution containing [Hbet]Cl (1 M) which has a pK_a of 1.83.[43]

homogeneous phase during the leaching process to avoid the loss of metal ions to the water phase.[41] A mix of YOX, HALO, BAM and LAP was added to the ionic liquid (4×10 mg g^{-1}) and stirred (600 rpm) at 90 °C. The water-free ionic liquid was compared with water-containing ionic liquid (1, 2.5 and 5 wt% water added). Closed vessels with screw caps were used to contain the small amounts of water at elevated temperatures. The results show that the addition of water has a positive influence on the leaching of YOX due to the lower viscosity and better ion diffusion. With a water content of 5 wt% (50 μL g^{-1}) in the ionic liquid, full dissolution of YOX was observed after 24 h (Fig. 2). More importantly, under these conditions very little dissolution of HALO was observed (<0.05 wt%) (Fig. 3) and no leaching of BAM and LAP could be detected. Higher water contents are not advisable since this will lead to increasing dissolution of HALO (Fig. 3). It was also confirmed in a separate experiment that SiO_2 and Al_2O_3 do not dissolve in the [Hbet][Tf_2N] ionic liquid.[37,42]

It is clear from Fig. 2 and 3 that under water-poor conditions (<5 wt% H_2O in the ionic liquid) Y_2O_3:Eu^{3+} dissolves much better than HALO. This is surprising considering that in dilute acidic aqueous solutions (*e.g.* 1 M [Hbet]Cl), HALO dissolves much more easily than Y_2O_3:Eu^{3+}. To explain this unusual behaviour a hypothesis is proposed based on the difficult solvation of anions in [Hbet][Tf_2N]. While metal cations (*e.g.* rare-earth ions) can be coordinated efficiently in [Hbet][Tf_2N] by the carboxylate groups of the deprotonated betaine, this is not the case for anions.[36–38] It was previously observed by Nockemann *et al.* that the solubility of oxides in [Hbet][Tf_2N] was much higher than that of chloride salts, which is in agreement with our hypothesis.[36] This hypothesis was supported by the observation that NaCl, $EuCl_3$ and YCl_3 could not be dissolved in the pure ionic liquid, while it was possible to dissolve their corresponding oxides. It was also observed that when [Hbet][Tf_2N] was brought in contact with an aqueous YCl_3 solution some yttrium was extracted to the ionic liquid phase but no chloride was extracted. The extraction of metal ions is based on the release of protons by $[Hbet]^+$ and the coordination of the metal ion by zwitterionic betaine groups, but there is no suitable mechanism for the coordination or solvation of anions in the ionic liquid. Since the dissolution of metal oxides does not create anions, they easily dissolve in this ionic liquid (eqn (2)) while metal salts like rare-earth chlorides (eqn (3)) (or even NaCl) do not, due to the formation of anions. This behaviour is the opposite of what is found in aqueous solutions, where chlorides dissolve much easier than oxides which require the presence of acid. Only when sufficient amounts of water are added to the ionic liquid, it will dissolve (some) chloride salts because water can solvate anions (eqn (3)). The same is true for HALO, where many phosphate and chloride ions need to be solvated in order for HALO to dissolve (eqn (1)). HALO dissolves very fast in dilute acidic aqueous solutions, but very little dissolution (<0.05 wt%) is observed in [Hbet][Tf_2N] when less than 5 wt% of water is present. That is why such a drastic change in the dissolution behavior of HALO is observed when the water content is increased (Fig. 3). The leaching of metal oxides like YOX is also accelerated in the presence of water but this is mainly due to the lower viscosity and faster diffusion of protons in the ionic liquid.[36,37] YOX forms, upon dissolution, only water and cations, which are efficiently solvated by the betaine groups, and does not form anions (eqn (2)). The water content is therefore the most crucial parameter as the control of the water content in the ionic liquid allows selective dissolution of YOX, without dissolving HALO.

$$Ln_2O_3 + 6H^+ \rightarrow 2Ln^{3+} + 3H_2O \quad (2)$$

$$LnCl_3 \rightarrow Ln^{3+} + 3Cl^- \quad (3)$$

It is important to keep the dissolution of HALO to an absolute minimum, not only from an economic point of view

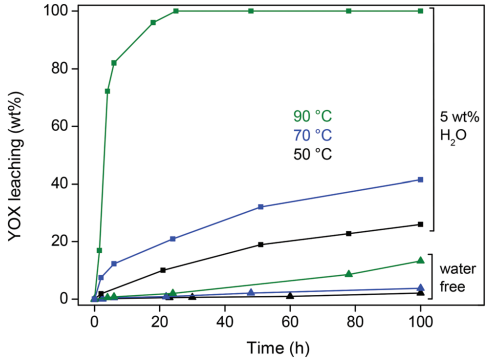

Fig. 4 Dissolution (wt%) of YOX in water-free [Hbet][Tf_2N] and water-containing (5 wt% H_2O) [Hbet][Tf_2N] as a function of time and temperature.

but also from a chemical point of view as it constitutes up to 50 wt% of the waste. The dissolution of HALO consumes a large amount of acid and releases unwanted metal ions (eqn (1)), which means that purification methods (*e.g.* solvent extraction) are required to retrieve pure rare earths. The dissolution of HALO also leads to the formation of phosphate ions (eqn (1)) which can form very insoluble YPO_4 and $EuPO_4$ with the dissolved Y^{3+} and Eu^{3+} from the YOX. This hampers further processing because rare-earth phosphates are very difficult to dissolve (like LAP and monazite). The optimal leaching system is therefore a compromise between the fast dissolution of YOX and keeping the leaching of HALO as low as possible. [Hbet][Tf_2N] with 5 wt% of H_2O (90 °C, 24 h) seems to be the best compromise between speed and selectivity. Under these conditions, the leaching of YOX and HALO is 100 wt% and 0.04 wt% respectively, and BAM and LAP leaching below the detection limit (Fig. 2 and 3).

The influence of temperature on the leaching of YOX was also investigated for this optimized ionic liquid system (5 wt% H_2O) and compared with water-free ionic liquid (Fig. 4). In both cases a noticeable increase in leaching speed was observed with increasing temperature (Fig. 4). A temperature of 90 °C with 5 wt% (50 μL g^{-1}) of H_2O in the ionic liquid was chosen as the optimal system because of its high leaching efficiency and the fact that the water pressure is still manageable.

A higher temperature is favorable because it accelerates the dissolution reaction and lowers the viscosity of the ionic liquid, which improves the diffusion. This is important because the leaching rate of this solid material is diffusion-controlled. The viscosity was measured as a function of the water content in the ionic liquid and the temperature (Table 2). It is clear that higher water content and temperature drastically diminish the viscosity. The viscosity of the ionic liquid with 5 wt% water at 80 °C is only 25 cP. The viscosity at 90 °C could not be measured with our equipment but it will be

Table 2 Viscosity (cP) of [Hbet][Tf_2N] as a function of the water content and temperature

	Viscosity (cP) at 30 °C	Viscosity (cP) at 50 °C	Viscosity (cP) at 80 °C
[Hbet][Tf_2N] (1 wt% H_2O)	925	252	65
[Hbet][Tf_2N] (5 wt% H_2O)	172	67	25
[Hbet][Tf_2N] (water-sat.)[a]	22	12	6

[a] Water-saturated [Hbet][Tf_2N] contains approximately 13 wt% H_2O.[41]

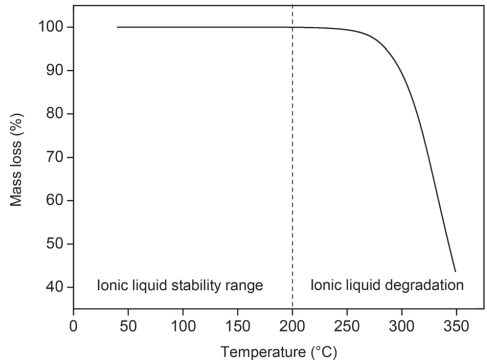

Fig. 5 Thermogravimetric analysis of [Hbet][Tf_2N], measured from 40 to 350 °C (2 °C min^{-1}) under a nitrogen atmosphere.

even lower. Of course, the viscosity of the leaching system used in this work (ionic liquid with 5 wt% H_2O at 90 °C) is still higher than that of water (0.3 cP at 90 °C) but it is sufficiently low in order not to be an issue.

The thermal stability of [Hbet][Tf_2N] was tested by thermogravimetric analysis (TGA) and ^{13}C NMR. The thermal stability is an important characteristic since the ionic liquid will be used for leaching at temperatures up to 90 °C for prolonged amounts of time. The Tf_2N^- anion is known to have a high relative stability compared to other common ionic liquid anions.[39] For TGA, the ionic liquid was first dried under reduced pressure at 80 °C until all the remaining traces of water were removed and the mass of the ionic liquid was stable. The ionic liquid was then heated (2 °C min^{-1}) under a nitrogen atmosphere, from room temperature to 350 °C. The results of the dynamic TGA show that the ionic liquid only starts to degrade at temperatures around 200 °C, which proves that it is definitely stable at 90 °C (Fig. 5). A static measurement at 90 °C for a period of 24 h showed negligible (<0.01%) degradation of the ionic liquid. ^{13}C NMR was used to investigate the degradation of water-containing ionic liquid under experimental conditions (90 °C, 5 wt% H_2O, 600 rpm, 48 h). A ^{13}C NMR spectrum was taken before and after the experiment to confirm the stability of the ionic liquid under these conditions.

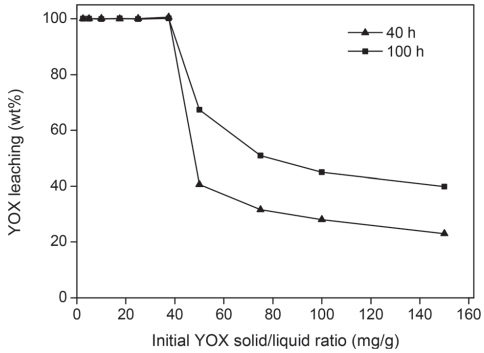

Fig. 6 Dissolution (wt%) of YOX in [Hbet][Tf_2N] (5 wt% H_2O) as a function of the initial YOX concentration in the ionic liquid (solid/liquid ratio). The dissolutions were carried out at 90 °C for 40 h and 100 h.

The loading capacity, meaning the amount of YOX that can be dissolved in the ionic liquid, was also investigated. The theoretical maximal stoichiometric solubility of Y_2O_3 in the ionic liquid amounts to 95 mg g^{-1}. However, this requires the addition of more water under reflux conditions in order to be sufficiently fast.[36] This would undermine the selectivity of this system since under these conditions the HALO would easily dissolve in the water phase. Higher loadings also resulted in higher viscosities due to the highly charged rare-earth ions in the ionic liquid, making the system much more difficult to handle. It was shown that under the previously mentioned optimized conditions (90 °C, 5 wt% H_2O), up to 40 mg g^{-1} of YOX could be fully dissolved in the ionic liquid after 40 h (Fig. 6). The parameter optimization in this work was done for a YOX loading of 10 mg g^{-1} (10 000 ppm), but it is possible to work under more concentrated conditions (solid/liquid ratio) without significant modifications. As shown in Fig. 6, a dissolution of 40 mg g^{-1} of YOX in the ionic liquid would correspond to a solid/liquid ratio of 200 mg g^{-1} (200 g kg^{-1}) of waste in the ionic liquid, since fluorescent lamp waste contains around 20 wt% of YOX.

The dissolved Y^{3+} and Eu^{3+} (YOX) in [Hbet][Tf_2N] was recovered by a stripping step. This was achieved either by bringing the loaded ionic liquid in contact with an acidic water phase to extract the rare-earth ions (method 1) or by directly precipitating the rare earths from the ionic liquid using pure (solid) oxalic acid (method 2). Stripping method 1 has important limitations due to the loss of ionic liquid to the water phase. Stripping with pure oxalic acid (method 2) is clearly a better alternative since no ionic liquid is lost and the YOX phosphor can be immediately regenerated from the yttrium/europium oxalate salt in a simple calcination step. However, it is still interesting to also investigate the stripping with HCl and quantify the loss of ionic liquid to the water phase even if it is not the best method. Both stripping systems are discussed separately and compared.

Stripping method 1: recovery of yttrium and europium using an acidic aqueous phase

The first stripping system involves the use of an acidic aqueous phase, which is brought in contact with the loaded ionic phase. In this process the rare-earth ions (Ln) are transferred to the water phase as soluble compounds (*e.g.* chlorides). The acidic protons protonate the betaine ligands and regenerate the ionic liquid (eqn (4)).

$$[\mathrm{Ln(bet)_3}][\mathrm{Tf_2N}]_3 + 3\mathrm{HCl} \rightarrow \mathrm{LnCl_3} + 3[\mathrm{Hbet}][\mathrm{Tf_2N}] \quad (4)$$

The fact that a two-phase system is now used means that it is necessary to look at possible losses of ionic liquid to the water phase. The loss of ionic liquid depends on the phase ratio and the amount and type of dissolved ions.[44–46] Ions can be classified as salting-in (*e.g.* NO_3^-) and salting-out (*e.g.* Cl^-, SO_4^{2-}) agents as described by the Hofmeister series.[45,47] The former class of ions tends to lead to an improved mixing of ionic liquid/water, while the latter leads to a better separation of ionic liquid/water and therefore a smaller loss of ionic liquid to the water phase. The loss of ionic liquid to the water phase (1 : 1 phase ratio by mass) was quantified using ^{1}H NMR spectroscopy with 1,4-dioxane as an internal standard and D_2O instead of H_2O as the water phase. The loss of [Hbet][Tf_2N] to a (pure) water phase was determined to be 13 wt%. Lowering the pH increases the loss of ionic liquid to the water phase even more to 15.1%, 15.4% and 18.1% for 1 M H_2SO_4, HCl and HNO_3 respectively. This is in agreement with the sequence found in the literature.[45] Although stripping with H_2SO_4 resulted in the lowest loss of ionic liquid, stripping with HCl is still the better choice because the solubility of rare-earth sulfates in water is much lower than the corresponding rare-earth chlorides. The loss of ionic liquid is very significant and it is cumbersome to recover the ionic liquid from the water phase, even though various techniques exist to recover ionic liquids at a later stage using for example strong salting-out agents, adsorbents, special membranes, electrodialysis or nanofiltration.[48–52] That is why the oxalic acid precipitation route (method 2) is the preferred method.

The different stripping parameters were then investigated for stripping with HCl, starting with the influence of acid concentration. First, 10 mg g^{-1} of YOX was dissolved in [Hbet][Tf_2N] (5 wt% H_2O). Then, the loaded ionic liquid was contacted with aqueous solutions containing varying concentrations of HCl (1 : 1 phase ratio by mass) and shaken (1500 rpm) for 1 h at 25 °C. The remaining metal content in the ionic liquid was then analyzed using TXRF. The results showed that bringing the ionic liquid in contact with 1 M HCl resulted in 99.6% and 99.7% stripping of Y^{3+} and Eu^{3+} respectively (Fig. 7). A sufficient amount of HCl is needed to protonate the betaine and to form the water-soluble YCl_3 and $EuCl_3$ compounds. In this set-up, the stoichiometric HCl concentration is 0.3 M in the water phase, but an excess of HCl is required to obtain full stripping (1 M) (Fig. 7). An interesting observation is the fact that under dilute acidic conditions with an excess of rare-earth ions compared to HCl, Y^{3+} is easier to strip than

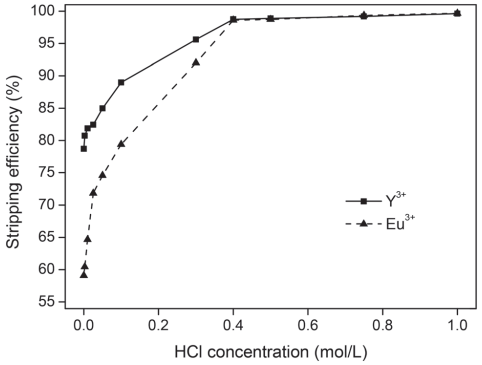

Fig. 7 Stripping of Y^{3+} and Eu^{3+} from [Hbet][Tf_2N], previously loaded with 10 mg g^{-1} of YOX. The influence of the HCl concentration on the stripping efficiency for Y^{3+} and Eu^{3+} is shown. The biphasic system was shaken (1500 rpm) at 25 °C for 1 h.

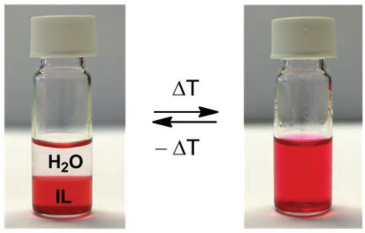

Fig. 8 Reversible formation of a homogeneous phase when increasing the temperature above the cloud point (55 °C for a pure water/ionic liquid system in a 1 : 1 ratio).[44] A coloring agent (methyl red sodium salt) was dissolved in the transparent ionic liquid phase to help the visualization. The density of the [Hbet][Tf_2N] liquid is higher than that of water.

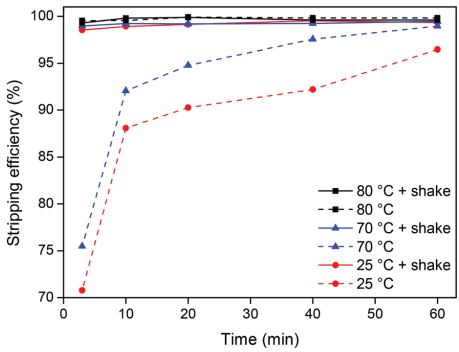

Fig. 9 Stripping kinetics and the influence of shaking (1500 rpm) are shown for 25 °C, 70 °C and 80 °C with 1 M HCl. The cloud point temperature is 74 °C and so at 80 °C the system is one homogeneous phase which explains the efficient stripping without shaking. For 25 °C and 70 °C it consists of two phases, a water phase and an ionic liquid phase, making shaking essential for an efficient stripping process.

Eu^{3+}. This is in agreement with previous reports where yttrium(III) had a slightly lower affinity for betaine ligands compared to europium(III).[44] For HCl concentrations >0.4 M no difference was observed and the stripping process became very efficient and reproducible. An HCl concentration of 1 M was retained as the optimal stripping concentration because of the fast and reliable stripping.

Secondly, the stripping kinetics was investigated. When dealing with a biphasic system, the process kinetics is controlled by the extent of the interface since the exchange of ions can only happen at this interface. The area of the interface is usually increased by intense stirring or shaking; however, a special feature of the [Hbet][Tf_2N]/H_2O system is that it shows thermomorphic behavior with an upper critical solution temperature.[44] This means that the biphasic system will become one homogeneous phase above a certain temperature called the cloud point temperature. This is very interesting since the process kinetics will be much faster as they are then no longer limited by the diffusion across an interface. In order to obtain phase separation, the mixture has to be heated above the cloud point and shaken briefly (1 s) to overcome the metastable state, but the homogeneous state then remains stable as long as the temperature is above the cloud point. Below the cloud point, the phase separation automatically occurs again (Fig. 8).

The cloud point is dependent not only on the amount and type of ions present in the water phase, but also on the loading of the ionic liquid and the water to ionic liquid ratio.[41] The cloud point was determined for this stripping system consisting of one phase with 1 g of ionic liquid in which Y_2O_3: Eu^{3+} was dissolved (10 mg g^{-1}), brought in contact with another phase consisting of a 1 g HCl solution (1 M) in a 1 : 1 phase ratio. The cloud point was found to be 74 °C by heating the sample to 80 °C and then slowly cooling it down, keeping it steady at every degree for 5 min to see whether it would become cloudy when gently shaken which indicates that the mixture starts to phase separate.[53] This cloud point is higher than that for a pure H_2O/[Hbet][Tf_2N] system, because of the H^+, Cl^-, Y^{3+} and Eu^{3+} ions dissolved in it.[41]

The stripping kinetics was then investigated at room temperature (25 °C) and just below (70 °C) and above (80 °C) the cloud point temperature (74 °C) both with and without shaking (1500 rpm) (Fig. 9).

Raising the temperature from 25 °C to 70 °C only slightly increases the stripping speed. However, when the temperature is raised to 80 °C, which is above the cloud point temperature, the stripping is much faster due to the disappearance of the interface between the ionic liquid and the water phase and the formation of one homogeneous phase. It is also clear that shaking has a major influence when working at temperatures below the cloud point temperature because the system is then a biphasic mixture. Shaking the samples at 80 °C (above the

cloud point) has no influence since the system is then one homogeneous phase. It is clear from this experiment (Fig. 9) that from an energy-saving point of view, the best choice for stripping is either to work with a biphasic mixture at 25 °C while shaking or to work at 80 °C without shaking thanks to the formation of a homogeneous phase. Other combinations require more energy and are less efficient.

Stripping method 2: recovery of yttrium and europium using pure oxalic acid

The problem of the loss of ionic liquid to the water phase can be avoided by stripping with solid oxalic acid, directly in the ionic liquid phase. This acid forms insoluble oxalate complexes with the rare-earth ions (eqn (5)) and precipitates them while regenerating the ionic liquid. This stripping precipitation method is very efficient for rare-earth ions. The rare-earth oxalate precipitate can then be separated from the ionic liquid and thermally decomposed in an oven at high temperature to form the corresponding rare-earth oxides.[54] By carefully choosing the conditions it is also possible to directly resynthesize the Y_2O_3:Eu^{3+} phosphor by calcination of the mixed yttrium/europium oxalate (eqn (6)), as described by the Solvay patent.[55] The advantage is that the yttrium and europium are already present in the right ratio to manufacture the YOX phosphor, since they have been selectively leached from the used lamp phosphors in the first place. This stripping system is therefore definitely the preferred choice compared to the stripping system using an acidic water phase. The oxalic acid stripping is much more convenient and can be carried out directly in the ionic liquid, meaning that there is no loss of ionic liquid to the water phase.

$$2(Y^{3+}, Eu^{3+}) + 3H_2C_2O_4 \rightarrow (Y, Eu)_2(C_2O_4)_{3(s)} + 6H^+ \quad (5)$$

$$(Y, Eu)_2(C_2O_4)_{3(s)} + \frac{3}{2}O_2 \xrightarrow{950\,^{\circ}C} Y_2O_3{:}\,Eu^{3+}{}_{(s)} + 6CO_2 \quad (6)$$

The different parameters of this stripping method were investigated. The results show that a stoichiometric amount (eqn (5)) of oxalic acid compared to the amount of rare-earth ions (3 : 2) is sufficient to obtain a stripping efficiency of 100% (Fig. 10). Oxalic acid does not show individual selectivity for yttrium or europium under these conditions.

The influence of temperature on the stripping kinetics of this heterogeneous stripping process was investigated. The viscosity of this pure ionic liquid is obviously higher than that for a biphasic water–ionic liquid mixture, but it is still very manageable especially at higher temperatures (Table 2). An ionic liquid containing 10 mg g^{-1} of YOX and 5 wt% H_2O was reused, and a stoichiometric amount of oxalic acid was added compared to the amount of rare-earth ions (3 : 2). The samples were then stirred (600 rpm) at different temperatures and for increasing amounts of time. The results show a drastic increase in the stripping efficiency when raising the temperature from 25 °C to 50 °C and 70 °C (Fig. 11). This increase is attributed to the lower viscosity (Table 2) and the improved diffusion of the oxalic acid in the ionic liquid. At 70 °C, a stripping efficiency of 100% was obtained after only 10 min, which is a very satisfactory result.

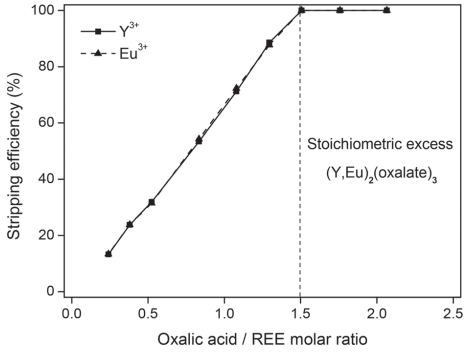

Fig. 10 Stripping of yttrium and europium from [Hbet][Tf_2N] using pure (solid) oxalic acid. The influence of oxalic acid concentration on the stripping efficiency is shown. A ratio of 1.5 : 1 is the stoichiometric amount of oxalic acid required to precipitate all rare-earth ions (REE = Y + Eu) in solution as $(Y,Eu)_2(C_2O_4)_3$ and results in a stripping efficiency of 100%.

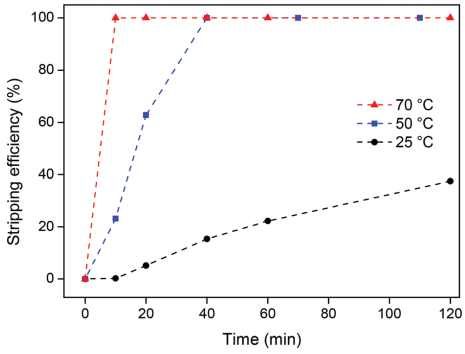

Fig. 11 Stripping of yttrium and europium from the [Hbet][Tf_2N] ionic liquid, using a stoichiometric amount (3 : 2) of pure (solid) oxalic acid. The influence of time and temperature on the total stripping efficiency (Y + Eu) is shown.

It can be concluded that this oxalate stripping process is very efficient since stoichiometric amounts of oxalic acid suffice to get full stripping of the rare-earth ions from the ionic liquid. The formation of the rare-earth oxalate precipitate is also very convenient since the oxalate salt can be transformed into a new YOX phosphor Y_2O_3:Eu^{3+} by a simple calcination step. The major advantage of this stripping system compared to the biphasic system (method 1) is the fact that no ionic liquid is lost. The drawback is that this stripping system is kinetically slower and therefore requires heating at 70 °C for 10 min (Fig. 11). The biphasic stripping system using HCl

could be carried out efficiently by shaking at room temperature for 10 min (Fig. 9). All things considered, the oxalic acid stripping method was retained for the final recycling process.

Regenerating the Y_2O_3:Eu^{3+} phosphor

The $(Y,Eu)_2(C_2O_4)_3$ precipitate was separated from the ionic liquid by filtration with a Büchner funnel and washed with water to lower the viscosity of the ionic liquid. Afterwards the water can be removed by evaporation. An alternative could be to filter at 70 °C at which point the viscosity of the [Hbet][Tf_2N] (5 wt% H_2O) becomes very low. The mixed oxalate was then dried in a vacuum oven at 50 °C for 12 h. The dry $(Y,Eu)_2(C_2O_4)_3$ was then placed in an oven at 950 °C for 5 h to obtain the Y_2O_3:Eu^{3+} phosphor. The YOX particles were characterized using ICP-MS, SEM imaging, luminescence spectroscopy and powder XRD, and compared with the purchased YOX. The purity of the recycled YOX was determined to be >99.9 wt% by TXRF and ICP-MS with only small traces of calcium (<0.1 wt%). The purchased YOX had a certified purity of >99 wt%. SEM images can be found in the ESI (Fig. S1†). They showed that the particles had a size of 4.11 ± 1.41 μm which is in range with the commercial YOX phosphor (3.61 ± 1.52 μm). However, the recycled YOX phosphor had a rougher surface than the purchased phosphor (Fig. S1†). Powder XRD was carried out to compare the commercial YOX with the recycled YOX. The diffractograms were essentially identical, which confirmed the successful synthesis of Y_2O_3:Eu^{3+} (Fig. S2†). The luminescence of this material was also compared with the commercially obtained Y_2O_3:Eu^{3+} phosphor (Fig. 12). When the spectra are scaled to have the same intensity of the $^5D_0 \rightarrow {}^7F_1$ transition, it is interesting to compare the intensity of the $^5D_0 \rightarrow {}^7F_2$ transition (around 612 nm) since this is a so-called hypersensitive transition, meaning its intensity is very dependent on its environment.[56–58] It can be seen that the maximum intensity peak ($^5D_0 \rightarrow {}^7F_2$) has the same intensity for the recycled phosphor as for the commercial phosphor. The luminescence lifetime was also measured by studying the decay of the $^5D_0$ emitting state of Eu^{3+}. The samples were excited with 254 nm light and the emission light was collected at 612 nm. The decay curves (Fig. S3†) were fitted as a mono-exponential decay, resulting in a luminescence lifetime of 0.989 ms (R^2 = 0.998) and 1.003 ms (R^2 = 0.997) for the recycled and purchased YOX phosphor respectively. The very good luminescence and luminescence lifetime of the recycled YOX confirms that the recycling process yields a sufficiently pure yttrium/europium oxalate product to allow direct resynthesis of the YOX phosphor (>99.9 wt% purity). This process is only possible because of the highly selective dissolution of YOX in the ionic liquid, because any dissolution of HALO, BAM or LAP would lead to an impure product and a significant decrease in luminescence. Optimization of the calcination process (flux agents, temperature, time, *etc.*) could further improve the luminescence properties and particle morphology to obtain an optimal red phosphor, but this is outside the scope of this work and has been studied by others.[55,59]

An overview of the proposed recycling process is shown in Fig. 13. This process selectively recovers the YOX which represents 80 wt% of the critical rare-earths in the lamp phosphor waste powder and approximately 70% of the value.[14] Only oxalic acid is consumed (cheap chemical) and it creates no waste besides some CO_2 (the ionic liquid is entirely reusable). This process is a sustainable alternative compared to mineral acid leaching and could be applied on industrial scale as an on-site valorization method for recyclers since no complex solvent extraction installations are needed.

This process was optimized using a synthetic mix of phosphors (HALO, YOX, BAM, LAP). However, it is also applicable to real lamp phosphor waste because the other components

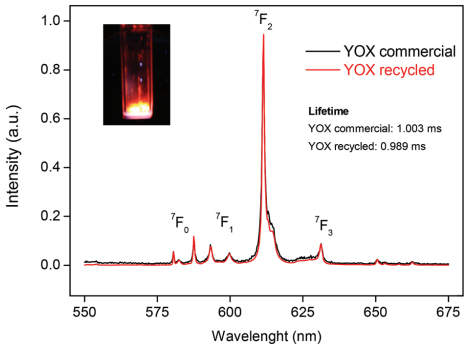

Fig. 12 Luminescence spectra (λ_{exc} = 254 nm) of the commercial red Y_2O_3:Eu^{3+} (YOX) phosphor, compared with the spectrum of the recycled YOX phosphor after calcination of the $(Y,Eu)_2(C_2O_4)_3$ precipitate. The spectra were scaled to have the same intensity for the $^5D_0 \rightarrow {}^7F_1$ transition in order to compare the intensity of the hypersensitive $^5D_0 \rightarrow {}^7F_2$ transition. Picture: recycled YOX phosphor in a quartz container irradiated with 254 nm light. The luminescence lifetimes are also shown (Fig. S3†).

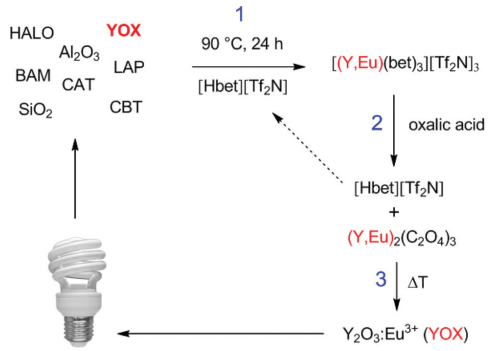

Fig. 13 Overview of the proposed recycling process for lamp phosphor waste, based on the selective dissolution and revalorization of YOX with the protonated functionalized ionic liquid [Hbet][Tf_2N]. Step 1: selective dissolution of YOX, step 2: stripping with pure oxalic acid (regenerates the ionic liquid), step 3: direct resynthesis of YOX.

(CAT, CBT, SiO_2, Al_2O_3) do not interfere with this process as they do not dissolve in [Hbet][Tf_2N].[37,42] The influence of mercury on this process was not investigated, but many techniques exist to remove mercury from the phosphor powders.[3,9,21,60–62] At the end of the recycling scheme, no additional waste has been created. The rest of the lamp phosphor waste (SiO_2, Al_2O_3, HALO, BAM, LAP, CAT, CBT) can be discarded or further processed, for example by doing a rough separation of the HALO with physical separation methods.[3,63] This would result in a terbium concentrate (≈8 wt% Tb) held in LAP, CAT and CBT. The terbium content in this concentrate is much higher than that in any commercially exploited ore from primary mining (<1.3 wt% Tb).[4] The high demand for terbium could therefore make it worthwhile to dissolve the LAP, CAT and CBT phosphors in a final stage, but these phosphors are much more difficult to dissolve and require a lot of energy input.[14]

Microwave heating

In most of our experiments, the ionic liquid was heated by a conventional heating source. However, since the leaching of YOX in the ionic liquid requires high temperatures over prolonged periods of time, it is interesting to note that ionic liquids can be heated in a very energy-efficient way by microwave irradiation. Ionic liquids consist entirely of ions as opposed to water or organic solvents which explains the high adsorption of microwave radiation.[64] Microwaves do not interfere with the dissolution process and provide a highly economical way to heat an ionic liquid in an industrial context.[64,65] The immediate on/off behavior of microwave irradiation is also useful for process control. A programmable microwave oven with temperature and pressure control was used to test this. At 100 W, the ionic liquid [Hbet][Tf_2N] was heated to a temperature of 100 °C in less than 15 s (Fig. 14). The temperature can be kept constant at a low cost.

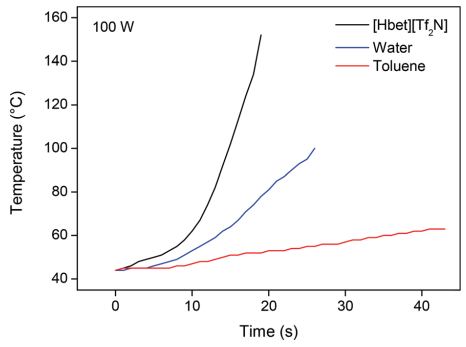

Fig. 14 Heating of different solvents in a microwave oven (100 W), equipped with an infrared temperature probe.

Conclusion

The ionic liquid leaching system described in this work is a major improvement compared to mineral acid leaching, since it allows the selective dissolution of Y_2O_3:Eu^{3+} (YOX) without dissolving the other phosphors (HALO, BAM, LAP). An interesting feature of the process is that the $(Sr,Ca)_{10}(PO_4)_6(Cl,F)_2$:$Sb^{3+}$, Mn^{2+} phosphor was not leached by the ionic liquid (<0.05 wt%). This non-valuable broad-band white phosphor known as "halophosphate" (HALO) can make up as much as 50 wt% of the lamp phosphor waste fraction. Dissolution of HALO is unavoidable when using dilute mineral acids, especially under the conditions required for the dissolution of Y_2O_3:Eu^{3+}. The unusual selectivity of the ionic liquid was attributed to the fact that the [Hbet][Tf_2N] is unable to solvate anions efficiently, which explains why it is only able to dissolve metal oxides efficiently and not metal salts like ($LnCl_3$, NaCl). The yttrium and europium dissolved in the ionic liquid [Hbet][Tf_2N] were then stripped with an HCl solution or by adding pure (solid) oxalic acid directly to the ionic liquid. The oxalic acid route precipitates the rare earths as a mixed (yttrium, europium) oxalate salt, which can be transformed into a new Y_2O_3:Eu^{3+} phosphor by a simple calcination step at 950 °C. The ionic liquid is automatically regenerated during the stripping step and can be reused. This innovative approach offers selectivity, mild conditions and reusability, which make this a promising green technology for the targeted recovery of Y_2O_3:Eu^{3+} and the valorization of lamp phosphor waste. 70% of the value and 80% of the critical rare earths in the lamp phosphor waste are recovered this way. Further processing of the terbium-rich rest fraction can be done but requires much harsher conditions. No additional waste is generated during this process and there is no need for additional solvent extraction steps since the YOX is dissolved selectively and immediately regenerated. This opens the way to a more simple, economical and energy-efficient industrial process for the revalorization of lamp phosphor waste.

Acknowledgements

The authors wish to thank the KU Leuven (projects GOA/13/008 and IOF-KP RARE^3) and the FWO Flanders (PhD fellowship to DD) for financial support. The authors would like to thank Dorien Baeten for the help with TGA measurements, Prof. Erik van der Eycken and Geert Hooyberghs for access to microwave oven facilities and Michèle Vanroelen for the ICP-MS measurements. Jeroen Sniekers is also thanked for helping with the SEM images and Neil Brooks for powder XRD characterization.

Notes and references

1 D. Schüler, M. Buchert, R. Liu, G. S. Dittrich and C. Merz, *Study on rare earths and their recycling*, Öko-Institut, Darmstadt, 2011.

2 Ad-Hoc Working Group on Defining Critical Raw Materials, *Report on Critical Raw Materials for the EU*, European Commission, DG Enterprise & Industry, Brussels, 2014.
3 K. Binnemans, P. T. Jones, B. Blanpain, T. Van Gerven, Y. Yang, A. Walton and M. Buchert, *J. Cleaner Prod.*, 2013, **51**, 1–22.
4 D. Sandalow, D. Bauer, D. Diamond, J. Li, M. McKittrick and P. Telleen, *Critical Materials Strategy*, U.S. Department of Energy, USA, 2010.
5 K. Binnemans, P. T. Jones, K. Acker, B. Blanpain, B. Mishra and D. Apelian, *JOM*, 2013, **65**, 846–848.
6 M. Tanaka, T. Oki, K. Koyama, H. Narita and T. Oishi, in *Handbook on the Physics and Chemistry of Rare Earths*, ed. J.-C. G. Bünzli and V. K. Pecharsky, Elsevier-Amsterdam, 2013, ch. 255, vol. 43, pp. 159–212.
7 Y. Wu, X. Yin, Q. Zhang, W. Wang and X. Mu, *Resour., Conserv., Recycl.*, 2014, **88**, 21–31.
8 Solvay, Press release, http://www.solvay.com, 2012.
9 K. Binnemans and P. T. Jones, *J. Rare Earth*, 2014, **32**, 195–200.
10 T. Vander Hoogerstraete, S. Wellens, K. Verachtert and K. Binnemans, *Green Chem.*, 2013, **15**, 919–927.
11 S. Wellens, R. Goovaerts, C. Moller, J. Luyten, B. Thijs and K. Binnemans, *Green Chem.*, 2013, **15**, 3160–3164.
12 T. Vander Hoogerstraete and K. Binnemans, *Green Chem.*, 2014, **16**, 1594–1606.
13 K. Larsson, C. Ekberg and A. Ødegaard-Jensen, *Waste Manage.*, 2013, **33**, 689–698.
14 J. J. Braconnier and A. Rollat, *Solvay, European Patent*, EP 2419377 A1, 2012.
15 T. Hirajima, A. Bissombolo, K. Sasaki, K. Nakayama, H. Hirai and M. Tsunekawa, *Int. J. Miner. Process.*, 2005, **77**, 187–198.
16 T. Hirajima, K. Sasaki, A. Bissombolo, H. Hirai, M. Hamada and M. Tsunekawa, *Sep. Purif. Technol.*, 2005, **44**, 197–204.
17 G. Mei, P. Rao, M. Mitsuaki and F. Toyohisa, *J. Wuhan. Univ. Technol., Mater. Sci. Ed.*, 2009, **24**, 418–423.
18 V. Innocenzi, I. De Michelis, B. Kopacek and F. Vegliò, *Waste Manage.*, 2014, **34**, 1237–1250.
19 H. Liu, S. Zhang, D. Pan, J. Tian, M. Yang, M. Wu and A. A. Volinsky, *J. Hazard. Mater.*, 2014, **272**, 96–101.
20 M. A. Rabah, *Waste Manage.*, 2008, **28**, 318–325.
21 C. Tunsu, C. Ekberg and T. Retegan, *Hydrometallurgy*, 2014, **144–145**, 91–98.
22 F. Yang, F. Kubota, Y. Baba, N. Kamiya and M. Goto, *J. Hazard. Mater.*, 2013, **254–255**, 79–88.
23 H. L. Yang, W. Wang, H. M. Cui, D. L. Zhang, Y. Liu and J. Chen, *J. Chem. Technol. Biotechnol.*, 2012, **87**, 198–205.
24 G. Mei, P. Rao, M. Mitsuaki and F. Toyohisa, *J. Wuhan Univ. Technol., Mater. Sci. Ed.*, 2009, 24.
25 R. Otto and A. Wojtalewicz, *US patent*, 0027651 A1, 2012.
26 A. P. Abbott, G. Frisch, S. J. Gurman, A. R. Hillman, J. Hartley, F. Holyoak and K. S. Ryder, *Chem. Commun.*, 2011, **47**, 10031–10033.
27 S. Wellens, T. Vander Hoogerstraete, C. Möller, B. Thijs, J. Luyten and K. Binnemans, *Hydrometallurgy*, 2014, **144–145**, 27–33.
28 A. Rout, S. Wellens and K. Binnemans, *RSC Adv.*, 2014, **4**, 5753–5758.
29 S. Wellens, B. Thijs, C. Moller and K. Binnemans, *Phys. Chem. Chem. Phys.*, 2013, **15**, 9663–9669.
30 A. P. Abbott, G. Frisch, J. Hartley and K. S. Ryder, *Green Chem.*, 2011, **13**, 471–481.
31 S. Wellens, B. Thijs and K. Binnemans, *Green Chem.*, 2012, **14**, 1657–1665.
32 Y. Gu, *Green Chem.*, 2012, **14**, 2091–2128.
33 Q. Zhang, S. Zhang and Y. Deng, *Green Chem.*, 2011, **13**, 2619–2637.
34 T. Welton, *Green Chem.*, 2011, **13**, 225–225.
35 N. V. Plechkova and K. R. Seddon, *Chem. Soc. Rev.*, 2008, **37**, 123–150.
36 P. Nockemann, B. Thijs, S. Pittois, J. Thoen, C. Glorieux, K. Van Hecke, L. Van Meervelt, B. Kirchner and K. Binnemans, *J. Phys. Chem. B*, 2006, **110**, 20978–20992.
37 P. Nockemann, B. Thijs, T. N. Parac-Vogt, K. Van Hecke, L. Van Meervelt, B. Tinant, I. Hartenbach, T. Schleid, V. T. Ngan, M. T. Nguyen and K. Binnemans, *Inorg. Chem.*, 2008, **47**, 9987–9999.
38 P. Nockemann, B. Thijs, K. Lunstroot, T. N. Parac-Vogt, C. Görller-Walrand, K. Binnemans, K. Van Hecke, L. Van Meervelt, S. Nikitenko, J. Daniels, C. Hennig and R. Van Deun, *Chem. – Eur. J.*, 2009, **15**, 1449–1461.
39 R. Reddy, *J. Phase Equilib. Diffus.*, 2006, **27**, 210–211.
40 T. Vander Hoogerstraete, S. Jamar, S. Wellens and K. Binnemans, *Anal. Chem.*, 2014, **86**, 3931–3938.
41 T. Vander Hoogerstraete, B. Onghena and K. Binnemans, *Int. J. Mol. Sci.*, 2013, **14**, 21353–21377.
42 B. Thijs, PhD thesis, KU Leuven – University of Leuven, Belgium, 2007.
43 R. M. C. Dawson, *Data for Biochemical Research*, Oxford University Press, New York, 3rd edn, 1986, pp. 8–9.
44 T. Vander Hoogerstraete, B. Onghena and K. Binnemans, *J. Phys. Chem. Lett.*, 2013, **4**, 1659–1663.
45 M. G. Freire, P. J. Carvalho, A. M. S. Silva, L. M. N. B. F. Santos, L. P. N. Rebelo, I. M. Marrucho and J. A. P. Coutinho, *J. Phys. Chem. B*, 2008, **113**, 202–211.
46 M. G. Freire, C. M. S. S. Neves, P. J. Carvalho, R. L. Gardas, A. M. Fernandes, I. M. Marrucho, L. M. N. B. F. Santos and J. A. P. Coutinho, *J. Phys. Chem. B*, 2007, **111**, 13082–13089.
47 Y. Zhang and P. S. Cremer, *Curr. Opin. Chem. Biol.*, 2006, **10**, 658–663.
48 L. Bai, X. Wang, Y. Nie, H. Dong, X. Zhang and S. Zhang, *Sci. China: Chem.*, 2013, **56**, 1811–1816.
49 C. M. S. S. Neves, M. G. Freire and J. A. P. Coutinho, *RSC Adv.*, 2012, **2**, 10882–10890.
50 C. Abels, C. Redepenning, A. Moll, T. Melin and M. Wessling, *J. Membr. Sci.*, 2012, **405–406**, 1–10.
51 J. F. Fernández, D. Waterkamp and J. Thöming, *Desalination*, 2008, **224**, 52–56.
52 J. Lemus, J. Palomar, F. Heras, M. A. Gilarranz and J. J. Rodriguez, *Sep. Purif. Technol.*, 2012, **97**, 11–19.
53 B. Onghena, J. Jacobs, L. Van Meervelt and K. Binnemans, *Dalton Trans.*, 2014, **43**, 11566–11578.

54 G. Adachi, N. Imanaka and Z. C. Kang, *Binary Rare Earth Oxides*, Kluwer Academic Publishers, Dordrecht, 2006.
55 X. Wan, *Solvay, China Patent*, EP 2176375 A1, 2010.
56 C. R. Ronda, T. Jüstel and H. Nikol, *J. Alloys Compd.*, 1998, **275–277**, 669–676.
57 N. C. Chang, *J. Appl. Phys.*, 1963, **34**, 3500–3504.
58 K. Binnemans and C. Gorller-Walrand, *J. Rare Earth*, 1996, 173–180.
59 T. Hirai, T. Hirano and I. Komasawa, *J. Mater. Chem.*, 2000, **10**, 2306–2310.
60 M. Jang, S. M. Hong and J. K. Park, *Waste Manage.*, 2005, **25**, 5–14.
61 W. A. Durão Jr., C. A. de Castro and C. C. Windmöller, *Waste Manage.*, 2008, **28**, 2311–2319.
62 C. Raposo, C. C. Windmöller and W. A. Durão Júnior, *Waste Manage.*, 2003, **23**, 879–886.
63 T. Horikawa and K. Machida, *Mater. Integr.*, 2011, **24**, 37–43.
64 J. Hoffmann, M. Nuchter, B. Ondruschka and P. Wasserscheid, *Green Chem.*, 2003, **5**, 296–299.
65 A. Arfan and J. P. Bazureau, *Org. Process Res. Dev.*, 2005, **9**, 743–748.

Paper 2: Recycling of rare earths from NdFeB magnets

Title:

Recycling of Rare Earths from NdFeB Magnets Using a Combined Leaching/Extraction System Based on the Acidity and Thermomorphism of the Ionic Liquid [Hbet][Tf_2N]

Type: Full paper + Inside front cover
Journal: Green Chemistry (IF 8.02)
Publisher: Royal Society of Chemistry (RSC)
Publication date: 02/03/2015

Reprint with permission from:
D. Dupont and K. Binnemans, *Green Chem.*, **2015**, 17, 2150-2163

Electronic Supplementary Information (ESI) available: http://pubs.rsc.org.

Graphical abstract

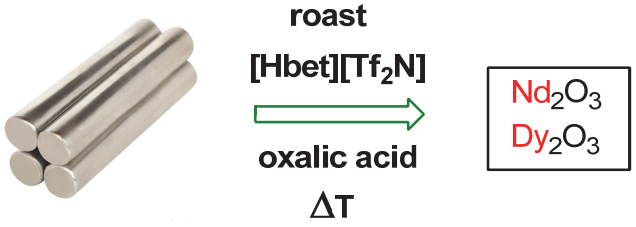

A new recycling process was developed to recover the rare earths from roasted NdFeB magnets using the thermomorphic and acidic properties of the ionic liquid [Hbet][Tf_2N] to achieve a combined leaching/extraction system.

Volume 17 | Number 4 | April 2015 | Pages 1929–2588

Green Chemistry

Cutting-edge research for a greener sustainable future

www.rsc.org/greenchem

ISSN 1463-9262

ROYAL SOCIETY OF CHEMISTRY

PAPER

David Dupont and Koen Binnemans

Recycling of rare earths from NdFeB magnets using a combined leaching/extraction system based on the acidity and thermomorphism of the ionic liquid [Hbet][Tf_2N]

Green Chemistry

PAPER

View Article Online
View Journal | View Issue

Cite this: *Green Chem.*, 2015, **17**, 2150

Recycling of rare earths from NdFeB magnets using a combined leaching/extraction system based on the acidity and thermomorphism of the ionic liquid [Hbet][Tf_2N]†

David Dupont and Koen Binnemans*

The continuous miniaturization of electric motors, hard disks and wind turbines is causing an increasing demand for high-performance neodymium–iron–boron magnets (NdFeB). The supply risk for the rare-earth elements (REEs) used in these magnets is a growing concern and has sparked the development of recycling schemes for these end-of-life products. In this paper a new recycling process for (microwave) roasted NdFeB magnets is proposed, based on the carboxyl-functionalized ionic liquid: betainium bis(trifluoromethylsulfonyl)imide, [Hbet][Tf_2N]. Using the thermomorphic properties of the [Hbet][Tf_2N]–H_2O system, a combined leaching/extraction step was designed. The change from a homogeneous system during leaching (80 °C) to a biphasic system at room temperature causes the dissolved metal ions to distribute themselves amongst the two phases. The valuable elements (Nd, Dy, Co) are thus separated from the iron with high separation factors. The stripping was done very efficiently using oxalic acid to precipitate the REE(III) and cobalt(II) ions while transferring the iron(III) from the ionic liquid to the water phase as a soluble oxalate complex. The cobalt (present in certain magnets) was removed by treating the mixed (REE/Co) oxalate precipitate with aqueous ammonia. The remaining REE oxalate was then calcined to form the REE oxides (99.9% pure). The ionic liquid is regenerated during the stripping step and contamination of the water phase was avoided by salting-out the ionic liquid with Na_2SO_4. This innovative recycling process features a combined leaching/extraction in mild conditions using a reusable acidic ionic liquid and an energy-efficient microwave roasting of the magnets. These aspects all contribute towards the green character of this process which can be considered as a sustainable and efficient alternative to mineral acid leaching and solvent extraction.

Received 22nd January 2015,
Accepted 2nd March 2015

DOI: 10.1039/c5gc00155b

www.rsc.org/greenchem

Introduction

The rare-earth elements (REEs) include the 15 lanthanides plus yttrium and scandium. They are used in many high-tech applications including wind turbines, electric vehicles, NiMH batteries, hard disk drives and fluorescent lamps.[1–5] The demand for these elements is expected to grow by more than 8% per year, mainly driven by the increasing demand for the strong neodymium–iron–boron (NdFeB) magnets.[2–6] NdFeB magnets contain two critical REEs, neodymium (Nd) and dysprosium (Dy), and the demand for these elements is expected to grow by 700% and 2600% respectively over the next 25 years as the NdFeB market expands rapidly.[2] Currently, China dominates the REE supply from primary mining (>90% of the global production in 2013) and the worldwide recycling rate is still very low (<1%).[4,6,7] Since the tightening of the Chinese export quota for rare earths in 2010, the rare-earth elements have been labeled as critical raw materials by the European Commission and the U.S. Department of Energy.[1,3,4,6,8] Opening or reopening mines outside China requires time and large financial investments. Therefore recycling of REEs from end-user products like NdFeB magnets (38% of the market by value) could help to secure the supply of these critical elements.[3] It is estimated that by 2020 over 200 000 tonnes of REEs will be held in NdFeB magnets worldwide in wind turbines, electric motors, hard disk drives, speakers, *etc.*[3] Efficient recycling of these NdFeB magnets could therefore help to secure the supply of neodymium and dysprosium and to create a closed-loop system in order to solve the balance problem which is caused by the unwanted co-production of

KU Leuven, Department of Chemistry, Celestijnenlaan 200F – P.O. Box 2404, 3001 Leuven, Belgium. E-mail: Koen.Binnemans@chem.kuleuven.be

†Electronic supplementary information (ESI) available: Characterization of the NdFeB magnet particles with full ICP-MS analysis, XRD diffractograms and SEM images. The TXRF analysis procedure and water treatment process are also discussed. Finally, the salting-out effect of salt anions on the water-solubility of [Hbet][Tf_2N] is shown. See DOI: 10.1039/c5gc00155b

other rare-earth elements during primary mining.[3,9] For example, the market for light rare earths is mainly driven by the demand for neodymium for NdFeB magnets, which means that enough ore has to be mined in order to meet the demand for neodymium, causing excess production of lanthanum and cerium which are far more abundant in most ores.[9] This unwanted co-production has led to the accumulation of large stocks of certain elements (La, Ce) while facing shortages of others (Y, Eu, Tb, Nd, Dy).[3,4,8–12] To remediate this problem and to secure the supply of certain critical REEs, new and increasingly efficient recycling schemes are being developed, opening up new possibilities for urban mining and rare-earth waste revalorization.[1,3,10,11,13–18] The potential for direct recycling from end-user products instead of storing the materials in landfills is very high. Unfortunately, the collection of used NdFeB magnets is still not widely organized, but manufacturers are now putting in place initiatives to collect end-of-life consumer products to retrieve the valuable magnets. Examples include air conditioning manufacturer Hitachi, that has started collecting and recycling initiatives for the NdFeB magnets in their products.[3] High quality cars are also being considered, since these can contain as much as hundred magnets per car. The number of recycling schemes for NdFeB magnets is growing rapidly as researchers try to develop more efficient processes to recover the rare earths. Many approaches have been proposed, not only hydrometallurgical routes, but also pyrometallurgical routes, glass slag methods, liquid metal extraction, gas-phase extraction methods, *etc*.[3] Several hydrometallurgical processes involve a preliminary roasting step to transform the NdFeB magnets into the metal oxides.[3,12] The dissolution of roasted magnets is partially selective since the dissolution of iron and cobalt oxides is kinetically slower than the dissolution of rare-earth oxides, but the iron and cobalt will always go into solution to a certain extent. It has been demonstrated by Vander Hoogerstraete *et al.* that by leaching with HCl while controlling the pH, the leached iron can be immediately reprecipitated as iron(III) hydroxide, effectively removing iron from the solution.[12]

The process described in this paper proposes an alternative that uses a fully *reusable* ionic liquid leaching agent instead of consuming mineral acids such as HCl, HNO_3 or H_2SO_4.[3] The carboxyl-functionalized ionic liquid betainium bis(trifluoromethylsulfonyl)imide, [Hbet][Tf_2N], (Fig. 1) is a particularly interesting ionic liquid because of its ability to selectively dissolve metal oxides.[19–22] It has also been used as organic phase in solvent extraction studies.[23–29] Recently, [Hbet][Tf_2N] was used for the design of a highly efficient and sustainable recycling process for rare earths from lamp phosphor waste powders.[22] While that recycling process was based on a different concept, it does however show that this ionic liquid is very suitable for the green recycling and processing of metal oxide containing materials. Such task-specific ionic liquids and ionometallurgy in general, continue to show great potential for this type of specialized applications, opening up new possibilities compared to traditional hydrometallurgy.[22,30–34] Many other domains such as extraction, electrochemistry, organic synthesis and catalysis, have also benefitted from the unique properties of ionic liquids. On many occasions, ionic liquids have shown to be very efficient green solvents and improve the safety of a process thanks to their negligible vapor pressure, low-flammability and relatively low toxicity.[15,17,34–39]

Here, [Hbet][Tf_2N] was used to selectively dissolve the valuable rare-earth oxides from the roasted NdFeB magnets, leaving most of the iron oxide matrix behind. Moreover, [Hbet][Tf_2N]–H_2O mixtures display thermomorphic behavior with an upper critical solution temperature (UCST) meaning that they will form one homogeneous phase above the cloud point temperature (55 °C for a 1 : 1 wt/wt system) and two phases below that temperature.[21] The metals will then selectively distribute between both phases. Such a combined leaching/extraction system that automatically separates the metals when cooling down the leaching solution is innovative and applicable to NdFeB magnet recycling. The resulting process is a sustainable alternative to mineral acid leaching processes that often require solvent extraction and produce significant volumes of waste water. Since [Hbet][Tf_2N] is a fluorinated ionic liquid, contamination of the water phase with ionic liquid should be avoided during the process. The loss of ionic liquid was circumvented by salting-out with Na_2SO_4.

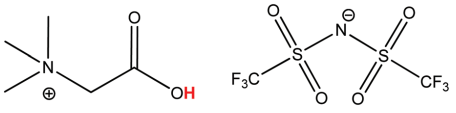

Fig. 1 Structure of the ionic liquid betainium bis(trifluoromethylsulfonyl)imide [Hbet][Tf_2N]. The acidic proton of the betaine group (pK_a 1.83), responsible for the dissolution of metal oxides, is highlighted in red.[40]

Experimental

Chemicals

$MgCl_2$ (98%), $Mg(NO_3)_2{\cdot}6H_2O$ (99%), $LiNO_3$ (99%), NaCl (98%), $NaClO_4{\cdot}H_2O$ (98%) and D_2O (99.9 atom% D) were obtained from Sigma-Aldrich (Diegem, Belgium), $CaCl_2$ (99.5%), $NaNO_3$ (99%), KNO_3 (99%), $Ca(NO_3)_2{\cdot}4H_2O$ (99%) and Na_2SO_4 (99%) were obtained from Chem-Lab (Zedelgem, Belgium). KCl (99.5%) and NaI (99.5%) were purchased from AppliChem (Darmstadt, Germany) and LiCl (99%) from Fisher Chemical (UK). $Nd(NO_3)_3{\cdot}6H_2O$ (99%) was obtained from Alfa Aeser (Karlsruhe Germany) and NH_4NO_3 (99%) from Chempur (Karlsruhe, Germany). NH_4Cl (99.5%), $Dy(NO_3)_3{\cdot}6H_2O$ (99%), $Co(NO_3)_2{\cdot}6H_2O$ (99%), 1,4-dioxane (99.9 wt%) and betaine hydrochloride (HbetCl) (99%) were obtained from Acros Organics (Geel, Belgium). Lithium bis(trifluoromethylsulfonyl)-imide (LiTf_2N) (99%) was purchased from IoLiTec (Germany). Oxalic acid dihydrate (>99.5%) and $Fe(NO_3)_3{\cdot}9H_2O$ (99%) were purchased from J.T. Baker. The silicone solution in isopropanol was obtained from SERVA Electrophoresis GmbH

(Germany) and the praseodymium, holmium and erbium standard solutions (1000 mg L^{-1}) were obtained from Merck (Overijse, Belgium). All chemicals were used as received without further purification.

Equipment and characterization

^{1}H NMR spectra were recorded on a Bruker Avance 300 spectrometer, operating at a frequency of 300 MHz. The samples were prepared by dissolving a small amount of product in heavy water (D_2O). The viscosity of the ionic liquid was measured using an automatic Brookfield plate cone viscometer, Model LVDV-II CP (Brookfield Engineering Laboratories, USA). The morphology and size distribution was determined by scanning electron microscopy (SEM) using a Philips XL 30 FEG device equipped with EDX. Powder X-ray diffraction (XRD) was carried out on an Agilent SuperNova X-ray diffractometer, using Mo Kα radiation (λ = 0.71073 Å) and a CCD detector. A Retsch ZM100 centrifugal mill (Gemini BV), a Retsch RS100 vibratory disc mill and a Retsch PM400 planetary ball mill were used for grinding of the magnet and a muffle furnace for roasting. A Heraeus Megafuge 1.0 centrifuge was used to separate the magnet residue from the ionic liquid after the leaching experiments. Total reflection X-ray fluorescence spectroscopy (TXRF) was performed with a Bruker S2 Picofox TXRF spectrometer equipped with a molybdenum source. For the sample preparation, plastic microtubes were filled with a small amount of ionic liquid sample (50 mg), 1 : 1 vol/vol ethanol–H_2O (700 μL) and a mix of standard solutions (1000 mg L^{-1}): praseodymium (100 μL), holmium (50 μL) and erbium (25 μL). This mix is the result of an optimization procedure to find suitable standards with X-ray energies that closely match the energy of the probed elements (Nd, Fe, Dy, Co) in order to reduce the effects of secondary absorption of X-rays by the matrix (ESI, Fig. S3 and Table S1†). High-matrix ionic liquid containing samples require such a procedure, while low-matrix aqueous solutions can be accurately analyzed using just one standard. The microtubes were then vigorously shaken on a vibrating plate (IKA MS 3 basic). Finally, a 1 μL drop of this solution was put on a quartz plate, previously treated with a silicone–isopropanol solution (Serva®) to avoid spreading of the sample droplet on the quartz plate. The quartz plates were then dried for 30 min at 60 °C prior to analysis. Each sample was measured for 5 min.

Synthesis of [Hbet][Tf_2N]

The ionic liquid [Hbet][Tf_2N] was synthesized according to a one-step literature method based on the reaction between HbetCl and $LiTf_2N$.[21,22] The level of chloride impurities was below 1 ppm (TXRF). Dry ionic liquid was obtained using a rotary evaporator. Increasing amounts of water were then added to obtain ionic liquids with different water contents. The water-saturated ionic liquid was prepared by keeping the ionic liquid in contact with an excess of water and then using the water-saturated ionic liquid phase (contains 14 wt% H_2O).

Magnet pre-processing: roasting and milling

The demagnetized NdFeB magnets were obtained from the University of Birmingham (UK) and Goudsmit Magnetics, and had the following composition (Table 1). The full ICP-MS trace analysis results are given in the ESI, Table S1.† The main difference between various NdFeB magnets lies in the cobalt and dysprosium content, which is added to high-end magnets in order to improve their magnetic and thermal properties. In reality, few magnets contain as much cobalt as magnet 1, but it is interesting to trace the movement of the valuable cobalt in any proposed recycling process. In this paper, the experiments were therefore mainly carried out with the magnet of type 1. At the end, the full recycling process was also tested for the magnet of type 2. Both magnets were demagnetized and then crushed and milled to obtain a magnet powder with a particle size < 400 μm.

The powders were then roasted using a conventional oven at 950 °C for 15 h to assure full conversion to the metal oxides as described by Vander Hoogerstraete *et al.*[12] An XRD diffractogram of the roasted magnet powder is given in the ESI (Fig. S2†). A proof-of-concept is also given for the roasting of magnets with microwaves. An analytical (monomodal) high-temperature microwave set-up was used to study the heating and roasting of NdFeB magnets with microwaves (Fig. 2).

The oven-roasted particles were then crushed to obtain three different particle sizes. In the first case, the particles were crushed with a pestle and mortar to obtain large particles with an average diameter of (310 ± 140) μm. The other two particle sizes were obtained by using a ball mill and passing the powder through 90 μm, 60 μm and 40 μm sieves. Two fractions were retained: the fraction <90 μm that did not pass the 60 μm sieve, and the <40 μm fraction. These fractions had an average diameter of (73 ± 40) μm and (6 ± 3) μm, respectively. The particle size was determined by SEM and ImageJ software (Fig. S1†).

Leaching experiments

Small glass vials (4 mL) were filled with a fixed amount of [Hbet][Tf_2N] (1 g) and 10 mg of roasted magnet particles which resulted in a solid/liquid ratio of 10 mg g^{-1}. Water-containing

Table 1 Main composition (wt%) of two different NdFeB magnets. Magnet 1 is a high-performance cobalt- and dysprosium-rich magnet, while magnet 2 is a standard hard disk drive magnet with small amounts of cobalt and dysprosium

Magnet 1	Composition (wt%)	Magnet 2	Composition (wt%)
Fe	58.16	Fe	66.01
Nd	25.95	Nd	29.17
Dy	4.22	Dy	1.98
Co	4.21	Co	0.36
B	1.00	B	1.02
Total[a]	93.5	Total[a]	98.54

[a] The total does not add up to 100% due to the presence of trace elements (Al, Nb, Pr, Cu, Mn, N, O, C, Si,...) and the analytical error associated with ICP-MS measurements. The full detailed composition is given in the ESI, Table S1.

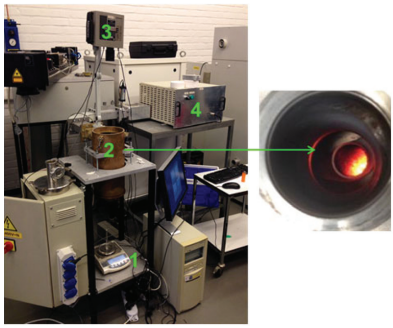

Fig. 2 Analytical (monomodal) high-temperature microwave set-up, consisting of a microwave cavity (2) with a quartz table connected to a balance (1), an infra-red temperature probe (3) and a high-power microwave source (4).

ionic liquid (2.5–10 wt%) or a 1 : 1 wt/wt [Hbet][Tf_2N]–H_2O mixture was used depending on the experiment. A magnetic stirring bar was then added to each of the vials and they were sealed using a plastic screw cap. The dissolution experiments were carried out in an oil bath at a set temperature while stirring (600 rpm). The samples were then placed in a centrifuge (5300 rpm, 30 min) to precipitate the undissolved magnet residue. The metal content in the ionic liquid was determined using total reflection X-ray fluorescence spectroscopy (TXRF).

Quantitative ^{1}H NMR

The dissolution of ionic liquid in the water phase was studied and optimized in order to assure that no ionic liquid would be lost during the process and no contamination of the water phase would occur. The concentration of ionic liquid in the aqueous phase was determined using quantitative ^{1}H NMR with 1,4-dioxane as an internal standard. A sample of the water phase was taken (100 mg) and a known amount of 1,4-dioxane–D_2O solution was added so that the concentration of 1,4-dioxane internal standard would be comparable to the amount of ionic liquid in the water phase. The ^{1}H NMR spectrum of 1,4-dioxane shows one peak at δ = 3.6, corresponding to its 8 equivalent protons and does not overlap with the spectrum of water or [Hbet][Tf_2N]. The relative concentration *versus* 1,4-dioxane and the absolute concentration of [Hbet][Tf_2N] were calculated by integration of the peaks using Spinworks software.

Optimized full recycling process

First the magnets were roasted. This was done in a conventional oven as described by Vander Hoogerstraete *et al.*,[12] or in a microwave oven at 950 °C. The second method is preferred since it is more energy-efficient. The roasted magnets were then crushed/milled to reduce their particle size. This powder was leached in a 1 : 1 wt/wt [Hbet][Tf_2N]–H_2O mixture for 24–48 h (80 °C) to obtain full leaching of the REEs (Nd and Dy) and partial leaching of cobalt and iron. Thanks to the thermomorphic properties of the [Hbet][Tf_2N]–H_2O system, the solution is homogeneous during leaching (80 °C) but phase separates when cooling it to room temperature (25 °C). The dissolved metals distribute amongst the two phases with iron(III) going to the ionic liquid phase and the REEs and cobalt(II) going to the aqueous phase. $NaNO_3$ is used as an additive to enhance the separation of the metals. The two phases were then separated from each other and the metal content was determined by TXRF. The water phase was stripped with stoichiometric amounts of pure (solid) oxalic acid (10 min, 25 °C, stirring) to precipitate the REEs and cobalt(II) as a mixed oxalate. The oxalate precipitate was removed by filtration and the cobalt(II) was fully removed by contacting the precipitate with aqueous ammonia and shaking it (2000 rpm) for 10 min at 25 °C. The resulting, highly pure, REE oxalate (>99.9 wt%) can be calcined to obtain the rare-earth oxides. The iron(III)-containing ionic liquid was stripped with an oxalic acid solution. This transfers the iron(III) to the water phase as a soluble oxalate complex, effectively cleaning the ionic liquid and regenerating it by reprotonation of the carboxylate groups. The waste water was cleaned using Na_2SO_4 to salt-out the remaining traces of ionic liquid, and $Ca(OH)_2$ to precipitate the $[Fe(C_2O_4)_3]^{3-}$ complex as $Fe(OH)_{3(s)}$ and $CaC_2O_{4(s)}$.

Results and discussion

Roasting

Roasting or oxidative roasting of NdFeB magnets transforms all the elements in the magnet into their respective oxides. The resulting roasted magnet consisted mainly of Fe_2O_3, Nd_2O_3, Dy_2O_3 and CoO. The roasting of metallic cobalt at 950 °C leads to the formation of cobalt(II) oxide.[41] The oxidative roasting of NdFeB magnets was done in an oven as described by Vander Hoogerstraete *et al.* (950 °C, 3–15 h).[12] But here a proof-of-concept is also given for an alternative, more sustainable, roasting process based on microwave heating. Microwave energy has a lot of potential in mineral treatment operations such as heating, drying, leaching, roasting and smelting.[42–44] Hua *et al.* reported for example a 4 to 17 times increase in roasting speed for a copper sulfide concentrate.[44] Microwave heating is a non-contact and on/off heating technique that offers a number of advantages over conventional heating such as material-selective and rapid heating due to the fact that the material is heated from the inside (the material itself is the heating source). This significantly reduces the energy consumption and also improves the safety of the process.[42] The strong coupling of microwaves with magnetic metals results in a very fast heating of the magnet (Fig. 3) and an energy-efficient roasting compared to traditional oven roasting where the air has to be heated first.[45] The fact that the (demagnetized) magnet powder can be heated to 1000 °C in a few seconds is quite remarkable and shows the potential of microwave roasting. The very fast heating can also be used to

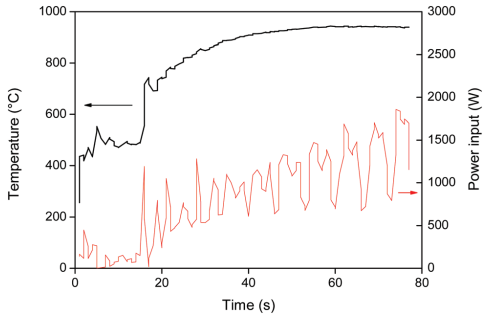

Fig. 3 Heating of demagnetized NdFeB magnet particles (≈400 μm) with a monomodal high-temperature microwave set-up. The temperature was raised in two steps: first it was stabilized at 500 °C and then at 950 °C. The power input (W) and temperature (°C) are shown *versus* time (s). The temperature range under 250 °C was not accessible with the infra-red temperature probe.

quickly demagnetize NdFeB magnets by raising the temperature above the Curie temperature (312 °C).[46] Slower heating speeds are of course also achievable by reducing the power input.

Leaching of NdFeB magnets in [Hbet][Tf_2N]

The protonated carboxyl-functionalized ionic liquid betainium bis(trifluoromethylsulfonyl)imide [Hbet][Tf_2N] (Fig. 1) has the ability to dissolve certain metal oxides, including rare-earth oxides (eqn (1)).[20,21]

$$REE_2O_3 + 6[Hbet][Tf_2N] \rightarrow 2[REE(bet)_3][Tf_2N]_3 + 3H_2O \quad (1)$$

Other metal oxides like iron and cobalt oxides are poorly soluble in [Hbet][Tf_2N].[20,21] This difference in solubility can be exploited to obtain the (partially) selective dissolution of the valuable REE oxides from the roasted NdFeB magnets. Important parameters affecting the selectivity and kinetics are the roasted magnet particle size and the water content in the ionic liquid. Water accelerates the dissolution of metal oxides because it lowers the viscosity, facilitates the exchange of protons from the betaine groups and enhances the solvation of ions in the ionic liquid.[20–22] The dissolution of metal oxides was studied by Nockemann *et al.* and is driven by the reactivity of the carboxylic acid group (pK_a 1.83) located on the cation of the ionic liquid.[20,21,40,47] The deprotonated zwitterionic betaine groups are also responsible for the complexation of the dissolved metal ions. The Tf_2N^- anions do not participate in the complex formation but they are essential for the formation of betainium-based *hydrophobic* ionic liquid, with a low viscosity and good thermal stability.[22,47,48]

First, water-containing ionic liquid was tested (2.5, 5, 7.5 and 10 wt% H_2O) without exceeding the solubility limit of water in the ionic liquid (14 wt%). Roasted NdFeB magnet particles were then added to the ionic liquid (10 mg g^{-1}) and stirred (600 rpm) at 90 °C for increasing amounts of time. The influence of the water content on the leaching kinetics of the roasted magnet is shown for three different particle sizes (310 ± 140) μm, (73 ± 40) μm and (6 ± 3) μm. The leaching of the largest particles (≈300 μm) is relatively slow but more selective towards the REE oxides (Fig. 4). The addition of water accelerates the leaching but it is clear that the leaching of the large particles is still too slow to fully dissolve the REE oxides from these roasted magnet particles within 100 h (Fig. 4). This is not due to the solubility of these oxides, since in the same conditions, commercial Nd_2O_3 and Dy_2O_3 could be fully dissolved in [Hbet][Tf_2N] within 24 h. The reason is that the particles are large (≈300 μm) and consist mainly of iron oxides (≈60 wt%), which are very poorly soluble in [Hbet][Tf_2N]. The leaching of the REE oxides embedded in this insoluble iron oxide matrix is therefore a slow process.

The fact that the particles consist of a large insoluble Fe_2O_3 matrix hampers the efficient dissolution of the rare-earth oxides because it is very difficult for the ionic liquid to create deep channels in these iron oxide particles. SEM images and surface EDX analysis revealed that on the surface, all the Nd_2O_3 had been leached selectively without dissolving the Fe_2O_3 (Fig. 5). This confirms that it is possible to selectively leach the Nd_2O_3 from these particles. However, the penetration of the acidic ionic liquid in the particles was insufficient to dissolve the rare-earth oxides held in the core of the particles (Fig. 6). The particle size before and after leaching did not change significantly which shows that the large iron matrix is not dissolved and that the rare-earth oxides are leached, leaving behind the iron oxide matrix as a porous structure (Fig. 6). The visible denting of the surface is around 10–20 μm deep (Fig. 6) and EDX shows that the surface is free of Nd_2O_3 (Fig. 5). By reducing the particle size, the dissolution of rare-

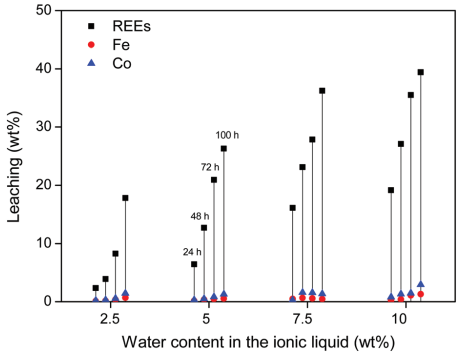

Fig. 4 Leaching (%) of Co, Fe and REEs (Nd + Dy) from large roasted NdFeB particles (≈300 μm). The leaching is shown as function of time (24, 48, 72 and 100 h) and as function of the water content in the ionic liquid (2.5, 5, 7.5 and 10 wt%). The solutions were stirred at 600 rpm and 90 °C.

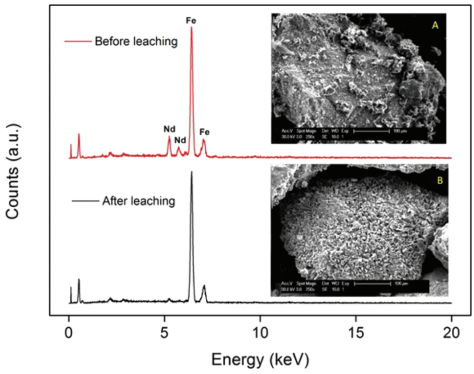

Fig. 5 SEM images (magnified 250×) and EDX spectrum of the surface of the large NdFeB particles (≈300 μm) before (A) and after (B) leaching.

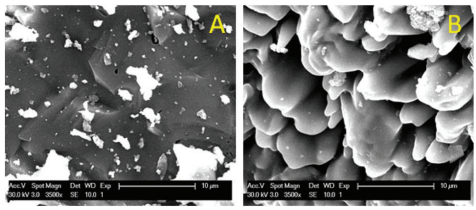

Fig. 6 SEM images (magnified 3500×) of the surface of the particles before (A) and after (B) leaching.

earth oxides should therefore be much faster, while retaining a certain selectivity towards the rare-earth oxides.

The leaching of these smaller particles (≈70 μm and 6 μm) was investigated in the same manner as the large particles, by measuring the leaching of rare earths, iron and cobalt in the ionic liquid with increasing water content. It is clear from Fig. 7 that the leaching of the milled powder is much faster and allows full leaching of the REE content within 48–72 h. Unfortunately, the leaching of iron and cobalt also increases significantly.

While these results are encouraging, the leaching in water-unsaturated ionic liquid is clearly slow and selective for large particles (Fig. 4) or fast and less selective for smaller particles (Fig. 7). To get full dissolution of the REEs, small particles must be used and too much iron and cobalt goes into solution. This would require additional solvent extraction steps to isolate the REEs and would complicate the recycling process. Instead, an alternative leaching system is proposed based on the same ionic liquid but with an excess of water (>13 wt%) so that it forms a biphasic system at room temperature. This system is very promising and innovative as it combines leaching with metal extraction (separation) in one convenient step

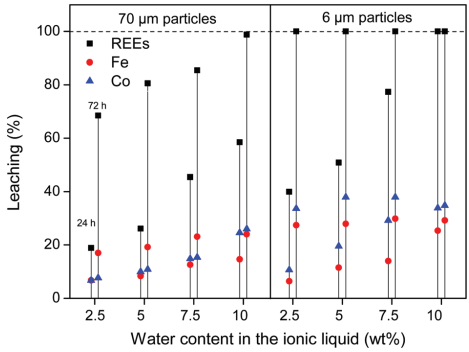

Fig. 7 Leaching (%) of Co, Fe and REEs (Nd + Dy) from two different milled roasted NdFeB magnets (≈70 μm and 6 μm). The leaching is shown as function of time (24 and 72 h) and as function of the water content in the ionic liquid (2.5, 5, 7.5 and 10 wt%). The solutions were stirred 600 rpm at 90 °C.

thanks to the thermomorphic properties of this ionic liquid/water system.

Thermomorphic leaching/extraction in a [Hbet][Tf_2N]–H_2O system

The [Hbet][Tf_2N]–H_2O system shows thermomorphic behavior with an upper critical solution temperature (UCST).[21,26,27] This means that above a certain temperature, called the cloud point temperature, it forms one homogeneous phase and under this temperature it is a biphasic system.[26,27] In this biphasic system, the iron is mostly present in the ionic liquid phase, while the rare-earth ions and cobalt are mostly present in the water phase due to the higher affinity of Fe(III) ions for betaine compared to REE(III) and Co(II) ions. This observation led us to investigate the possibilities of a thermomorphic leaching system with its automatic metal separation once the system becomes biphasic at room temperature. Such a thermomorphic leaching/extraction system has to the best of our knowledge not been described in the literature yet. The combined leaching/extraction process starts by leaching the roasted NdFeB magnets in a 1 : 1 wt/wt blend of [Hbet][Tf_2N]–H_2O at 80 °C (above the cloud point temperature) so that it forms one homogeneous phase. Afterwards, the solution is cooled again to room temperature so the mixture can phase separate into a valuable REE/cobalt-enriched water phase and an iron-enriched ionic liquid phase (Fig. 8).

First, the leaching of the roasted NdFeB particles was tested using a 1 : 1 wt/wt [Hbet][Tf_2N]–H_2O mixture. The leaching of different particle sizes is again shown (300 μm, 70 μm and 6 μm) over time at 80 °C. At this temperature the system forms one homogeneous phase. The samples were then cooled to room temperature to phase separate and centrifuged to precipitate the remaining magnet residue. The total leaching percentage was determined by combining the measured metal

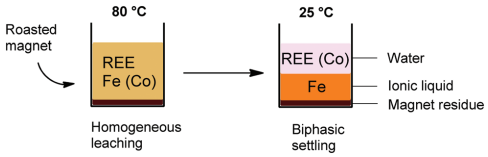

Fig. 8 Schematic overview of the biphasic leaching-settling process using a thermomorphic ionic liquid. The [Hbet][Tf_2N]–H_2O mixture forms one homogeneous phase at 80 °C and forms two phases at room temperature.

content in the water phase and in the ionic liquid phase. The leaching is faster compared to experiments with lower water contents in the ionic liquid (Fig. 4 and 7). The effect of the particle size is similar in the sense that full leaching of the REEs is achieved faster for smaller particles but with less selectivity and slower for larger particles but with higher selectivity (Fig. 9).

The leaching temperature of the process was set at 80 °C, because the leaching is sufficiently fast at this temperature in this water-saturated system. At 80 °C the thermomorphic ionic liquid/water system is also certainly homogeneous (cloud point temperature is 55 °C for a 1 : 1 wt/wt [Hbet][Tf_2N]–H_2O system). Although closed vials were used, temperatures should not exceed 90 °C due to pressure buildup. At 80 °C, the viscosity of the ionic liquid/water system is also sufficiently low and almost equal to pure water (Fig. 10). The high temperature and low viscosity are important because the leaching kinetics of this material is slow, especially since the rare earths are held in a largely insoluble iron oxide matrix.

Next, the metal separation over the two phases was optimized by studying the distribution of Nd(III), Dy(III), Fe(III) and

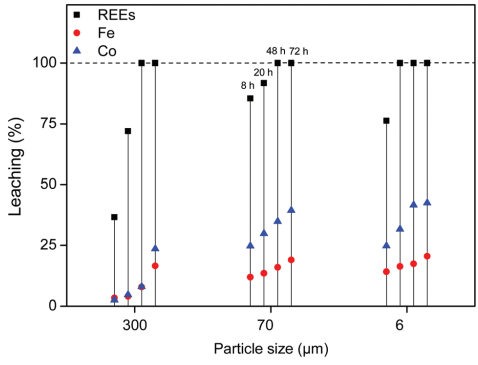

Fig. 9 Leaching (%) of REEs, iron and cobalt from roasted NdFeB magnets (10 mg) using a 1 : 1 wt/wt [Hbet][Tf_2N]–H_2O system (2 g). The leaching was carried out at 80 °C for 8 h, 20 h and 48 h while stirring (600 rpm).

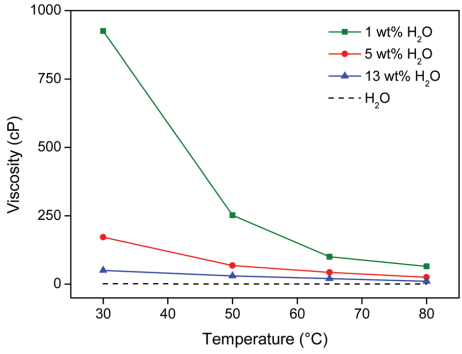

Fig. 10 Viscosity (cP) of [Hbet][Tf_2N] as function of its water content (wt%) and the temperature (°C). The viscosity of water is shown as a reference.

Co(II) ions between the ionic liquid and the water phase. Onghena and Binnemans recently showed that Fe(III) can be extracted to the [Hbet][Tf_2N] phase, while the REE(III) ions remain in the aqueous phase.[29] We also tested the effect of inorganic salts in the water phase on the distribution of the metals. The advantage of the [Hbet][Tf_2N] ionic liquid is that Tf_2N^- is one of the most difficult anions to displace from the ionic liquid so that no anion exchange reactions will occur for [Hbet][Tf_2N]. A high salt concentration could therefore be used in the water phase without detecting any traces of the anions in the ionic liquid. A distinction must be made between the effect of salt anions and salt cations. Water-soluble salt anions can form complexes with the metal ions and therefore change the affinity of the metal ions for the water phase. Additionally, salt anions and cations can influence the solubility of the ionic liquid in the water phase.[49] It was therefore interesting to investigate if salts could influence the betaine content in the water phase and thus influence the distribution of iron(III) as it forms iron-betaine complexes rather than aqua complexes. A synthetic mix (4 × 1000 ppm) of hydrated $Nd(NO_3)_3$, $Dy(NO_3)_3$, $Fe(NO_3)_3$ and $Co(NO_3)_2$ was mixed with a 1 : 1 wt/wt [Hbet]-[Tf_2N]–H_2O system. This ionic liquid/water mixture was heated for 15 min at 80 °C to obtain a homogeneous phase similar to the one formed during leaching. The mixture was then allowed to cool so that it would phase separate and equilibrate. The metal content was determined in each phase and expressed as the distribution ratio between the water phase and the ionic liquid phase (eqn (2)). A distribution ratio larger than 1 corresponds to a greater affinity for the water phase than for the ionic liquid phase.

$$D = \frac{[M]_{aq}}{[M]_{IL}} \quad (2)$$

First the effect of salt anions is shown. It is clear from Fig. 11 that this biphasic leaching process effectively allows

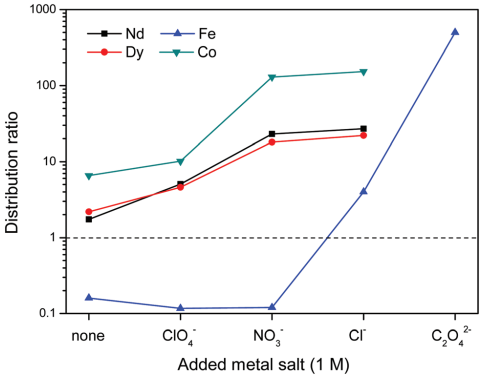

Fig. 11 Influence of added metal salts (1 M) with varying anions on the distribution ratio of Nd(III), Dy(III), Fe(III) and Co(II) ions in a biphasic [Hbet]-[Tf_2N]–H_2O system. A high distribution ratio corresponds to a greater affinity for the water phase. Oxalate forms highly insoluble complexes with REE(III) and Co(II) ions.

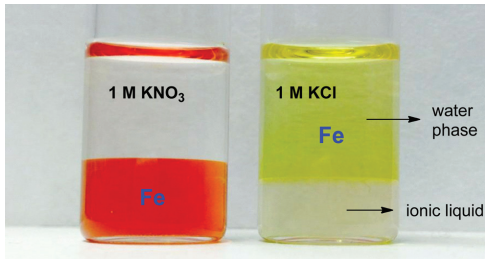

Fig. 12 Reversal of iron(III) distribution when adding a non-coordinating salt (KNO_3) compared to a salt with coordinating anions (KCl). The upper and lower phase consist of water and [Hbet][Tf_2N], respectively.

the separation of the valuable elements (Nd, Dy, Co) from iron. The separation of iron(III) from the REE(III) and Co(II) ions is quite efficient because the strong iron-betaine complexes cause the iron to stay in the ionic liquid, while the Nd, Dy and Co ions are present in the water phase as aqua complexes.

The increased distribution factors for Nd(III), Dy(III) and Co(II) when adding coordinating anions are due to a better coordination of metal ions in the water phase compared to the situation with non-coordinating ions such as Tf_2N^- (in the case of pure water) or ClO_4^-. The presence of coordinating anions such as nitrates or chlorides significantly improves the solubility of the REE(III) and Co(II) ions in the water phase, but too strongly coordinating anions such as sulfates or oxalates cause precipitation. However, the most striking feature in Fig. 11 is the transfer of iron(III) to the water phase in the presence of strongly coordinating anions such as chloride or oxalate anions (1 M). More weakly-coordinating anions such as nitrates and perchlorates do not cause transfer of iron(III) to the water phase because iron is preferentially present as the iron-betaine complex in that case. A photograph has been added to help visualize the reversal of the iron(III) distribution when adding coordinating anions such as chloride anions or oxalate anions (Fig. 12). To the best of our knowledge, this is the first time that this is described for the [Hbet][Tf_2N]–H_2O system. Switching between salt media effectively creates a tunable extraction system for iron(III). This phenomenon will also be used to strip iron from the water phase using oxalate anions which form the highly water-soluble $[Fe(C_2O_4)_3]^{3-}$ complex, resulting in high distribution factors.

Salt cations on the other hand, cannot form complexes with the metal ions. They can however impact the solubility of ionic liquid in the water phase and therefore also the solubility of betaine, which would (slightly) affect the distribution factor for iron(III) which is present as an iron-betaine complex. In this context, the concept of salting-in and salting-out salts is important. The "Hofmeister series" ranks different anions and cations according to their salting-in or salting-out behavior, meaning their ability to influence the solubility of organic compounds or proteins in the water phase.[50] Salting-out ions diminish the solubility of organic molecules in aqueous solutions and cause aggregation, while salting-in ions enhance the solubility of organic molecules (ionic liquid) in aqueous solutions.[49–54] The effect of anions and cations on the ionic liquid [Hbet][Tf_2N] was determined by measuring the [Hbet]-[Tf_2N] content in the water phase when adding different salts. This was done using ^{1}H NMR and 1,4-dioxane as an internal standard. The value obtained for the pure [Hbet][Tf_2N]–H_2O system was 14.0 wt% which is in good agreement with the values reported in the literature.[29] The discussion of the salting-out effect is limited here to the effect of salt cations (Fig. 13) because salt anions form complexes with metal ions which affects the metal distribution much more than their salting-out effect. The salting-out effect of anions is however included in the ESI (Fig. S4†). The salting-out effect for cations follows the order $NH_4^+ < K^+ < Na^+ < Li^+ < Ca^{2+} < Mg^{2+}$ (Fig. 13) and the salting-out effect of anions follows the order $ClO_4^- < I^- < NO_3^- < Cl^- < SO_4^{2-}$ (Fig. S4†). This is in agreement with the effect of salts on other ionic liquid/water systems such as [C_4mim][CF_3SO_3]–H_2O and [C_4mim][Tf_2N]–H_2O.[51,53,54] Furthermore, a higher salt concentration increases the salting-in or salting-out effect of a salt, respectively.

The distribution ratios for Co(II), Nd(III), Dy(III) and Fe(III) were then determined using these same salts (Fig. 14). When salts cause a salting-in effect compared to pure water (*e.g.* NH_4NO_3 or KNO_3), the iron is more present in the water phase (D increases). For salts that cause a salting-out compared to pure water, the iron is less present in the water phase (D decreases). This is in agreement with the hypothesis that the solubility of betaine in the water phase is lowered by salting-out salts and therefore the affinity of iron(III) for the water phase is lowered since it has more affinity for betaine than water. Note however, that the salting-out effect of cations on

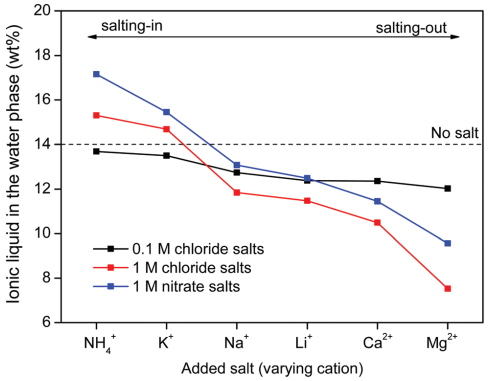

Fig. 13 [Hbet][Tf_2N] content (wt%) in the water phase when adding salts with varying cations and concentrations. The [Hbet][Tf_2N] content was determined using ^1H NMR and 1,4-dioxane as an internal standard. When no salt is added, the water phase contains 14 wt% of [Hbet]-[Tf_2N].[29]

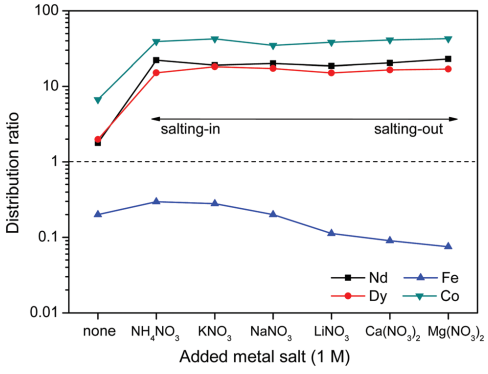

Fig. 14 Influence of added metal salts (1 M) with varying cations on the distribution ratio of Nd(III), Dy(III), Fe(III) and Co(II) ions in a biphasic [Hbet]-[Tf_2N]–H_2O system. A high distribution ratio corresponds to a greater affinity for the water phase.

the distribution factor of iron(III) (Fig. 14) is much smaller than the coordination effect of the anions (Fig. 11). The distribution of the other metal ions Nd(III), Dy(III) and Co(III) shows no dependence on salting-in or salting-out salts since they are present as aqua-complexes in the water phase as their affinity for betaine is much lower. They do however show a large difference between pure water and water + salt systems since the presence of counter ions such as nitrate ions significantly enhances the solubility of these aqua complexes by providing water-miscible counter ions, which are not formed during the dissolution of the metal oxides.

To support the fact that salting-out behavior is directly responsible for the decrease of iron(III) in the water phase, several nitrate salts (1 M) were added and the resulting Nd/Fe separation factors α (eqn (3)) were plotted *versus* the ionic liquid content in the water phase (wt%) (Fig. 15). The separation factors are positive because D_{Nd} is larger than D_{Fe}, meaning that neodymium has a larger affinity for the water phase as defined by eqn (2).

$$\alpha_{Fe}^{Nd} = \frac{D_{Nd}}{D_{Fe}} \quad (3)$$

Salt cations do not directly interact with the iron(III) cations, which is why the observed effects (Fig. 15) can be solely attributed to changes in the water-solubility of betaine due to salting-in or salting-out salts.

The trend follows the cation salting-out series (Fig. 13) which is a strong indicator that the salting-out effect of the salts is indeed responsible for the trend in REE/iron separation. In general, the addition of nitrate salts also improves the separation compared to a system without nitrates, because of the availability of counter-ions (NO_3^-) for the dissolved REE(III) and Co(II) ions in the water phase. Based on Fig. 15, it is evident that the addition of the right inorganic salt is beneficial for this leaching/extraction system. It is however important to find a salt that does not interfere with the leaching or stripping process and that is not too expensive. $NaNO_3$ was chosen because it significantly enhances the transfer of Nd(III), Dy(III) and Co(II) ions to the water phase while keeping iron(III) in the ionic liquid phase. $NaNO_3$ is not the best salting-out agent but $LiNO_3$ is too expensive and Ca^{2+} or Mg^{2+} salts cannot be used due to the fact that they would co-precipitate with oxalic acid, which was used for stripping the metal ions later on. NaCl cannot be used since chloride ions cause transfer of Fe(III) ions to the water phase. The $NaNO_3$ present in [Hbet]-[Tf_2N]–H_2O enhances the properties of the extraction system

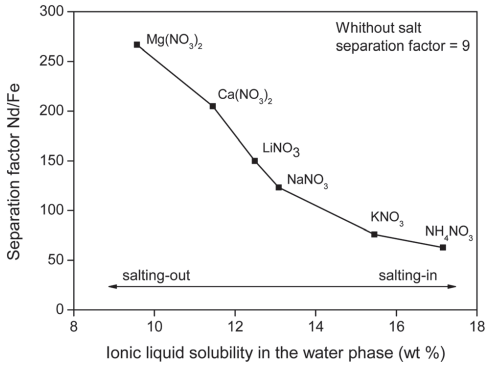

Fig. 15 Nd/Fe separation factor as function of the [Hbet][Tf_2N] content in the water phase (wt%). The corresponding salts (1 M) are shown as labels.

Table 2 Relative metal composition of the water phase (wt%) prior to stripping. Two different types of magnets and various particle sizes are shown. The water phase contained 1 M $NaNO_3$ to optimize the metal separation. During stripping the product is further purified

NdFeB Magnet	Type 1	Type 1	Type 1	Type 2
Particle size (μm)	300	70	6	350
REEs (wt%)	98.5	93.8	92.1	98.1
Fe (wt%)	1.1	2.3	2.8	1.8
Co (wt%)	0.4	3.9	5.1	<0.1

but will not cause impurities in the ionic liquid (no extraction of NO_3^- and Na^+ in the ionic liquid) and will not cause impurities in the final rare-earth product since it does not precipitate with oxalic acid. The salt can be added after leaching, just before cooling down (phase separation) or it can be added from the beginning of the process since it was tested that the presence of $NaNO_3$ (1 M) had no effect on the leaching speed, efficiency or selectivity.

The result of this combined leaching/extraction process is that a REE-rich aqueous phase is obtained while keeping iron in the ionic liquid. This allows the use of less selective (faster) leaching conditions (*e.g.* 6 μm particles), since the co-leached iron is automatically separated from the leached REEs (Fig. 15) once the mixture cools down and phase separates. The resulting purity of the aqueous REE-rich phase after leaching for 48 h (full REE leaching) is shown in Table 2. Besides REEs, cobalt and traces of iron still remain in the water phase. These will be fully removed during the stripping step and a cobalt-removal step. In this way, a final REE oxide can be obtained with a purity >99.9 wt%, without the need for solvent extraction.[15,17] The results are also shown for a magnet of type 2 that contains very little cobalt (Table 1).

Metal stripping and recovery of ionic liquid

After separating the magnet residue, the metal ions are removed and the ionic liquid can be fully regenerated without losses. The most convenient technique is to separate the two phases and to add oxalic acid to the water phase, which forms polymeric precipitates with the REE(III) and Co(II) ions (eqn (4) and (5)). Any traces of iron in the water phase will not co-precipitate which results in a highly pure mixed REE/cobalt oxalate precipitate.[55] The REE content in the oxalate varies between 95–100 wt% (Table 2) depending on the initial cobalt content (Table 1).

$$2REE^{3+}_{(aq.)} + 3H_2C_2O_4 \rightarrow (REE)_2(C_2O_4)_{3(s)} + 6H^+ \quad (4)$$

$$Co^{2+}_{(aq.)} + H_2C_2O_4 \rightarrow CoC_2O_{4(s)} + 2H^+ \quad (5)$$

The oxalate precipitation stripping method is very efficient, meaning that stoichiometric amounts of oxalic acid are sufficient to obtain 100% stripping (Fig. 16). The stripping is fast (complete within 10 min) even at room temperature.

This rare-earth oxalate product with traces of cobalt, can be further purified by treating it with aqueous ammonia which

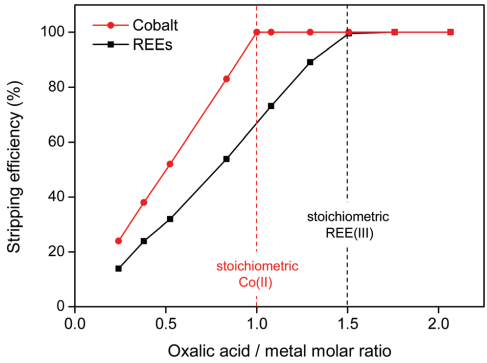

Fig. 16 Precipitation stripping of REE(III) (Nd + Dy) and Co(II) ions from the water phase, using solid oxalic acid (stir 600 rpm, 10 min at 25 °C). A stoichiometric amount of oxalic acid (3 : 2 for REEs and 1 : 1 for Co) is sufficient to achieve full precipitation.

readily dissolves the cobalt(II) oxalate as an hexaamine complex (eqn (6)).[56]

$$CoC_2O_{4(s)} + 6NH_3 \rightarrow [Co(NH_3)_6]^{2+} + C_2O_4{}^{2-} \quad (6)$$

This cobalt removal step is very efficient and fast (<10 min at 25 °C) and is capable of removing more than 99.9 wt% of the cobalt(II) (Fig. 17). An NH_3/cobalt(II) molar ratio of 100 is required to obtain full removal of the cobalt (Fig. 17), but this is still a small amount since cobalt is only present in trace amounts in the oxalate product.

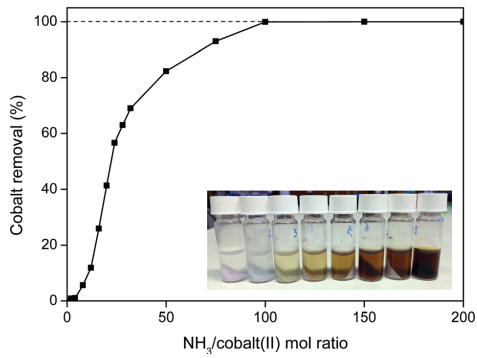

Fig. 17 Cobalt(II) removal from the mixed REE/Co(II) oxalate precipitate, using increasing concentrations of aqueous ammonia. The ammonia/cobalt(II) ratio is plotted *versus* the cobalt removal efficiency (%). As inset, the color change is shown using some of the samples, with increasing amounts of ammonia from left to right. The samples were shaken (2000 rpm) for 10 min.

The resulting pure REE oxalate after cobalt removal has a high purity (>99.9 wt%) and can be calcined in an oven to obtain the rare-earth oxides (Nd_2O_3 and Dy_2O_3) (eqn (7)) which can be used as precursor for the synthesis of NdFeB magnets.[57,58]

$$(REE)_2(C_2O_4)_{3(s)} + \frac{2}{2}O_2 \xrightarrow{950\,^{\circ}C} REE_2O_{3(s)} + 6CO_2 \quad (7)$$

Next, the iron(III) is removed from the ionic liquid by contacting it with an oxalic acid (aqueous) solution or by reusing the (just cleaned) water phase and adding some solid oxalic acid. The samples are then shaken to form the iron(III) oxalate complex that is transferred to the water phase (eqn (8)).

$$[Fe(bet)_3][Tf_2N]_3 + 3H_2C_2O_4 \rightarrow [Fe(C_2O_4)_3]^{3-} + 3[Hbet][Tf_2N] + 3H^+ \quad (8)$$

Iron(III) oxalate is very soluble in water as the complex $[Fe(C_2O_4)_3]^{3-}$, which means that the iron will be fully transferred to the water phase (Fig. 18) with a high distribution factor, as was shown previously (Fig. 11). A slight excess of oxalic acid is sufficient to obtain >99% stripping (back extraction) as shown in Fig. 18. The ionic liquid is also automatically regenerated by the reprotonation of the betaine groups (eqn (8)) and can be reused as such since it is now free of metal ions.

The complete stripping process is summarized in Fig. 19. It is highly efficient since it only consumes small (stoichiometric) amounts of oxalic acid to achieve both the cleaning of the ionic liquid phase from iron(III) and the precipitation of REEs and cobalt(II) from the water phase. The REE oxalate product was calcined to obtain the corresponding oxides with high purity (>99.9 wt%). After stripping, the ionic liquid can be reused as such.

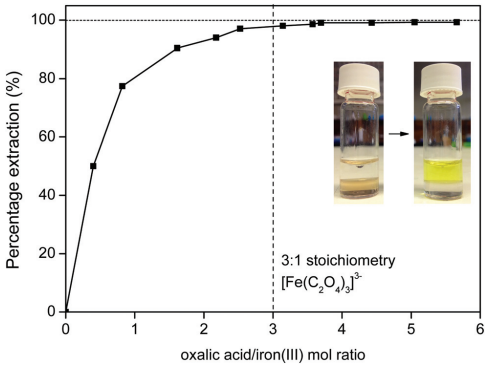

Fig. 18 Stripping of iron(III) from the ionic liquid to the water phase using oxalic acid. The oxalic acid regenerates the ionic liquid and transfers the iron(III) ions to the water phase as the highly soluble $Fe(C_2O_4)_3^{3-}$ complex. The photograph shows the transfer of iron from the ionic liquid phase (left) to the water phase (right).

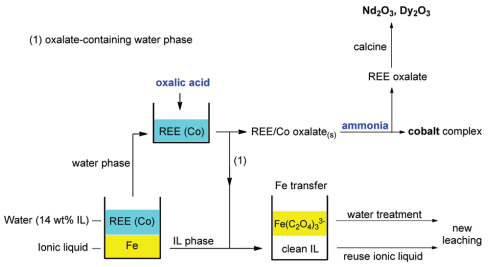

Fig. 19 Overview of the proposed stripping process based on oxalic acid precipitation of REE(III) and Co(II) ions and phase transfer of iron(III) as a water-soluble oxalate complex. This process allows full recovery of the ionic liquid. The cobalt can be removed by treating the mixed REE/Co oxalate precipitate with aqueous ammonia.

The water phase can be further treated to remove the iron(III) oxalate complex and fully retrieve the ionic liquid that is still dissolved in the water phase. An efficient water treatment method was designed, which is discussed in detail in the ESI (Fig. S5†). Basically, the iron is removed by adding $Ca(OH)_2$ to precipitate the soluble $[Fe(C_2O_4)_3]^{3-}$ complex as $Fe(OH)_{3(s)}$ and $CaC_2O_{4(s)}$. The recovery of ionic liquid from the water phase can be done with various techniques such as adsorbents, specialized membranes, electrodialysis or nanofiltration.[59–63] However, a very straightforward approach is the salting-out of the ionic liquid using strong (cheap) salting-out agents such as Na_2SO_4 (Fig. 20). This strong salting-out agent reduces the loss of ionic liquid in the water phase to less than 0.15 wt% (compared to 14 wt% without salt). This guarantees an almost full recovery of the ionic liquid which is required to avoid contamination of the water phase. In order to avoid consumption of Na_2SO_4, this salting-out step can be performed in an evapor-

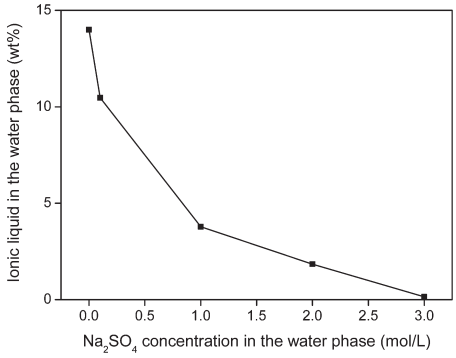

Fig. 20 Salting-out of ionic liquid from water using Na_2SO_4. This way, loss of ionic liquid can be avoided.

ation pond in which the rate of incoming water is equal to the evaporation rate, effectively keeping the Na_2SO_4 concentration constant while continuously salting-out the ionic liquid from the incoming waste water.

No regeneration or cleaning of the ionic liquid is necessary because [Hbet][Tf_2N] does not undergo anion exchange. According to the Hofmeister series, Tf_2N^- cannot be displaced by salt anions such as NO_3^-, Cl^- or SO_4^{2-} which lie at the opposite side of the Hofmeister series. High concentrations of Na_2SO_4 will therefore not affect the purity of the ionic liquid. Even at 3 M Na_2SO_4, the sulfate content in the ionic liquid was below detection limit (TXRF). It was shown in previous work that the ionic liquid also had an excellent thermal stability up to 200 °C.[22] This guarantees a good reusability and explains why no loss of efficiency was observed after 3 leaching/stripping cycles. An overview of the proposed recycling process is shown in Fig. 21. This process recovers over 99% of the rare earths in the NdFeB magnet with a purity >99.9 wt%, without the need for solvent extraction. The ionic liquid was also fully recovered to avoid contamination of the water phase. This process is therefore a sustainable alternative compared to mineral acid leaching and solvent extraction.

As a final remark it is interesting to discuss the possibility of microwave heating of ionic liquids. In most of our experiments, the ionic liquid was heated by a conventional heating source. However, since the leaching of the REE oxides in the ionic liquid requires heating (80–90 °C) over prolonged periods of time, it is interesting to note that ionic liquids can be heated in a very energy-efficient way by microwave irradiation. Ionic liquids consist entirely of ions as opposed to water or organic solvents which explains the very high adsorption of microwave radiation.[22,64] Microwaves do not interfere with the chemical dissolution process but provide a more economical way to heat an ionic liquid in an industrial context.[42,43,64,65] Several reactor designs exist where the radiation of an external microwave source is guided through a non-magnetic hollow metal tube (waveguide) into the reaction vessel.[42] The immediate on/off behavior of microwave irradiation and the fact that the liquid is heated from the inside as opposed to conventional heating, is also useful for process control and safety.[42,64,66]

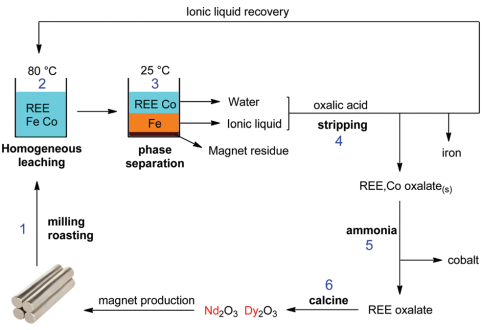

Fig. 21 Overview of the proposed recycling process for roasted NdFeB magnets, based on the acidity and thermomorphism of the functionalized ionic liquid [Hbet][Tf_2N]. Step 1: crushing and (microwave) roasting of the magnets. Step 2: Leaching of the roasted magnets in [Hbet][Tf_2N]–H_2O at 80 °C (homogeneous phase). Step 3: Biphasic settling at room temperature and automatic distribution of the metals across the two phases. Step 4: stripping of both separate phases with oxalic acid, which regenerates the ionic liquid, removes the iron and produces a mixed REE/Co oxalate. Step 5: removal of the cobalt by treatment with aqueous ammonia. Step 6: Calcination of the REE oxalate to form the oxides (purity > 99.9 wt%), which can be used as a precursor for the production of new NdFeB magnets.[58]

Conclusion

The combined ionic liquid leaching/extraction system described in this work is an innovative approach to NdFeB magnet recycling. The process is based on the leaching of (microwave) roasted NdFeB magnets in the carboxyl-functionalized ionic liquid [Hbet][Tf_2N]. The special thermomorphic properties of the [Hbet][Tf_2N]–H_2O system cause the mixture to be homogeneous during leaching at 80 °C (temperature above the cloud point temperature) and biphasic when cooling back down to room temperature. The formation of a biphasic system induces metal separation where Fe(III) goes to the ionic liquid phase and the REE(III) and Co(II) ions to the water phase with high separation factors. Such a thermomorphic leaching system offers many advantages and was studied in detail, including the effect of inorganic salts on the metal distribution. Oxalic acid was used to precipitate the REE(III) and cobalt(II) ions, while stripping iron(III) by back extraction as a soluble iron oxalate complex. The cobalt was then removed from the oxalate product using aqueous ammonia. The final REE oxalate had a purity above 99.9 wt% and could be calcined to obtain the pure oxides which can be used as precursors for the production of new NdFeB magnets.[58] The stripping step also automatically regenerated the ionic liquid and a salting-out method was designed (using Na_2SO_4) to exclude any loss of ionic liquid or contaminate on of the water phase. Therefore, this closed-loop system only generates little waste and offers selectivity, mild conditions and reusability, which make this a promising green technology for the targeted recovery of REEs from NdFeB magnets. Considering the supply risk for these elements (mainly Nd and Dy) and the high demand for NdFeB magnets this technology could help to secure the demand for these critical elements by providing a sustainable and efficient alternative for the recycling of spent NdFeB magnets.

Acknowledgements

The authors wish to thank the KU Leuven (projects GOA/13/008 and IOF-KP RARE^3), the FWO Flanders (PhD fellowship to DD and research project G.0900.13) for financial support. The

University of Birmingham (UK) and Goudsmit Magnetics are acknowledged for providing the demagnetized NdFeB magnets, Jeroen Sniekers for helping with the SEM and EDX measurements, Neil Brooks for powder XRD characterization, Tom Vander Hoogerstraete for the help with milling and roasting of the magnets, Clio Deferm for milling of the magnets, Jef Vleugels for the useful discussions and Carlo Groffils, Sam Buls and Olivier Van Roey for their help with the microwave set-up and the microwave experiments.

Notes and references

1 D. Schüler, M. Buchert, R. Liu, G. S. Dittrich and C. Merz, *Study on rare earths and their recycling*, Öko-Institut, Darmstadt, 2011.
2 E. Alonso, A. M. Sherman, T. J. Wallington, M. P. Everson, F. R. Field, R. Roth and R. E. Kirchain, *Environ. Sci. Technol.*, 2012, **46**, 3406–3414.
3 K. Binnemans, P. T. Jones, B. Blanpain, T. Van Gerven, Y. Yang, A. Walton and M. Buchert, *J. Cleaner Prod.*, 2013, **51**, 1–22.
4 M. Humphries, *Rare Earth Elements: The Global Supply Chain*, Congressional Research Service, USA, 2013.
5 S. Massari and M. Ruberti, *Resour. Policy*, 2013, **38**, 36–43.
6 Report on Critical raw materials for the EU, European Commission, DG Enterprise & Industry, Brussels, 2014.
7 A. Golev, M. Scott, P. D. Erskine, S. H. Ali and G. R. Ballantyne, *Resour. Policy*, 2014, **41**, 52–59.
8 U.S. Department of Energy, *Critical Materials Strategy*, USA, 2011.
9 K. Binnemans, P. T. Jones, K. Acker, B. Blanpain, B. Mishra and D. Apelian, *JOM*, 2013, **65**, 846–848.
10 M. Tanaka, T. Oki, K. Koyama, H. Narita and T. Oishi, in *Handbook on the Physics and Chemistry of Rare Earths*, ed. J.-C. G. Bünzli and V. K. Pecharsky, Elsevier, Amsterdam, 2013, *ch. 255*, vol. 43, pp. 159–212.
11 Y. Wu, X. Yin, Q. Zhang, W. Wang and X. Mu, *Resour., Conserv. Recycl.*, 2014, **88**, 21–31.
12 T. Vander Hoogerstraete, B. Blanpain, T. Van Gerven and K. Binnemans, *RSC Adv.*, 2014, **4**, 64099–64111.
13 Solvay, Press release, http://www.solvay.com, 2012.
14 K. Binnemans and P. T. Jones, *J. Rare Earths*, 2014, **32**, 195–200.
15 T. Vander Hoogerstraete, S. Wellens, K. Verachtert and K. Binnemans, *Green Chem.*, 2013, **15**, 919–927.
16 S. Wellens, R. Goovaerts, C. Moller, J. Luyten, B. Thijs and K. Binnemans, *Green Chem.*, 2013, **15**, 3160–3164.
17 T. Vander Hoogerstraete and K. Binnemans, *Green Chem.*, 2014, **16**, 1594–1606.
18 K. Larsson, C. Ekberg and A. Ødegaard-Jensen, *Waste Manage.*, 2013, **33**, 689–698.
19 C. Jagadeeswara Rao, K. A. Venkatesan, K. Nagarajan and T. G. Srinivasan, *Radiochim. Acta*, 2008, **96**, 403–409.
20 P. Nockemann, B. Thijs, T. N. Parac-Vogt, K. Van Hecke, L. Van Meervelt, B. Tinant, I. Hartenbach, T. Schleid, V. T. Ngan, M. T. Nguyen and K. Binnemans, *Inorg. Chem.*, 2008, **47**, 9987–9999.
21 P. Nockemann, B. Thijs, S. Pittois, J. Thoen, C. Glorieux, K. Van Hecke, L. Van Meervelt, B. Kirchner and K. Binnemans, *J. Phys. Chem. B*, 2006, **110**, 20978–20992.
22 D. Dupont and K. Binnemans, *Green Chem.*, 2015, **17**, 856–868.
23 K. Sasaki, K. Takao, T. Suzuki, T. Mori, T. Arai and Y. Ikeda, *Dalton Trans.*, 2014, **43**, 5648–5651.
24 K. Sasaki, T. Suzuki, T. Mori, T. Arai, K. Takao and Y. Ikeda, *Chem. Lett.*, 2014, **43**, 775–777.
25 D. P. Fagnant, G. S. Goff, B. L. Scott, W. Runde and J. F. Brennecke, *Inorg. Chem.*, 2013, **52**, 549–551.
26 T. Vander Hoogerstraete, B. Onghena and K. Binnemans, *Int. J. Mol. Sci.*, 2013, **14**, 21353–21377.
27 T. Vander Hoogerstraete, B. Onghena and K. Binnemans, *J. Phys. Chem. Lett.*, 2013, **4**, 1659–1663.
28 B. Onghena, J. Jacobs, L. Van Meervelt and K. Binnemans, *Dalton Trans.*, 2014, **43**, 11566–11578.
29 B. Onghena and K. Binnemans, *Ind. Eng. Chem. Res.*, 2015, **54**, 1887–1898.
30 A. P. Abbott, G. Frisch, S. J. Gurman, A. R. Hillman, J. Hartley, F. Holyoak and K. S. Ryder, *Chem. Commun.*, 2011, **47**, 10031–10033.
31 S. Wellens, T. Vander Hoogerstraete, C. Möller, B. Thijs, J. Luyten and K. Binnemans, *Hydrometallurgy*, 2014, **144–145**, 27–33.
32 A. Rout, S. Wellens and K. Binnemans, *RSC Adv.*, 2014, **4**, 5753–5758.
33 S. Wellens, B. Thijs, C. Moller and K. Binnemans, *Phys. Chem. Chem. Phys.*, 2013, **15**, 9663–9669.
34 A. P. Abbott, G. Frisch, J. Hartley and K. S. Ryder, *Green Chem.*, 2011, **13**, 471–481.
35 S. Wellens, B. Thijs and K. Binnemans, *Green Chem.*, 2012, **14**, 1657–1665.
36 Y. Gu, *Green Chem.*, 2012, **14**, 2091–2128.
37 Q. Zhang, S. Zhang and Y. Deng, *Green Chem.*, 2011, **13**, 2619–2637.
38 T. Welton, *Green Chem.*, 2011, **13**, 225–225.
39 N. V. Plechkova and K. R. Seddon, *Chem. Soc. Rev.*, 2008, **37**, 123–150.
40 R. M. C. Dawson, in *Data for Biochemical Research*, Oxford University press, New York, 3rd edn, 1986, pp. 8–9.
41 G. Brauer, in *Handbook of Preparative Inorganic Chemistry*, Academic Press, New York, 2nd edn, 1963, ch. 28, pp. 1513–1559.
42 K. E. Haque, *Int. J. Miner. Process.*, 1999, **57**, 1–24.
43 M. Al-Harahsheh and S. W. Kingman, *Hydrometallurgy*, 2004, **73**, 189–203.
44 Y. Hua, C. Cai and Y. Cui, *Sep. Purif. Technol.*, 2006, **50**, 22–29.
45 K. Miura, M. Masuda, M. Itoh, T. Horikawa and K.-i. Machida, *J. Alloys Compd.*, 2006, **408–412**, 1391–1395.
46 S. Pan, *Rare Earth Permanent-Magnet Alloys' High Temperature Phase Transformation: In Situ and Dynamic Observation and Its Application in Material Design*, Springer, Berlin, Heidelberg, 2014.

47 P. Nockemann, B. Thijs, K. Lunstroot, T. N. Parac-Vogt, C. Görller-Walrand, K. Binnemans, K. Van Hecke, L. Van Meervelt, S. Nikitenko, J. Daniels, C. Hennig and R. Van Deun, *Chem. – Eur. J.*, 2009, **15**, 1449–1461.
48 R. Reddy, *J. Phase Equilib. Diffus.*, 2006, **27**, 210–211.
49 M. G. Freire, A. R. R. Teles, J. N. Canongia Lopes, L. P. N. Rebelo, I. M. Marrucho and J. A. P. Coutinho, *Sep. Sci. Technol.*, 2011, **47**, 284–291.
50 Y. Zhang and P. S. Cremer, *Curr. Opin. Chem. Biol.*, 2006, **10**, 658–663.
51 M. G. Freire, P. J. Carvalho, A. M. S. Silva, L. M. N. B. F. Santos, L. P. N. Rebelo, I. M. Marrucho and J. A. P. Coutinho, *J. Phys. Chem. B*, 2009, **113**, 202–211.
52 M. G. Freire, C. M. S. S. Neves, P. J. Carvalho, R. L. Gardas, A. M. Fernandes, I. M. Marrucho, L. M. N. B. F. Santos and J. A. P. Coutinho, *J. Phys. Chem. B*, 2007, **111**, 13082–13089.
53 S. Shahriari, C. M. S. S. Neves, M. G. Freire and J. A. P. Coutinho, *J. Phys. Chem. B*, 2012, **116**, 7252–7258.
54 L. I. N. Tomé, F. R. Varanda, M. G. Freire, I. M. Marrucho and J. A. P. Coutinho, *J. Phys. Chem. B*, 2009, **113**, 2815–2825.
55 J.-S. Sohn, D.-H. Yang, S.-M. Shin and J.-G. Kang, *Geosyst. Eng.*, 2006, **9**, 81–86.
56 D. Nicholls, in *The Chemistry of Iron, Cobalt and Nickel*, Pergamon, Exeter, 1st edn, 1973, pp. 1053–1107.
57 A. K. Galwey and E. Brown, *Thermal Decomposition of Ionic Solids: Chemical Properties and Reactivities of Ionic Crystalline Phases*, Elsevier Science, 1999.
58 G. Qi, M. Hino and A. Yazawa, *Mater. Trans. JIM*, 1990, **31**, 463–470.
59 L. Bai, X. Wang, Y. Nie, H. Dong, X. Zhang and S. Zhang, *Sci. China: Chem.*, 2013, **56**, 1811–1816.
60 C. M. S. S. Neves, M. G. Freire and J. A. P. Coutinho, *RSC Adv.*, 2012, **2**, 10882–10890.
61 C. Abels, C. Redepenning, A. Moll, T. Melin and M. Wessling, *J. Membr. Sci.*, 2012, **405–406**, 1–10.
62 J. F. Fernández, D. Waterkamp and J. Thöming, *Desalination*, 2008, **224**, 52–56.
63 J. Lemus, J. Palomar, F. Heras, M. A. Gilarranz and J. J. Rodriguez, *Sep. Purif. Technol.*, 2012, **97**, 11–19.
64 J. Hoffmann, M. Nuchter, B. Ondruschka and P. Wasserscheid, *Green Chem.*, 2003, **5**, 296–299.
65 A. Arfan and J. P. Bazureau, *Org. Process Res. Dev.*, 2005, **9**, 743–748.
66 C. O. Kappe and D. Dallinger, *Nat. Rev. Drug Discovery*, 2006, **5**, 51–63.

Paper 3: Recycling of antimony from lamp phosphor waste

Title:
Antimony recovery from the halophosphate fraction in lamp phosphor waste: a zero-waste approach

Type: Full paper
Journal: Green Chemistry (IF 8.02)
Publisher: Royal Society of Chemistry (RSC)
Publication date: 14/09/2015

Reprint with permission from:
D. Dupont and K. Binnemans, *Green Chem.*, **2016**, 18, 176-185.

Electronic Supplementary Information (ESI) available: http://pubs.rsc.org.

Graphical abstract

This paper describes a zero-waste valorization process for the recovery of antimony from lamp phosphor waste.

Green Chemistry

PAPER

View Article Online
View Journal | View Issue

Cite this: *Green Chem.*, 2016, **18**, 176

Antimony recovery from the halophosphate fraction in lamp phosphor waste: a zero-waste approach

David Dupont and Koen Binnemans*

Antimony is becoming an increasingly critical element as the supply-demand gap is expected to exceed 10% over the period 2015–2020. Antimony production is primarily concentrated in China (90%) and as the industrial demand for this metal surges, attention has to turn towards the recovery of antimony from (industrial) waste residues and end-of-life products in order to guarantee a sustainable supply of antimony. Although lamp phosphor waste is usually considered as a source of rare earths, it also contains significant amounts of antimony in the form of the white halophosphate phosphor $(Ca,Sr)_5(PO_4)_3(Cl,F):Sb^{3+}$, Mn^{2+} (HALO). HALO phosphor readily dissolves in dilute acidic conditions, making antimony far more accessible than in the main production route which is the energy intensive processing of stibnite ore (Sb_2S_3). HALO makes up 50 wt% of the lamp phosphor waste, but it has been systematically overlooked and treated as an undesired residue in the efforts to recover rare earths from lamp phosphor waste. In this paper, the feasibility of antimony recovery is discussed and an efficient process is proposed. The HALO phosphor is first dissolved in dilute HCl at room temperature, followed by a selective extraction of antimony with the ionic liquid Aliquat® 336. The remaining leachate is valorized as apatite which is a feed for the phosphate and fertilizer industry. A zero-waste valorization approach was followed, meaning that no residue or waste was accepted and that all the elements were converted into useful products. This paper thus emphasizes the potential of lamp phosphor waste as a secondary source of antimony and describes a sustainable process to recover it. The process can be integrated in lamp phosphor recycling schemes aimed at recovering rare earths.

Received 29th July 2015,
Accepted 14th September 2015

DOI: 10.1039/c5gc01746g

www.rsc.org/greenchem

Introduction

The word antimony comes from the Greek "anti monos", meaning "never (found) alone" which explains why the metal was only isolated and correctly identified in the 16th century even though it had been known since ancient times as a cosmetic product.[1] The abundance of antimony in the earth's crust is 0.2 ppm, making this element scarcer than the heavy rare-earth elements.[2] Antimony (Sb) is mainly produced from stibnite (Sb_2S_3) which is found in quartz veins.[1] Today, 90% of the global antimony supply is produced in China. This country also holds the largest reserves.[1] Antimony is mostly used in the form of Sb_2O_3 as flame retardant due to its synergetic effect with halogenated flame retardants. Sb_2O_3 has become crucial to guarantee the safety of inherently flammable materials such as plastics, coatings and electronics and takes up the majority of the world's antimony production. Sb_2O_3 is also the main catalyst for the production of PET plastic and it is used as additive in glass and ceramics. Antimony metal is less important, although it is used in some types of lead alloys.[1] Due to its economic importance and high supply risk, antimony was listed among the most critical elements in the critical raw material report from the European Commission (2014).[3] The report forecasts that in the period 2015–2020 the supply-demand gap for antimony will be the most severe amongst all the considered strategic metals, exceeding 10% on an annual basis. Due to the strong concentration of production in China and the lack of new deposits, increasing attention should go to the recovery of antimony from secondary sources such as industrial waste residues and end-of-life consumer products. Recycling of critical metals and elemental sustainability is becoming increasingly important as resources become scarcer. In this context, lamp phosphor waste from collected end-of-life fluorescent lamps can be very interesting due to its relatively high antimony content (0.5–1 wt%) and its known rare-earth content, which adds value.[4–7] Stibnite ore (Sb_2S_3) has an average grade of 2.7 wt%, but requires a lot of energy and chemicals to extract the antimony.[1] The antimony

KU Leuven, Department of Chemistry, Celestijnenlaan 200F - P.O. Box 2404, B-3001 Heverlee, Belgium. E-mail: Koen.Binnemans@chem.kuleuven.be

in the lamp phosphor waste can be recovered in milder conditions (room temperature, dilute acid) and contains far less contaminants since lamp phosphors are synthesized using high purity products.[8–12] Stibnite ore often contains impurities such as Pb, As and Fe.[1]

Lamp phosphors are fluorescent powders coated on the inside of the glass and are responsible for the emission of visible light in normal or compact fluorescent lamps (CFLs).[8–12] Their luminescence is based on the adsorption of UV-radiation emitted by the mercury atoms in the gas filling of the lamps. Two important classes of lamp phosphors can be distinguished: the white halophosphate phosphors and the so-called "tri-band" phosphors which use a mixture of red, green and blue phosphors to generate white light. The white HALO phosphor was invented in 1942 and large amounts of this phosphor were produced as it found widespread use in fluorescent tubes.[8–10,12] Small differences exist, but it's main structure is a fluoro–chloro apatite doped with manganese(II) and antimony(III).[8–10] Its luminescence and shade of white can be adjusted by tuning the ratio of blue emitting antimony dopant and orange emitting manganese dopant or the fluorine-to-chlorine ratio.[8–10,13] Some of the calcium can also be substituted by strontium to obtain narrower emission bands.[8–10] The tri-band phosphors are more recent and have largely replaced halophosphate phosphors due to their better color rendering index, higher efficiency and excellent stability. Tri-band phosphors are composed of separate red (YOX), blue (BAM) and green (LAP/CAT) phosphors (Table 1), which together generate white light.[10] The tri-band phosphors were crucial for the development of CFLs because the high wall temperature and higher UV flux of these lamps would quickly degrade the less resistant halophosphate phosphors. Their downside is that they rely on expensive rare-earth elements (REEs) for their luminescence, namely Eu(III), Tb(III) and Eu(II) for the red, green and blue phosphors, respectively. As a compromise between phosphor cost and performance, a double coating scheme can be applied.[10] A base layer of inexpensive and more-easily-damaged halophosphate phosphor is coated with a resistant REE phosphor blend in order to protect it from the electron discharge and generate white light with high efficiency and good color rendering index. Despite the fact that since the 1990s the tri-band phosphors have largely replaced HALO phosphor, enormous amounts of HALO have been produced over the years and are either still in use or have been stockpiled or landfilled by recyclers.[14,15] Today, processed lamp phosphor waste contains around 50 wt% of HALO, making it the largest component (Table 1).[5]

With annual sales of CFL's topping 2.5×10^9 units per year (2007), the volume of lamp phosphor waste is expected to grow rapidly as fluorescent lamps reach their end-of-life.[16,17] Fluorescent lamps are considered as hazardous waste due to their mercury content, and have to be collected separately.[14,15] While the glass and metal in the lamps is often recycled, the lamp phosphor powders are usually simply stockpiled or discarded despite their significant critical metal content (Table 1).[14,15,18] However, the interest in this waste fraction has been growing since the rare-earth crisis of 2011.[15,19] The REEs are present in the red (YOX), green (LAP/CAT) and blue (BAM) tri-band phosphors and many studies have been carried out to recover these valuable elements.[14,15,18,20–27] Since 2012, the recycling of REEs from fluorescent lamps is also carried out on industrial scale by Solvay in France.[5] However, the broadband antimony-containing phosphor $(Sr,Ca)_5(PO_4)_3(Cl,F):Sb^{3+},Mn^{2+}$ (HALO) does not contain rare earths and is therefore usually considered as a non-valuable residue even though it makes up around 50 wt% of the lamp phosphor waste (Table 1).[14,15,18] As rare-earth prices have come down from their highs of 2011, more attention should go to this halophosphate phosphor as a potentially interesting secondary source of antimony. Antimony is crucial for many growing applications as described earlier but its recycling from end-of-life consumer waste has not been considered so far. The recovery of antimony should be integrated in REE recycling processes for fluorescent lamp phosphor waste in the larger attempt to valorize this valuable consumer waste product. The HALO content in these powders is too large to ignore or discard as a useless side product. In this paper, the feasibility of antimony recovery is discussed and a new process is presented to efficiently recover the antimony from the HALO phosphor using minimal amounts of chemicals. The resulting product is pure Sb_2O_3, which is the main commercial form of antimony and an apatite residue which is the primary feedstock for the phosphate and fertilizer industry. A zero-waste valorization strategy was followed, meaning that no waste was tolerated and all of the elements in HALO were valorized into useful products, not just antimony. The process was developed using commercial HALO phosphor in order to study the chemistry of this phosphor in detail. However, the implementation of the HALO valorization process in lamp phosphor recycling schemes is also discussed in this paper.

Table 1 Overview of the approximate lamp phosphor waste composition and average stoichiometry of the different commercial phosphors[15]

Name	Formula	Fraction[a] (wt%)
HALO[b]	$Ca_{4.86}Mn_{0.10}Sb_{0.04}Sr_{0.004}(PO_4)_3Cl_{0.10}F_{0.90}$	50
YOX	$Y_{1.92}Eu_{0.08}O_3$	20
BAM	$Ba_{0.86}Eu_{0.14}MgAl_{10}O_{17}$	5
LAP	$La_{0.60}Ce_{0.27}Tb_{0.13}PO_4$	5
CAT	$Ce_{0.63}Tb_{0.37}MgAl_{11}O_{19}$	5

[a] The remaining consists of SiO_2 (fine glass particles) and Al_2O_3 (binder). [b] For convenience, a shorter formula for HALO is used in this paper: $(Sr,Ca)_5(PO_4)_3(Cl,F):Sb^{3+},Mn^{2+}$.

Experimental

Materials and chemicals

The lamp phosphors $(Ca,Sr)_5(PO_4)_3(Cl,F):Sb^{3+},Mn^{2+}$ (HALO), $Y_2O_3:Eu^{3+}$ (YOX), $LaPO_4:Ce^{3+},Tb^{3+}$ (LAP) and $BaMgAl_{10}O_{17}:Eu^{2+}$

Table 2 Composition of the HALO phosphor expressed in wt% and mol%

Element	Concentration (wt%)	Concentration (mol%)
PO_4	55.71	33.32
Ca	38.06	53.95
F	3.33	9.94
Sb	1.05	0.49
Mn	1.06	1.10
Cl	0.73	1.16
Sr	0.06	0.04
Total	100%	100%

(BAM) were purchased from Nichia (Japan) (>99%). The exact composition of the commercial HALO is shown in Table 2. $CeMgAl_{11}O_{19}:Tb^{3+}$ (CAT), [A336][Cl] (Aliquat® 336) and $SbCl_3$ (>99%) were obtained from Sigma-Aldrich (Diegem, Belgium). HCl (37%) and H_2SO_4 (96%) were purchased from Acros Organics (Geel, Belgium). NaOH (>99%) was purchased from VWR (Leuven, Belgium). The silicone solution in isopropanol was purchased from SERVA Electrophoresis GmbH (Germany) and the indium standard solution (1000 ppm) from Merck (Belgium). All chemicals were used as received without further purification.

Equipment and characterization

A TMS-200 thermoshaker (Nemus Life) was used to facilitate mixing of the samples and a centrifuge Heraeus Megafuge 1.0 was used to sediment the undissolved residue. The metal concentrations in the samples were determined by total reflection X-ray fluorescence spectroscopy (TXRF) on a Bruker S2 Picofox TXRF spectrometer equipped with a molybdenum source. For the sample preparation, plastic microtubes were filled with an amount of aqueous sample (100–200 mg) and 3 M HCl solution (200 μL) to avoid hydrolysis of Sb(III) ions. For the analysis of the ionic liquid (IL) phase, smaller samples were taken (50 mg) and diluted in EtOH (200 μL). Then, 50 μL of a 1000 ppm indium standard solution was added as an internal standard. Indium was chosen as a standard because this element has an X-ray energy very similar to both calcium and antimony, which reduces the effects caused by adsorption of secondary X-rays (matrix effects).[28] The microtubes were vigorously shaken on a vibrating plate (IKA MS 3 basic). Finally, a 2 μL drop of this solution was put on a quartz plate, previously treated with a silicone/isopropanol solution (Serva®) to avoid spreading of the sample droplet on the quartz plate. The quartz plates were then dried for 30 min at 60 °C prior to analysis. Each sample was measured for 10 min.

Dissolution experiments

The solid material (*e.g.* HALO) was introduced in small glass vials (4 mL) together with the desired acidic solution (2 mL). A solid/liquid ratio of 25 mg g^{-1} was used in most experiments. The samples were then shaken (2000 rpm) at 25 °C for a certain amount of time (depending on the experiment). Finally, the vials were centrifuged for 5 min (5000 rpm) to sediment the residue and a sample was taken from the supernatant to determine the metal concentrations in solution (TXRF).

Solvent extraction experiments

A batch of leachate (20 mL) was prepared by dissolving HALO in 1 M HCl (25 mg g^{-1} solid/liquid ratio) and stirring the solution (500 rpm) at 25 °C until the dissolution was complete and a clear solution was obtained (5–10 min). The aqueous leachate was then divided into 2 g portions and contacted with the water saturated ionic liquid phase (1 g) using 4 mL vials with screw caps. The water-saturated IL was used to avoid volume changes when contacted with the leachate during solvent extraction experiments. The IL Aliquat® 336 was presaturated with water by contacting a large batch of pure IL with water, shaking it (1 h, 2000 rpm) and allowing it to phase separate. The extraction vials were then shaken for 30 min (2000 rpm) at 25 °C to guarantee a good mixing of the two phases. Finally, the vials were centrifuged for 10 min (5000 rpm) to accelerate phase separation and a sample was taken of the aqueous and IL phase to determine the metal concentrations (TXRF).

Scrubbing and stripping experiments

The loaded IL phase (1 g) was contacted with an aqueous solution (1 g) containing NaCl for scrubbing experiments or NaOH for stripping experiments. The vials were then shaken for 10 min (2000 rpm) at 25 °C. A sample of the IL phase was taken to determine the remaining metal concentration in the IL (TXRF).

Precipitation of the residue

The aqueous phase obtained after the extraction was used to conduct these precipitation experiments. NaOH was added to set the pH and the formed precipitate was settled by centrifugation. A sample of the supernatant was taken after 10 min and 24 h to determine the remaining metal concentrations (TXRF) in the effluent.

Results and discussion

Feasibility of antimony recycling from lamp phosphor waste

Before describing the recycling process, we chose to first discuss the feasibility of antimony recycling from lamp phosphor waste, as well as the general zero-waste valorization strategy. The first hurdle to antimony recycling is that antimony is only present in one phosphor (HALO). It is therefore important to avoid co-dissolution of the other components in the lamp phosphor waste as this would cause significant complications (Table 1). Luckily, it is well-known that the HALO phosphor is more easy to dissolve in acid than the other phosphors (HALO > YOX ≫ LAP/CAT/BAM).[5,15,18,29] This was confirmed by our experiments in HCl solutions with separate commercial phosphors (Table 3).

Table 3 Time required for full dissolution of HALO in a 25 mg g^{-1} solution. The dissolutions were carried out at 25 °C while shaking (2000 rpm) at constant pH (HCl). The dissolution of the other phosphors in the same conditions (but in separate vials) is also shown

pH	Time for full HALO dissolution (min)	YOX leaching (wt%)	LAP/CAT/BAM leaching (wt%)
0	5	2.7 (5 min)	<D.L.[a] (5 min)
0.25	25	8.3 (25 min)	<D.L.[a] (25 min)
0.50	60	11.8 (60 min)	<D.L.[a] (60 min)
1.00	Partial hydrolysis Sb		

[a] Detection limit for rare-earths elements in TXRF < 10 ppb.

It is clear from these results that HALO is indeed more easily dissolved than the other phosphors. Amongst the other components, only YOX is partially dissolved. It is important to avoid the co-dissolution of YOX since it is a valuable phosphor and dissolving it together with HALO, which releases phosphoric acid, would cause the Y(III) and Eu(III) ions to reprecipitate as water-insoluble phosphates: YPO_4 and $EuPO_4$ ($K_{sp} \approx 10^{-25}$) (eqn (1) and (2)).[30]

$$(Y, Eu)_2O_3 + 6HCl \rightarrow 2(Y, Eu)Cl_3 + 6H_2O \quad (1)$$

$$(Y, Eu)^{3+} + H_3PO_4 \rightarrow (Y, Eu)PO_{4(s)} + 3H^+ \quad (2)$$

There are two ways to avoid partial co-dissolution of YOX and the consequent loss of yttrium and europium. The first is to minimize the dissolution of YOX by careful pH control (*e.g.* 5 min, pH 0), but this cannot fully exclude the dissolution of YOX (Table 3),[5,29] The other approach is to selectively remove the YOX in a prior process step. This was not possible until recently because of the faster dissolution of HALO in acidic aqueous solutions. However, we recently developed a process to achieve this in the carboxyl-functionalized ionic liquid betainium bis(trifluoromethylsulfonyl)imide [Hbet][Tf_2N], which can selectively dissolve metal oxides such as YOX.[27] This selective dissolution of YOX allows the direct recycling of the most valuable component in the lamp phosphor waste and has the additional advantage of removing YOX from the lamp phosphor waste so that in a next step, HALO can be dissolved quickly and selectively in acid.[27] The antimony recovery process described in this paper, can then be applied without further complications. This way, the valorization of HALO can fit in a general rare-earth recycling scheme for lamp phosphor waste, finally allowing the valorization of this major component of the lamp phosphor waste (50 wt%), instead of discarding it as a non-valuable waste residue.[5,15,20]

Waste valorization strategy

The aim of this work was to recover antimony from the HALO phosphor using a zero-waste approach.[31] This is a key process requirement since it is not desirable to end up with more waste than the waste that is being treated in the first place. The key to HALO valorization lies in its resemblance to the industrially very important phosphate rock.[31–37] The phosphor $Ca_5(PO_4)_3(Cl,F):Sb^{3+},Mn^{2+}$ (HALO) has a typical apatite structure, in which some of Ca(II) ions are substituted by Sb(III) and Mn(II) ions.[8–10] Apatites have the general formula $Ca_5(PO_4)_3X$ (X = OH, F, Cl) and are the main component of phosphate rock which is the primary source of phosphoric acid and phosphate-based fertilizers.[31–37] The importance of phosphate rock for the fertilizer industry is based on the H_2SO_4 (eqn (3)), H_3PO_4 (eqn (4)) or HNO_3 (eqn (5)) route .[37]

$$Ca_5(PO_4)_3X + 5H_2SO_4 + 10H_2O \rightarrow 3H_3PO_4 + 5CaSO_4 \cdot 2H_2O + HX \quad (3)$$

$$Ca_5(PO_4)_3X + 7H_3PO_4 \rightarrow 5Ca(H_2PO_4)_2 + HX \quad (4)$$

$$Ca_5(PO_4)_3X + 10HNO_3 \rightarrow 5Ca(NO_3)_2 + 3H_3PO_4 + HX \quad (5)$$

The sulfuric acid route yields phosphoric acid and phosphogypsum, while the phosphoric acid route directly forms a phosphate fertilizer with the formula $Ca(H_2PO_4)_2$, called triple superphosphate (TSP) (Fig. 1).[37] The nitric acid route is less common but can be used to avoid phosphogypsum formation. Ammonia and potash can be used to obtain NP and NPK fertilizers (Fig. 1).[37] Phosphate rock digestion is also an industrial production route for hydrofluoric acid (HF). An important drawback of phosphate rock is that it usually contains traces of heavy metals (*e.g.* Cd, As, Pb) and radioactive elements such as U, Th and Ra.[31,37,38] The fast depletion of phosphate rock reserves is also a major concern as it is the cornerstone of the entire phosphate and fertilizer industry.[31–37]

Therefore we have developed a process which not only recovers the valuable and critical antimony from the HALO, but also amounts to a pure calcium phosphate product which can be integrated in the phosphate industry. The absence of radioactive elements in the HALO phosphor, make it an interesting source of phosphate and phosphoric acid. The production of new HALO phosphor has also faded out as this lamp phosphor has been replaced by the rare-earth containing tri-band phosphors. This means that the recycling of HALO present in lamps and waste stockpiles can be a net input to the phosphate cycle.[31–37]

Dissolution of HALO

Having discussed the general feasibility and strategy of the valorization process, we now describe in detail a potential recycling scheme. The first step is to dissolve the HALO and obtain

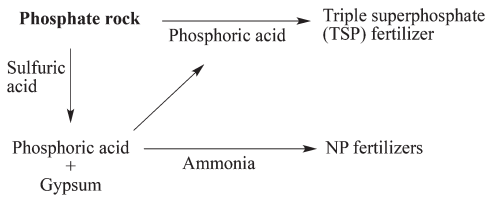

Fig. 1 Main industrial production routes for phosphate fertilizers.

a stable leachate. HCl and H_2SO_4 were considered since these are cheap and largely available acids. HNO_3 is not a good choice as antimony(III) nitrate solutions are less stable and nitrate effluents have a large impact on the environment.[39] When dissolving HALO in HCl, highly soluble Ca(II), Mn(II) and Sb(III) chlorides are formed (eqn (6)). The dissolution mechanism of apatites has been studied in detail, but at low pH values (pH < 0.5) it is sufficient to consider the full dissolution reactions as it occurs fast.[40,41]

$$\mathrm{Ca_5(PO_4)_3(Cl,F):Sb^{3+},Mn^{2+}} + x\mathrm{HCl} \rightarrow 5\mathrm{CaCl_2} + 3\mathrm{H_3PO_4} + \mathrm{SbCl_3} + \mathrm{MnCl_2} + \mathrm{HF} \quad (6)$$

Raising the pH above 1 causes precipitation of insoluble Ca(II), Sb(III) and Mn(II) phosphates and also hydrolysis of Sb(III) ions.[1,42–47] The room temperature hydrolysis of Sb(III)–HCl solutions was studied in detail by Hashimoto *et al.* and they showed that at low pH (1–4) Sb(III) ions are hydrolyzed to form $SbOCl_{(s)}$ and $Sb_4O_5Cl_{2(s)}$, and above pH 4.5 $Sb_2O_{3(s)}$ is formed.[47] Unfortunately, controlled hydrolysis of Sb(III) to isolate the antimony, is not an option in this case since the hydrolysis is incomplete at low pH and increasing the pH above pH 2 will cause parrallel precipitation of calcium and manganese phosphates. Therefore, the best strategy was to obtain a stable leachate, which could be further purified by solvent extraction. The experiments were carried out for leachates with a HALO content of 25 g L^{-1}, but the solid/liquid ratio can be further increased since the solubility of these chloride salts is very high. If H_2SO_4 is used instead of HCl, calcium is precipitated as insoluble $CaSO_{4(s)}{\cdot}2H_2O$ (eqn (7)).

$$\mathrm{Ca_5(PO_4)_3(Cl,F):Sb^{3+},Mn_{(s)}^{2+}} + x\mathrm{H_2SO_{4(aq)}} \rightarrow 5\mathrm{CaSO_4{\cdot}2H_2O_{(s)}} + 3\mathrm{H_3PO_{4(aq)}} + \mathrm{Sb_2(SO_4)_{3(aq)}} + \mathrm{MnSO_{4(aq)}} + \mathrm{HF_{(aq)}} \quad (7)$$

At 1 N acid, HALO is fully dissolved in both HCl and H_2SO_4, but calcium is precipitated with H_2SO_4 (Fig. 2). The removal of calcium with H_2SO_4 could be useful due to the large excess of calcium ions (110 : 1 : 2 Ca : Sb : Mn mol ratio).[48,49] In aqueous sulfate solutions the remaining solubility of calcium is approximately 2000 ppm., but this can lowered by adding ethanol which decreases the solubility of $CaSO_4$ (Fig. 3).[50] In a 1 : 1 vol/vol EtOH–H_2O solution, the soluble calcium could be reduced to 10 ppm in this HALO leachate.

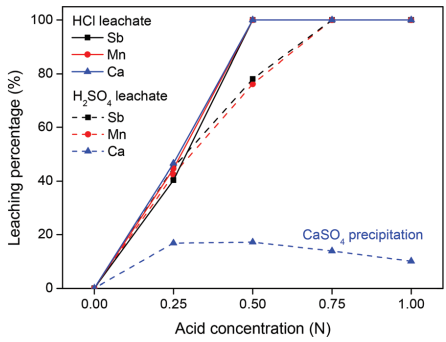

Fig. 2 Dissolution of HALO (25 mg g^{-1}) in increasingly concentrated HCl and H_2SO_4 solutions. The samples were shaken (2000 rpm) for 1 h at 25 °C.

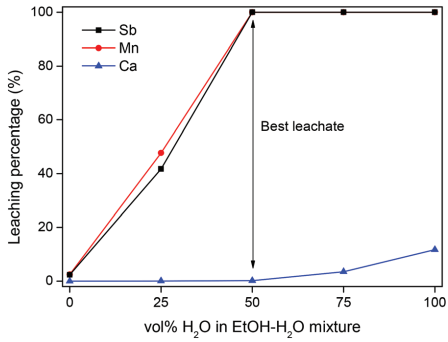

Fig. 3 Influence of the EtOH–H_2O ratio on the dissolution of HALO with 1 N H_2SO_4. The samples were shaken (2000 rpm) for 1 h at 25 °C.

The absence of calcium in the leachate is advantageous, but the HCl dissolution route (1 M, 10 min) is still preferred, because in the sulfuric acid process large amounts of $CaSO_4{\cdot}2H_2O$ are created as a useless residue. Extraction of antimony with basic extractants from sulfate media is also less efficient than from chloride media.[51,52] Antimony forms strong chloride complexes and can therefore be extracted as tetrachloroantimonate(III) complex $SbCl_4^-$.[52,53] No waste residue is created with the HCl route, since neutralization of the HCl leachate with NaOH will precipitate a valuable calcium phosphate apatite product and a NaCl-containing effluent which can be discarded in sea water.

Separation of antimony

We previously mentioned that controlled hydrolysis of Sb(III) is not an option to isolate the antimony, because the hydrolysis is incomplete at low pH and increasing the pH above 2 will also cause precipitation of calcium and manganese phosphates. Therefore, antimony must be removed by other means such as solvent extraction or selective electrodeposition of antimony metal. The latter will not be discussed in this work as the demand for antimony metal is much lower than the demand for antimony(III) oxide.[1] Electrodeposition of antimony metal in water can also cause formation of highly toxic stibine gas (SbH_3) in certain conditions.[54] Therefore, selective extraction of the Sb(III) ions is the best option. Sb(III) removal by solvent extraction has been studied previously, although the main focus has been to separate antimony from heavy and precious metal ions (Cd(II), Pb(II), Sn(II), Te(IV), Se(IV), Bi(IV), As(III), ...) and from Cu(II) electroplating solutions.[51,52,55–65] Most studies

have focused on the use of neutral and acidic organophosphorus extractants or the use of secondary and tertiary amines as basic extractants (eqn (9) and (10)).[51,52,55–65] These extractants are usually dissolved in organic solvents such as toluene, xylene or kerosene. Some studies have also proposed the use of ion exchange resins and sorbents but these are restricted to the removal of trace amounts of antimony from wastewater.[66–68] While solvent extraction is certainly promising for the separation of Sb(III), the use of volatile and flammable organic solvents and highly concentrated acidic solutions often limits their applicability. Here, we propose the use of an ionic liquid (IL) as organic phase to selectively extract the Sb(III) ions from the leachate in mild conditions. Ionic liquids are ideal replacements for organic solvents in solvent extraction processes since they are reusable, non-volatile and non-flammable compounds. The commercial ionic liquid Aliquat® 336 was used here (undiluted). This ionic liquid consists mainly of trioctyl(methyl)ammonium chloride $[N_{8881}][Cl]$ but is in fact a mixture of C8 and C10 chains with C8 predominating. It is abbreviated here as [A336][Cl]. Aliquat® 336 has been used previously for solvent extraction studies of a wide variety of metal ions.[53,69] It is a basic extractant, which means it extracts the Sb(III) ions as the anionic complex $SbCl_4^-$ (eqn (8)).[51–53]

$$[A336]Cl_{(IL)} + SbCl_4^-{}_{(aq)} \rightarrow [A336][SbCl_4]_{(IL)} + Cl^-{}_{(aq)} \quad (8)$$

This mechanism is similar to the one observed for secondary and tertiary amine extractants (eqn (9) and (10)).[51–53]

$$R_3N_{(org)} + HCl_{(aq)} \rightarrow [R_3NH][Cl]_{(org)} \quad (9)$$

$$[R_3NH][Cl]_{(org)} + SbCl_4^-{}_{(aq)} \rightarrow [R_3NH][SbCl_4]_{(org)} + Cl^-{}_{(aq)} \quad (10)$$

However, secondary and tertiary amines are generally less efficient than quaternary ammonium extractants such as the ionic liquid Aliquat® 336 and require higher chloride concentrations.[53] The extraction of Sb(III), Ca(II) and Mn(II) by Aliquat® 336 was tested on a HALO leachate which was prepared by dissolving HALO (25 g L^{-1}) in a diluted HCl solution (1 M). The composition of the leachate is shown in Table 4.

The leachate was then contacted with water-saturated ionic liquid in a 2 : 1 leachate/IL phase ratio (wt : wt) and shaken 10 min (2000 rpm) at room temperature. The metal concentrations in the IL phase and the aqueous phase were measured by TXRF to determine the percentage extraction %E (eqn (11)).

Table 4 Metal concentrations in the leachate (mg L^{-1}) after dissolving HALO (25 g L^{-1}) in a diluted HCl solution (1 M). The dissolution was carried out room temperature while stirring (500 rpm) for 10 min

Ion	Concentration (mg L^{-1})
Ca(II)	9515
Sr(II)	15
Sb(III)	263
Mn(II)	265

$$\%E = \frac{n_{IL}}{n_{IL} + n_{aq}} \quad (11)$$

Here, n_{IL} and n_{aq} are the number of moles in the IL phase and aqueous phase after extraction, respectively. First, the percentage extraction is plotted *versus* the chloride concentration by addition of NaCl to the aqueous phase (Fig. 4). The extraction of Sb(III) ions is very strong from the HCl leachate and 100% extraction efficiency is observed even without addition of NaCl. Mn(II) ions are only extracted at very high chloride concentrations as the complex $MnCl_4^-$.[53] Ca(II) and Sr(II) ions do not form anionic chloro complexes in these conditions, and are therefore barely extracted in these conditions.

The fact that the quaternary ammonium IL Aliquat® 336 allows direct extraction of Sb(III) from the HCl leachate without addition of extra NaCl or HCl, is a significant improvement compared to the use of secondary and tertiary amine extractants which require higher HCl concentrations to fully extract Sb(III).[51–53] The use of an ionic liquid also eliminates the need for volatile and flammable organic solvents which reduces the environmental impact of the process. A pure ionic liquid phase is therefore preferred, but sometimes addition of an organic diluent such as toluene can be advantageous for example to diminish the viscosity in order to accelerate the extraction kinetics and facilitate phase separation. Diluting the IL with toluene did not significantly influence the extraction percentage of antimony ($SbCl_4^-$) (Fig. 5).

When the extraction is carried out directly from the leachate with a pure ionic liquid, the Ca(II) and Mn(II) extraction efficiency is 0.98% and 1.03%, respectively. This may seem low, but due to the large excess of Ca(II) in the leachate this is actually a large amount and it has to be removed in order to obtain a pure Sb_2O_3 end-product. Therefore, a scrubbing step is required, where the IL is contacted with an aqueous solution

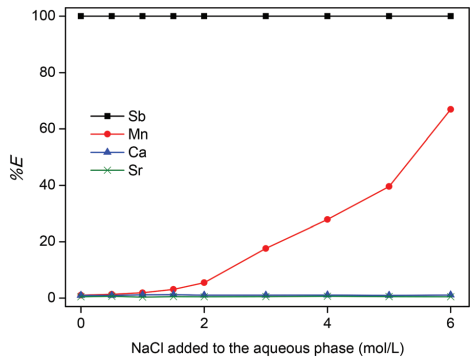

Fig. 4 Percentage extraction (%E) of Sb(III), Mn(II), Ca(II) and Sr(II) ions as function of the addition of NaCl to the HALO leachate (the aqueous phase). The HALO leachate was prepared by dissolving 25 g L^{-1} of HALO in 1 M HCl. A 2 : 1 phase ratio (wt : wt) was used for the aqueous phase and the IL phase [A336][Cl].

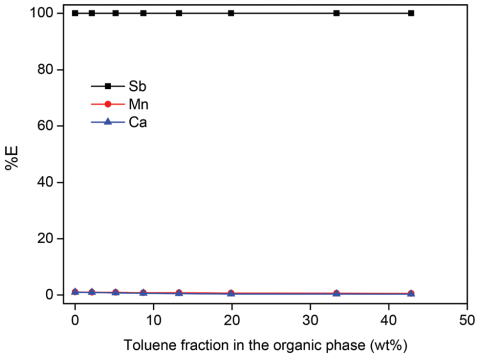

Fig. 5 Influence of toluene in the IL phase on the extraction of Sb(III), Mn(II) and Ca(II) ions. The extraction was done from a HALO leachate, prepared by dissolving 25 g L^{-1} of HALO in 1 M HCl. A 2 : 1 phase ratio (wt : wt) was used for the aqueous phase and the IL phase [A336][Cl].

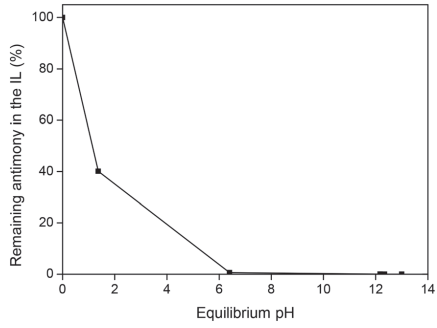

Fig. 6 Stripping of Sb(III) ions from the ionic liquid phase as function of the equilibrium pH, using a water phase with increasing amounts of NaOH.

in order to remove the unwanted elements: Mn(II) and Ca(II) and the co-extracted HCl from the IL. Different scrubbing solutions were tested, but NaCl (1 M) is the best as it removes >99.9% of the Ca(II) and Mn(II) while keeping Sb(III) in the IL (Table 5).

Next, the Sb(III) ions have to be removed (stripped) from the IL. This can be done by contacting the IL phase with an alkaline aqueous phase to transfer the Sb(III) ions to the water phase. Ammonia and NaOH solutions are frequently used bases for stripping of Sb(III) from amine extractants.[52] Depending on the pH, the Sb(III) ions can then be hydrolyzed and precipitated as $SbOCl_{(s)}$ or $Sb_2O_{3(s)}$. The stripping also simultaneously regenerates the IL (eqn (12) and (13)).[46,47] NaOH is preferred here as it forms a (non-toxic) NaCl effluent.

$$[A336][SbCl_4] + 2NaOH \rightarrow [A336][Cl] + SbOCl_{(s)} + 2NaCl + H_2O \quad (12)$$

$$2[A336][SbCl_4] + 6NaOH \rightarrow 2[A336][Cl] + Sb_2O_{3(s)} + 6NaCl + 3H_2O \quad (13)$$

Fig. 6 shows the remaining antimony content in the IL after contacting the Sb(III)-loaded IL with a NaOH-containing aqueous phase. The stripping is sufficiently efficient (>99.99%) above pH 7. Higher pH values are not needed, since the further improvement in stripping efficiency is negligible.

Table 5 Scrubbing (removal) efficiency (%) for Sb(III), Mn(II) and Ca(II) from the ionic liquid using different scrubbing solutions

Scrubbing solution	Sb (%)	Mn (%)	Ca (%)
H_2O	4.5	>99.9	88.9
HCl (1 M)	1.1	>99.9	93.4
NaCl (1 M)	<0.1	>99.9	> 99.9

The precipitation of Sb_2O_3 from aqueous chloride solutions at pH 4.5–12 is the main hydrometallurgical pathway to Sb_2O_3 and has been sufficiently demonstrated.[1,42–47] It is widely used in the purification of antimony and the production of high-quality Sb_2O_3.[1,42–47] The resulting Sb_2O_3 product, is the most important commercial form of antimony as it accounts for more than 90% of the antimony market. An important advantage of recovering antimony from lamp phosphor waste is that lamp phosphor waste contains much less contaminants compared to stibnite ore which is frequently polluted with elements such as lead, arsenic, iron and copper. The purity of the final Sb_2O_3 precipitate was >99.99 wt% with calcium and manganese levels below detection limit for TXRF (10 ppb and 1 ppb, respectively).

Zero-waste valorization of the residue

The HALO leachate (pH 0–0.5), from which the antimony has been initially extracted, is not discarded as waste but is neutralized with NaOH to obtain a clean effluent and a valuable residue. Fig. 7 shows the remaining concentration of calcium and manganese in the leachate as function of pH. At pH 7 (the desired effluent pH), the remaining manganese concentration is below detection limit of TXRF (1 ppb).[70] Calcium removal is not complete at pH 7 (≈85% removal), because at this pH calcium phosphates are still partially soluble.[71,72] However, since calcium is not toxic, it is more favorable to emit the manganese-free $NaCl/CaCl_2$ effluent at pH 7 than to further increase the pH to remove the remaining calcium ions. The effluent is certainly free of fluoride at pH 7 due to large excess of Ca(II) ions and the low solubility of CaF_2 ($K_{sp} = 3.9 \times 10^{-11}$).

The composition of the effluent (excluding NaCl) and the maximum contaminant levels (MCL) allowed in drinking water in the USA, are shown in Table 6.[73] Note that the quality requirements are stricter than the ones applicable to the disposal of wastewater. The effluent meets all regulatory limits

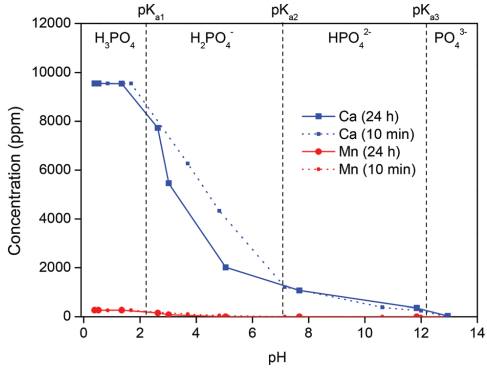

Fig. 7 The remaining metal concentration in solution is shown to evaluate the precipitation of the apatite residue as function of pH. The initial pH of the leachate after extraction was 0.37 and the pH was increased by using NaOH.

Table 6 Composition of the effluent (pH 7) as well as the maximum contaminant levels (MCL) permitted in drinking water (USA)[73]

Element	Effluent (mg L^{-1})	MCL (mg L^{-1})
Ca	1405	No regulatory limit
Sr	15	No regulatory limit
Sb	<0.005	0.006
Mn	<0.001	0.05
F	<0.02	4
P	<0.1	No regulatory limit

and can therefore be discarded in the sea.[73] Seawater contains 35 g L^{-1} (0.6 M) of NaCl on average.[74]

The precipitate evolves over time as it ripens and this is accompanied by a decrease of the pH (Fig. 7). The main species to precipitate out of solution around pH 7 are $CaHPO_4$ (eqn (14)) and a mixture of chloro-, fluoro- and hydroxoapatite: $Ca_5(PO_4)_3(OH,F,Cl)$ (eqn (15)).[71,72]

$$CaCl_2 + H_3PO_4 + 2NaOH \rightarrow CaHPO_{4(s)} + 2NaCl + 2H_2O \quad (14)$$

$$5CaCl_2 + 3H_3PO_4 + 10NaOH \rightarrow Ca_5(PO_4)_3(OH)_{(s)} + 10NaCl + 9H_2O \quad (15)$$

Manganese is co-precipitated and the stages of manganese precipitation can be visualized by the color change of the precipitate (Fig. 8). Below pH 2, no precipitation occurs and the solution is clear. Between pH 3 and 5 the Mn(II) ions are partially coprecipitated with the calcium phosphate, resulting in the typical pink color of Mn(II) salts. Above pH 7, manganese is fully removed as $Mn(OH)_{2(s)}$, which is cream colored and gradually turns brown upon standing (especially at high pH) due to the oxidation of Mn(II) and formation of Mn_2O_3.[75] Note

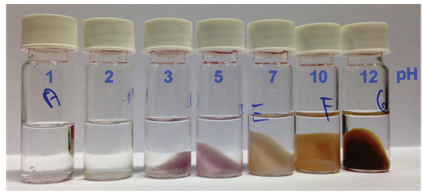

Fig. 8 Precipitation of the remaining elements present in the leachate after extraction of antimony. The pH was adjusted with NaOH.

the strong color of the precipitate despite the small manganese content (<1 wt%).

The calcium phosphate precipitate can be used in the phosphate and fertilizer industry since it is very similar to phosphate rock which is also a mixture of calcium phosphates and apatites.[31–37] Phosphate rock is the primary industrial feed for the production of phosphoric acid, phosphate fertilizers and hydrofluoric acid.[37] The small amounts of manganese in the precipitate can be removed in a separate step, but it may be more interesting to keep it since manganese is an important plant micronutrient.[76] The high purity of the recycled apatite, contrasts with the apatite in phosphate rock which contains traces of As, Pb and Cd.[31,37,38] Phosphate rock is also known for its radioactivity caused by U, Th, Ra and their decay products.[31,37,38] The precipitate produced in this process is thus a welcome source of phosphate. An overview of the entire process is shown in Fig. 9.

Note that in this process only HCl and NaOH are consumed and no waste is created except the NaCl effluent. The ionic liquid [A336][Cl] is entirely reusable and non-volatile so no losses occur. This recycling process for the recovery of critical antimony from the HALO lamp phosphor is therefore a good example of a zero-waste valorization approach. It is in theory

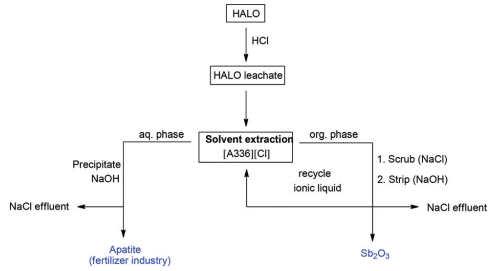

Fig. 9 Schematic overview of the proposed recycling process. After full dissolution in diluted HCl, the antimony is selective extracted from the leachate using the ionic liquid Aliquat® 336 and pure Sb_2O_3 is obtained after scrubbing and stripping. The remaining elements in the leachate are then reprecipitated as an apatite which can serve as feedstock in the fertilizer industry. The only waste of this process is an aqueous NaCl effluent which can be discarded in the sea.

also possible to regenerate HCl and NaOH by electrolysis of the NaCl solution in a membrane cell (eqn (16)), followed by the recombination of H_2 and Cl_2 to form HCl (eqn (17))

$$2NaCl + H_2O + E(V) \rightarrow 2NaOH + H_2 + Cl_2 \quad (16)$$

$$Cl_2 + H_2 \rightarrow 2HCl \quad (17)$$

This would result in a completely closed-loop recycling process as the reagents can be regenerated from the effluent and only energy would be consumed. Although the electrolysis of NaCl and synthesis of HCl is carried out in this way industrially on very large scale, it is probably more interesting for medium-sized recycling plants to purchase HCl and NaOH and discard the clean NaCl solution in the sea.

Conclusion

Halophosphate is the largest component in lamp phosphor waste (50 wt%), but is usually discarded as a non-valuable residue in rare-earth recycling even though it contains industrially important antimony. The increasing supply risk for antimony combined with decreasing rare-earth prices should turn the attention of researchers to the valorization of this lamp phosphor waste component. Here, a process is proposed to efficiently recover the antimony (>99.99 wt% purity) and to valorize the remaining elements as a high-quality feedstock for the phosphate industry. This green process operates at room temperature and no waste is created except a NaCl effluent, which makes it a more sustainable source of antimony than the energy-intensive processing of stibnite ore. The process can be integrated in lamp phosphor recycling schemes aimed at recovering rare earths. The main advantage of this step-wise and selective approach to lamp phosphor recycling is that less chemicals and energy are consumed to obtain pure end-products. Selective valorization of the most valuable components is a better strategy than full dissolution followed by separation, when dealing with a highly complex feedstock such as lamp phosphor waste. It is our hope that this paper will highlight the potential of lamp phosphor waste as an overlooked source of antimony and stimulate the inclusion of antimony recovery in future lamp phosphor waste recycling schemes.

Acknowledgements

The authors wish to thank the KU Leuven (projects GOA/13/008 and IOF-KP RARE^3) and the FWO Flanders (PhD fellowship to DD) for financial support.

Notes and references

1 C. G. Anderson, *Chem. Erde.*, 2012, **72**, 3–8.
2 G. B. Haxel, J. B. Hedrick and G. J. Orris, *Rare Earth Elements Critical Resources for High Technology - Fact Sheet 087-02*, U.S. Geological Survey, 2002.
3 Report on Critical raw materials for the EU, European Commission, DG Enterprise & Industry, Brussels, 2014.
4 G. Belardi, N. Ippolito, L. Piga and M. Serracino, *Thermochim. Acta*, 2014, **591**, 22–30.
5 J. J. Braconnier and A. Rollat, *Solvay, European Patent*, EP 2419377 A1, 2012.
6 T.-C. Chang, S.-F. Wang, S.-J. You and A. Cheng, *J. Environ. Eng. Manage.*, 2007, 435–439.
7 R. Dobrowolski and J. Mierzwa, *Mater. Chem. Phys.*, 1993, **34**, 270–273.
8 S. T. Henderson, A. M. Marsden and L. Thorn Lighting, *Lamps and lighting: a manual of lamps and lighting*, Edward Arnold, London, 1972.
9 K. Shinde, S. J. Dhoble, H. C. Swart and K. Park, in *Phosphate Phosphors for Solid-State Lighting*, Springer, Berlin Heidelberg, 2012, vol. 174, ch. 6, pp. 151–189.
10 A. M. Srivastava and T. J. Sommerer, *Electrochem. Soc. Interface*, 1998, **7**, 28–31.
11 C. R. Ronda, T. Jüstel and H. Nikol, *J. Alloys Compd.*, 1998, **275–277**, 669–676.
12 S. Shionoya, W. M. Yen and H. Yamamoto, *Phosphor Handbook*, Taylor & Francis, Boca Raton, 2006.
13 T. F. Soules, in *Physics and Chemistry of Luminescent Materials*, ed. C. R. Ronda, L. E. Shea and A. M. Srivastava, Electrochemical Society, Pennington, USA, 2000, vol. 40, pp. 56–68.
14 K. Binnemans and P. T. Jones, *J. Rare Earths*, 2014, **32**, 195–200.
15 K. Binnemans, P. T. Jones, B. Blanpain, T. Van Gerven, Y. Yang, A. Walton and M. Buchert, *J. Cleaner Prod.*, 2013, **51**, 1–22.
16 B. J. Baliga, *The IGBT Device: Physics, Design and Applications of the Insulated Gate Bipolar Transistor*, Elsevier Science, 2015.
17 Compact Fluorescent Lamps Could Nearly Halve Global Lighting Demand for Electricity, http://www.worldwatch.org/node/5918.
18 Y. Wu, X. Yin, Q. Zhang, W. Wang and X. Mu, *Resour., Conserv. Recycl.*, 2014, **88**, 21–31.
19 K. Binnemans, P. T. Jones, K. Acker, B. Blanpain, B. Mishra and D. Apelian, *JOM*, 2013, **65**, 846–848.
20 V. Innocenzi, I. De Michelis, B. Kopacek and F. Vegliò, *Waste Manage.*, 2014, **34**, 1237–1250.
21 H. Liu, S. Zhang, D. Pan, J. Tian, M. Yang, M. Wu and A. A. Volinsky, *J. Hazard. Mater.*, 2014, **272**, 96–101.
22 G. Mei, P. Rao, M. Mitsuaki and F. Toyohisa, *J. Wuhan Univ. Technol., Mater. Sci. Ed.*, 2009, **24**, 418–423.
23 C. Tunsu, C. Ekberg and T. Retegan, *Hydrometallurgy*, 2014, **144–145**, 91–98.
24 I. Urniezaite, G. Denafas and D. Jankunaite, *Waste Manage. Res.*, 2010, **28**, 609–614.
25 F. Yang, F. Kubota, Y. Baba, N. Kamiya and M. Goto, *J. Hazard. Mater.*, 2013, **254–255**, 79–88.
26 H. L. Yang, W. Wang, H. M. Cui, D. L. Zhang, Y. Liu and J. Chen, *J. Chem. Technol. Biotechnol.*, 2012, **87**, 198–205.

27 D. Dupont and K. Binnemans, *Green Chem.*, 2015, **17**, 856–868.
28 J. H. Hubbell and S. M. Seltzer, National Institute of Standards and Technology (NIST), NIST X-ray Attenuation Databases, http://physics.nist.gov/PhysRefData/XrayMassCoef/tab3.html, 2014.
29 R. Otto and A. Wojtalewicz, *US patent* 2012/0027651 A1, 2012.
30 F. H. Firsching and S. N. Brune, *J. Chem. Eng. Data*, 1991, **36**, 93–95.
31 K. Binnemans, P. T. Jones, B. Blanpain, T. Van Gerven and Y. Pontikes, *J. Cleaner Prod.*, 2015, **99**, 17–38.
32 C. J. Dawson and J. Hilton, *Food Policy*, 2011, **36**(Supplement 1), S14–S22.
33 R. H. E. M. Koppelaar and H. P. Weikard, *Global Environ. Chang.*, 2013, **23**, 1454–1466.
34 L. Reijnders, *Resour., Conserv. Recycl.*, 2014, **93**, 32–49.
35 R. W. Scholz, A. E. Ulrich, M. Eilittä and A. Roy, *Sci. Total Environ.*, 2013, **461–462**, 799–803.
36 P. Walan, S. Davidsson, S. Johansson and M. Höök, *Resour., Conserv. Recycl.*, 2014, **93**, 178–187.
37 T. P. Hignett, *Fertilizer Manual*, Springer, Netherlands, 2013.
38 M. Chen and T. E. Graedel, *J. Cleaner Prod.*, 2015, **91**, 337–346.
39 N. C. Norman, *Chemistry of Arsenic, Antimony and Bismuth*, Springer, 1998.
40 S. V. Dorozhkin, *Comments Inorg. Chem.*, 1999, **20**, 285–299.
41 S. V. Dorozhkin, *World J. Methodol.*, 2012, **2**, 1–17.
42 A. H. Abdullah, N. H. M. Noor, I. Ramli and M. Hashim, *Mater. Chem. Phys.*, 2008, **111**, 201–204.
43 X. Y. Chen, H. S. Huh and S. W. Lee, *J. Solid State Chem.*, 2008, **181**, 2127–2132.
44 M. Vuković, Z. Branković, D. Poleti, A. Rečnik and G. Branković, *J. Sol–Gel Sci. Technol.*, 2014, **72**, 527–533.
45 M. Filella, N. Belzile and Y.-W. Chen, *Earth-Sci. Rev.*, 2002, **59**, 265–285.
46 J.-g. Yang and Y.-t. Wu, *Hydrometallurgy*, 2014, **143**, 68–74.
47 H. Hashimoto, T. Nishimura and Y. Umetsu, *Mater. Trans.*, 2003, **44**, 1624–1629.
48 Y. Ling and G. P. Demopoulos, *J. Chem. Eng. Data*, 2004, **49**, 1263–1268.
49 A. Al-Othman and G. P. Demopoulos, *Hydrometallurgy*, 2009, **96**, 95–102.
50 V. Gomis, M. D. Saquete and J. García-Cano, *Fluid Phase Equilib.*, 2013, **360**, 248–252.
51 A. Alian and W. Sanad, *Talanta*, 1967, **14**, 659–669.
52 B. M. Sargar, M. M. Rajmane and M. A. Anuse, *J. Serb. Chem. Soc.*, 2004, **69**, 283–298.
53 F. G. Seeley and D. J. Crouse, *J. Chem. Eng. Data*, 1966, **11**, 424–429.
54 L. Tomlinson, *J. Electrochem. Soc.*, 1964, **111**, 592–596.
55 P. Navarro, J. Simpson and F. J. Alguacil, *Hydrometallurgy*, 1999, **53**, 121–131.
56 A. R. Byrne and D. Gorenc, *Anal. Chim. Acta*, 1972, **59**, 81–89.
57 E. M. Donaldson and M. Wang, *Talanta*, 1986, **33**, 35–44.
58 S. Facon, G. Cote and D. Bauer, *Solvent Extr. Ion Exch.*, 1991, **9**, 717–734.
59 A. P. Grimanis and I. Dore Hadzistelios, *Anal. Chim. Acta*, 1968, **41**, 15–21.
60 J. N. Iyer and P. M. Dhadke, *Indian J. Chem. Technol.*, 2003, **10**, 665–669.
61 N. V. Kirichenko, A. I. Nikolaev, V. G. Maiorov, A. V. Tyuremnov and E. G. Il'in, *Russ. J. Inorg. Chem.*, 2013, **58**, 474–480.
62 H. K. Lin, *Hydrometallurgy*, 2004, **73**, 283–291.
63 S. G. Sarkar and P. M. Dhadke, *Sep. Purif. Technol.*, 1999, **15**, 131–138.
64 J. A. N. Szymanowski, *Miner. Process. Extr. Metall. Rev.*, 1998, **18**, 389–418.
65 R. G. Vibhute and S. M. Khopkar, *Talanta*, 1989, **36**, 957–959.
66 N. V. Deorkar and L. L. Tavlarides, *Hydrometallurgy*, 1997, **46**, 121–135.
67 P. Navarro and F. J. Alguacil, *Hydrometallurgy*, 2002, **66**, 101–105.
68 L. Łukaszczyk and W. Żyrnicki, *J. Pharm. Biomed. Anal.*, 2010, **52**, 747–751.
69 S. Wellens, B. Thijs and K. Binnemans, *Green Chem.*, 2012, **14**, 1657–1665.
70 Bruker, Detection limits for the NIST 1640 reference standard, https://www.bruker.com/products/x-ray-diffraction-and-elemental-analysis/micro-xrf-and-txrf/s2-picofox/applications.html.
71 J. F. De Rooij, J. C. Heughebaert and G. H. Nancollas, *J. Colloid Interface Sci.*, 1984, **100**, 350–358.
72 J. W. Sausville, *U.S. Patent*, US3663473 A, 1972.
73 (EPA), Environmental Protection Agency, *National Primary Drinking Water Regulations*, USA, 2009.
74 M. H. Sharqawy, J. H. Lienhard and S. M. Zubair, *Desalin. Water Treat.*, 2010, **16**, 354–380.
75 G. Rayner-Canham, in *Descriptive Inorganic Chemistry, Freeman*, New York, 1996, ch. 8.
76 G. DalCorso, A. Manara, S. Piasentin and A. Furini, *Metallomics*, 2014, **6**, 1770–1788.

Paper 4: A critical review of secondary antimony sources

Title:
Antimony recovery from end-of-life products and industrial process residues: a critical review

Type: Review paper
Journal: Journal of Sustainable Metallurgy
Publisher: Springer
Publication date: 08/02/2016

Reprint with permission from:
D. Dupont, S. Arnout, P. T. Jones, K. Binnemans, *J. Sustain. Metall.*, **2016**, 2, 79-103.

J. Sustain. Metall. (2016) 2:79–103
DOI 10.1007/s40831-016-0043-y

REVIEW ARTICLE

Antimony Recovery from End-of-Life Products and Industrial Process Residues: A Critical Review

David Dupont[1] · Sander Arnout[2] · Peter Tom Jones[3] · Koen Binnemans[1]

Published online: 8 February 2016

Abstract Antimony has become an increasingly critical element in recent years, due to a surge in industrial demand and the Chinese domination of primary production. Antimony is produced from stibnite ore (Sb_2O_3) which is processed into antimony metal and antimony oxide (Sb_2O_3). The industrial importance of antimony is mainly derived from its use as flame retardant in plastics, coatings, and electronics, but also as decolourizing agent in glass, alloys in lead-acid batteries, and catalysts for the production of PET polymers. In 2014, the European Commission highlighted antimony in its critical raw materials report, as the element with the largest expected supply–demand gap over the period 2015–2020. This has sparked efforts to find secondary sources of antimony either through the recycling of end-of-life products or by recovering antimony from industrial process residues. Valuable residues are obtained by processing of gold, copper, and lead ores with high contents of antimony. Most of these residues are currently discarded or stockpiled, causing environmental concerns. There is a clear need to move to a more circular economy, where waste is considered as a resource and zero-waste valorization schemes become the norm, especially for rare elements such as antimony. This paper gives a critical overview of the existing attempts to recover antimony from secondary sources. The paper also discusses the possibility of waste valorization schemes to guarantee a more sustainable life cycle for antimony.

Keywords Antimony · Recovery · Recycling · Secondary sources

Introduction

The history of antimony goes back to as early as 3100 BC, when it was used by the Egyptians as cosmetic in the form of black Sb_2S_3 [1]. Antimony was later used by alchemists in the form of antimony oxychloride SbOCl, which acted as a powerful emetic and thus became known as "mercury of life" or "algarot" [2]. The etymology of the current name "antimony" is still subject of discussion. Some believe it comes from the Greek word *antimonos* ("never found alone"), others have suggested it is derived from the greek word *anthos* ("flower"), due to the petal-like appearance of stibnite ore, and some even argued that it is derived from the Greek word *anti-monachos* or the French word *antimoine* ("against monks"), which could refer to the poisonous properties of antimony and the fact that many early alchemists were monks [1, 2]. Despite its long history, antimony metal was isolated and identified as late as the 16th century. Today, antimony is used in a wide variety of products and processes. It is mainly produced from stibnite

The contributing editor for this article was Diran Apelian.

✉ Koen Binnemans
Koen.Binnemans@chem.kuleuven.be

David Dupont
David.Dupont@chem.kuleuven.be

Sander Arnout
sander.arnout@inspyro.be

Peter Tom Jones
Peter.Jones@mtm.kuleuven.be

[1] Department of Chemistry, KU Leuven, Celestijnenlaan 200F, P.O. Box 2404, 3001 Heverlee, Belgium

[2] InsPyro NV, Kapeldreef 60, 3001 Heverlee, Belgium

[3] Department of Materials Engineering, KU Leuven, Kasteelpark Arenberg 44, P.O. Box 2450, 3001 Heverlee, Belgium

ore (Sb_2S_3), but also occurs as oxide (Sb_2O_3), and as antimonides and sulphoantimonides of metals like lead, copper, zinc, silver, and gold [3]. Antimony is mainly used in the form of Sb_2O_3, as flame retardant in plastics, coatings, and electronics, due to its synergetic effect with halogenated flame retardants, which minimizes the amount of halogenated flame retardant required [4]. This application takes up the majority of the world's antimony production [4, 5]. Antimony is also used in catalysts for the production of polyethylene terephthalate (PET) polymers and as additive in glass in the form of sodium antimonite, which acts as a decolourizing agent for optical glass in cameras, photocopiers, binoculars, and fluorescent light tubes [3, 6]. Antimony metal is used as a hardener in lead alloys such as the lead electrodes in lead-acid (LA) batteries [1, 7]. The average antimony content of automotive battery alloys has declined from 7 to 1.6 % in recent years, as Ca, Al, and Sn alloys have been used as replacements. However, the increasing car sales partly compensate for the declining use of antimony in LA batteries [5, 7]. Other minor uses include paint pigments (Sb_2O_3, Sb_2S_3, Sb_2S_5), semiconductors (e.g., AsSb, GaSb, InSb), IR-reflecting camouflage paints (Sb_2S_3), matchboxes (Sb_2S_3), and vulcanizing agents in the production of red rubber (Sb_2S_5) [2, 7]. Antimony compounds are also used in certain phosphors (for instance the halophosphate lamp phosphors), pesticides, ammunition, and medicine [7]. Overall, it is estimated that the global antimony consumption is distributed to flame retardants 52 %, lead alloys and lead-acid batteries 38 %, catalysts for the production of polyethylene terephthalate (PET) 6 %, and chemicals, ceramics, and glass less than 3 %, down from 13 % in 2000 [3]. More detailed overviews of the antimony market and applications can be found in industry reports and government reports [3, 5].

Antimony mining is currently dominated by China ($\approx$78 % of global production), which also holds the largest reserves (Table 1) [1]. The dependence on China, combined with the strong industrial demand for antimony, has raised concerns over the supply security, especially since the abundancy of antimony in the earth's crust is quite low (0.2 ppm) and current reserves (1,800,000 t) allow for only 10–11 more years of production at the current speed (Table 1) [8].

Table 1 Antimony world mine production and reserves (tons) in 2014 [8]

Country	Mine production 2014	Reserves (recoverable)
China	125,000	950,000
Burma	9000	NA
Russia	7000	350,000
Bolivia	5000	310,000
Tajikistan	4700	50,000
Other	8300	177,000
Total	160,000	1,800,000

Figure 1 shows the distribution of primary and secondary production as well as the portion of illegal (non-reported) primary mining based on a 2011 consulting report [3]. Despite the presence of some deposits, no antimony is currently mined in Europe or in the U.S.A. [1, 7].

These observations have led the European Commission to highlight antimony as a critical raw material in 2014, with an expected supply–demand gap exceeding 10 % over the period 2015–2020, which is the highest amongst all critical metals [9]. The processing of antimony ores and the production of antimony metal is also concentrated in China, due to its high smelting capacity. Most of the antimony industry in Europe and the U.S.A. is therefore dependent on the import of Chinese antimony metal and is focused on the production of high-purity products and applications.

The aim of this paper is to give an overview of antimony-containing waste streams and to analyze their potential as secondary sources of antimony. Furthermore, the existing valorization methods are discussed as well as the environmental hazard associated with antimony. Finally, an overview is given of the existing water purification and air treatment methods to recover traces of antimony and avoid unwanted release of antimony into the environment. Secondary supply, through recycling and valorization of industrial residues could be a solution to ensure a more secure long-term supply of antimony [9]. Secondary production of antimony could also make Europe and the U.S.A. less reliable on Chinese antimony, thus lowering geopolitical risks. Roskill Consulting estimated that in 2010 around 20 % of the global antimony supply originated from secondary production [3]. Today, secondary production of antimony is mainly restricted to the recycling of antimony-containing lead alloys from lead-acid battery recycling plants [3]. However, interesting future secondary sources could include industrial residues (e.g., mine tailings, process residues, manufacturing scrap) from the production of lead, copper, gold, and antimony [7]. The large production volumes, especially for copper and lead, mean that these residues have the potential to replace a large portion of the primary antimony production [7]. Secondary antimony sources also include end-of-life products such as lead-acid batteries, plastics with antimony-containing flame retardants, antimony-containing glass, and phosphor powders from spent fluorescent lamps [7]. At this moment, only lead-acid batteries are being recycled on a large scale [10, 11]. Antimony could also be recycled from spent fluid catalytic cracking (FCC) catalysts or from catalysts used for the production of PET polymers [12]. Finally, efforts have been made to recover antimony

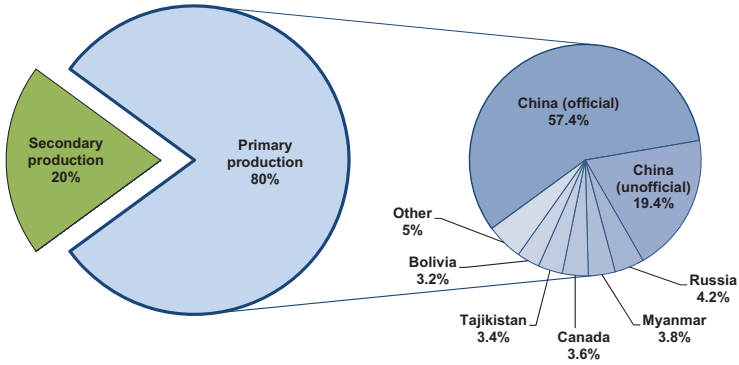

Fig. 1 Distribution of antimony ore production in 2010 (196,484 t), using data compiled by Roskill [3]

from landfills and municipal solid waste incineration (MSWI) ashes [13–15]. A schematic overview of the antimony life cycle, with its waste streams and possible recycling routes, is depicted in Fig. 2.

Recovery from Industrial Residues

Antimony Production

The primary production and metallurgy of antimony has been reviewed by Anderson (2012) [1]. However, in order to discuss the secondary production of antimony from industrial residues, a short overview must be given here of the main production routes, process residues, and metal-containing waste streams. The main pyro- and hydrometallurgical pathways to produce antimony metal and antimony oxide (Sb_2O_3), are shown in Fig. 3.

Hydrometallurgical methods are based on two steps: leaching (alkaline sulfide or acidic chloride system), followed by the electrodeposition of antimony metal at the cathode, or hydrolysis with NaOH or NH_4OH to produce Sb_2O_3 [1]. At this moment, mainly pyrometallurgical processes are used, but hydrometallurgical processes based on alkaline sulfide leaching have been employed industrially in the former Soviet Union, China, Australia, and the United States [1]. Alkaline sulfide technology has the advantage of having a high selectivity toward antimony,

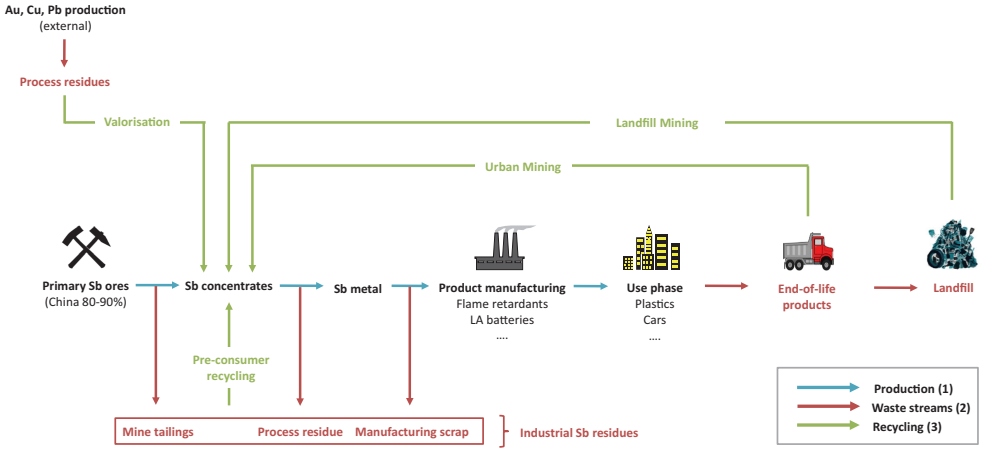

Fig. 2 Schematic overview of the antimony life cycle, which includes (*1*) the main value chain between primary mining and final disposal, (*2*) the major waste streams, and (*3*) the possible secondary antimony production routes through recycling and recovery of antimony-containing waste (Color figure online)

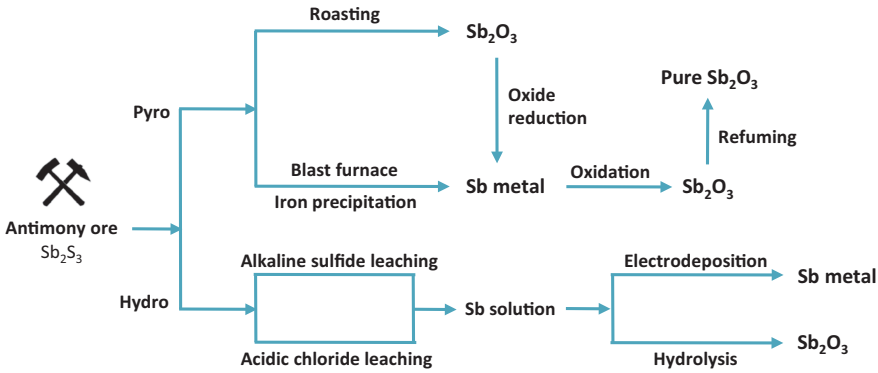

Fig. 3 Primary production of antimony through pyrometallurgical and hydrometallurgical methods

and having less issues with corrosion. However, a considerable amount of research and pilot-scale work has been undertaken to utilize chloride-based technology [1, 16, 17]. A more detailed overview of the pyrometallurgical pathways and process residues is given in Fig. 4.

A stibnite concentrate is first produced by grinding, milling, flotation, and gravity concentration [1]. These steps are usually carried out close to the mining site, and result in Sb-containing mine tailings. Depending on the grade of antimony in the concentrate, different pyrometallurgical methods can be used to extract antimony [1]. For low-grade ores (5–25 % Sb), *oxide volatilization* is used. The ores are roasted at 1000 °C, and the volatile Sb_2O_3 is recovered. Intermediate grade ores (25–40 % Sb), and Sb-rich residues, slags, mattes, and flue dusts are smelted in a blast furnace at 1300–1400 °C which produces antimony metal, SO_2 gas, and a slag. Sb-rich ores (45–60 % Sb) can be treated by *liquation* and *iron precipitation*. Liquation consists of heating the ore to 550–600 °C under a reducing atmosphere, to extract liquid Sb_2S_3 from the ore. This product is called crude, liquated, or needle antimony. The liquation residue (12–30 % Sb) can be treated to further improve the recovery of antimony. The *iron precipitation* method is used to produce antimony metal from concentrated antimony ores or from the crude antimony issued from the liquation process. In this process, scrap iron is added to molten Sb_2S_3 to displace the antimony in order to form antimony metal and a *matte* which contains iron sulfide. The reduction of Sb_2O_3 to antimony metal is done with charcoal in a reverberatory furnace (1200 °C), with the formation of a slag. The loss of antimony by volatilization is high (12–20 %), meaning that the flue

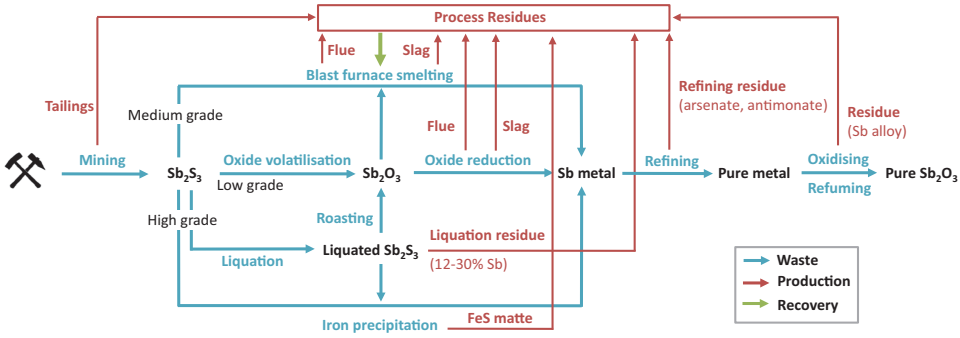

Fig. 4 Pyrometallurgical pathways (*blue*) and metal-containing waste streams (*red*) for the primary production of antimony from stibnite ore. The different process residues can be used as secondary antimony sources and fed back into the blast furnace (*green*) (Color figure online)

dusts must also be caught and then reprocessed in a blast furnace. Finally, refining steps are needed to obtain pure antimony metal (e.g., arsenic removal with NaOH). This creates arsenate- and antimonate-containing residues. Highly pure Sb_2O_3 is usually obtained by oxidation of technical grade antimony metal (99.0–99.8 % pure), followed by a refuming process (volatilization + condenzation) [2]. These oxidation processes produce dusts and residues, which can also contain important quantities of antimony. It is clear from Fig. 4 that antimony production creates many residues. The composition of these residues is highly variable on the type of feed material and the process parameters, but some representative compositions are given in Table 2.

In some countries, these residues are stockpiled or landfilled, causing metal pollution in the areas around antimony mining sites and processing plants [18, 22–24]. A better approach is to try to immobilize these waste residues by applying various stabilization, solidification, and geopolymerization techniques [22]. However, a better solution is to valorize these residues, thus creating *secondary sources* of antimony. This increases the extraction efficiency of antimony from the initial ore and also eliminates or reduces the need to discard residues containing toxic metals [18]. Guo et al. [18] characterized the process residues (e.g., slags, flue dusts) from an antimony smelting plant in Xikuangshan area in China (the "antimony capital"). They found large amounts of antimony in the flue dust of the blast furnace (23.4 wt%) and in the residue from the arsenic removal process (37.8 wt%). The leaching of the different residues was studied in an effort to remove the antimony and other metals (e.g., Hg, Pb, As, Cr) from these waste residues. Fuxu et al. investigated the use of a three-phase fluidized bed reactor for arsenic removal from Sb-refining residue (20–40 % Sb, 3–5 % As) [21]. Their set-up achieved a 97 % removal rate of arsenic, leaving behind a valuable antimony concentrate. Kequiang et al. [21] prepared Sb_2O_3 (98.50 % pure) from Sb-containing slag, using a vacuum evaporation method. The slag was placed in the vacuum chamber and heated (893–1073 K) in order to selectively evaporate the volatile Sb_2O_3. Luo et al. [20] studied the recovery of gold and antimony from antimony smelting slag by direct reduction in an electric furnace. Using this method, the antimony content in the slag was reduced from 32 to <1 wt%. During the pyrometallurgical production of antimony oxide from antimony metal, waste residues are also created, which contain alloys of antimony and other base and precious metals. Anderson [7] studied the recovery of antimony from these pyrometallurgical production residues. Using alkaline sulfide leaching, 99.5 % of antimony was recovered.

Table 2 Heavy metal content (wt%) in various process residues from the primary production of antimony

Residue	Sb	As	Hg	Zn	Pb	Cu
Smelter slag [18]	1.11	0.57		0.07		0.01
Smelter flue dust [18]	23.4	0.13	0.93	0.03	0.05	0.04
Gas treatment slag [18]	0.69	0.07	0.05			
Refining residue [18]	37.8	11.4				
Refining residue [19]	34.85	4.41				
High-Sb slag [20]	32.00	0.63			0.30	
High-Sb slag [21]	39.49					
Sb oxidation residue [7]	63.0				18.0	12.0

The data are based on literature reports [18–20]

At the same time, research is still ongoing to optimize the primary production of antimony from stibnite ore and to reduce the amount of (toxic) waste streams [7, 16, 25, 26]. Yang et al. [25], for example, developed a low-temperature sulfur-fixing smelting process, using a NaOH–Na_2CO_3 flux with ZnO to fix the sulfur as ZnS. This approach reduces SO_2 emissions (98.61 % sulfur-fixing) and results in an antimony recovery rate of 97.07 % in the form of antimony metal. Ye et al. [26] investigated a similar system, using a eutectic Na_2CO_3–NaCl molten salt and ZnO as a sulfur-fixing agent. Under optimum conditions, the average recovery ratio of antimony reached 92.88 %. Also of interest, are the efforts to recover antimony from a low-grade or complex stibnite ore, as well as from secondary antimony minerals. Yang and Wu [16] developed a new hydrometallurgical process to recover antimony from complex stibnite concentrate. They dissolved antimony using a chlorination–oxidation procedure to obtain an $SbCl_3$ solution. Using electrodeposition, hydrolysis, hydrolysis–smelting, or hydrolysis–washing, they obtained cathode antimony metal (99.98 %), Sb_2O_3 (99.9 %), crude antimony metal (99 %), or SbOCl (99.9 %), respectively. Gök (2014) published a hydrometallurgical method for the catalytic production of antimonate from stibnite concentrate [27]. Alkaline leaching was used to extract the antimony, followed by the oxidation of Sb(III) in a hydroquinone-catalyzed alkaline electrolyte, which precipitates antimony as sodium hydroxyantimonate $NaSb(OH)_6$ (with 90 % recovery).

Besides stibnite, researchers are also investigating other, complex antimony minerals. An overview of complex antimony minerals and their mineralogy has been compiled by Roper et al. [28]. Complex antimony minerals often require adapted flowsheets in order to ensure the recovery of antimony and the other main metal constituents. The last primary producer of antimony in the U.S.A. (Sunshine Mining & Refining Company) was mining the complex copper-silver-antimony sulfide: freibergite $(Cu,Ag)_{12}Sb_4S_{13}$ [1]. This mine produced both silver and antimony concentrates until its closure in 2001. Other interesting Sb-

containing minerals are tetrahedrite $(Cu,Fe)_{12}Sb_4S_{13}$ and jamesonite $Pb_4FeSb_6S_{14}$. Baláž et al. [29] investigated the leachability of antimony and arsenic from tetrahedrite and jamesonite with alkaline sulfide leaching. Awe and Sandström [30] also studied the selective leaching of arsenic and antimony from a tetrahedrite-rich complex sulfide concentrate and concluded that by removing these elements, a valuable copper concentrate was obtained, which could be used as a feedstock for copper smelting. Yang et al. [31] developed a flowsheet for the recovery of antimony from a low-grade jamesonite concentrate ($Pb_4FeSb_6S_{14}$). They used sodium sulfide to dissolve the antimony as sodium thioantimonate (Na_3SbS_4) and subsequently used air oxidation to produce sodium pyroantimonate. ($Na_2H_2Sb_2O_7$). Duchao et al. [32] improved this process by using pressured air oxidation. Under optimum conditions, the precipitation ratio of antimony was 99.38 %. Gold, copper, and lead production are also associated with large amounts of antimony impurities, which end up in the process residues.

Gold Production

Gold-bearing sulfide ores often contain important amounts of antimony (Table 3). Kyle et al. [38, 39] made a series of reports on the occurrence and deportment of trace elements (Sb, Bi, Se, Te, As, Hg, Cd, Pb) in gold processing. They estimated that in Australia alone, total emissions of antimony (air, water, land) reach as much as 3.8 t/year during mining and 8.7 t/year during metal manufacturing. This represents a significant loss of valuable antimony and it is a challenge to find better processing technologies which can minimize the loss of antimony by valorizing the different gold-mining residues and waste streams.

These "refractory" gold ores are resistant against the standard gold recovery method of cyanidation and carbon adsorption, because the sulfide mineral traps the gold particles, making it difficult for the cyanide leach solution to complex with the gold [2, 40]. Pretreatment is therefore required to make the cyanidation effective. Different pretreatment options exist: chemical leaching, roasting, bacterial oxidation, pressure oxidation, and ultrafine grinding [2, 40]. The choice of pretreatment process depends on the type of ore and the impurities present in the ore and may be preceded by a flotation concentration step. Depending on the concentrations of gold and antimony, different categories of Au-Sb-containing sulfide ores can be distinguished: (1) ores in which gold is the main valuable component and antimony is a harmful impurity, (2) gold-bearing ores in which the amount of antimony is considerable and for which it is economically viable to recover antimony as a commercial byproduct, (3) antimony ores in which gold is a minor accompanying element, the recovery of which could increase the economic efficiency of the process [38, 41]. For the ores of group (1) and (3), standard gold-processing and antimony-processing technology is applied, respectively. The recovery of traces of gold and antimony from these ores is only interesting for waste products, as this does not cause losses in the recovery of the main metal. The processing of the second group of ores (2), usually requires changes in the flowsheet in order to ensure the recovery of both the gold and antimony fraction. For this type of ores, alkaline sulfide leaching is a preferred pretreatment method as it isolates antimony and simultaneously increases the recovery rate of gold in the consequent cyanidation step (Fig. 5).

Ubaldini et al. [40] used alkaline sulfide leaching as a pretreatment step, to remove antimony from a gold-bearing stibnite ore. Antimony was then recovered by electrodeposition. Results showed that this pretreatment improved the recovery of gold in the consequent cyanidation process from 30 to 75 %. Celep et al. [35, 42] studied similar antimonial refractory gold and silver ores. Their findings confirmed that alkaline NaOH and Na_2S leaching were appropriate pretreatment methods to recover antimony prior to the conventional cyanidation for the recovery of the noble metals. Using this approach, 85 % of antimony could be leached out and during the subsequent cyanidation step, silver recovery rates increased from less than 18 % up to 90 % and gold extraction was also enhanced by 20–30 %. Solozhenkin et al. (2010) investigated the complex antimony ores and gold-antimony concentrates, found in the Sarylakhsky and Sentachansky deposits in Russia [34, 43]. They developed different hydrometallurgical processes to treat these ores and produce both gold and antimony concentrates with antimony recovery rates of

Table 3 Literature examples of Au-Sb-rich ores and waste from which both gold and antimony can be valorized into concentrates

Antimony concentrate	Au (g/t)	Ag (g/t)	Sb (wt%)	As (wt%)
Refractory Sb-Au ore 1 [33]	3.6		0.3	0.4
Refractory Sb-Au ore 2 [34]	7.4		16.73	
Refractory Sb-Au ore 3 [34]	42.2		28.7	
Refractory Sb-Au ore 4 [35]	20	220	1.6	0.03
Refractory Sb-Au ore 5 [36]	10.5	2.1	0.22	1.67
Electrorefining Slime [37]	210		0.31	

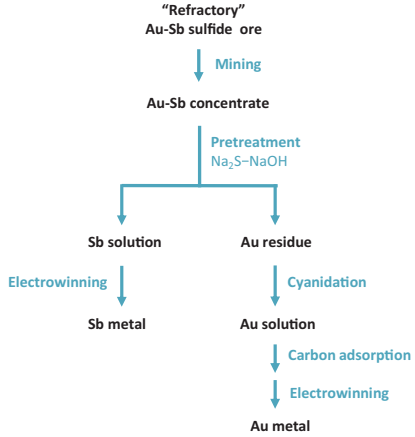

Fig. 5 Schematic visualization of the pretreatment of refractory Au-Sb sulfide ore with alkaline sulfide leaching. The pretreatment method improves the cyanidation of gold and allows the recovery of antimony [40]

95–98 %. The studied methods include antimonite flotation, sodium dimethyldithiocarbamate treatment, and biotreatment of the ores. The authors also introduced a processing plant for Sb-Au-bearing alloys and demonstrated the successful electrolytic refining and production of cathode antimony and noble metal slurry [39, 43]. Kanarskii et al. [38] investigated the concentration and isolation of antimony and arsenic in Sb-As-bearing gold ores by flotation. They demonstrated the flotation separation of antimonite and arsenopyrite into separate products, thus increasing process efficiency and profit by improving the gold recovery rate and reducing the consumption of cyanide. Karimi et al. [36] investigated the influence of different pretreatment methods (H_2O_2/air oxidation, roasting, and HNO_3/HCl leaching) on the cyanidation of Sb-rich gold ores and the movement of antimony and impurities. Saleh et al. [37], examined the recovery of Au, Sb, and Sn from gold electrorefining slime. The solid waste was dissolved in HCl (2 M), before extracting the metal ions with the quaternary ammonium chloride extractant Aliquat® 336.

Copper Production

Copper is mainly produced from copper ores such as chalcopyrite, $CuFeS_2$, which often contain antimony, arsenic, and bismuth as impurities [2]. These impurities must be removed and therefore end up in various residues. The formation of the residues is discussed here, as well as the recovery of antimony from these residues. In the past, the copper concentrate (20–40 % Cu) was first roasted and then introduced in blast furnaces or reverberatory furnaces, but nowadays direct smelting is favored using for example Outokumpu Flash furnaces or Isasmelt furnaces [2, 44]. During smelting, silica is added as a flux to remove iron as an iron-silicate *slag,* which floats on top and which can be used as building material. A *copper matte* is also formed which is a mixture of copper, iron, and sulfur that is enriched in copper. The copper matte (30–70 % Cu) produced in the smelter is then introduced in a converter, where air is blown into the matte to remove the sulfur as SO_2 gas and to form *blister copper* (>98 % Cu) and an iron-silicate "Fayalite" slag (Fe_2SiO_4). The blister copper is then put into an anode furnace (fire refining), where it is purified to *anode-grade copper* by removing most of the remaining sulfur, oxygen, and iron. Oxygen is usually removed by blowing natural gas through the melt (*poling*). The resulting *anode copper* (>99 % Cu) is further purified by electrorefining. The copper anodes are placed in an electrolysis set-up filled with an aqueous solution of $CuSO_4$ and H_2SO_4. By applying a voltage, copper and the less noble metals (e.g., Fe, Ni, Co, Zn, Pb, Sb, Bi, As) dissolve at the anode, while the more noble metals (e.g., Ag, Au, Se, Te) settle at the bottom of the cell as *anode slime.* The Cu(II) ions migrate through the electrolyte to the cathode, and copper metal is deposited. Part of the less noble metal ions remain in solution as soluble sulfates (e.g., Fe, Ni, Co, Zn), while others precipitate as insoluble sulfates (Pb) or hydrolyzed species (As, Sb, Sn, Bi) and are therefore found in the anode slime on the bottom of the cell, together with the noble metals. The electrolyte solution and anode slimes are valuable by-products of copper electrorefining and can be further treated. Metals can also accumulate in the *flue dust* of the smelter or converter. A detailed overview of the existing copper production processes has been compiled by Moskalyk and Alfantazi [45]. Here, a condensed (schematic) overview of the copper production process and its residues is given (Fig. 6).

The composition of the process residues is very dependent on the type of ore and the process that is used to extract the copper. However, some representative examples can be found in the literature (Table 4).

Antimony-containing residues are an increasingly big issue in copper processing due to the deteriorating quality of primary copper ores. However, no recycling activities are currently carried out on industrial scale although there is a strong commitment to develop these in the future. Antimony is found in different intermediates and residues of the copper production process, and a wide variety of processes has been developed on laboratory scale to recover antimony from these waste streams. Awe et al. [53] developed a flowsheet to remove antimony from copper concentrates which feed the copper industry. Alkaline

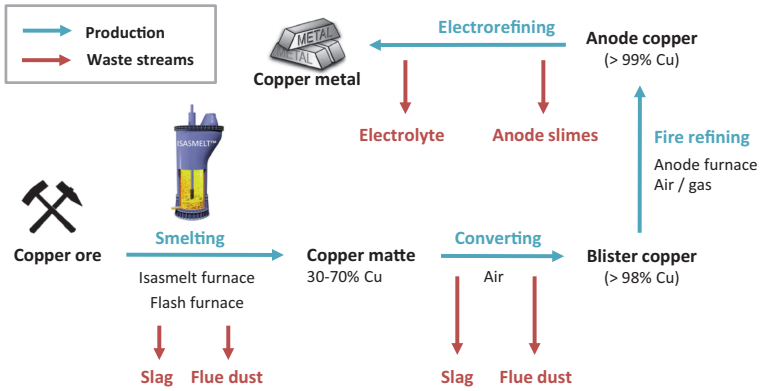

Fig. 6 Schematic overview of primary copper production from copper ores (Color figure online)

Table 4 Literature examples of copper processing residues and their metal contents (wt%) [7, 46–51]

Residue	Sb	Cu	Ni	Se	Te	As	Bi	Pb	Zn	Ag	Sn	Fe
Slag [46]		0.4										49.3
Flue dust [47]	3.1	5.3				2.8	2.8	28	8.9		12.0	1.2
Anode slime 1 [48]	3.0	25.4		8.2	1.3	3.4	0.8	2.9		14.5		
Anode slime 2 [49]	24.6	1.44	2.4					0.5			17.7	2.4
Anode slime 3 [7]	8.3	1.0	1.0	0.2	0.2	2.0	2.0	35.7		18.2		
Anode slime 4 [50]	5.09	11.9		5.2	0.6	4.1		16.2		10.5	1.0	
Electrolyte [51]	1.0	90.3				7.51	1.2	0.1				
Electrolyte [52]	1.0	97.5					0.6					1.0

sulfide leaching was used (Na_2S/NaOH) to extract antimony from the ore, which was then electrodeposited as antimony metal. Using this approach, the antimony content in the concentrate was reduced from 1.7 % to less than 0.1 % Sb, which is desirable for copper. Zhang et al. [54] studied the recovery of antimony and bismuth from pressure-leached flue dust created during the smelting of copper. They used a three-step process consisting of a kerosene desulfurization step, a chloride leaching step, and a final hydrolysis step to recover 95.80 % of Bi and 90.8 % of Sb. Vircikova et al. [47] investigated the removal of arsenic from converter flue dust as well as the behavior of antimony and bismuth. Arsenic was leached using a Na_2S solution and then precipitated using different methods. Recovery rates up to 99.9 % were achieved for arsenic but only 6.6 % for antimony. Fernández et al. [48] investigated the leaching of antimony and arsenic from anode slimes in the electrorefining of copper. The oxidized arsenic and antimony compounds in the anode slimes were selectively and almost completely dissolved in 0.4 M KOH at 80 °C. Meng et al. [49] studied the recovery of antimony(V) from the chloride leachate of copper anode slimes. Antimony was recovered by hydrolysis in the form of Sb_2O_5 with a recovery rate of 97 %. Anderson [7] reported the selective leaching of antimony and arsenic from copper electrorefining slimes, using alkaline sulfide leaching (Na_2S–NaOH). Recovery rates were 99.3 % for Sb and 99.5 % for As. Li et al. [50] investigated alkaline fusion leaching as a method to recover valuable metals from copper anode slimes. The slime was fused with NaOH and $NaNO_3$, followed by water leaching. Se, As, Sn, and Pb were leached out, leaving behind a valuable concentrate of Cu, Sb, Te, and precious metals (Ag, Au, Pt).

Much research has also been carried out to remove impurities (e.g., Sb, Bi, As, Pb) from copper electrolyte solutions with sorbents and solvent extraction methods [55]. Some metals such as antimony can cause passivation of the electrodes during electrorefining and is therefore important to remove these from the electrolyte solution [56]. Ando and Tsuchida [52] studied the recovery of trace impurities (Sb and Bi) from copper electrolyte solutions, using adsorbents with aminophosphonic acid functional groups. High recovery rates of 99.5 % for Bi and 100 % for Sb were achieved. Deorkar and Tavlarides [57]

investigated the use of a silica gel ceramic support, functionalized with covalently bonded pyrogallol groups as a sorbent to separate antimony from copper and lead. The bed was regenerated by desorbing Sb(III) with HCl (4 M) and potassium hydrogen tartrate (0.05 M), resulting in a concentration factor of 25–30. Navarro and Alguacil [58] reported the adsorption of antimony and arsenic from a copper electrorefining solution onto activated carbon. Wang et al. [51] developed a new adsorbent based on Sb(V) and $BaSO_4$ as a carrier to recover impurities (e.g., Sb, Bi) from a copper electrolyte solution. Sb(V) can combine with Bi(III) and Sb(III) to precipitate these ions as $Bi(SbO_4)$ and $Sb(SbO_4)$. The sorbent was able to remove 90 % of Bi and 80 % of Sb from the acidic copper electrolyte solution. Xiao et al. [59] conducted studies on the removal of antimony and bismuth impurities from synthetic copper electrolyte solution. They used As(III) ions as collector to precipitate the impurities, but low removal rates were reported: 53 and 52 % for Sb and Bi, respectively. Xiao et al. [60] also studied the removal of Sb, As and Bi impurities using Sb(III) ions as collector to precipitate these impurities from a synthetic copper electrolyte solution, but with low recovery rates: 48.0 % for Sb and 38.4 % for Bi.

Solvent extraction has also been studied as a way to purify the copper electrolyte solutions and to extract valuable metals such as antimony or bismuth [61]. Szymanowski [61] discussed the use of phosphor-based extractants (e.g., TBP, DEHPA, Cyanex® 923), hydroxamic acids, and (poly)alcohols as a way to recover Sb, As, and Bi from copper electrolytes. Navarro et al. [62] studied the extraction of antimony from copper electrorefining solutions with the hydroxamic acid extractant LIX 1104SM and HCl as a stripping agent. They found that the order of extraction was Sb(III) > As(V) > Fe(III) ≫ Cu(II), with a distribution factor *D* for Sb of 299. Sarkar and Dhadke [63] studied the solvent extraction separation of Sb(III) and Bi(III) with bis(2,4,4-trimethylpentyl) monothiophosphinic acid (Cyanex® 302) from H_2SO_4 and HCl solutions. They reported quantitative extraction of antimony and bismuth and separated the metals by first stripping with HNO_3 (2 M) to remove bismuth and then H_2SO_4 (8.5 M) to strip antimony. Iyer and Dhadke [64] reported the quantitative extraction and separation of Sb(III) and Bi(III) from aqueous H_2SO_4 and HCl solutions with the trialkyl phosphine oxide extractant Cyanex® 925. Sb(III) was stripped from the organic phase with H_2SO_4 (8 M) and Bi(III) with HNO_3 (2–3 M). Other relevant studies include the work of Fuyii et al. [65] on the extraction behavior of Sb(III) in the TRUEX® system and a study of the co-extraction of Sb(III) by the Cu(II) extractant Acorga® CLX50 performed by Lin [66]. This pyridine-3,5-dicarboxylate ester extractant is used in the CUPREX® process to produce cathode-grade copper with a hydrometallurgical process in which sulfide ore concentrates are leached in chloride medium [67]. The extraction of Sb(III) and Sb(V) ions with amine extractants in different acid solutions and the separation from other relevant metal ions (e.g., Bi(III), Sn(II), Cd(II), Te(IV), Se(IV), Pb(II), Cu(II), Au(III), Fe(III), and Zn(II)), have been studied extensively by Alian and Sanad [68] and Sargar et al. [69]. Facon et al. [70] also investigated the removal of Sb(III) from Bi(III), Pb(II), and Sn(IV) with Cyanex® 301 from chloride solutions.

Lead Production

Antimony is also connected to primary and secondary lead production because it occurs in primary lead ores (e.g., galena PbS) as well as in the lead alloys used in lead-acid (LA) batteries, which use up the majority of the world's lead (76.7 % in 2006) [10]. Due to the large production volumes of lead (11,000,000 t/year in 2014), compared to antimony (160,000 t/year in 2014), lead production residues are considered as important secondary feedstocks of antimony [71]. Stringent environmental regulations and the exhaustion of high-quality primary lead deposits have caused an accelerated shift toward lead recycling as the main supply source [10]. In 2006, 60 % of the world's annual lead consumption was met by recycling of LA batteries, lead pipes, etc. [10]. In the U.S.A., secondary supply meets more than 80 % of the demand for lead and in countries such as Austria, the Netherlands, Spain, and Belgium the entire lead production is based on secondary raw materials from lead recycling [72]. Here, an overview is given of primary and secondary lead production with an emphasis on the formation of the different Sb-containing residues (e.g., slags, drosses, speiss, slimes) and the existing technologies to recover antimony from these residues (Fig. 7). Almost all antimony in secondary lead is currently being recycled [73]. For example, antimonial drosses are used to produce antimonial lead [73]. Efforts have also started to upgrade the process in order to produce pure Sb_2O_3 from these secondary lead residues [74–76]. Residues with low antimony contents such as the slags and matte are less interesting when it comes to antimony recycling, but can have other applications [73]. Lead refiners are highly interested in valorizing the valuable Sb-containing waste streams both from an economic and environmental standpoint. The composition of the different process residues is dependent on the feed, equipment, and process, but some representative examples are shown in Table 5.

Primary lead production from lead sulfide ores (Galena: PbS) starts with the concentration of the ore, followed by a roasting and sintering step to form sinter (Fig. 7) [81, 82]. The lead concentrate is then fed into a blast furnace

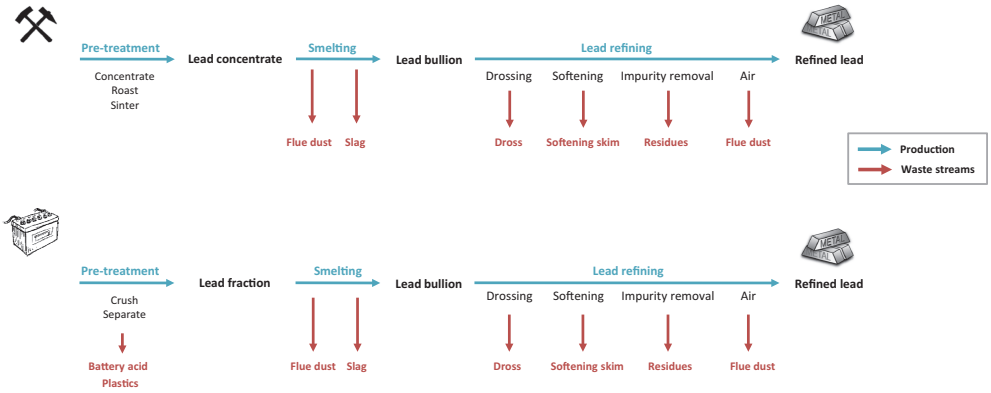

Fig. 7 Schematic overview of primary lead production from lead ores, and secondary lead production from spent lead-acid (LA) batteries. The different metal-containing waste streams and residues are indicated in *red* [73] (Color figure online)

Table 5 Literature examples of lead processing residues and their metal contents (wt%) [7, 76–80]

Residue	Sb	Pb	Cu	As	Fe	Ni	Zn	Ag	Sn	Bi
Slag [77]		2.8	0.1		37.1		11.2			
Harris dross [78]	8.2	67.0			0.8		0.7			
Speiss [7]	3.3	14.8	43.5	12.2	1.7	1.4	0.9	0.9	0.5	
Matte [80]	0.9	41.1	45.3	0.6	0.3	0.3	0.4			
Softening skim [7]	31.7	52.9		3.3						
Sb dust [76]	42.4	7.5	0.12	10.4						0.6
Slime [79]	63.6	12.6	1.47	4.0				1.1		3.3

together with limestone (flux) and coke in order to reduce the oxides to the metal [81]. New reactor designs also allow the roasting and smelting in a single reactor (e.g., Isasmelt furnace) [2, 82]. The non-metallic fraction (e.g., sulfides, silicates) forms a slag with the fluxing materials. During the smelting, a lighter phase is formed which is known as *speiss*. Speiss consist mainly of iron arsenides and antimonides, and other elements such as Pb, Cu, Ni, Sn, and significant levels of precious metals (Ag 9 kg/t and Au 45 g/t) [7]. It rises to the top of the melt and can be skimmed off. Furthermore, a *matte* layer consisting of copper and other metal sulfide impurities is formed. The speiss and matte can be sold to copper smelters, where they are refined for copper recovery. The lead coming from the smelting furnace, called lead bullion, still contains many impurities (e.g., Cu, As, Sb, Sn, Bi, Zn, Ag, Au), and needs to be refined. First, copper is removed in a drossing process [81]. The melt is cooled to decrease the solubility of copper, and a *copper dross* is formed on the surface [81]. Sulfur can also be added to remove the last traces of copper. Dross is usually skimmed off and sent to a dross furnace to recover the non-lead components. The lead is then subjected to further purification steps either by thermal refining or by electrorefining [81]. In thermal refining, the lead is heated and cooled under different conditions and at different temperatures to oxidize or to remove the metal impurities from the lead. Arsenic, tin, and antimony are best removed in a softening step, which consists of heating the lead in a furnace in the presence of air, which causes the impurities with a greater affinity for oxygen than lead, to be oxidized. The *softening skims* can then be collected from the surface of the bath. An alternative is the *Harris process*, which uses a flux of molten NaOH and $NaNO_3$ to remove the impurities as sodium arsenate, stannate, and antimonate [83, 84]. Further purification steps are used to remove gold and silver (Parkes process), zinc (vacuum distillation), bismuth (Kroll–Betterton process), and other impurities such as antimony (caustic refining) [2, 82, 84–86]. These refining processes are combined to obtain a lead bullion with sufficient purity, before casting it into ingots [81]. Instead of this sequence of thermal refining steps, pure lead can also be obtained by electrorefining after the

initial decoppering step [87]. Solutions of H_2SiF_6 (Betts process) or HBF_4 are used and the work-lead is cast into anodes and then dissolved [88]. The metals that are more noble than lead (e.g., As, Sb, Bi, Au, Ag) do not dissolve and are collected in the *anode slimes* [2]. The advantage of electrorefining is that unlike thermal refining all the impurities are removed in one step and 99.999 % pure lead is obtained [2]. In the sintering, smelting, and refining stages, fumes and dusts may contain between 10 and 60 % Pb and a wide range of other metals (e.g., Cu, Zn, As, Sb, Sn, Cd, Ag, Au, Bi). Plants are normally designed to capture these *flue dusts* in filters in order to discard them safely or resmelt them in certain cases [81].

Secondary lead production is almost entirely dependent on the recycling of spent lead-acid batteries (Fig. 7) [2, 73]. After removing the acid, the batteries are crushed to separate lead from the plastic. The lead can be separated in a lead metal fraction and a lead oxide fraction by a mechanical process [2]. The lead metal is then simply remelted, whereas the lead oxide is reduced in several types of furnaces (e.g., rotary furnaces or Isasmelt furnaces) [2, 11]. Besser et al. reviewed the different types of furnace designs and processes for battery recycling as well as their efficiency, and ability to produce pure lead and lead-antimony alloys for battery grid manufacturers and other lead alloy applications [10, 89]. The lead is refined using similar processes as the primary lead production and the same type of residues (e.g., skims, drosses, flue dust) are obtained [73].

The recovery of antimony from lead production residues has been investigated for some time [73]. Anderson [7], studied the use of alkaline sulfide leaching as a way to selectively remove antimony (and arsenic) from lead smelting residues. A mixture of Na_2S and NaOH was used to solubilize antimony as thioantimonite Na_3SbS_3. High antimony recovery rates were reported for lead smelter speiss (99.4 %), skims (89.0 %), and flue dust (95 %) [7]. Singh [78] reported the recovery of antimony from the antimony-containing Harris dross (8.2 % Sb) of the refining section of a lead plant. HCl was used to leach antimony from the dross (95 % recovery) and Sb_2O_3 was formed by hydrolysis (73.6 % recovery) [78]. Peterson and Twidwell [90] investigated the removal of arsenic and antimony from lead smelter speiss, using volatilization techniques. The removal of antimony from antimony dust captured during the direct lead smelting process has been studied by Liu et al. They proposed a pyrometallurgical process based on reduction smelting, alkaline refining, and oxidation to extract antimony from antimony dust and produce Sb_2O_3 with a purity above 99.8 % [76]. Cao et al. studied the recovery of antimony from lead anode slimes, using a potential-controlled chlorination leaching ((Cl_2) leaching) and continuous distillation [79]. High-purity $SbCl_3$ was prepared, with an antimony recovery rate of more than 95 %. The process forms a closed loop and no waste is created [79]. Itoh et al. [91], proposed an alternative process to recover antimony from the anode slimes (Pb–Bi-Sb alloy) of spent lead-acid battery processing. In a method called *volatile oxide formation,* antimony is selectively oxidized due to its higher affinity for oxygen compared to lead or bismuth. Sb_2O_3 is then evaporated because of its high vapor pressure. Lin and Qiu [92] also developed a process to recover antimony and arsenic from anode slimes. They used a new process called v*acuum dynamic flash reduction* to evaporate the volatile oxides of antimony and arsenic, leaving silver behind. A recovery of 93.67 % was achieved for antimony and 98.92 % for arsenic. The vacuum treatment eliminates much of the air pollution and material losses associated with other conventional treatment methods. Qui et al. also used vacuum evaporation technology to recover antimony from Sb-rich anode slimes from the lead industry [93]. The antimony recovery rate was 92 %, and a 99.7 % pure antimony oxide distillate was obtained. Binz et al. [75] developed a bottom-up process to recover antimony from lead-refining residues. They investigated a more selective oxidation during lead softening and the carbothermic reduction of the slag to produce a concentrated antimony slag and improve the recovery of antimony. Kaporal et al. [94] studied the feasibility of antimony removal from accumulator acid found in spent lead-acid batteries. They achieved 100 % removal of antimony from synthetic solutions, using electrodeposition with a copper electrode. Bergmann and Kaporal [95] continued this work and studied the electrochemical recovery of antimony from real spent accumulator acid found in lead-acid batteries. They managed to reduce antimony levels from 5 ppm to less than 0.15 ppm, while also regenerating the accumulator acid. Copper and graphite cathodes produced the best results.

Spent Antimony Catalyst

Antimony is also used in several catalysts [96–101]. When these catalysts reach their end-of-life, antimony can be recovered and reused. The most important application is the production of polyethylene terephthalate (PET), one of the most common polyester thermoplastic polymers. This polymer is mostly used in textile fibers and as container for food or liquids. PET is produced by the Sb(III)-catalyzed polycondenzation of bis(hydroxyethyl)terephthalate (BHET) (Fig. 8). This precursor is either synthesized by the transesterification of dimethyl terephthalate (DMT) or the esterification of terephthalic acid (TPA). Titanium-based catalysts have been proposed, but today more than 90 % of the world's polyester production still runs on Sb-based catalysts (150–300 ppm) [96, 102].

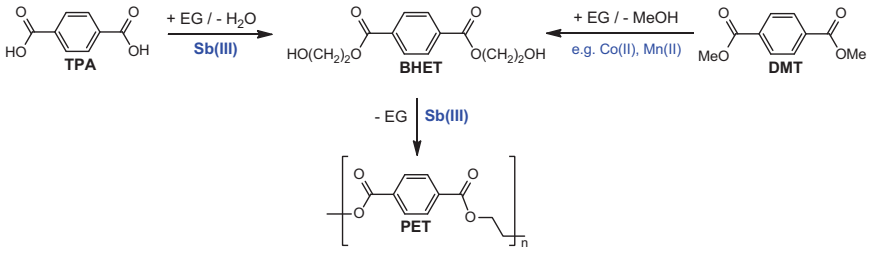

Fig. 8 Two pathways for the production of PET (*EG* ethylene glycol)

The most common forms are Sb_2O_3, $Sb(OCH_2CH_2O)_3$, and $Sb(OAc)_3$ [103]. High-purity compounds are required, especially in regard to arsenic since the catalyst will be present in the final PET polymer used for making plastic bottles. Despite the efficiency of antimony catalysts, there are drawbacks such as the decomposition, which deposits antimony metal particles [103]. This causes a grayish discolouration in the polymer, especially at concentrations >250 ppm Sb [96]. The mechanism behind the formation of antimony metal during PET polymerization and the discolouration was studied in detail by Aharoni [104]. Although antimony is present in the PET polymer (100–300 ppm), it has been demonstrated that water stored in PET bottles contains less than 1 ppb of Sb, which is far below the EEC limit of 20 ppb [96, 105]. The mass recycling of PET plastic could therefore be an opportunity to recover antimony, although antimony contents are typically lower than in plastics containing antimony-based flame retardants. Therefore, most studies have focused on the recovery of antimony from spent catalysts so far. Dougherty and Garska [12] developed a process to recover antimony from spent ethylene glycol residues resulting from the manufacture of PET polymers. Their method consists of combusting the spent glycol residues to produce an ash, from which antimony can be recovered. Several patents have also been published on the recovery of antimony from halocarbon solutions, because Sb-containing catalysts (e.g., $HF/SbCl_5$) are used in the fluorination of chlorinated hydrocarbons [99, 106, 107]. Fernschild et al. [106] described a method for the recovery of an Sb-containing catalyst by chlorination, followed by the distillation of $SbCl_5$. Hyatt [107] developed an alternative process based on the reduction of $SbCl_5$ to $SbCl_3$, followed by extraction of $SbCl_3$ from the halocarbon solution to an acidic aqueous phase. Finally, Anderson [7] also studied the recovery of antimony from a spent catalyst used in the production of acrolein from propylene. Antimony was successfully leached out (99.5 %) using HCl, leaving the silica substrate intact.

End-of-Life Products and Municipal Waste

Antimony can be found in a variety of products, which eventually end up as waste. It is therefore important to understand the presence of antimony in different items, in order to assure that no antimony is released into the environment. The high antimony content in certain products also makes them very interesting as secondary sources of antimony either through direct recycling or through municipal waste incineration. Table 6 gives an overview of the different antimony products and their approximate growth rates [3].

Municipal Solid Waste Incineration

Municipal solid waste incineration (MSWI) is a vital part of many waste management systems. The residues formed during the incineration contain many valuable elements and have been investigated as secondary source of ferrous and non-ferrous metals. In a MSWI plant, the waste is incinerated at a temperature of 850–1000 °C, forming a solid bottom ash fraction and flue gas, which is captured and cooled to form boiler ash, fly ash, and air pollution control (ACP) residues. A schematic overview of a MSWI plant is shown in Fig. 9.

The waste incineration residues can undergo different treatments (e.g., dry, wet, thermal, mechanical) aimed at removing ferrous and non-ferrous metals and/or valorizing it as a granulate for the construction industry, e.g., in road foundation. A lot of different elements are present in these ashes, but the discussion is restricted here to the recovery of antimony. Jung et al. [109] and Allegrini et al. [13] compiled an overview of the composition of MSWI bottom ash, fly ashes, and other waste incineration residues, and compared this with typical ore concentrations to determine the recovery potential (Table 7) [13, 109]. The typical ore concentration given in Table 7 reflects the average grade of the deposits, but does not take into account the ore's abundance. The widely available incinerator residues could

Table 6 Antimony consumption (tons) in 2000 and 2010 per product category and its main market drivers (Source: Roskill consulting) [3]

Product	2000 (t)	2010 (t)	Annual growth rate (%)	Market driver
Flame retardants	70,000	103,500	4.0	Plastics
Lead-acid batteries	40,000	53,000	2.9	Automotive
Lead alloys	11,000	23,000	7.7	Construction
PET catalysts	6000	11,400	6.6	PET
Heat stabilizer	1,400	2600	6.4	PVC
Ceramics	1700	2500	3.9	Construction
Glass	16,000	1700	−20.1	CRT glass
Others	1500	1840	2.1	
Total	147,600	199,540	4.1	

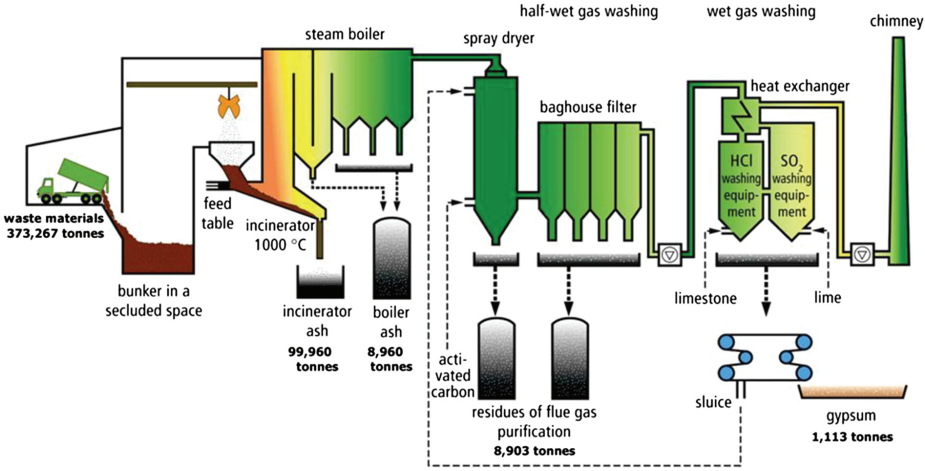

Fig. 9 Schematic representation of the MSWI plant in Doel, Belgium. This figure is reproduced with permission from KU Leuven SIM^2 [108]

therefore become an attractive secondary resource. Fly ashes are particularly interesting, due to the volatility of antimony which results in an important enrichment of antimony in the fly ashes. However, presorting of materials with high antimony contents (e.g., plastics with flame retardants), could drastically improve the efficiency of such an incineration process.

Nakamura et al. [111] investigated the origin of antimony, lead, and cadmium in incinerator waste. They concluded that the relatively high content of antimony in these incineration residues is mainly due to the presence of antimony in plastics, glass, and textiles (Table 8). Curtain fabrics had a particularly high antimony content (2100 ppm), due to the use of flame retardant coatings

Table 7 Content (mg kg^{-1}) of a selection of metals in MSWI bottom ash, boiler ash, and fly ash, compared to typical ores

Element	Bottom ash	Boiler ash	Fly ash	Typical ore
Sb	10–400	200–1000	260–1100	27,000
As	1–200	20–60	40–300	1000–40,000
Cu	300–8000	500–1000	600–3200	5000–20,000
Pb	100–14,000	1000–35,000	5300–26,000	300,000–400,000
Sn	2–400	200–700	550–2000	4000

Note: these are representative values, but other reports may differ [109]

A range is given, based on the work of Van Gerven et al. [110] and Allegrini et al. [13, 110]

[111]. In general, Watanabe et al. [112] estimated that raw incinerator waste contains approximately 40–50 mg kg^{-1} of antimony.

The removal of antimony from incinerator residues has been an important topic of discussion, mainly because of its toxicity and the risk for uncontrolled release of antimony. Osaka et al. [113] wrote a report on the risks associated with the presence of antimony in municipal waste incineration residues. They studied the influence of the pH on the leaching of antimony from these residues and proposed risk management measures. Paoletti et al. (2001) and Nakamura et al. (1996) studied the movement and distribution of antimony in the different incinerator residues [111, 114]. These risk management studies focused mainly on limiting the leaching of antimony from these residues. However, due to the high criticality of antimony, the recovery of antimony from these residues may become of higher interest, especially since consumer waste contains important amounts of antimony in textiles, plastics, and glass (Table 8). Miravet et al. [115] analyzed the leachability and speciation of antimony in incinerator fly ash. They used citrate solutions to leach out antimony and concluded that Sb(V) was the main Sb-containing species. The extraction of metals from incinerator residues through leaching was also studied by Van Gerven et al. [110]. They performed column and batch leaching tests with acidified water (HNO_3) to estimate the leachability of a wide range of metals from MSWI bottom ash, boiler ash, fly ashes, and air pollution control (APC) residues. Van Gerven et al. [116] also studied the removal of heavy metals from MSWI bottom ashes using organic solutions of citric acid and ammonium citrate. Cornelis et al. [14, 15] investigated the influence of the pH on the leaching of antimony from carbonated and non-carbonated MSWI bottom ash. Hong et al. studied the extraction of heavy metals from MSW incinerator fly ashes, using acids (HCl), and chelating agents (NTA, EDTA, DTPA) in batch experiments. The leaching test on the residues after the treatment with chelating agents showed that the fly ashes were successfully detoxified to meet the guideline for landfilling. Okkenhaug et al. [117] showed that iron-rich sulfuric acid waste is efficient to immobilize antimony in MSWI air pollution control residues. These technologies are all promising but the winning technology will be the one that can *selectively* remove certain elements such as antimony. Due to the mix of elements in these residues, it is crucial to develop methods which can deal with the complexity of these powders in a low-cost and efficient manner. Despite the technical challenges, there is a significant opportunity to recover valuable metals from these ashes as they are available in large quantities.

Table 8 Antimony content and contribution in crushed municipal waste

Waste type	Sb content (mg kg^{-1})	Contribution to waste (%)
Plastics	180	44.7
Glass	1008	15.2
Textiles	111	14.7
Wood	11	9.3
Other	93	16.1

The data were adapted from Nakamura et al. [111]

Flame Retardants in Plastics

In 2014, the world consumption of flame retardants was more than 2.2 million tons, representing a market of approximately 5 billion EUR with a 4–5 % annual growth rate due to rising safety standards worldwide [4, 118]. Flame retardants are crucial to guarantee the safety of plastics, construction materials, electronics, textiles, and coated products [119, 120]. There are three main classes of flame retardants: (1) metal hydroxides such as $Al(OH)_3$ (ATH) and $Mg(OH)_2$ (MDH), (2) organohalogen compounds (chlorinated or brominated) in combination with antimony trioxide (Sb_2O_3), and (3) organophosphorus compounds [119]. An overview of the flame retardant market (2007) is given in Fig. 10.

Continuous research and regulations are driving new developments in the different categories of flame retardants. For example, research is being conducted to graft flame retardant groups in the structure of the polymer, thus avoiding the release of the flame retardants into the environment [122–124]. The most effective commercial fire retardant systems are currently based on brominated organic compounds (known as brominated flame retardants

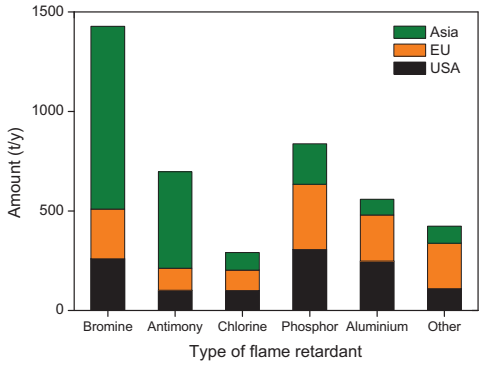

Fig. 10 Flame retardant sales per region and per category (2007), expressed in t/year. Adapted from SRI-Consulting [121] (Color figure online)

(BFRs)), preferably in conjunction with antimony trioxide Sb_2O_3 due to the strong synergetic effect [120]. Flame retardants were responsible for 52 % of the demand for antimony in 2010 (≈103,500 t) [3]. Camino and Costa [119], reviewed the performance and mechanisms of antimony fire retardants in polymers. They attributed the synergetic effect to the fact that metal halides are far more effective flame inhibitors, compared to the hydrogen halides formed in the absence of the metal compound [120]. In reality, a variety of different oxyhalide metal species are formed and their thermal stability and chemical reactivity have therefore been studied in great detail [125]. A discussion of the fire retardant mechanism is beyond the scope of this work, and what follows is therefore only a discussion of the possible recovery of antimony from plastics, electronics, and coatings. The antimony content in plastics is highly dependent on the type of plastic and the application. Table 9 provides an overview of the typical formulations used to fireproof different polymers [6].

Non-halogenated polymers are inherently flammable and require large amounts of halogenated flame retardants in combination with Sb_2O_3 to be flame resistant [6]. Halogenated polymers (e.g., PVC, PVDC) on the other hand, are already partially flame retarded due to their chlorine content and do not require the addition of halogenated compounds. Smaller amounts of Sb_2O_3 can be added to these polymers to ensure their fire resistance [6]. Due to the inherent risk for fires, polymers used in building materials, electronics, and some textiles are often made fireproof using these halogenated compounds and Sb_2O_3. Plastics used for food and beverages or plastics that do not require fire-proofing, do not contain significant quantities of antimony. PET bottles are an exception, as these contain some antimony (0.2–0.3 wt%) due to the use of an antimony catalyst for the production of PET polymers [126]. Efficient recovery of antimony from plastics requires adapted screening and sorting methods to identify plastics with high antimony contents. X-ray fluorescence spectroscopy (XRF) could provide a fast and non-destructive screening. Other interesting techniques are X-ray transparency and laser-induced breakdown spectroscopy (LIBS). Bellara et al. [127] also developed a method for the direct determination of antimony in solid PVC samples by graphite furnace atomic absorption spectrometry (GFAAS). They concluded that this screening technique provides sufficiently reliable results in a reasonably short time, but it is difficult to implement in a continuous process. Once sorted, the antimony-containing plastics can be placed in special ovens for the pyrolysis of the polymer, where antimony is caught in the residues (bottom ashes or fly ashes). A patent of Nippon Electric Co (1994) described a method to decompose a resin, containing flame retardants, and capture the bromine and antimony in a gas mixture (e.g., HBr, $SbBr_3$, CO_2, H_2O) [128]. By washing the gas mixture with an alkaline aqueous solution (e.g., NaOH), NaBr and Sb_2O_3 could be obtained. The thermal decomposition could be operated under air-free conditions or by combustion. In a follow-up patent, Masatochi et al. [129] specifically described the recovery of antimony from decomposition gasses, originating from the pyrolysis of flame resistant plastics. Masatoshi and Ikuta [130] also described the pyrolysis-based recovery of antimony and bromine from molding resins used in electronics. The electronic parts consisted of an epoxy resin, a silica filler, and flame retardants consisting of brominated compounds and Sb_2O_3. This study investigated the best pyrolysis conditions to obtain a pure silica product. The exhaust gasses generated in the pyrolysis of the molding resin were treated to remove the bromine and convert the antimony bromides to Sb_2O_3. Jakab et al. [131] studied the thermal decomposition of flame-retarded high-impact polystyrene. In a detailed overview of the decomposition pathways and mechanisms, they concluded that the brominated additives themselves do not change the decomposition temperature of polystyrene, but Sb_2O_3 reduces the thermal stability of the samples by acting as an initiator for the decomposition of the brominated flame retardants. Klein et al. [132] also studied the behavior of antimony during thermal treatment of antimony-rich halogenated waste. Their aim was to ensure the environmentally friendly waste incineration of antimony-rich plastic waste, by strengthening the knowledge about the fate of antimony and the potential formation of harmful species as function of temperature, residence time and flow rate of air in the furnace. Their investigations showed that under moderate oxidative conditions, the partition of antimony between the residual bottom ash (≈64 %) and the gas phase (≈36 %) was constant regardless of the temperature. However, they observed that at 850 °C antimony was mainly present in the gas phase as Sb(III), while around 1100 °C, Sb(V) was favored. Wu et al. [133] studied the thermal degradation of high-impact

Table 9 Required Sb_2O_3 to make polymers flame resistant [6]

Plastic	Flammability	Sb_2O_3 (wt%)	BFR required?
PE	High	8–16	Yes
PP	High	5–15	Yes
PS	High	10	Yes
PU	High	10	Yes
SBR	High	5–30	Yes
ABS	High	5–12	Yes
PVC	Low	1–10	No

Polymer abbreviations: *PE* polyethylene, *PP* polypropylene, *PS* polystyrene, *PU* polyurethane, *SBR* styrene-butadiene rubber, *ABS* acrylonitrile–butadiene–styrene, *PVC* polyvinylchloride, *BFR* brominated flame retardant

polystyrene, containing brominated flame retardants and Sb_2O_3. Bauxite residue (red mud) was used as an additive to catch the bromine and antimony in a residue, while producing a valuable pyrolysis oil. Mitan et al. [134] investigated the controlled pyrolysis of polyethylene/polypropylene/polystyrene mixed with brominated high-impact polystyrene. Their work describes the effect of the brominated flame retardants and Sb_2O_3 on the pyrolysis process and the distribution of pyrolysis products. Brebu et al. [135] also looked at the effect of flame retardants and Sb_2O_3 synergists on the thermal decomposition of high-impact polystyrene and on its debromination by ammonia treatment. More than 90 wt% of initial bromine could be recovered as inorganic NH_4Br. Hall et al. [136] developed a method for the co-pyrolysis of flame-retarded high-impact polystyrene and polyolefins in a fixed bed reactor. They looked at the effect that the different types of brominated aryl compounds and Sb_2O_3 have on the pyrolysis products.

Besides pyrolysis, other methods have also been proposed. Omwudili and Williams [137] attempted the alkaline reforming of high-impact polystyrene and traced the movement of bromine and antimony. The waste polymer was reacted in supercritical water and NaOH in a pressure reactor in order to neutralize the corrosive inorganic bromine species released during the reactions. They observed that the presence of the alkaline supercritical water led to 97 wt% debromination of the product oil, producing a valuable bromine-free oil feedstock. Furthermore, a 98 % removal rate was achieved for antimony. The same method was also used for acrylonitrile–butadiene–styrene polymers [138]. Another unusual approach was tested by Lateef et al. [139]. They used imidazolium- and pyridinium-based ionic liquids to extract brominated flame retardants and Sb_2O_3 from high-impact polystyrene. They identified 1-hexylpyridinium bromide as the most suitable for solid–liquid and liquid–liquid extraction, achieving extraction percentages of 92.7 % for the brominated flame retardants and 99.9 % for Sb_2O_3. Furthermore, they demonstrated that the chain length of the polymer was not degraded by the extraction process, thus forming a polymer residue which can be recycled. Another approach could be the depolymerization of the polymers to recover Sb_2O_3 and the building blocks (e.g., ethylene, HCl). This approach has not been investigated in detail so far, but some projects have looked into the possibility of separating, cleaning, and reusing bromine- and antimony-containing plastics [140].

Plastics in Waste Electrical and Electronic Equipment

A subcategory of flame retardant plastics are the plastics used in waste electrical and electronic equipment (WEEE) [141]. WEEE is already being recycled on a large scale, mainly to recover the precious metals (e.g., Co, In, Te, Se, Au, Ag) used in the electronic components such as printed circuit boards (PCBs) (Table 10) [142]. Besides the metallic fraction, there is also a large non-metallic fraction in WEEE [143]. Even for PCBs the non-metallic fraction is still more than 70 % [143]. This non-metallic fraction includes the silicon substrates and the plastics used in these products. The strict safety regulations for electrical and electronic equipment (EEE), require large amounts of brominated flame retardants and Sb_2O_3 to be used in order to guarantee the safe use of these plastics [142]. As explained previously, approximately 52 % of antimony is consumed in flame retardants, of which 70 % is used for plastics in electrical and electronic equipment (Table 6) [3, 142].

This clearly shows the potential of WEEE plastics as a secondary feedstock of antimony. Table 9 showed that certain plastics require as much as 5–15 wt% of antimony to be fire resistant, making WEEE particularly rich in antimony. The most important plastics under investigation are acrylonitrile–butadiene–styrene (ABS) and high-impact polystyrene (HIPS) as these are the most-used polymers in EEE (Fig. 11) [141]. These polymers typically contain 5–10 wt% of Sb_2O_3 and an even larger amount of brominated flame retardants. [142]. Different studies have been carried out to deal with these polymers in WEEE recycling schemes. The toxic brominated compounds and antimony-containing plastics have been a source of concern for the recycling of WEEE. Regulations for the emission of brominated compounds are very strict and therefore solutions have been investigated to capture the bromine efficiently during the pyrolysis of the WEEE [142]. The fact that antimony is also present in the plastic fraction, means that bromine and antimony are intrinsically connected in WEEE recycling.

De Marco et al. and Moltó et al. reviewed the pyrolysis of electrical and electronic wastes but did not discuss in detail the recovery of antimony or bromine flame retardants [144, 145]. Guo et al. [143] reviewed the recycling of non-metallic fractions (NMFs) from waste printed circuit boards (PCBs) and demonstrated the importance of finding a solution for the recycling of this important fraction of WEEE. The non-metallic fraction was usually treated by combustion or landfilling in the past. However, uncontrolled combustion causes the formation of highly toxic polybrominated dibenzodioxins and dibenzofurans, while landfilling of the NMFs will lead to secondary pollution caused by heavy metals and brominated flame retardants (BFRs) leaching to the groundwater. This had been previously demonstrated by the work of Gullet et al. [146], who characterized the emissions and residual ash from open air burning of electronic wastes during simulated rudimentary

Table 10 Metal consumption for electrical and electronic equipment EEE (t/year)

	Yearly demand for EEE (t/year)	Percentage of total production (%)
Cu	4,500,000	30
Sn	90,000	33
Sb	65,000	50
Co	11,000	19
Ag	6000	30
Bi	900	16
In	380	79
Au	300	12
Se	240	17

The data are obtained from the work of Buekens and Yang [142]

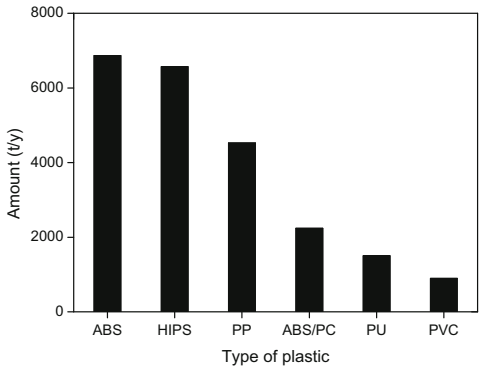

Fig. 11 Flows of the major plastic types in Swiss WEEE products for the year 2007 [141]. *ABS* acrylonitrile–butadiene–styrene, *HIPS* high-impact polystyrene, *PP* polypropylene, *PC* polycarbonate, *PU* polyurethane, *VC* polyvinylchloride

recycling operations. They analyzed the fly ash and particulate matter and characterized the organic and metallic components in the air emissions. Therefore, Guo et al. [143] concluded that more advanced processes are required such as pyrolysis, gasification, depolymerization, or hydrogen degradation in order to convert the non-metallic fraction to chemical feedstocks and fuels. These methods have the advantage of eliminating hazardous substances such as brominated organic compounds from this waste fraction and allow the recovery of antimony from the plastic waste. In later work, Guo et al. [147] analyzed the pyrolysis of scrap printed circuit board plastic particles in a fluidized bed reactor. The gas products, liquid products, and solid residues were analyzed and it was found that the liquid yields increased with an increase in pyrolysis temperature. The main compositions of liquid products were aromatic compounds including substituted benzenes, whereas the solid products mainly contained char and fiberglass. Morf et al. [148] also tracked the movement of brominated flame retardants and antimony in WEEE recycling plants. Hall et al. [149] investigated the fast pyrolysis of plastics recovered from computer waste. The computer case was made from PVC, but the computer monitor cover consisted of brominated acrylonitrile–butadiene–styrene and had an antimony content between 3.9 and 4.5 wt%. The pyrolysis was carried out in a fluidized bed reactor at 500 °C, and the composition products were studied. They concluded that the high bromine and chlorine content was a nuisance and that in-process sorption of the halogens was required to obtain a high-quality oil. In later work, Hall et al. [150] used zeolite catalysts and fluidized catalytic cracker (FCC) catalysts to destroy the toxic organobromines during pyrolysis of brominated high-impact polystyrene (4.6 wt% Sb) and acrylonitrile–butadiene–styrene (3.2 wt% Sb), found in WEEE. The movement of antimony in the oil and char residues was also tracked. Tostar et al. [151] specifically investigated the leaching of antimony in plastics from WEEE with various acids and gamma irradiation. The most efficient leaching medium was a heated solution of sodium hydrogen tartrate in dimethyl sulphoxide, which leached approximately 50 % of the antimony from the acrylonitrile–butadiene–styrene plastic. Gamma irradiation did not significantly change the amount of leached antimony. A patent by Zhenming et al. [152] also describes vacuum distillation as a way to recover antimony from printed circuit board waste. Yang et al. [153] reviewed the pyrolysis and dehalogenation of plastics from waste electrical and electronic equipment. The conclusion from these works is that there are technologies available to valorize the plastic components of WEEE, but that additional research needs to be done to improve the efficiency of these processes before upscaling becomes economically feasible. These plastics have to be processed appropriately due to their high content of toxic brominated compounds. The focus up till now has been on limiting the emission of brominated compounds and producing useful fuel oils. However, the high antimony content present in these same plastics offers a unique opportunity to combine the necessary treatment of these brominated plastics with the recovery of valuable antimony. Valorizing antimony from WEEE plastics could improve the economics of the total WEEE recycling process and offset the additional cost of de-brominating during the processing of WEEE plastics.

Lamp Phosphor Waste

Antimony is used in the halophosphate (HALO) lamp phosphors, found in fluorescent lamps [154, 155]. These

lamp phosphors are coated on the inside of the glass and are responsible for the emission of visible light [156–159]. The HALO phosphor was invented in 1942 and large amounts of this phosphor were produced as it found widespread use in fluorescent tubes due to its emission of intense white light [156–159]. This phosphor usually consists of a fluoro-chloro apatite doped with Mn(II) and Sb(III) and has the general formula $(Sr,Ca)_5(PO_4)_3(Cl,F):Sb^{3+}$, Mn^{2+} [156–158]. Antimony is added as a blue dopant to adjust the shade of white [156–158, 160]. Today, lamp phosphor waste contains around 50 wt% of HALO, making it the largest component [154, 155, 161]. This corresponds to approximately 0.5–1 wt% of antimony which is similar to a low-grade stibnite ore [1, 155, 157, 161, 162]. With annual sales of CFLs topping 2.5×10^9 units/y (2007), the volume of lamp phosphor waste is expected to continue growing at a rapid pace as fluorescent lamps reach their end-of-life [163, 164]. Due to their mercury content, fluorescent lamps are considered as hazardous waste and are therefore collected separately in most countries [165, 166]. The interest in lamp phosphor powders as a secondary resource has been growing recently due to their high rare-earth content (in tri-band phosphor), and the recovery of these valuable elements has been studied extensively [165–175]. Currently, a recycling process is operated on industrial scale (>1000 t/y) by Solvay in France [161]. So far, the Sb-containing HALO phosphor is often still discarded as a non-valuable residue due to the absence of rare earths [165, 166, 172]. However, the HALO content in these powders is too high to ignore (50 wt%) and could serve as an interesting secondary source of antimony [176]. Our group therefore recently developed a zero-waste valorization method to recover antimony from HALO and to valorize the remaining as a calcium phosphate (apatite) product, which is a feedstock for the fertilizer industry (Fig. 12) [176]. The valorization of HALO and the recovery of antimony can be integrated in rare-earth recovery schemes and in the broader effort to recycle these lamp phosphor powders [175, 176].

Antimony Emissions and Recovery

Antimony Emissions: Land, Water, Air

Antimony is also lost through emissions in the air, in the water, and on the land [177]. Total antimony emissions are difficult to estimate, but it has been shown that in Australia alone, total emissions of antimony (air, water, land) reach as much as 3.8 t/year during mining and 8.7 t/year during metal manufacturing. A better understanding of these losses can help limit the unwanted emissions of antimony and increase the available supply of antimony at the same time. Land emissions are important, especially around antimony mining and processing sites. An overview of antimony emissions in the soil and decontamination procedures has been compiled by Wilson et al. [178] and since this antimony is often very localized and difficult to access, it is not discussed here in detail. Air emissions on the other hand are very relevant to the topic of secondary sources of antimony. We previously discussed how air pollution control residues, flue dusts, and fly ashes in lead, copper, gold, and antimony processing can contain important amounts of antimony. An overview was also given of the different valorization methods and antimony recovery processes for these residues. However, the capture of antimony air emissions still needs to be improved. Tian et al. [177] made a study of global yearly air emissions and calculated that in 2005 global air emissions of antimony reached 2232 t, and then gradually declined to about 1904 t in 2010. Atmospheric emissions are mostly caused by fuel combustion (42 %), waste incineration (24 %), brake wear (17 %), and metal production (17 %) [177]. China is the largest emitter of atmospheric antimony (649 t in 2010) due to the large-scale combustion of coal and the production of metals, as China currently has 114 antimony mines dispersed over 18 provinces [177]. The emission of antimony from coal power plants, waste incinerators, and metal production sites, can be lowered by the implementation of better filters and air pollution control systems, from which the antimony can then be recovered and reused. However, the emissions of antimony through the wear of vehicle brake linings and brake pads has proven to be a larger concern as antimony emissions are not localized and no simple solutions are available. Sb_2S_3 is used as a lubricant in disc brake pads and drum brake pads, with concentrations as high as 46 g/kg, depending on the type of brake [179, 180]. Uexküll et al. [180] and Varrica et al. [179] studied the speciation of these brake wear particles and concluded that while the brake linings are mainly composed of Sb_2S_3, this compound is decomposed during the abrasion process leading to a mix of Sb_2O_3 and Sb_2O_5 in the airborne particulate. Finally, there is the emission of antimony to surface water, which has been reviewed by Filella et al. [181]. These emissions can also be important secondary sources of antimony if proper filtration systems are set in place. In concentrated industrial flows and mine drainage this is simple to implement, but even for very dilute water streams, decontamination is mandatory, so these large volumes can result overall in a significant amount of recovered antimony.

Antimony Removal from Waste Water

Antimony removal from waste water was recently reviewed by Ungureanu et al. [182]. This extensive review

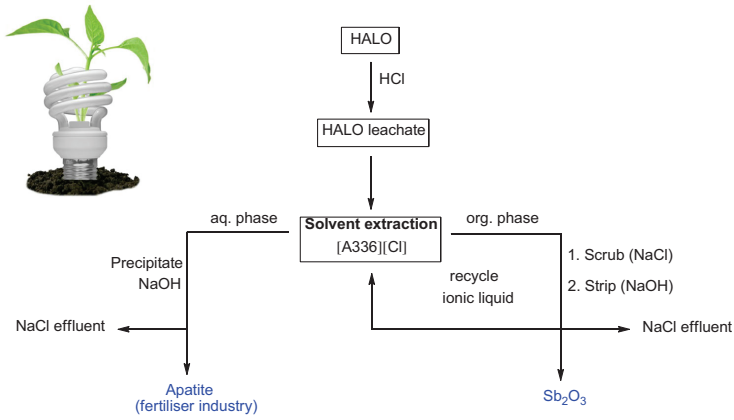

Fig. 12 Zero-waste valorization process for the recovery of antimony from the halophosphate fraction of lamp phosphor waste. The phosphor is first dissolved in HCl, followed by the selective extraction of Sb(III) with Aliquat® 336. Pure Sb_2O_3 is then obtained after a scrubbing (NaCl) and stripping step (NaOH). The remaining leachate is precipitated as apatite (fertilizer precursor). Reproduced with permission from Ref. [176]. Copyright Royal Society of Chemistry (2016) [176]

gives an overview of the analytic techniques for antimony speciation and the existing removal techniques [182]. Different removal techniques have been proposed such as ion-exchange, adsorption, membrane separation, electrochemical methods, bio-removal methods, or coagulation/flocculation followed by filtration or sedimentation [182]. The very large number of papers written on this topic, clearly demonstrated the importance of antimony removal from waste water [182]. In these studies, the focus is systematically on the removal of antimony to obtain clean water. This field of study is different from the previous chapters in this review, as it deals with very dilute antimony waste streams. However, the large volumes represent a sizeable amount of antimony, which should not go to waste. Antimony removal from wastewater is therefore an opportunity to collect antimony efficiently, using automatic (continuous) technologies such as column filtration with specialized sorbents. These techniques lead to a strong concentration of the antimony, which can then be used as a source of antimony, when renewing or regenerating the sorbent or filter.

The most common treatment techniques for antimony removal are flocculation–coagulation followed by filtration or sedimentation, or the use of adsorbents [182]. Flocculation–coagulation is one of the most employed treatments to produce drinking water, and has been investigated for antimony removal as well, with ferric chloride being the most suitable coagulant [182–185]. The drawback of this technique is that it is difficult to automate, it creates toxic sludge and it is not 100 % effective at removing antimony. Researchers have therefore increasingly turned to adsorbents due to the convenient automatization in a continuous set-up and the generally higher antimony-removal efficiencies [182]. The use of sorbents requires only a periodic regeneration, which is an opportunity to recover (pure) antimony. A large variety of sorbents have been investigated to this effect, and a full list is not included here since these have already been reviewed by Ungureanu et al. [182]. The investigated materials include chars, activated carbons, graphene, alumina, metal oxides, minerals, resins, biosorbents, and sorbents based on waste materials and residues. The benchmark was set by Xu et al. [186] who achieved the highest adsorption capacity (214 mg/g) using a binary iron-manganese oxide, whose adsorption capacity significantly outperformed the individual oxides [182, 186]. However, it should be stated that this result is an outlier, with most adsorbents having an adsorption capacity around 50–100 mg/g [182]. The second best material was prepared by Biswas et al. [187], who used saponified orange waste, loaded with Zr(IV) and Fe(III), as a sorbent for the adsorptive removal of Sb(III) and Sb(V) from waste water. They reported adsorption capacities around 114–145 mg/g. However, the review by Ungureanu et al. [182] does not yet include the latest results and an overview of some additional recent examples is given here, which boast high adsorption capacities (>100 mg/g). Wang et al. prepared iron-modified aerobic granules to remove Sb(V) from waste water and investigated the adsorption mechanism in detail [188]. They reported a maximal adsorption capacity of 125 mg/g. Dou et al. [189] investigated hierarchical macro- and mesoporous amorphous alumina as a sorbent for Sb(V). The results were compared with five different commercial alumina adsorbents and showed that this material had the highest adsorption capacity (118 mg/g) and fast adsorption kinetics. Dong et al. [190] made nanocomposites from graphene oxide and schwertmannite (iron oxyhydroxysulphate mineral) to adsorb Sb(V) from aqueous solutions. A synergetic effect

on Sb(V) uptake was observed for this composite adsorbent, which had a maximum Sb(V) adsorption capacity of 158.6 mg/g. Sb(V) in spiked tap water (100 μg/L), simulated river water (6400 μg/L), and acid mine drainage (50,000 μg/L) was adsorbed by this sorbent to levels well below the regulation levels for these waters. An interesting subcategory of water purification is the removal of antimony from mine drainage. These flows are often much more concentrated and more acidic and therefore demand different solutions. Zhu et al. used electrocoagulation to partially remove antimony from mine flotation waste water [191]. The remaining concentration was still 1 mg/L, which far exceeds the drinking water limit, but meets the emission standards established by the state department of environmental protection of China [191].

Conclusion and Outlook

Antimony is one of the most critical elements, but has remained largely out of the spotlights. However, the gap between supply and demand is expected to exceed 10 % in the coming years, making antimony supply far more critical than for example the rare-earth elements. Similar to the rare earths, antimony production is dominated by China and as the grades of primary ores diminishes, it becomes increasingly difficult to meet the demand for antimony. Antimony is an important industrial commodity and is used in flame retardants for plastics and electronics, but also in catalysts for the production of PET polymers and in lead-acid batteries. To meet demand, it is crucial that attention shifts to secondary sources such as industrial process residues and end-of-life consumer items. This review gives an overview of existing waste streams which could be of importance as secondary sources of antimony. It also encourages researchers to look at unusual sources such as air pollution control residues, low-grade ores, and unusual products such as lamp phosphor waste. Sufficient technologies are available to make antimony recycling a success and current recycling rates of approximately 20 % are expected to rise as China struggles to increase its output. However, one of the remaining obstacles for the implementation of antimony recycling in the industry is the upscaling from laboratory methods to industrial processes. Further work needs to be carried out on pilot scale to see which methods are sufficiently robust and flexible. Another challenge is the changing composition of various residues depending on the ore or product that is being processed. Changes in composition of the input material can greatly affect the performance of the recovery processes. Finally, economic feasibility studies and life cycle assessments need to be carried out to determine which techniques are the most promising for industrial upscaling. We expect copper producers to invest in antimony recovery techniques in coming years as this is a growing problem that needs to be addressed in the copper production flowsheets. Other very interesting sources include incineration ashes from concentrated fractions such as textiles or flame retardant plastics. Recycling of antimony through the recycling of lead-acid batteries is currently carried on industrial scale and should continue to provide a steady stream of secondary antimony. Current primary antimony production is unsustainable as current reserves account for only 10–11 years of production at current levels which could be aggravated by rising demand from existing and future antimony applications such as liquid–metal batteries and thermoelectric materials. Moreover, antimony is also associated with environmental problems, so a better management of antimony resources is mandatory and the antimony life cycle must become more circular in the coming years.

Acknowledgments The authors wish to thank the KU Leuven (Projects GOA/13/008 and IOF-KP RARE^3) and the FWO Flanders (PhD fellowship to DD) for financial support.

Compliance with Ethical Standards

Conflict of interest The authors declare no competing financial interest.

References

1. Anderson CG (2012) The metallurgy of antimony. Chem Erde 72:3–8. doi:10.1016/j.chemer.2012.04.001
2. Claude F (2002) Non-ferrous metal: from Ag to Zn. Lannoo, Tielt
3. Chegwidden J (2011) Study of the antimony market. Roskill Consulting Group Ltd, London
4. Satterthwaite K (2014) Flame retardant markets to 2018. Roskill Consulting Industrial Minerals Event, Budapest
5. Schmidt M, Liedke M, Domer U (2015) Rohstoffrisikobewertung—Antimon. Deutsche Rohstoffagentur (DERA) in der Bundesanstalt für Geowissenschaften und Rohstoffe (BGR), Berlin, Germany
6. Uses and Formulations. (2015) United States Antimony Corportation. http://www.usantimony.com/2013_uses_formulations.htm
7. Anderson CG (2001) Hydrometallurgically treating antimony-bearing industrial wastes. JOM 53:18–20. doi:10.1007/s11837-001-0156-y
8. Antimony Statistics and Information (2014) U.S. Geological Survey (USGS), USA
9. Report on Critical raw materials for the EU (2014) European Commission, DG Enterprise & Industry, Brussels
10. Besser AD, Sorokina VS, Sokolov OK, Paretskii VM (2009) Processing of utilized lead-acid storage batteries—the basis of lead recycling. Russ Metall 2009:781–787. doi:10.1134/S0036029509080217
11. Ramus K, Hawkins P (1993) Lead/acid battery recycling and the new Isasmelt process. J Power Sources 42:299–313. doi:10.1016/0378-7753(93)80159-M

12. Dougherty SJ, Garska KJ (1978) Recovery of sodium and antimony values from spent ethylene glycol residues. U.S. Patent US4100253 A
13. Allegrini E, Maresca A, Olsson ME, Holtze MS, Boldrin A, Astrup TF (2014) Quantification of the resource recovery potential of municipal solid waste incineration bottom ashes. Waste Manage 34:1627–1636. doi:10.1016/j.wasman.2014.05.003
14. Cornelis G, Gerven TV, Vandecasteele C (2012) Antimony leaching from MSWI bottom ash: modelling of the effect of pH and carbonation. Waste Manage 32:278–286. doi:10.1016/j.wasman.2011.09.018
15. Cornelis G, Van Gerven T, Vandecasteele C (2006) Antimony leaching from uncarbonated and carbonated MSWI bottom ash. J Hazard Mater 137:1284–1292. doi:10.1016/j.jhazmat.2006.04.048
16. Yang J-G, Wu Y-T (2014) A hydrometallurgical process for the separation and recovery of antimony. Hydrometallurgy 143:68–74. doi:10.1016/j.hydromet.2014.01.002
17. Macdonald MD, Stevens DA, Thibault JD (1997) Process for producing antimony trioxide. WO 1998011021 A1
18. Guo X, Wang K, He M, Liu Z, Yang H, Li S (2014) Antimony smelting process generating solid wastes and dust: characterization and leaching behaviors. J Environ Sci 26:1549–1556. doi:10.1016/j.jes.2014.05.022
19. Fuxu H, Hongjiu R, Zhe S, Qingwen L (1989) Three-phase fluidized bed leaching of antimony refining slag. Hydrometallurgy 23:119–125. doi:10.1016/0304-386X(89)90022-4
20. Luo H-L, Liu W, Qin W-Q, Zheng Y-X, Yang K (2016) Cleaning of high antimony smelting slag from an oxygen-enriched bottom-blown by direct reduction. Rare Metals. doi:10.1007/s12598-015-0468-7
21. Keqiang Q, Rongliang Z (2006) Research on preparation of nanometer antimony trioxide from slag containing antimony by vacuum evaporation method. Vacuum 80:1016–1020. doi:10.1016/j.vacuum.2006.01.010
22. Salihoglu G (2014) Immobilization of antimony waste slag by applying geopolymerization and stabilization/solidification technologies. J Air Waste Manag Assoc 64:1288–1298. doi:10.1080/10962247.2014.943352
23. Courtin-Nomade A, Rakotoarisoa O, Bril H, Grybos M, Forestier L, Foucher F, Kunz M (2012) Weathering of Sb-rich mining and smelting residues: insight in solid speciation and soil bacteria toxicity. Chem Erde 72:29–39. doi:10.1016/j.chemer.2012.02.004
24. Anawar H, Freitas MC, Canha N, Santa Regina I (2011) Arsenic, antimony, and other trace element contamination in a mine tailings affected area and uptake by tolerant plant species. Environ Geochem Health 33:353–362. doi:10.1007/s10653-011-9378-2
25. Yang J-G, Tang C-B, Chen Y-M, Tang M-T (2011) Separation of antimony from a stibnite concentrate through a low-temperature smelting process to eliminate SO_2 emission. Metall Mater Trans B 42:30–36. doi:10.1007/s11663-010-9453-6
26. Ye L, Tang C, Chen Y, Yang S, Yang J, Zhang W (2015) One-step extraction of antimony from low-grade stibnite in sodium carbonate—sodium chloride binary molten salt. J Clean Prod 93:134–139. doi:10.1016/j.jclepro.2015.01.018
27. Gök Ö (2014) Catalytic production of antimonate through alkaline leaching of stibnite concentrate. Hydrometallurgy 149:23–30. doi:10.1016/j.hydromet.2014.06.007
28. Roper AJ, Williams PA, Filella M (2012) Secondary antimony minerals: phases that control the dispersion of antimony in the supergene zone. Chem Erde 72:9–14. doi:10.1016/j.chemer.2012.01.005
29. Baláž P, Achimovičová M (2006) Selective leaching of antimony and arsenic from mechanically activated tetrahedrite, jamesonite and enargite. Int J Miner Process 81:44–50. doi:10.1016/j.minpro.2006.06.004
30. Awe SA, Sandström Å (2010) Selective leaching of arsenic and antimony from a tetrahedrite rich complex sulphide concentrate using alkaline sulphide solution. Miner Eng 23:1227–1236. doi:10.1016/j.mineng.2010.08.018
31. Yang T-Z, Jiang M-X, Lain Q-L, Chen J-Z (2005) Sodium sulfide leaching of low-grade jamesonite concentrate in production of sodium pyroantimonate. J Cent South Univ Technol 12:290–294
32. Duchao Z, Qingkai X, Weifeng L, Lin C, Tianzu Y, Younian L (2015) Pressure oxidation of sodium thioantimonite solution to prepare sodium pyroantimonate. Hydrometallurgy 151:91–97. doi:10.1016/j.hydromet.2014.11.014
33. Kanarskii AV, Adamov EV, Krylova LN (2012) Flotation concentration of the sulfide antimony-arsenic gold-bearing ore. Russ J Non-Ferr Met 53:120–124. doi:10.3103/S1067821212020058
34. Solozhenkin PM, Alekseev AN (2010) Innovative processing and hydrometallurgical treatment methods for complex antimony ores and concentrates. Part I. J Miner Sci 46:203–209. doi:10.1007/s10913-010-0026-5
35. Celep O, Alp İ, Deveci H (2011) Improved gold and silver extraction from a refractory antimony ore by pretreatment with alkaline sulphide leach. Hydrometallurgy 105:234–239. doi:10.1016/j.hydromet.2010.10.005
36. Karimi P, Abdollahi H, Amini A, Noaparast M, Shafaei SZ, Habashi F (2010) Cyanidation of gold ores containing copper, silver, lead, arsenic and antimony. Int J Miner Process 95:68–77. doi:10.1016/j.minpro.2010.03.002
37. Saleh SM, Said SA, El-Shahawi MS (2001) Extraction and recovery of Au, Sb and Sn from electrorefined solid waste. Anal Chim Acta 436:69–77. doi:10.1016/S0003-2670(01)00866-2
38. Kyle JH, Breuer PL, Bunney KG, Pleysier R (2012) Review of trace toxic elements (Pb, Cd, Hg, As, Sb, Bi, Se, Te) and their deportment in gold processing: part II: deportment in gold ore processing by cyanidation. Hydrometallurgy 111–112:10–21. doi:10.1016/j.hydromet.2011.09.005
39. Kyle JH, Breuer PL, Bunney KG, Pleysier R, May PM (2011) Review of trace toxic elements (Pb, Cd, Hg, As, Sb, Bi, Se, Te) and their deportment in gold processing. Part 1: mineralogy, aqueous chemistry and toxicity. Hydrometallurgy 107:91–100. doi:10.1016/j.hydromet.2011.01.010
40. Ubaldini S, Vegliò F, Fornari P, Abbruzzese C (2000) Process flow-sheet for gold and antimony recovery from stibnite. Hydrometallurgy 57:187–199. doi:10.1016/S0304-386X(00)00107-9
41. Milham L, Craw D (2009) Antimony mobilization through two contrasting gold ore processing systems, New Zealand. Mine Water Environ 28:136–145. doi:10.1007/s10230-009-0071-y
42. Celep O, Alp İ, Paktunç D, Thibault Y (2011) Implementation of sodium hydroxide pretreatment for refractory antimonial gold and silver ores. Hydrometallurgy 108:109–114. doi:10.1016/j.hydromet.2011.03.005
43. Solozhenkin PM, Alekseev AN (2010) Innovative processing and hydrometallurgical treatment methods for complex antimony ores and concentrates. Part II: hydrometallurgy of complex antimony ores. J Min Sci 46:446–452. doi:10.1007/s10913-010-0056-z
44. Korhonen JM, Välikangas L (2014) Handbook of organizational and entrepreneurial ingenuity. Edward Elgar Publishing Inc, Cheltenham, U.K
45. Moskalyk RR, Alfantazi AM (2003) Review of copper pyrometallurgical practice: today and tomorrow. Miner Eng 16:893–919. doi:10.1016/j.mineng.2003.08.002
46. Zivković Ž, Mitevska N, Mihajlović I, Nikolić Đ (2009) The influence of the silicate slag composition on copper losses

during smelting of the sulfide concentrates. J Min Metall Sect B 45:23–24. doi:10.2298/JMMB0901023Z
47. Vircikova E, Havlik M (1999) Removing as from converter dust by a hydrometallurgical method. JOM 51(9):20–23. doi:10.1007/s11837-999-0152-1
48. Fernández MA, Segarra M, Espiell F (1996) Selective leaching of arsenic and antimony contained in the anode slimes from copper refining. Hydrometallurgy 41:255–267. doi:10.1016/0304-386X(95)00061-K
49. Meng L, Zhang S-G, Pan D-A, Li B, Tian J-J, Volinsky AA (2015) Antimony recovery from $SbCl_5$ acid solution by hydrolysis and aging. Rare Met 34:436–439. doi:10.1007/s12598-015-0480-y
50. Li D, Guo X, Xu Z, Tian Q, Feng Q (2015) Leaching behavior of metals from copper anode slime using an alkali fusion-leaching process. Hydrometallurgy 157:9–12. doi:10.1016/j.hydromet.2015.07.008
51. Wang X, Chen Q, Yin Z, Zhang P, Long Z, Su Z (2003) Removal of impurities from copper electrolyte with adsorbent containing antimony. Hydrometallurgy 69:39–44. doi:10.1016/S0304-386X(03)00026-4
52. Ando K, Tsuchida N (1997) Recovering Bi and Sb from electrolyte in copper electrorefining. JOM 49:49–51. doi:10.1007/s11837-997-0033-4
53. Awe SA, Sundkvist JE, Bolin NJ, Sandstrom A (2013) Process flowsheet development for recovering antimony from Sb-bearing copper concentrates. Miner Eng 49:45–53. doi:10.1016/j.mineng.2013.04.026
54. Zhang B, Li Q, Shen W, Min X (2012) Recovery of bismuth and antimony metals from pressure-leaching slag. Rare Met 31:102–106. doi:10.1007/s12598-012-0471-1
55. Hoffmann J (2004) The purification of copper refinery electrolyte. JOM 56(7):30–33. doi:10.1007/s11837-004-0088-4
56. Möller CA, Myagmarsuren B, Friedrich B (2010) Effect of As, Sb, Bi and oxygen in copper anodes during electrorefining. In: Copper 2010: Proceedings, Hamburg, Germany
57. Deorkar NV, Tavlarides LL (1997) A chemically bonded adsorbent for separation of antimony, copper and lead. Hydrometallurgy 46:121–135. doi:10.1016/S0304-386X(97)00006-6
58. Navarro P, Alguacil FJ (2002) Adsorption of antimony and arsenic from a copper electrorefining solution onto activated carbon. Hydrometallurgy 66:101–105. doi:10.1016/S0304-386X(02)00108-1
59. Xiao F, Mao J, Cao D, Shen X, Volinsky AA (2012) The role of trivalent arsenic in removal of antimony and bismuth impurities from copper electrolytes. Hydrometallurgy 125–126:76–80. doi:10.1016/j.hydromet.2012.05.011
60. F-x Xiao, Cao D, J-w Mao, X-n Shen, F-z Ren (2013) Role of trivalent antimony in the removal of As, Sb, and Bi impurities from copper electrolytes. Int J Min Met Mater 20:9–16. doi:10.1007/s12613-013-0687-6
61. Szymanowski JAN (1998) Removal of toxic elements from copper electrolyte by solvent extraction. Miner Process Extr Metall 18:389–418. doi:10.1080/08827509808914162
62. Navarro P, Simpson J, Alguacil FJ (1999) Removal of antimony(III) from copper in sulphuric acid solutions by solvent extraction with LIX 1104SM. Hydrometallurgy 53:121–131. doi:10.1016/S0304-386X(99)00033-X
63. Sarkar SG, Dhadke PM (1999) Solvent extraction separation of antimony(III) and bismuth(III) with bis(2,4,4-trimethylpentyl) monothiophosphinic acid (Cyanex 302). Sep Purif Technol 15:131–138. doi:10.1016/S1383-5866(98)00088-4
64. Iyer JN, Dhadke PM (2003) Solvent extraction and separation studies of antimony(III) and bismuth(III) by using cyanex-925. Indian J Chem Technol 10:665–669
65. Fujii T, Aoki K, Yamana H (2007) Extraction behavior of antimony in a TRUEX system. J Nucl Sci Technol 44:1301–1305. doi:10.1080/18811248.2007.9711375
66. Lin HK (2004) Extraction of antimony by a copper chloride extractant. Hydrometallurgy 73:283–291. doi:10.1016/j.hydromet.2003.12.008
67. Dalton RF, Diaz G, Price R, Zunkel AD (1991) The cuprex metal extraction process: recovering copper from sulfide ores. JOM 43(8):51–56. doi:10.1007/BF03221105
68. Alian A, Sanad W (1967) Extraction of antimony with tertiary amines. Talanta 14:659–669. doi:10.1016/0039-9140(67)80033-X
69. Sargar BM, Rajmane MM, Anuse MA (2004) Selective liquid-liquid extraction of antimony(III) from hydrochloric acid media by N-n-octylaniline in xylene. J Serb Chem Soc 69:283–298
70. Facon S, Cote G, Bauer D (1991) Solvent extraction of antimony(III), bismuth (III), lead(II), tin(IV) with bis(2,4,4-trimethylpentyl)phosphinodithioic acid (Cyanex 301 ®). Solvent Extr Ion Exch 9:717–734. doi:10.1080/07366299108918080
71. Mineral Commodity Summaries (2015). U.S.A
72. Thornton I, Rautiu R, Brush M (2001) Chapter 4: lead industry profile. Lead the facts. Ian Allan Printing Ltd, Hersham, U.K., pp 47–65
73. Blanpain B, Arnout S, Chintinne M, Swinbourne DR (2014) Chapter 8—lead recycling. In: Worrell E, Reuter MA (eds) Handbook of recycling. Elsevier, Boston, MA, pp 95–111. doi:10.1016/B978-0-12-396459-5.00008-8
74. Liu W-F, Yang T-Z, Xia W-T, Xie Z-F, Liu W, Huang C (2009) Principle and practice of producing qualified antimony white from lead-antimony alloy by blowing directly. In: Proceedings of the symposium of the extraction and processing division, held at the TMS 2009 annual meeting and exhibition. TMS, Warrendale Pennsylvania, USA, pp. 483–492
75. Binz F, Friedrich B (2015) Recovery of antimony trioxide flame retardants from lead refining residues by slag conditioning and fuming. Chem Ing Tech 87:1569–1579. doi:10.1002/cite.201500071
76. Liu W, Yang T, Zhang D, Chen L, Liu Y (2014) A new pyrometallurgical process for producing antimony white from by-product of lead smelting. JOM 66(9):1694–1700. doi:10.1007/s11837-014-1026-8
77. Osmani A, Rizaj M, Terziqi A, Kamberaj N (2009) Slag Valorisation of reductive smelting process by shaft furnace in the lead metallurgy of "Trepça" complex with economical and environmental effects. J Int Environ Appl Sci 4:198–206
78. Singh LN (1990) Synthesis of potassium antimony tartrate from the antimony dross of lead smelters. Hydrometallurgy 25:19–25. doi:10.1016/0304-386X(90)90061-6
79. H-z Cao, J-z Chen, H-j Yuan, G-q Zheng (2010) Preparation of pure $SbCl_3$ from lead anode slime bearing high antimony and low silver. Trans Nonferrous Met Soc China 20:2397–2403. doi:10.1016/S1003-6326(10)60661-9
80. Minić D, Štrbac N, Mihajlović I, Živković Ž (2005) Thermal analysis and kinetics of the copper-lead matte roasting process. J Therm Anal Calorim 82:383–388. doi:10.1007/s10973-005-0906-0
81. Barry DL, Cannell JF, Catterall JA, Chave PA, Harris M, Read R, Taylor MRG (1995) Metal manufacturing, refining and finishing works. Ruislip, UK
82. Jaeck ML (1989) Primary and secondary lead processing. In: Proceedings of the international symposium on primary and secondary lead processing. Halifax, Canada, Elsevier Science
83. Henry H (1926) Refining lead. U.S. Patent US1573830 A
84. Nikolić BG (1997) Processing of alkali antimony intermediate products in a lead refinery. Hydrometallurgy 47:31–36. doi:10.1016/S0304-386X(97)00023-6
85. Ojebuoboh FK (1996) One ton of bismuth in the lead smelter and 60 years of Kroll-Betteron. CIM Bull 89:76–79

86. Mallaley K, Morris DR (1990) Analysis of the Kroll-Betterton process—the removal of bismuth from lead bullion. Can Metal Q 29:67–71
87. Brecka G, Hein K, Lange HJ, Paschen P (1997) A pyrometallurgical alternative: the refining electrolysis of lead and solder. JOM 49(4):62–64. doi:10.1007/BF02914881
88. González-Domínguez JA, Peters E, Dreisinger DB (1991) The refining of lead by the Betts process. J Appl Electrochem 21:189–202. doi:10.1007/BF01052570
89. Felder A, Prengaman RD (2006) Lead alloys for permanent anodes in the nonferrous metals industry. JOM 58(10):28–31. doi:10.1007/s11837-006-0197-3
90. Peterson M, Twidwell LG (1985) Removal of arsenic from lead smelter speiss. J Hazard Mater 12:225–229. doi:10.1016/0304-3894(85)85009-3
91. Itoh S, Ono J, Hino M, Nagasaka T (2005) Kinetic study on recovery of antimony in anode slime from used lead batteries utilizing volatile oxide formation. Mater Trans 46:658–664. doi:10.2320/matertrans.46.658
92. Lin D, Qiu K (2011) Removal of arsenic and antimony from anode slime by vacuum dynamic flash reduction. Environ Sci Technol 45:3361–3366. doi:10.1021/es103424u
93. Qiu K, Lin D, Yang X (2012) Vacuum evaporation technology for treating antimony-rich anode slime. JOM 64:1321–1325. doi:10.1007/s11837-012-0458-2
94. Koparal AS, Özgür R, Öğütveren ÜB, Bergmann H (2004) Antimony removal from model acid solutions by electrodeposition. Sep Purif Technol 37:107–116. doi:10.1016/j.seppur.2003.09.001
95. Bergmann MEH, Koparal AS (2011) Electrochemical antimony removal from accumulator acid: results from removal trials in laboratory cells. J Hazard Mater 196:59–65. doi:10.1016/j.jhazmat.2011.08.073
96. Thiele UK (2004) Quo vadis polyester catalyst? Chem Fibers Int 54:162–163
97. Albonetti S, Blanchard G, Burattin P, Masetti S, Tagliani A, Trifirò F (1998) A new ternary mixed oxide catalyst for ammoxidation of propane: Sn/V/Sb. Catal Lett 50:17–23. doi:10.1023/A:1019046430749
98. Trimm DL, Gabbay DS (1971) Kinetics and mechanism of oxidation of butene isomers over a tin oxide + antimony oxide catalyst. T Faraday Soc 67:2782–2792. doi:10.1039/TF9716702782
99. Santacesaria E, Di Serio M, Basile G, Carra S (1989) Kinetics of chloroform fluorination by HF catalyzed by antimony pentachloride. J Fluorine Chem 44:87–111. doi:10.1016/S0022-1139(00)84373-0
100. Ono T, Hillig KW, Kuczkowski RL (1990) The mechanism of the oxidation of propene to acrolein over antimony-tin mixed oxide catalysts. J Catal 123:236–244. doi:10.1016/0021-9517(90)90172-G
101. Zhang C, Catlow CRA (2008) The mechanism of propene oxidation to acrolein on iron antimony oxide. J Catal 259:17–25. doi:10.1016/j.jcat.2008.06.027
102. Thiele UK (2001) The current status of catalysis and catalyst development for the industrial process of poly(ethylene terephthalate) polycondensation. Int J Polym Mater 50:387–394. doi:10.1080/00914030108035115
103. Biros SM, Bridgewater BM, Villeges-Estrada A, Tanski JM, Parkin G (2002) Antimony ethylene glycolate and catecholate compounds: structural characterization of polyesterification catalysts. Inorg Chem 41:4051–4057. doi:10.1021/ic020204b
104. Aharoni SM (1998) The cause of the grey discoloration of PET prepared by the use of antimony-catalysts. Polym Eng Sci 38:1039–1047. doi:10.1002/pen.10272
105. Takahashi Y, Sakuma K, Itai T, Zheng G, Mitsunobu S (2008) Speciation of antimony in PET bottles produced in Japan and China by X-ray absorption fine structure spectroscopy. Environ Sci Technol 42:9045–9050. doi:10.1021/es802073x
106. Fernschild G, Rudolph W, Massonne J (1977) Process for the recovery of antimony pentachloride from used catalyst solutions. U.S. Patent US4005176 A
107. Hyatt DE (1988) Recovery or arsenic and antimony from spent antimony catalyst. U.S. Patent US4722774 A
108. Van Brecht A, Konings A (2011) In: Jones PT et al (eds) Second international slag valorisation symposium: The transition to sustainable materials management. KU Leuven, Leuven, pp 215–227
109. Jung C-H, Osako M (2009) Metal resource potential of residues from municipal solid waste (MSW) melting plants. Resour Conserv Recy 53:301–308. doi:10.1016/j.resconrec.2009.01.004
110. Van Gerven T, Geysen D, Stoffels L, Jaspers M, Wauters G, Vandecasteele C (2005) Management of incinerator residues in Flanders (Belgium) and in neighbouring countries. A comparison. Waste Manage 25:75–87. doi:10.1016/j.wasman.2004.09.002
111. Nakamura K, Kinoshita S, Takatsuki H (1996) The origin and behavior of lead, cadmium and antimony in MSW incinerator. Waste Manage 16:509–517. doi:10.1016/S0956-053X(96)00093-1
112. Watanabe N, Inoue S, Ito H (1999) Antimony in municipal waste. Chemosphere 39:1689–1698. doi:10.1016/S0045-6535(99)00069-7
113. Osako M, Machida N, Tanaka M (1996) Risk management measures against antimony in residue after incineration of municipal waste. Waste Manage 16:519–526. doi:10.1016/S0956-053X(96)00103-1
114. Paoletti F, Seifert H, Vehlow J, Sirini P (2000) Oxyanions forming elements in waste combustion- partitioning of antimony. Waste Manage Res 18:141–150. doi:10.1177/0734242x0001800206
115. Miravet R, López-Sánchez JF, Rubio R (2006) Leachability and analytical speciation of antimony in coal fly ash. Anal Chim Acta 576:200–206. doi:10.1016/j.aca.2006.06.003
116. Van Gerven T, Cooreman H, Imbrechts K, Hindrix K, Vandecasteele C (2007) Extraction of heavy metals from municipal solid waste incinerator (MSWI) bottom ash with organic solutions. J Hazard Mater 140:376–381. doi:10.1016/j.jhazmat.2006.10.037
117. Okkenhaug G, Breedveld GD, Kirkeng T, Lægreid M, Mæhlum T, Mulder J (2013) Treatment of air pollution control residues with iron rich waste sulfuric acid: does it work for antimony (Sb)? J Hazard Mater 248–249:159–166. doi:10.1016/j.jhazmat.2012.12.041
118. Beard A, Klimes M (2013) Searching for safe flame retardants—an update on regulatory status and environmental assessments. PINFA and CEFIC, San Francisco, CA. http://www.flameretardants-online.com/images/userdata/pdf/375_EN.pdf
119. Camino G, Costa L (1988) Performance and mechanisms of fire retardants in polymers—a review. Polym Degrad Stab 20:271–294. doi:10.1016/0141-3910(88)90073-0
120. Camino G, Costa L, Luda di Cortemiglia MP (1991) Thermal stabilisation and flammability of polymers and composites: overview of fire retardant mechanisms. Polym Degrad Stab 33:131–154. doi:10.1016/0141-3910(91)90014-I
121. SRI-Consulting (2008) Global market of flame retardants. http://flameretardants-online.com/web/en/106/114.htm
122. Cheema HA, El-Shafei A, Hauser PJ (2013) Conferring flame retardancy on cotton using novel halogen-free flame retardant bifunctional monomers: synthesis, characterizations and applications. Carbohydr Polym 92:885–893. doi:10.1016/j.carbpol.2012.09.081
123. Abou-Okeil A, El-Sawy SM, Abdel-Mohdy FA (2013) Flame retardant cotton fabrics treated with organophosphorus polymer. Carbohydr Polym 92:2293–2298. doi:10.1016/j.carbpol.2012.12.008

124. Edwards B, El-Shafei A, Hauser P, Malshe P (2012) Towards flame retardant cotton fabrics by atmospheric pressure plasma-induced graft polymerization: synthesis and application of novel phosphoramidate monomers. Surf Coat Technol 209:73–79. doi:10.1016/j.surfcoat.2012.08.031
125. Costa L, Goberti P, Paganetto G, Camino G, Sgarzi P (1990) Thermal behaviour of chlorine-antimony fire-retardant systems. Polym Degrad Stab 30:13–28. doi:10.1016/0141-3910(90)90114-M
126. Keresztes S, Tatár E, Mihucz VG, Virág I, Majdik C, Záray G (2009) Leaching of antimony from polyethylene terephthalate (PET) bottles into mineral water. Sci Total Environ 407: 4731–4735. doi:10.1016/j.scitotenv.2009.04.025
127. Belarra MA, Belategui I, Lavilla I, Anzano JM, Castillo JR (1998) Screening of antimony in PVC by solid sampling-graphite furnace atomic absorption spectrometry. Talanta 46: 1265–1272. doi:10.1016/S0039-9140(97)00390-1
128. Minozaki M, Kachi M (1994) Method and apparatus for recovery of bromine and/or antimony from heat-resistant resins. Japan Patent JP 06144801 A
129. Masatochi J, Juji I, Daisuke A, Shinji S (1995) Treatment of decomposition gases of flame-resistant plastics. Japan Patent JP 08299759, A
130. Masatoshi I, Ikuta Y (1998) Pyrolysis-based material recovery from molding resin for electronic parts. J Environ Eng 124:821–828. doi:10.1061/(ASCE)0733-9372
131. Jakab E, Uddin MA, Bhaskar T, Sakata Y (2003) Thermal decomposition of flame-retarded high-impact polystyrene. J Anal Appl Pyrolysis 68–69:83–99. doi:10.1016/S0165-2370(03)00075-5
132. Klein J, Dorge S, Trouvé G, Venditti D, Durécu S (2009) Behaviour of antimony during thermal treatment of Sb-rich halogenated waste. J Hazard Mater 166:585–593. doi:10.1016/j.jhazmat.2008.12.006
133. Wu H, Shen Y, Harada N, An Q, Yoshikawa K (2014) Production of pyrolysis oil with low bromine and antimony contents from plastic material containing brominated flame retardants and antimony trioxide. Energy Environ Res 4:105–118. doi:10.5539/eer.v4n3p105
134. Mitan NMM, Bhaskar T, Hall WJ, Muto A, Williams PT, Sakata Y (2008) Effect of decabromodiphenyl ether and antimony trioxide on controlled pyrolysis of high-impact polystyrene mixed with polyolefins. Chemosphere 72:1073–1079. doi:10.1016/j.chemosphere.2008.04.011
135. Brebu M, Jakab E, Sakata Y (2007) Effect of flame retardants and Sb_2O_3 synergist on the thermal decomposition of high-impact polystyrene and on its debromination by ammonia treatment. J Anal Appl Pyrolysis 79:346–352. doi:10.1016/j.jaap.2007.02.003
136. Hall WJ, Mitan NMM, Bhaskar T, Muto A, Sakata Y, Williams PT (2007) The co-pyrolysis of flame retarded high impact polystyrene and polyolefins. J Anal Appl Pyrolysis 80:406–415. doi:10.1016/j.jaap.2007.05.002
137. Onwudili JA, Williams PT (2009) Alkaline reforming of brominated fire-retardant plastics: fate of bromine and antimony. Chemosphere 74:787–796. doi:10.1016/j.chemosphere.2008.10.029
138. Onwudili JA, Williams PT (2009) Degradation of brominated flame-retarded plastics (Br-ABS and Br-HIPS) in supercritical water. J Supercrit Fluids 49:356–368. doi:10.1016/j.supflu.2009.03.006
139. Lateef H, Grimes SM, Morton R, Mehta L (2008) Extraction of components of composite materials: ionic liquids in the extraction of flame retardants from plastics. J Chem Technol Biotechnol 83:541–545. doi:10.1002/jctb.1829
140. Freegard K, Tan G, Morton R (2006) Develop a process to separate brominated flame retardants from WEEE polymers: final reports. Oxon, UK
141. Wäger P, Böni H, Buser A, Morf L, Schluep M, Streicher M (2009) Recycling of plastics from waste electrical and electronic equipment (WEEE)—tentative results of a swiss study. In: R'09 Twin World Congress & World Resources Forum, Davos, Switzerland
142. Buekens A, Yang J (2014) Recycling of WEEE plastics: a review. J Mater Cycles Waste 16:415–434. doi:10.1007/s10163-014-0241-2
143. Guo J, Guo J, Xu Z (2009) Recycling of non-metallic fractions from waste printed circuit boards: a review. J Hazard Mater 168:567–590. doi:10.1016/j.jhazmat.2009.02.104
144. de Marco I, Caballero BM, Chomón MJ, Laresgoiti MF, Torres A, Fernández G, Arnaiz S (2008) Pyrolysis of electrical and electronic wastes. J Anal Appl Pyrolysis 82:179–183. doi:10.1016/j.jaap.2008.03.011
145. Moltó J, Font R, Gálvez A, Conesa JA (2009) Pyrolysis and combustion of electronic wastes. J Anal Appl Pyrolysis 84:68–78. doi:10.1016/j.jaap.2008.10.023
146. Gullett BK, Linak WP, Touati A, Wasson SJ, Gatica S, King CJ (2007) Characterization of air emissions and residual ash from open burning of electronic wastes during simulated rudimentary recycling operations. J Mater Cycles Waste 9:69–79. doi:10.1007/s10163-006-0161-x
147. Guo Q, Yue X, Wang M, Liu Y (2010) Pyrolysis of scrap printed circuit board plastic particles in a fluidized bed. Powder Technol 198:422–428. doi:10.1016/j.powtec.2009.12.011
148. Morf LS, Tremp J, Gloor R, Huber Y, Stengele M, Zennegg M (2005) Brominated flame retardants in waste electrical and electronic equipment: substance flows in a recycling plant. Environ Sci Technol 39:8691–8699. doi:10.1021/es051170k
149. Hall WJ, Williams PT (2006) Fast pyrolysis of halogenated plastics recovered from waste computers. Energy Fuels 20: 1536–1549. doi:10.1021/ef060088n
150. Hall WJ, Miskolczi N, Onwudili J, Williams PT (2008) Thermal processing of toxic flame-retarded polymers using a waste fluidized catalytic cracker (FCC) catalyst. Energy Fuels 22: 1691–1697. doi:10.1021/ef800043g
151. Tostar S, Stenvall E, Boldizar A, Foreman MRSJ (2013) Antimony leaching in plastics from waste electrical and electronic equipment (WEEE) with various acids and gamma irradiation. Waste Manage 33:1478–1482. doi:10.1016/j.wasman.2013.03.002
152. Zhenming X, Hongzhou L, Jia L, Yongqing W (2006) Vacuum distillation method for recovering antimony from waste printed circuit board. China Patent CN 1760385, A
153. Yang X, Sun L, Xiang J, Hu S, Su S (2013) Pyrolysis and dehalogenation of plastics from waste electrical and electronic equipment (WEEE): a review. Waste Manage 33:462–473. doi:10.1016/j.wasman.2012.07.025
154. Belardi G, Ippolito N, Piga L, Serracino M (2014) Investigation on the status of rare earth elements contained in the powder of spent fluorescent lamps. Thermochim Acta 591:22–30. doi:10.1016/j.tca.2014.07.015
155. Chang T-C, Wang S-F, You S-J, Cheng A (2007) Characterization of halophosphate phosphor powders recovered from the spent fluorescent lamps. J Environ Eng Manage 17:435–439
156. Henderson ST, Marsden AM, Thorn Lighting L (1972) Lamps and lighting: a manual of lamps and lighting. Edward Arnold, London
157. Shinde K, Dhoble SJ, Swart HC, Park K (2012) Some halophosphates phosphors. Phosphate phosphors for solid-state lighting, vol 174. Springer, Berlin, pp 151–189. doi:10.1007/978-3-642-34312-4_6
158. Srivastava AM, Sommerer TJ (1998) Fluorescent lamp phosphors. Electrochem Soc Interface 7:28–31
159. Shionoya S, Yen WM, Yamamoto H (2006) Phosphor handbook. Taylor & Francis, Boca Raton, FL

160. Soules TF (2000) Tailoring lamp phosphors. In: Ronda CR, Shea LE, Srivastava AM (eds) Physics and chemistry of luminescent materials, vol 40. Electrochemical Society, Pennington, NJ, pp 56–68
161. Braconnier JJ, Rollat A (2012) Method for recovering rare-earth elements from a solid mixture containing a halophosphate and a compound of one or more rare-earth elements. European Patent EP 2419377 A1
162. Dobrowolski R, Mierzwa J (1993) Investigation of activator (Mn, Sb) speciation in phosphors for fluorescent lamps. Mater Chem Phys 34:270–273. doi:10.1016/0254-0584(93)90046-O
163. Baliga BJ (2015) The IGBT device: physics, design and applications of the insulated gate bipolar transistor. Elsevier Science - William Andrew, Norwich, NY
164. Compact fluorescent lamps could nearly halve global lighting demand for electricity (2013). Worldwatch Institute, Washington, DC. http://www.worldwatch.org/node/5918
165. Binnemans K, Jones PT (2014) Perspectives for the recovery of rare earths from end-of-life fluorescent lamps. J Rare Earth 32:195–200. doi:10.1016/S1002-0721(14)60051-X
166. Binnemans K, Jones PT, Blanpain B, Van Gerven T, Yang Y, Walton A, Buchert M (2013) Recycling of rare earths: a critical review. J Clean Prod 51:1–22. doi:10.1016/j.jclepro.2012.12.037
167. Innocenzi V, De Michelis I, Kopacek B, Vegliò F (2014) Yttrium recovery from primary and secondary sources: a review of main hydrometallurgical processes. Waste Manage 34:1237–1250. doi:10.1016/j.wasman.2014.02.010
168. Liu H, Zhang S, Pan D, Tian J, Yang M, Wu M, Volinsky AA (2014) Rare earth elements recycling from waste phosphor by dual hydrochloric acid dissolution. J Hazard Mater 272:96–101. doi:10.1016/j.jhazmat.2014.02.043
169. Mei G, Rao P, Mitsuaki M, Toyohisa F (2009) Separation of red (Y_2O_3: Eu^{3+}), blue (Sr, Ca, Ba)$_{10}(PO_4)_6Cl_2$: Eu^{2+} and green ($LaPO_4$: Tb^{3+}, Ce^{3+}) rare earth phosphors by liquid/liquid extraction. J Wuhan Univ Technol 24:418–423. doi:10.1007/s11595-009-3418-0
170. Tunsu C, Ekberg C, Retegan T (2014) Characterization and leaching of real fluorescent lamp waste for the recovery of rare earth metals and mercury. Hydrometallurgy 144–145:91–98. doi:10.1016/j.hydromet.2014.01.019
171. Urniezaite I, Denafas G, Jankunaite D (2009) Characterization of residues from physicochemical treatment of waste fluorescent lamps. Waste Manage Res 28:606–614. doi:10.1177/0734242x09341074
172. Wu Y, Yin X, Zhang Q, Wang W, Mu X (2014) The recycling of rare earths from waste tricolor phosphors in fluorescent lamps: a review of processes and technologies. Resour Conserv Recy 88:21–31. doi:10.1016/j.resconrec.2014.04.007
173. Yang F, Kubota F, Baba Y, Kamiya N, Goto M (2013) Selective extraction and recovery of rare earth metals from phosphor powders in waste fluorescent lamps using an ionic liquid system. J Hazard Mater 254–255:79–88. doi:10.1016/j.jhazmat.2013.03.026
174. Yang HL, Wang W, Cui HM, Zhang DL, Liu Y, Chen J (2012) Recovery of rare earth elements from simulated fluorescent powder using bifunctional ionic liquid extractants (Bif-ILEs). J Chem Technol Biotechnol 87:198–205. doi:10.1002/Jctb.2696
175. Dupont D, Binnemans K (2015) Rare-earth recycling using a functionalized ionic liquid for the selective dissolution and revalorization of Y_2O_3:Eu^{3+} from lamp phosphor waste. Green Chem 17:856–868. doi:10.1039/C4GC02107J
176. Dupont D, Binnemans K (2016) Antimony recovery from the halophosphate fraction in lamp phosphor waste: a zero-waste approach. Green Chem 18:175–185. doi:10.1039/C5GC01746G
177. Tian H et al (2014) A comprehensive global inventory of atmospheric antimony emissions from anthropogenic activities, 1995–2010. Environ Sci Technol 48:10235–10241. doi:10.1021/es405817u
178. Wilson SC, Lockwood PV, Ashley PM, Tighe M (2010) The chemistry and behaviour of antimony in the soil environment with comparisons to arsenic: a critical review. Environ Pollut 158:1169–1181. doi:10.1016/j.envpol.2009.10.045
179. Varrica D, Bardelli F, Dongarrà G, Tamburo E (2013) Speciation of Sb in airborne particulate matter, vehicle brake linings, and brake pad wear residues. Atmos Environ 64:18–24. doi:10.1016/j.atmosenv.2012.08.067
180. von Uexküll O, Skerfving S, Doyle R, Braungart M (2005) Antimony in brake pads—a carcinogenic component? J Clean Prod 13:19–31. doi:10.1016/j.jclepro.2003.10.008
181. Filella M, Belzile N, Chen Y-W (2002) Antimony in the environment: a review focused on natural waters: I. Occurrence. Earth-Sci Rev 57:125–176. doi:10.1016/S0012-8252(01)00070-8
182. Ungureanu G, Santos S, Boaventura R, Botelho C (2015) Arsenic and antimony in water and wastewater: overview of removal techniques with special reference to latest advances in adsorption. J Environ Manage 151:326–342. doi:10.1016/j.jenvman.2014.12.051
183. Kang M, Kamei T, Magara Y (2003) Comparing polyaluminum chloride and ferric chloride for antimony removal. Water Res 37:4171–4179. doi:10.1016/S0043-1354(03)00351-8
184. Wu Z, He M, Guo X, Zhou R (2010) Removal of antimony (III) and antimony (V) from drinking water by ferric chloride coagulation: competing ion effect and the mechanism analysis. Sep Purif Technol 76:184–190. doi:10.1016/j.seppur.2010.10.006
185. Guo X, Wu Z, He M (2009) Removal of antimony(V) and antimony(III) from drinking water by coagulation–flocculation–sedimentation (CFS). Water Res 43:4327–4335. doi:10.1016/j.watres.2009.06.033
186. Xu W, Wang H, Liu R, Zhao X, Qu J (2011) The mechanism of antimony(III) removal and its reactions on the surfaces of Fe–Mn Binary Oxide. J Colloid Interface Sci 363:320–326. doi:10.1016/j.jcis.2011.07.026
187. Biswas BK, J-i Inoue, Kawakita H, Ohto K, Inoue K (2009) Effective removal and recovery of antimony using metal-loaded saponified orange waste. J Hazard Mater 172:721–728. doi:10.1016/j.jhazmat.2009.07.055
188. Wang L, C-l Wan, Zhang Y, Lee D-J, Liu X, X-f Chen, Tay J-H (2015) Mechanism of enhanced Sb(V) removal from aqueous solution using chemically modified aerobic granules. J Hazard Mater 284:43–49. doi:10.1016/j.jhazmat.2014.10.041
189. Dou X, Mohan D, Zhao X, Pittman CU Jr (2015) Antimonate removal from water using hierarchical macro-/mesoporous amorphous alumina. Chem Eng J 264:617–624. doi:10.1016/j.cej.2014.11.123
190. Dong S, Dou X, Mohan D, Pittman CU Jr, Luo J (2015) Synthesis of graphene oxide/schwertmannite nanocomposites and their application in Sb(V) adsorption from water. Chem Eng J 270:205–214. doi:10.1016/j.cej.2015.01.071
191. Zhu J, Wu F, Pan X, Guo J, Wen D (2011) Removal of antimony from antimony mine flotation wastewater by electrocoagulation with aluminum electrodes. J Environ Sci 23:1066–1071. doi:10.1016/S1001-0742(10)60550-5

Paper 5: Design of sulfonic acid ionic liquids for metal processing

Title:
Sulfonic Acid Functionalized Ionic Liquids for Dissolution of Metal Oxides and Solvent Extraction of Metal Ions

Type: Communication
Journal: Chemical Communication (IF 6.83)
Publisher: Royal Society of Chemistry (RSC)
Publication date: 24/04/2015

Reprint with permission from:
D. Dupont, S. Raiguel and K. Binnemans, *Chem. Commun.*, **2015**, 51, 9006-9009.[(a)]

[(a)]Experimental work carried out by Stijn Raiguel under my supervision.

Electronic Supplementary Information (ESI) available: http://pubs.rsc.org.

Graphical abstract

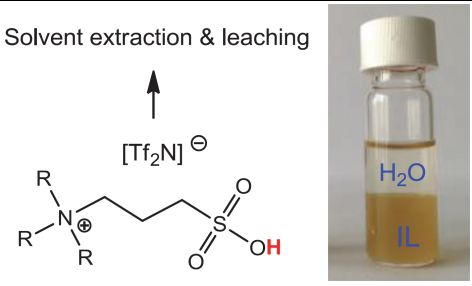

Sulfonic acid functionalized ionic liquids can dissolve metal oxides and extract metal ions very efficiently.

ChemComm

COMMUNICATION

View Article Online
View Journal | View Issue

Cite this: *Chem. Commun.*, 2015, **51**, 9006

Received 1st April 2015,
Accepted 27th April 2015

DOI: 10.1039/c5cc02731d

www.rsc.org/chemcomm

Sulfonic acid functionalized ionic liquids for dissolution of metal oxides and solvent extraction of metal ions†

David Dupont, Stijn Raiguel and Koen Binnemans*

New sulfonic acid functionalized ionic liquids (SAFILs) with bis(trifluoromethylsulfonyl)imide anions were synthesized. These ionic liquids are strong Brønsted acids and can solubilize metal oxides. Water-immiscible SAFILs were used as organic phases in solvent extraction studies.

Inorganic and organic acids are important in many chemical processes including organic synthesis, catalysis, processing of (bio)materials, dissolution of metal ores and as extractants in solvent extraction. Unfortunately, many (strong) acids produce noxious and corrosive fumes. Acid-functionalized ionic liquids are promising new materials as they combine the advantage of a liquid (large contact area), with the advantages of solid-state acids (negligible vapor pressure and reusability).[1,2] Another advantage is their versatility: an infinite number of ionic liquids (ILs) can be designed based on different cations, anions and functional groups.[3] The two main classes of Brønsted-acidic ILs are the carboxyl functionalized ILs and the sulfonic acid functionalized ILs (SAFILs).[2,4–16] Carboxyl functionalized ILs such as betainium bis(trifluoromethylsulfonyl)imide [Hbet][Tf_2N], have been used successfully for the dissolution of metal oxides and the separation of metals by solvent extraction.[4,5,17–23] So far, SAFILs have not been used for solvent extraction since no biphasic SAFIL–H_2O systems have been reported. The currently known SAFILs are hydrophilic (water miscible) due to the polar sulfonic acid functionalized cation and the choice of anion (Cl^-, Br^-, NO_3^-, HSO_4^-, BF_4^-, PF_6^-, $CH_3CO_2^-$, $CF_3SO_3^-$, $CH_3SO_3^-$, *p*-$CH_3C_6H_4SO_3^-$, *etc.*).[1,2,7–16,24,25] Because of their high melting points and viscosities, these SAFILs have been used mainly in diluted form as homogeneous catalyst in organic synthesis and for the hydrolysis of carbohydrates.[2,7–16] Their zwitterions have also been of interest as liquid crystals and as electrolytes in lithium ion batteries.[26–30] SAFILs with the right physical properties can open the way to new applications using the SAFILs in their pure form.

In this Communication, we introduce a series of new quaternary ammonium- and phosphonium-based SAFILs with bis(trifluoromethylsulfonyl)imide (Tf_2N^-) anions. The very stable Tf_2N^- anion is the conjugated base of the super acid HTf_2N and has a low coordinating ability which explains the superior physical properties of Tf_2N-containing ILs, including a relatively low viscosity, low melting point and high thermal stability.[26,31] These SAFILs can therefore be used undiluted. The combination of long alkyl chains and Tf_2N^- anions also allows synthesizing hydrophobic (water-immiscible) SAFILs. The new hydrophobic SAFILs were used as organic phase in solvent extraction systems for metal ions, while hydrophilic SAFILs were used for dissolution of metal oxides.

The SAFILs were prepared by reacting a trialkylamine or trialkylphosphine with 1,3-propanesultone to form sulfonate zwitterions (Scheme 1).[2,10,32,33] Then, a stoichiometric amount of the acid HTf_2N was added to the zwitterion to obtain the ionic liquid in quantitative yield. Detailed synthesis procedures and characterization data are provided in the ESI.† The physical properties of the ILs are summarized in Table 1. All the compounds are room-temperature ILs. When cooling the ILs in a DSC instrument, a glass transition was observed (no crystallization).

The phosphonium ILs have a better thermal stability and lower viscosity than their ammonium analogues, although the

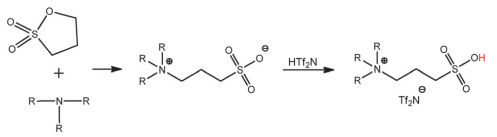

Scheme 1 Synthetic strategy for trialkylammoniumpropanesulfonic acid bis(trifluoromethylsulfonyl)imide ILs, abbreviated as [$N_{RRR}C_3SO_3H$][Tf_2N]. The same scheme applies for the phosphonium analogues [$P_{RRR}C_3SO_3H$][Tf_2N]. R = methyl (1), ethyl (2), propyl (3), butyl (4), hexyl (6), octyl (8) or phenyl (Ph).

KU Leuven, Department of Chemistry, Celestijnlaan 200F – P.O. Box 2404, B-3001 Heverlee, Belgium. E-mail: Koen.Binnemans@chem.kuleuven.be

† Electronic supplementary information (ESI) available: List of used chemicals, equipment, synthesis procedures for the ILs and characterization data (NMR, CHN, TGA, DSC, viscosity). See DOI: 10.1039/c5cc02731d

Table 1 Physical properties of the SAFILs described in this work

Nr	Ionic liquid	T_g[a] (°C)	Viscosity (cP) 30 °C/80 °C	T_{deg}[b] (°C)
1	$[PPh_3C_3SO_3H][Tf_2N]$	−39	≥10 000/482	319
2	$[N_{111}C_3SO_3H][Tf_2N]$	−48	3230/180	275
3	$[N_{222}C_3SO_3H][Tf_2N]$	−57	1463/79	275
4	$[N_{333}C_3SO_3H][Tf_2N]$	−37	≥10 000/229	275
5	$[N_{444}C_3SO_3H][Tf_2N]$	−40	≥10 000/310	275
6	$[P_{444}C_3SO_3H][Tf_2N]$	−50	1888/119	307
7	$[N_{666}C_3SO_3H][Tf_2N]$	−61	1347/111	270
8	$[P_{666}C_3SO_3H][Tf_2N]$	−64	621/62	300
9	$[N_{888}C_3SO_3H][Tf_2N]$	−61	1703/125	265
10	$[P_{888}C_3SO_3H][Tf_2N]$	−56	1916/116	320

[a] Glass transition temperature (T_g): measured with DSC. [b] Degradation temperature (T_{deg}): measured by TGA (5 °C min^{-1}, N_2). The TGA curves are shown in Fig. S1 (ESI).

Fig. 1 (A) The slightly colored, water-immiscible SAFIL (9) is shown as a $[N_{888}C_3SO_3H][Tf_2N]$–H_2O system (1 : 1 ratio wt/wt), before and after addition of ethanol (5 wt%) to suppress the gel formation. (B) The water-miscible SAFIL (6) is shown as a $[P_{444}C_3SO_3H][Tf_2N]$–H_2O system (1 : 1 ratio wt/wt) before and after adding sulfuric acid (2 M) to obtain an aqueous biphasic system.

viscosity of these ILs remains relatively high.[34] Increasing the temperature or adding water (Fig. S2, ESI†), greatly reduces the viscosity for all ILs which makes them easier to handle. SAFILs are usually hydrophilic due to the polar sulfonic acid group on the cation. To counter this effect, long alkyl side chains can be used in combination with the hydrophobic anion Tf_2N^-. The different SAFILs were contacted with water, acetone and toluene (1 : 1 wt/wt ratio) to test their miscibility (Table 2). SAFILs (1–6) were found to be hydrophilic (water-miscible) and are among the rare examples of water-miscible ILs with the Tf_2N^- anion. SAFILs (7–10) were found to be hydrophobic (water-immiscible). Without additives, the hydrophobic SAFILs form a gel when contacted with water. Gel formation can be suppressed by adding an alcohol as a modifier to the system. The best results were obtained adding ethanol (≈5 wt%) to SAFIL (8) or (9), and butanol (≈5 wt%) to SAFIL (10). The use of higher alcohols has been reported for solvent extraction systems with non-polar solvents like toluene.[35–38] Stable biphasic systems with a low viscosity and fast phase separation could be obtained this way for the water-immiscible SAFILs (8–10) (Fig. 1). An aqueous biphasic system with a sharp phase boundary was observed for the water-miscible SAFIL (6) $[P_{444}C_3SO_3H][Tf_2N]$ after addition of sulfuric acid (1–2 M) to the aqueous phase (Fig. 1). The acid suppresses the deprotonation of the sulfonic acid group of the IL and therefore decreases the polarity of the IL, thus inducing phase separation. This hypothesis is supported by the fact that the salting-out agent Na_2SO_4 did not cause phase separation.[39] The existence of biphasic SAFIL–H_2O systems opens the way to solvent extraction of metal ions. To the best of our knowledge, no reports exist on the use of sulfonic acid functionalized ILs for solvent extraction. Not much is known about solvent extraction with sulfonic acid extractants either, because their surfactant properties often cause micelle formation, which hampers phase separation.[40,41] A few papers mention solvent extraction using ILs with sulfonate anions, *e.g.* 1-butyl-3-methylimidazolium nonafluorobutanesulfonate, but their extraction mechanism is based on cation exchange (eqn (1)), leading to loss of IL cations to the aqueous phase.[42–44] On the other hand, the ILs described in this work have sulfonic acid functionalized cations, which can be deprotonated to form zwitterions. The SAFILs with long alkyl chains (hexyl, octyl) have water-immiscible zwitterions, which means that the acidic protons can be exchanged by metal ions, generally without transfer of IL cations or anions to the water phase (eqn (2)). This proton exchange mechanism is controlled by the pH. The same mechanism has been observed for ILs with carboxyl-functionalized cations such as $[Hbet][Tf_2N]$.[17,19]

$$M^{n+}_{(aq)} + n[Cat][RSO_3]_{(IL)} \rightarrow [M][RSO_3]_{n(IL)} + nCat^{+}_{(aq)} \quad (1)$$

$$M^{n+}_{(aq)} + n[RSO_3H][Tf_2N]_{(IL)} \rightarrow [(RSO_3)_nM][Tf_2N]_{n(IL)} + nH^{+}_{(aq)} \quad (2)$$

Table 2 Density (g cm^{-3}) (25 °C) and miscibility of the SAFILs in water, acetone and toluene (1 : 1 ratio wt/wt)[a]

IL	1	2	3	4	5	6	7	8	9	10
Density	1.50	1.57	1.55	1.42	1.35	1.36	1.32	1.26	1.17	1.20
Water	+	+	+	+	+	+	−	−	−	−
Acetone	+	+	+	+	+	+	+	+	+	+
Toluene	−	−	−	−	−	−	+	+	+	+

[a] Miscible (+) or immiscible (−).

The water-immiscible SAFIL $[N_{888}C_3SO_3H][Tf_2N]$ was contacted with water (1 : 1 ratio wt/wt) containing various metal chloride salts (1 mmol L^{-1}). Ethanol was added (5 wt%) to obtain a stable biphasic system with a sharp phase boundary (Fig. 1). The metal concentrations were measured by TXRF to determine the distribution ratio D (eqn (3)) and percentage extraction $\%E$ (eqn (4)):

$$D = \frac{[M]_{IL}}{[M]_{aq}} \quad (3)$$

$$\%E = \frac{n_{IL}}{n_{IL} + n_{aq}} \quad (4)$$

Here $[M]_{IL}$ and $[M]_{aq}$ are the equilibrium concentrations and n the corresponding number of moles in the IL phase and aqueous phase, respectively. Fig. 2 shows the extraction results without pH modification. The pH of the water phase is then in the range 0–0.2.

The SAFIL $[N_{888}C_3SO_3H][Tf_2N]$ is able to extract a wide range of metal ions (Fig. 2), with a particularly high affinity

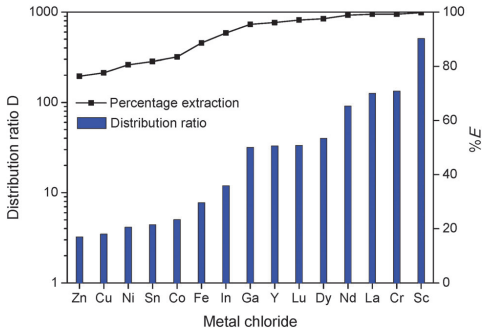

Fig. 2 Distribution ratio (*D*) and percentage extraction (%*E*) in $[N_{888}C_3SO_3H][Tf_2N]$–H_2O for the metal chlorides (1 mmol L^{-1}): Zn(II), Cu(II), Ni(II), Sn(II), Co(II), Fe(III), In(III), Ga(III), Y(III), Lu(III), Dy(III), Nd(III), La(III), Cr(III), Sc(III).

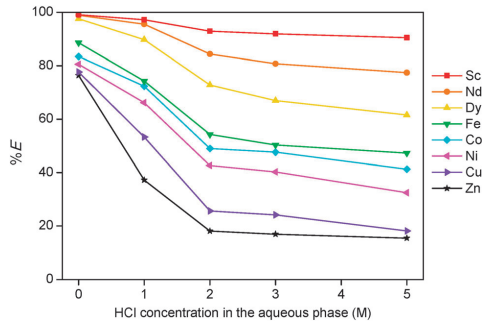

Fig. 3 Influence of the initial acid concentration in the aqueous phase on the extraction (%) of Zn(II), Cu(II), Ni(II), Co(II), Fe(III), Dy(III), Nd(III), Sc(III) ions.

for rare-earth ions especially compared to the affinity of carboxylic acid extractants and ILs at similar pH values.[17,45] Notice that the lanthanide ions are extracted in the reverse order (La(III) > Nd(III) > Dy(III) > Lu(III)) than the one expected on the basis of their charge density. This could be due to sterical hindrance of the sulfonate groups and octyl side chains which causes smaller lanthanides to be less efficiently coordinated. This reversal of the lanthanide extraction sequence is unusual, but sterical hindrance of ligands is known to influence the extraction sequence of the lanthanides and to eventually fully reverse it.[45–48] A typical example is the reversal when switching from linear thiocyanate ligands to more sterically demanding nitrate ligands in quaternary ammonium extraction systems.[47] Preston and du Preez attributed this behavior to the interplay of electrostatic and steric effects.[49] Since the extraction occurs *via* a proton exchange mechanism (eqn (2)), the extraction efficiencies and mutual separation of the metal ions can be modified by adjusting the pH of the aqueous phase (Fig. 3).[45]

Finally, the dissolution of metal oxides in the strongly Brønsted acidic SAFILs ($pK_a \approx -2$) was tested.[2] The dissolution of metal oxides has been described in detail for carboxylic acid functionalized ILs, but has not been investigated for the more strongly acidic SAFILs.[4,5,20,22] Metal salts (*e.g.* NaCl) are poorly soluble in conventional ILs due to the inefficient anion solvation.[20] Brønsted-acidic ILs can therefore selectively dissolve metal oxides because metal oxides form only metal cations and water when reacted with an acid (eqn (5)). This offers opportunities for the selective leaching of metal oxides from a mixture of minerals or salts or for the cleaning of oxidized metal surfaces.[20] Water can be added to accelerate the dissolution kinetics by lowering the viscosity and improving proton exchange, but the selectivity towards metal oxides is then reduced.[4,5,20]

$$NiO + 2[RSO_3H][Tf_2N] + nH_2O \rightarrow [Ni(RSO_3)_2(H_2O)_n][Tf_2N]_2 + H_2O \quad (5)$$

The dissolution of a range of metal oxides was tested in SAFIL–H_2O systems (1 : 1 ratio wt/wt) at 80 °C for SAFILs (2, 3, 9). In these conditions, the IL solutions have a low viscosity (<25 cP) (Fig. S2, ESI†). It was found that these ILs could dissolve large (stoichiometric) amounts of ZnO, CuO, NiO, La_2O_3, Nd_2O_3, Y_2O_3, MnO, CoO, Co_3O_4, Fe_2O_3 and to a lesser extent also TiO_2, Al_2O_3, Cr_2O_3, WO_3. This is an improvement compared to the carboxyl functionalized IL $[Hbet][Tf_2N]$ which cannot efficiently dissolve the more inert oxides: CoO, Co_3O_4, Fe_2O_3, TiO_2, Al_2O_3, Cr_2O_3, WO_3.[4,5] The strong acidity and high affinity of SAFILs for metal ions makes them very suitable for the dissolution of metal oxides (Fig. 4). For the same reason, methanesulfonic acid has also been highlighted as a promising leaching agent since it can dissolve a wide range of metal salts, many of them in significantly higher concentrations than in hydrochloric or sulfuric acid.[50] The use of IL analogues is therefore certainly an interesting evolution since ILs have the additional advantage of a negligible vapor pressure and improved reusability.

In summary, we have synthesized a range of new sulfonic acid functionalized ionic liquids (SAFILs) with Tf_2N^- anions showing excellent physical properties. Solvent extraction of metal ions was demonstrated using the new hydrophobic (water-immiscible) SAFILs. The highly acidic SAFILs were also used for the dissolution of metal oxides. This work will hopefully stimulate further research on these promising ILs besides their current use as homogeneous catalysts.

The authors wish to thank the KU Leuven (projects GOA/13/008 and IOF-KP RARE^3) and the FWO Flanders (PhD fellowship to DD) for financial support.

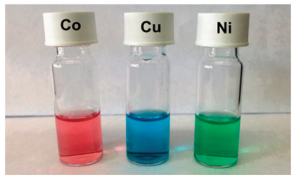

Fig. 4 Dissolution of Co_3O_4, CuO and NiO in $[N_{111}C_3SO_3H][Tf_2N]$ (50 mg g^{-1}).

Notes and references

1 A. Zare, F. Abi, A. R. Moosavi-Zare, M. H. Beyzavi and M. A. Zolfigol, *J. Mol. Liq.*, 2013, **178**, 113–121.
2 A. C. Cole, J. L. Jensen, I. Ntai, K. L. T. Tran, K. J. Weaver, D. C. Forbes and J. H. Davis, *J. Am. Chem. Soc.*, 2002, **124**, 5962–5963.
3 N. V. Plechkova and K. R. Seddon, *Chem. Soc. Rev.*, 2008, **37**, 123–150.
4 P. Nockemann, B. Thijs, T. N. Parac-Vogt, K. Van Hecke, L. Van Meervelt, B. Tinant, I. Hartenbach, T. Schleid, V. T. Ngan, M. T. Nguyen and K. Binnemans, *Inorg. Chem.*, 2008, **47**, 9987–9999.
5 P. Nockemann, B. Thijs, S. Pittois, J. Thoen, C. Glorieux, K. Van Hecke, L. Van Meervelt, B. Kirchner and K. Binnemans, *J. Phys. Chem. B*, 2006, **110**, 20978–20992.
6 Z. Fei, D. Zhao, T. J. Geldbach, R. Scopelliti and P. J. Dyson, *Chem. – Eur. J.*, 2004, **10**, 4886–4893.
7 J. Akbari, A. Heydari, H. Reza Kalhor and S. A. Kohan, *J. Comb. Chem.*, 2009, **12**, 137–140.
8 A. S. Amarasekara and A. Razzaq, *Carbohydr. Res.*, 2014, **386**, 86–91.
9 F. Jiang, Q. Zhu, D. Ma, X. Liu and X. Han, *J. Mol. Catal. A*, 2011, **334**, 8–12.
10 D. Fang, X.-L. Zhou, Z.-W. Ye and Z.-L. Liu, *Ind. Eng. Chem. Res.*, 2006, **45**, 7982–7984.
11 J. Shen, H. Wang, H. Liu, Y. Sun and Z. Liu, *J. Mol. Catal. A: Chem.*, 2008, **280**, 24–28.
12 S. Sim, S. Kwon and S. Koo, *Molecules*, 2012, **17**, 12804–12811.
13 D.-J. Tao, J. Wu, Z.-Z. Wang, Z.-H. Lu, Z. Yang and X.-S. Chen, *RSC Adv.*, 2014, **4**, 1–7.
14 A. Zare, A. R. Moosavi-Zare, M. Merajoddin, M. A. Zolfigol, T. Hekmat-Zadeh, A. Hasaninejad, A. Khazaei, M. Mokhlesi, V. Khakyzadeh, F. Derakhshan-Panah, M. H. Beyzavi, E. Rostami, A. Arghoon and R. Roohandeh, *J. Mol. Liq.*, 2012, **167**, 69–77.
15 M. A. Zolfigol, A. Khazaei, A. R. Moosavi-Zare, A. Zare, H. G. Kruger, Z. Asgari, V. Khakyzadeh and M. Kazem-Rostami, *J. Org. Chem.*, 2012, **77**, 3640–3645.
16 Q. Wu, H. Chen, M. Han, D. Wang and J. Wang, *Ind. Eng. Chem. Res.*, 2007, **46**, 7955–7960.
17 B. Onghena and K. Binnemans, *Ind. Eng. Chem. Res.*, 2015, **54**, 1887–1898.
18 T. Vander Hoogerstraete, B. Onghena and K. Binnemans, *J. Phys. Chem. Lett.*, 2013, **4**, 1659–1663.
19 K. Sasaki, K. Takao, T. Suzuki, T. Mori, T. Arai and Y. Ikeda, *Dalton Trans.*, 2014, **43**, 5648–5651.
20 D. Dupont and K. Binnemans, *Green Chem.*, 2015, **17**, 856–868.
21 D. P. Fagnant, G. S. Goff, B. L. Scott, W. Runde and J. F. Brennecke, *Inorg. Chem.*, 2013, **52**, 549–551.
22 D. Dupont and K. Binnemans, *Green Chem.*, 2015, **17**, 2150–2163.
23 A. P. Abbott, G. Frisch, J. Hartley and K. S. Ryder, *Green Chem.*, 2011, **13**, 471–481.
24 F. Fiegenbaum, E. M. Martini, M. O. de Souza, M. R. Becker and R. F. de Souza, *J. Power Sources*, 2013, **243**, 822–825.
25 A. Amarasekara and O. Owereh, *J. Therm. Anal. Calorim.*, 2011, **103**, 1027–1030.
26 S. Ueda, J. Kagimoto, T. Ichikawa, T. Kato and H. Ohno, *Adv. Mater.*, 2011, **23**, 3071–3074.
27 B. Soberats, M. Yoshio, T. Ichikawa, S. Taguchi, H. Ohno and T. Kato, *J. Am. Chem. Soc.*, 2013, **135**, 15286–15289.
28 R. Rondla, J. C. Y. Lin, C. T. Yang and I. J. B. Lin, *Langmuir*, 2013, **29**, 11779–11785.
29 S. Taguchi, T. Ichikawa, T. Kato and H. Ohno, *Chem. Commun.*, 2012, **48**, 5271–5273.
30 S. Taguchi, T. Matsumoto, T. Ichikawa, T. Kato and H. Ohno, *Chem. Commun.*, 2011, **47**, 11342–11344.
31 Y. Kohno and H. Ohno, *Chem. Commun.*, 2012, **48**, 7119–7130.
32 M. Yoshizawa, M. Hirao, K. Ito-Akita and H. Ohno, *J. Mater. Chem.*, 2001, **11**, 1057–1062.
33 S. Saita, Y. Mieno, Y. Kohno and H. Ohno, *Chem. Commun.*, 2014, **50**, 15450–15452.
34 K. Tsunashima and M. Sugiya, *Electrochem. Commun.*, 2007, **9**, 2353–2358.
35 Y. A. El-Nadi, *Int. J. Miner. Process.*, 2007, **82**, 14–22.
36 Y. Shen, D. Wang and J. Wu, *Chin. Sci. Bull.*, 1997, **42**, 1168–1172.
37 E. Anticó, A. Masana, M. Hidalgo, V. Salvadó, M. Iglesias and M. Valiente, *Anal. Chim. Acta*, 1996, **327**, 267–276.
38 M. Majdan, R. P. Sperline, W.-G. Gu, W.-H. Yu and H. Freiser, *Solvent Extr. Ion Exch.*, 1989, **7**, 987–1005.
39 M. G. Freire, A. F. M. Claudio, J. M. M. Araujo, J. A. P. Coutinho, I. M. Marrucho, J. N. C. Lopes and L. P. N. Rebelo, *Chem. Soc. Rev.*, 2012, **41**, 4966–4995.
40 E. O. Otu and A. D. Westland, *Solvent Extr. Ion Exch.*, 1991, **9**, 875–883.
41 G. Y. Markovits and G. R. Choppin, in *Ion Exch. Solvent Extr.*, ed. J. A. Marinsky and Y. Marcus, Marcel Dekker, New York, 1973, vol. 3, pp. 51–81.
42 N. Kozonoi and Y. Ikeda, *Monatsh. Chem.*, 2007, **138**, 1145–1151.
43 N. Asanuma, Y. Takahashi and Y. Ikeda, *Prog. Nucl. Energy*, 2011, **53**, 944–947.
44 N. Papaiconomou, J.-M. Lee, J. Salminen, M. von Stosch and J. M. Prausnitz, *Ind. Eng. Chem. Res.*, 2008, **47**, 5080–5086.
45 A. C. Du Preez and S. J. Preston, *Solvent Extr. Ion Exch.*, 1992, **10**, 207–230.
46 F. Xie, T. A. Zhang, D. Dreisinger and F. Doyle, *Miner. Eng.*, 2014, **56**, 10–28.
47 N. Krishnamurthy and C. K. Gupta, *Extractive Metallurgy of Rare Earths*, CRC Press, Boca Raton, FL, 2004.
48 T. C. Lo, M. H. I. Baird and C. Hanson, *Handbook of solvent extraction*, Wiley-Interscience, New York, 1983.
49 J. S. Preston and A. C. Du Preez, Solvent extraction processes for the separation of rare earths metals, in *Solvent Extraction 1990: proceedings of the International Solvent Extraction Conference (ISEC '90), Kyoto, Japan*, ed. T. Sekine, Part A, Elsevier, Amsterdam, 1990, pp. 883–894.
50 M. D. Gernon, M. Wu, T. Buszta and P. Janney, *Green Chem.*, 1999, **1**, 127–140.

Paper 6: Design of new alkylsulfuric acid ionic liquids

Title:
Alkylsulfuric acid ionic liquids: a promising class of strongly acidic room-temperature ionic liquids.

Type: Communication
Journal: Chemical Communication (IF 6.83)
Publisher: Royal Society of Chemistry (RSC)
Publication date: 01/03/2016

Reprint with permission from:
D. Dupont, E. Renders, and K. Binnemans, *Chem. Commun*., **2016**, DOI: 10.1039/C6CC00094K

[(a)]Experimental work carried out by Evelien Renders under my supervision.

Electronic Supplementary Information (ESI) available: http://pubs.rsc.org.

Graphical abstract

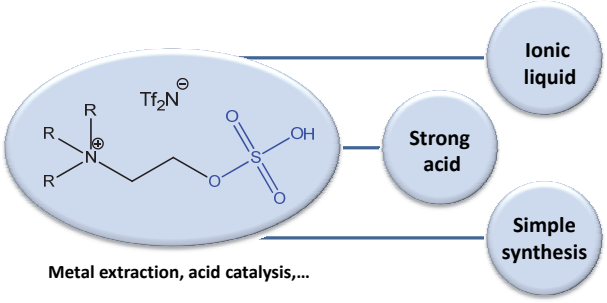

Alkylsulfuric acid ILs are simple to make and offer a more strongly acidic alternative to sulfonic acid ILs for applications in catalysis, metal extraction and dissolution of metal oxides.

ChemComm

COMMUNICATION

View Article Online
View Journal

Alkylsulfuric acid ionic liquids: a promising class of strongly acidic room-temperature ionic liquids†

David Dupont, Evelien Renders and Koen Binnemans*

Cite this: DOI: 10.1039/c6cc00094k

Received 5th January 2016,
Accepted 1st March 2016

DOI: 10.1039/c6cc00094k

www.rsc.org/chemcomm

Strongly acidic ($pK_a \approx -3.5$) room-temperature ionic liquids (ILs) with $-OSO_3H$ functionalized cations are introduced. The strong acidity, easy synthesis, and better physical properties of these R–OSO_3H ILs make them excellent alternatives to the well-known sulfonic acid (R–SO_3H) ILs, especially in the domain of metal processing.

Brønsted-acid ionic liquids (ILs) are a very interesting class of solvents.[1] They are highly tunable, soluble in a wide range of organic solvents, and often also reusable. The fact that they are non-volatile (no toxic fumes) also makes them safer and more convenient to handle than traditional mineral acids.[1] Acidic ILs have been used as catalysts in organic synthesis, but also for the dissolution of metal oxides, and as acidic extractants in solvent extraction of metal ions.[1–12] Currently, the two main classes of Brønsted-acid ILs are the carboxylic acid (–COOH) ILs and sulfonic acid (R–SO_3H) ILs.[1,4,13] The acid group is located on the IL cation so that upon deprotonation zwitterions are formed, which can effectively coordinate to metal ions.[1,5,10] Recently, we have synthesized the first examples of water-immiscible sulfonic acid ILs, which were liquid at room temperature.[10] Sulfonic acid extractants are typically avoided in traditional solvent extraction due to their detergent properties, micelle formation and low solubility in the organic phase.[14] These issues were solved by incorporating the sulfonic acid extractants in the structure of an IL.[10] However, the high charge density of the sulfonic acid group still caused a high viscosity, a tendency to form gels, and the need to use long alkyl chains (hexyl, octyl) to make the sulfonic acid ILs water-immiscible.[10] The synthesis of these compounds was therefore relatively expensive since cyclic sultones and amines with long alkyl chains were required.[1,10] As an answer to these problem, we present in this Communication a different class of strongly acidic room-temperature ILs which are simple to make and contain alkylsulfuric acid (R–OSO_3H) functionalized cations (Fig. 1). The synthesis, stability and physical properties are discussed, as well as their ability to dissolve and extract metal ions. The focus in this work is on metal processing in these ILs, but the increased acidity of R–OSO_3H groups ($pK_a \approx -3.5$),[15] compared to sulfonic acids (R–SO_3H) ILs ($pK_a \approx -2$),[16] should also improve their efficiency as Brønsted-acid catalyst and could be the object of future research.[15,17] The stronger acidity makes a difference for the protonation of organic species (*e.g.* carboxylic acids, aldehydes, ketones) in water-free solvents and therefore for the catalysis of certain reactions such as the Fischer esterification.[1,3,6,13,15–22] The additional oxygen atom of the R–OSO_3H group, compared to sulfonic acids (R–SO_3H), not only increases the acidity, but also decreases the charge density of the end group, thus lowering the viscosity and increasing the hydrophobicity. The direct consequence is that we were able to synthesize low-viscous, room-temperature ILs that are water-immiscible even with short alkyl chains (methyl, ethyl), instead of the hexyl or octyl chains required for similar sulfonic acid ILs.[10] Furthermore, alkylsulfuric acids and alkylsulfates are known for their low toxicity and biodegradability, which is why they are used as detergents in many household cleaning products (*e.g.* sodium dodecyl sulfate, SDS).[23,24] It is also possible to synthesize certain alkylsulfuric acid ILs starting from the widely available biomolecule and animal food additive choline chloride.[15,17,25,26] These ILs thus fit in the trend towards more bio-based and biodegradable ILs.[25–30]

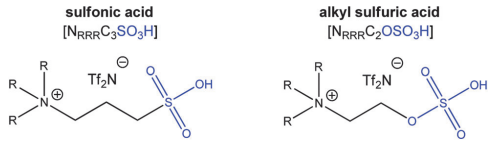

Fig. 1 Comparison between the well-known sulfonic acid ILs (left) and the alkylsulfuric acid ILs (right), described in this work.

The detailed synthesis and characterization are described in the ESI,† but a schematic overview is given here (Scheme 1).

KU Leuven, Department of Chemistry, Celestijnlaan 200F – P.O. Box 2404, B-3001 Heverlee, Belgium. E-mail: Koen.Binnemans@chem.kuleuven.be

† Electronic supplementary information (ESI) available: List of used chemicals, equipment, synthesis procedures, results and characterization data (NMR, FTIR, TGA, DSC, viscosity). See DOI: 10.1039/c6cc00094k

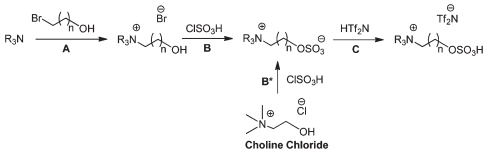

Scheme 1 General synthesis method for alkylsulfuric acid functionalized ammonium-based ILs. The same method applies for phosphonium-based ILs.

The general synthesis route started by alkylating a trialkylamine or trialkylphosphine with a linear ω-bromoalcohol (A), followed by the addition of chlorosulfonic acid to convert the alcohol to a sulfate group (B).[31] The zwitterion was then reacted with bistriflimic acid (HTf_2N) to produce the desired IL (C). The strong acidity of the IL cation makes it mandatory to use IL anions derived from even stronger acids, in order to avoid cross-protonation. Bis(trifluoromethylsulfonyl)imide (bistriflimide, Tf_2N^-) anions were chosen due to their tendency to form stable and low-viscous ILs.[32] The synthesis route depicted in Scheme 1 is flexible and allows control over the length of the alkyl chains on the amine and the length of the carbon linker attached to the $-OSO_3H$ group. Alternatively, the bio-compound choline chloride[25,26] can be used as building block to make the trimethyl IL in a convenient two-step method (B*).[15,17] An overview of the synthesized ILs and their physical properties is given in Table 1. The ILs are all liquid at room temperature and have relatively low viscosities even at 25 °C. Note that the glass transition temperatures and viscosities are lower than for the equivalent sulfonic acid ILs reported in our previous work.[10] We attributed this to the fact that the extra oxygen atom has an electron-withdrawing effect, thus lowering the intermolecular forces. The lower charge density of the alkylsulfuric acid group also translates in a more hydrophobic character, compared to sulfonic acid ILs.[10] The alkylsulfuric acid ILs cover a broad range of miscibility from water-miscible to miscible in hydrocarbons (Table 2), which is useful for a potential use as Brønsted-acid catalysts and even for non-aqueous (IL/hydrocarbon) solvent extraction systems.

The increased hydrophobicity of these ILs compared to sulfonic acid ILs, is also evident from the fact that the ILs with ethyl chains or longer (IL **2–6**) are water-immiscible (Table 2), while the analogue sulfonic acid ILs $[N_{RRR}C_3SO_3H][Tf_2N]$ required more expensive precursors with hexyl or octyl chains to be immiscible in water.[10] IL **1** is particularly interesting since it can form thermomorphic aqueous biphasic systems (ABS) when salts (*e.g.* NaCl, Na_2SO_4) are added to induce phase separation.[33–35] Such thermomorphic biphasic systems can mix reversibly with water above a certain temperature, called the *cloud point temperature*.[8,34,36–39] Similar behavior has been observed for the analogue carboxyl-functionalized IL: betainium bistriflimide [Hbet][Tf_2N] and this phenomenon is of great interest for solvent extraction as it effectively removes the phase boundary.[8,37,38,40] An overview of the influence of the salt concentration on the cloud point temperature of this ABS system is given in ESI† (Table S2). The best results were found for 1.0 M NaCl or 0.5 M Na_2SO_4, with excellent phase separation at room temperature and relatively low cloud point temperatures around 48 °C. Fig. 2 shows the mixing and demixing of IL **1** with water (1 : 1 wt/wt), containing 1.5 M of NaCl. The fact that IL **1** shows this interesting behavior is a lucky coincidence since this is the IL that can be prepared from choline chloride (Scheme 1).

Alkylsulfates can decompose in water to form the corresponding alcohol and sulfuric acid, but it is generally accepted that they have a relatively good kinetic resistance against hydrolysis.[27,33,41,42] To test the stability of the ILs, thermogravimetric analysis (TGA) was first carried out using a nitrogen atmosphere, which showed a degradation temperature of approximately 330 °C (ESI,† Fig. S1). Then, the stability of the ILs was tested with an air atmosphere (20–150 °C) and mixed with water (1 : 1 wt/wt) (20–80 °C) over a 24 h interval, using NMR to monitor the degradation, but no signs of degradation were observed (ESI,† Table S3).

From previous work, it is known that acidic ILs such as carboxylic acid ILs are able to efficiently dissolve metal oxides since only water and metal cations are formed, which can be solvated by the IL zwitterions created during the deprotonation.[2,5,9,43]

Table 1 Physical properties of the ionic liquids described in this work

Nr	Ionic liquid	T_g[a] (°C)	Viscosity (cP) 25 °C	Density 25 °C (g cm^{-3})
1	$[N_{111}C_2OSO_3H][Tf_2N]$	−28	324	1.58
2	$[N_{222}C_2OSO_3H][Tf_2N]$	<−80	378	1.46
3	$[N_{666}C_2OSO_3H][Tf_2N]$	<−80	1950	1.30
4	$[N_{888}C_2OSO_3H][Tf_2N]$	<−80	1538	1.28
5	$[P_{444}C_2OSO_3H][Tf_2N]$	<−80	739	1.40
6	$[P_{888}C_2OSO_3H][Tf_2N]$	<−80	1332	1.23
7	$[N_{111}C_3OSO_3H][Tf_2N]$	<−80	1337	1.59
8	$[N_{111}C_4OSO_3H][Tf_2N]$	<−80	1258	1.54

[a] Glass transition temperature (T_g): measured by DSC (lower limit: −80 °C).

Table 2 Miscibility of the alkylsulfuric acid ILs in different solvents[a]

ILs	1	2	3	4	5	6	7	8
Water	±	−	−	−	Gel	Gel	+	−
DMF	+	+	±	±	+	±	+	+
Acetonitrile	+	+	+	+	+	±	+	+
EG	+	+	−	−	−	−	+	+
Methanol	+	+	−	−	+	−	+	+
Ethanol	−	+	+	±	+	−	+	+
Acetone	+	+	+	+	+	+	+	+
Toluene	−	−	±	+	−	+	−	+
n-Heptane	−	−	−	−	−	−	−	+

[a] Miscible (+), partially miscible (±) or immiscible (−).

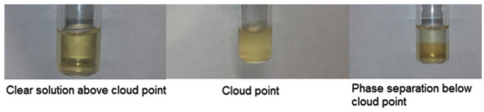

Fig. 2 Thermomorphic mixing/demixing of the $[N_{111}C_2OSO_3H][Tf_2N] : H_2O$ system (1 : 1 wt/wt) with NaCl (1.5 M). The cloud point of this system is 48 °C.

Metal salts (*e.g.* NaCl) are poorly soluble in these ILs due to the inefficient anion solvation.[9] These ILs thus offer the possibility to selectively dissolve metal oxides.[9] For alkylsulfuric acid ILs, the dissolution reaction of metal oxides (*e.g.* CuO) could be as follows (eqn (1)):

$$CuO + 2[ROSO_3H][Tf_2N] \rightarrow [(ROSO_3)_2Cu][Tf_2N]_2 + H_2O \quad (1)$$

The dissolution of a range of metal oxides was tested in IL–H_2O systems (20 wt% H_2O) at 80 °C (24 h) using $[N_{111}C_2OSO_3H][Tf_2N]$. This ionic liquid could efficiently dissolve metal oxides including CaO, CuO, NiO, La_2O_3, Nd_2O_3, Co_3O_4 and Fe_2O_3, which is not surprising considering its strong acidity and high affinity for metal ions. The alkylsulfuric acid IL allows the dissolution of the same metal oxides as the analogue sulfonic acid IL $[N_{111}C_3SO_3H][Tf_2N]$ ($pK_a \approx -2$),[10] prepared in previous work. This is expected due to the leveling effect of water. However, differences are observed when comparing the dissolution of metal oxides with the carboxylic acid IL $[N_{111}C_1COOH][Tf_2N]$ (=[Hbet][Tf_2N]) ($pK_a \approx 2$).[5,9,43] This ionic liquid cannot efficiently dissolve inert oxides such as Fe_2O_3 or Co_3O_4, but it has nevertheless shown a lot of promise for the treatment and recycling of metal-rich products and waste residues, due to its acidity, metal affinity and thermomorphic behavior.[2,9] The more strongly acidic alkylsulfuric acid ILs could be useful to speed up these leaching processes or allow the treatment of more inert residues such as bauxite residue or iron oxide slags.[44] The alkylsulfuric acid ILs are very strong acids and do not produce noxious fumes like most mineral acids (*e.g.* HCl, HNO_3).[1,16] This makes them particularly attractive as potentially green leaching agents. $[N_{111}C_2OSO_3H][Tf_2N]$ is preferred compared to the analogues with longer alkyl chains due to its easy synthesis and lower viscosity. An overview and comparison of metal oxide dissolution by these ILs is given in the ESI† (Table S4).

The water-immiscible alkylsulfuric acid ILs can also be used as organic phase to extract metal ions from aqueous solutions. These are interesting extractants, as their very strong acidity makes it possible to efficiently extract metal ions even from highly acidic solutions (pH < 0). This is not possible with weaker acids such as carboxylic acid or phosphoric acid extractants.[45] Unfortunately, alkylsulfuric acid or alkylsulfate extractants are difficult to use in traditional solvent extraction due to their detergent properties.[14,46,47] These polar extractants do not dissolve in the organic phase unless long alkyl chains are used, which in their turn cause micelle formation. Therefore, very little is known about solvent extraction with alkylsulfuric acid or alkylsulfate extractants. ILs thus offer a unique opportunity to study these "inaccessible" extractants, since no detergent behavior is observed and stable biphasic systems were obtained. Furthermore, the use of a pure ionic liquid phase with extractants incorporated in their structure, drastically increases the extractant concentration compared to organic solvents that typically have a low solubility for such acidic extractants.[48,49] The advantage of incorporating alkylsulfuric acid groups on the cation instead of using ILs with alkylsulfate anions is that acidic cations form zwitterions upon deprotonation, which can coordinate the metal ions.[11,38] This means that acidic protons are exchanged by metal ions (eqn (2)), instead of transferring organic cations to the aqueous phase as is commonly the case for ionic liquids with extracting anions (*e.g.* alkylsulfate anions).[45,50,51]

$$M^{n+}_{(aq)} + n[ROSO_3H][Tf_2N]_{(IL)} \rightarrow [(ROSO_3)_nM][Tf_2N]_{n(IL)} + nH^+_{(aq)} \quad (2)$$

The extraction efficiency was tested by contacting the ILs $[N_{111}C_2OSO_3H][Tf_2N]$ and $[N_{888}C_2OSO_3H][Tf_2N]$ with aqueous solutions (1 : 1 ratio wt/wt), containing metal chlorides (1 mmol L^{-1}, pH 2.7). NaCl (1.5 M) was added to the $[N_{111}C_2OSO_3H][Tf_2N]$ system to obtain a biphasic system. After extraction, the metal concentrations were measured by total reflection X-ray fluorescence (TXRF) to determine the percentage extraction %*E* (eqn (3)):

$$\%E = \frac{n_{IL}}{n_{IL} + n_{aq}} \times 100 \quad (3)$$

Here, n_{IL} and n_{aq} are the number of moles of the metal ion in the IL phase and aqueous phase, respectively. The results are shown in Fig. 3. The extraction efficiencies are intermediate between carboxyl-functionalized ILs such as [Hbet][Tf_2N] (poor extraction for most metal ions),[38] and sulfonic acid ILs which fully extract most studied metal ions from chloride solutions (>80%).[10] This trend is logical based on the charge density of the functional group: $R–COO^- < R–OSO_3^- < R–SO_3^-$. The intermediate extraction efficiency of the alkylsulfuric acid ILs is useful as it allows separation of metal ions. It is also very interesting to notice that the inversed extraction trend for rare-earth ions (La > Nd > Dy > Y), previously observed for sulfonic acid ILs, also occurs for these alkylsulfuric acid ILs. This confirms the hypothesis that bulky functional groups lead to a reversal of the normal (charge density based) extraction series for the rare-earth ions (La < Nd < Dy < Y), which is observed for carboxylic acid extractants.[10,38,52,53]

In conclusion, this Communication discusses a promising class of very acidic ILs with alkylsulfuric acid functionalized cations. These ILs can be synthesized cheaply and offer improved physical properties compared to sulfonic acid ILs,

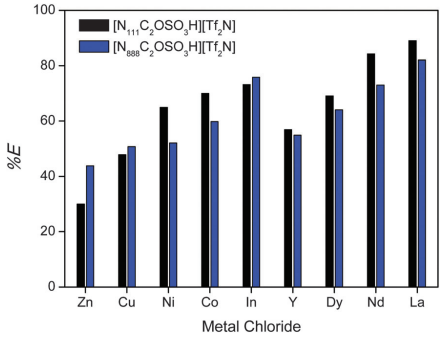

Fig. 3 Percentage extraction (%*E*) from a metal chloride solution (1 mmol L^{-1}, pH 2.7) using the IL $[N_{111}C_2OSO_3H][Tf_2N]$ and $[N_{888}C_2OSO_3H][Tf_2N]$ as org. phase. Zn(II), Cu(II), Ni(II), Co(II), In(III), Y(III), Dy(III), Nd(III) and La(III) were tested.

which are used as Brønsted-acid catalysts in organic synthesis. The stronger acidity of alkylsulfuric acid ILs and their miscibility in various organic solvents makes them excellent alternatives for sulfonic acid ILs. This Communication also focusses on the possibility of metal processing in these ILs, including the dissolution of metal oxides and the extraction of metal ions from aqueous solutions. These strongly acidic extractants can efficiently extract metal ions even from very acidic solutions (pH < 0), which is not possible with commonly used carboxylic acid or phosphoric acid extractants. Furthermore, incorporating alkylsulfuric acid groups into the structure of the IL finally allowed the study of this type of extractants, since in traditional solvent extraction alkylsulfuric acid extractants are difficult to use due to their strong detergent properties. These versatile alkylsulfuric acid ILs thus open up a range of interesting applications and it is our hope that this Communication will stimulate further research interest for these ILs.

The authors wish to thank the KU Leuven (projects GOA/13/008 and IOF-KP RARE[3]) and the FWO Flanders (PhD fellowship to DD) for financial support.

Notes and references

1 A. C. Cole, J. L. Jensen, I. Ntai, K. L. T. Tran, K. J. Weaver, D. C. Forbes and J. H. Davis, *J. Am. Chem. Soc.*, 2002, **124**, 5962–5963.
2 D. Dupont and K. Binnemans, *Green Chem.*, 2015, **17**, 2150–2163.
3 D. Fang, X.-L. Zhou, Z.-W. Ye and Z.-L. Liu, *Ind. Eng. Chem. Res.*, 2006, **45**, 7982–7984.
4 Z. Fei, D. Zhao, T. J. Geldbach, R. Scopelliti and P. J. Dyson, *Chem. – Eur. J.*, 2004, **10**, 4886–4893.
5 P. Nockemann, B. Thijs, S. Pittois, J. Thoen, C. Glorieux, K. Van Hecke, L. Van Meervelt, B. Kirchner and K. Binnemans, *J. Phys. Chem. B*, 2006, **110**, 20978–20992.
6 D.-J. Tao, J. Wu, Z.-Z. Wang, Z.-H. Lu, Z. Yang and X.-S. Chen, *RSC Adv.*, 2014, **4**, 1–7.
7 Q. Wu, H. Chen, M. Han, D. Wang and J. Wang, *Ind. Eng. Chem. Res.*, 2007, **46**, 7955–7960.
8 T. Vander Hoogerstraete, B. Onghena and K. Binnemans, *J. Phys. Chem. Lett.*, 2013, **4**, 1659–1663.
9 D. Dupont and K. Binnemans, *Green Chem.*, 2015, **17**, 856–868.
10 D. Dupont, S. Raiguel and K. Binnemans, *Chem. Commun.*, 2015, **51**, 9006–9009.
11 K. Sasaki, K. Takao, T. Suzuki, T. Mori, T. Arai and Y. Ikeda, *Dalton Trans.*, 2014, **43**, 5648–5651.
12 J. W. Freiderich, J. J. Stankovich, H. Luo, S. Dai and B. A. Moyer, *Eur. J. Inorg. Chem.*, 2015, 4354–4361.
13 C. Yue, D. Fang, L. Liu and T.-F. Yi, *J. Mol. Liq.*, 2011, **163**, 99–121.
14 G. Y. Markovits and G. R. Choppin, in *Ion Exchange and Solvent Extraction*, ed. J. A. Marinsky and Y. Marcus, Marcel Dekker, New York, USA, 1973, vol. 3, pp. 51–81.
15 H. Peng, S. Sun, Y. Hu, R. Xing and D. Fang, *Heteroat. Chem.*, 2015, **26**, 215–223.
16 J. P. Guthrie, *Can. J. Chem.*, 1978, **56**, 2342.
17 S. P. Satasia, P. N. Kalaria and D. K. Raval, *J. Mol. Catal. A: Chem.*, 2014, **391**, 41–47.
18 J. Gui, X. Cong, D. Liu, X. Zhang, Z. Hu and Z. Sun, *Catal. Commun.*, 2004, **5**, 473–477.
19 P. N. Muskawar, S. Senthil Kumar and P. R. Bhagat, *J. Mol. Catal. A: Chem.*, 2013, **380**, 112–117.
20 J. Shen, H. Wang, H. Liu, Y. Sun and Z. Liu, *J. Mol. Catal. A: Chem.*, 2008, **280**, 24–28.
21 Q. Zhang, S. Zhang and Y. Deng, *Green Chem.*, 2011, **13**, 2619–2637.
22 D. Zhao, J. Wang and E. Zhou, *Green Chem.*, 2007, **9**, 1219–1222.
23 A. Wibbertmann, I. Mangelsdorf, K. Gamon and R. Sedlak, *Ecotoxicol. Environ. Saf.*, 2011, **74**, 1089–1106.
24 K. Weisenberger, D. Mayer and S. R. Sandler, *Ullmann's Encyclopedia of Industrial Chemistry*, Wiley-VCH, Weinheim, Germany, 2000.
25 Y. Fukaya, Y. Iizuka, K. Sekikawa and H. Ohno, *Green Chem.*, 2007, **9**, 1155–1157.
26 K. D. Weaver, H. J. Kim, J. Sun, D. R. MacFarlane and G. D. Elliott, *Green Chem.*, 2010, **12**, 507–513.
27 M. T. Garcia, N. Gathergood and P. J. Scammells, *Green Chem.*, 2005, **7**, 9–14.
28 H. Ohno and K. Fukumoto, *Acc. Chem. Res.*, 2007, **40**, 1122–1129.
29 G.-H. Tao, L. He, W.-S. Liu, L. Xu, W. Xiong, T. Wang and Y. Kou, *Green Chem.*, 2006, **8**, 639–646.
30 G.-h. Tao, L. He, N. Sun and Y. Kou, *Chem. Commun.*, 2005, 3562–3564.
31 R. J. W. Cremlyn, *Chlorosulfonic Acid*, Royal Society of Chemistry, Cambridge, UK, 2002.
32 J. D. Holbrey, R. D. Rogers, R. A. Mantz, P. C. Trulove, V. A. Cocalia, A. E. Visser, J. L. Anderson, J. L. Anthony, J. F. Brennecke, E. J. Maginn, T. Welton and R. A. Mantz, *Ionic Liquids in Synthesis*, Wiley-VCH, Darmstadt, Germany, 2008, pp. 57–174.
33 F. J. Deive, A. Rodríguez, I. M. Marrucho and L. P. N. Rebelo, *J. Chem. Thermodyn.*, 2011, **43**, 1565–1572.
34 M. G. Freire, A. F. M. Claudio, J. M. M. Araujo, J. A. P. Coutinho, I. M. Marrucho, J. N. C. Lopes and L. P. N. Rebelo, *Chem. Soc. Rev.*, 2012, **41**, 4966–4995.
35 S. Shahriari, C. M. S. S. Neves, M. G. Freire and J. A. P. Coutinho, *J. Phys. Chem. B*, 2012, **116**, 7252–7258.
36 S. P. M. Ventura, C. M. S. S. Neves, M. G. Freire, I. M. Marrucho, J. Oliveira and J. A. P. Coutinho, *J. Phys. Chem. B*, 2009, **113**, 9304–9310.
37 D. Depuydt, L. Liu, C. Glorieux, W. Dehaen and K. Binnemans, *Chem. Commun.*, 2015, **51**, 14183–14186.
38 B. Onghena and K. Binnemans, *Ind. Eng. Chem. Res.*, 2015, **54**, 1887–1898.
39 Y. Kohno, S. Saita, Y. Men, J. Yuan and H. Ohno, *Polym. Chem.*, 2015, **6**, 2163–2178.
40 T. Vander Hoogerstraete, B. Onghena and K. Binnemans, *Int. J. Mol. Sci.*, 2013, **14**, 21353–21377.
41 R. Wolfenden and Y. Yuan, *Proc. Natl. Acad. Sci. U. S. A.*, 2007, **104**, 83–86.
42 T.-Y. Wu, S.-G. Su, S.-T. Gung, M.-W. Lin, Y.-C. Lin, C.-A. Lai and I. W. Sun, *Electrochim. Acta*, 2010, **55**, 4475–4482.
43 P. Nockemann, B. Thijs, T. N. Parac-Vogt, K. Van Hecke, L. Van Meervelt, B. Tinant, I. Hartenbach, T. Schleid, V. T. Ngan, M. T. Nguyen and K. Binnemans, *Inorg. Chem.*, 2008, **47**, 9987–9999.
44 K. Binnemans, P. T. Jones, B. Blanpain, T. Van Gerven and Y. Pontikes, *J. Cleaner Prod.*, 2015, **99**, 17–38.
45 A. C. Du Preez and S. J. Preston, *Solvent Extr. Ion Exch.*, 1992, **10**, 207–230.
46 E. O. Otu and A. D. Westland, *Solvent Extr. Ion Exch.*, 1991, **9**, 875–883.
47 T. Sekine and Y. Hasegawa, *Solvent extraction chemistry: fundamentals and applications*, Marcel Dekker, New York, USA, 1977.
48 A. E. Visser, R. P. Swatloski, W. M. Reichert, R. Mayton, S. Sheff, A. Wierzbicki, J. J. H. Davis and R. D. Rogers, *Chem. Commun.*, 2001, 135–136.
49 H. Zhao, S. Xia and P. Ma, *J. Chem. Technol. Biotechnol.*, 2005, **80**, 1089–1096.
50 N. Kozonoi and Y. Ikeda, *Monatsh. Chem.*, 2007, **138**, 1145–1151.
51 N. Papaiconomou, J.-M. Lee, J. Salminen, M. von Stosch and J. M. Prausnitz, *Ind. Eng. Chem. Res.*, 2008, **47**, 5080–5086.
52 J. S. Preston and A. C. Du Preez, Solvent Extraction Processes for the Separation of Rare Earths Metals, In Proceedings of International Solvent Extraction Conference Japan, 1990.
53 K. Larsson and K. Binnemans, *Hydrometallurgy*, 2015, **156**, 206–214.

Paper 7: Effect of salts on biphasic IL/water systems

Title:
Overview of the Effect of Salts on Biphasic Ionic Liquid/Water Solvent Extraction Systems: Anion Exchange, Mutual Solubility and Thermomorphic Properties

Type: Full paper
Journal: Journal of Physical Chemistry B (IF 3.30)
Publisher: American Chemical Society (ACS)
Publication date: 15/05/2015

Reprint with permission from:
D. Dupont, D. Depuydt and K. Binnemans, *J. Phys. Chem. B*, **2015**, 119, 6747-6757.

Electronic Supplementary Information (ESI) available: http://pubs.acs.org.

Graphical abstract

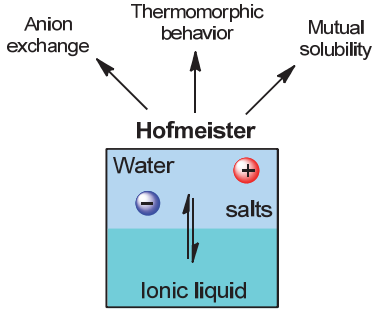

Implications of the Hofmeister series for biphasic IL/water extraction systems: anion exchange, mutual solubility and changes in cloud point temperature.

THE JOURNAL OF PHYSICAL CHEMISTRY B

Article

pubs.acs.org/JPCB

Overview of the Effect of Salts on Biphasic Ionic Liquid/Water Solvent Extraction Systems: Anion Exchange, Mutual Solubility, and Thermomorphic Properties

David Dupont, Daphne Depuydt, and Koen Binnemans*

KU Leuven, Department of Chemistry, Molecular Design and Synthesis, Celestijnenlaan 200F, P.O. Box 2404, B-3001 Heverlee, Belgium

Supporting Information

ABSTRACT: Hydrophobic (water-immiscible) ionic liquids (ILs) are frequently used as organic phase in solvent extraction studies. These biphasic IL/water extraction systems often also contain metal salts or mineral acids, which can significantly affect the IL trough (un)wanted anion exchange and changes in the solubility of IL in the aqueous phase. In the case of thermomorphic systems, variations in the cloud point temperature are also observed. All these effects have important repercussions on the choice of IL, suitable for a certain extraction system. In this paper, a complete overview of the implications of metal salts on biphasic IL/water systems is given. Using the Hofmeister series as a starting point, a range of intuitive prediction models are introduced, supported by experimental evidence for several hydrophobic ILs, relevant to solvent extraction. Particular emphasis is placed on the IL betainium bis(trifluoromethylsulfonyl)imide [Hbet][Tf_2N]. The aim of this work is to provide a comprehensive interpretation of the observed effects of metal salts, so that it can be used to predict the effect on any given biphasic IL/water system instead of relying on case-by-case reports. These prediction tools for the impact of metal salts can be useful to optimize IL synthesis procedures, extraction systems and thermomorphic properties. Some new insights are also provided for the rational design of ILs with UCST or LCST behavior based on the choice of IL anion.

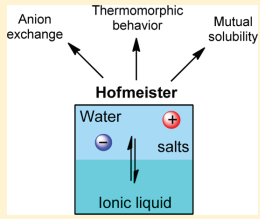

INTRODUCTION

The study of the effect of metal salts on the behavior of compounds in solution starts with Franz Hofmeister in 1888. He described the effect of salt cations and anions on the stability and solubility of the protein ovalbumin in aqueous solutions, and ranked the ions in the so-called Hofmeister series.[1] His observations were later transposed to explain the effect of metal salts and organic salts on the behavior of other proteins, colloids, and polymers in solution.[2−22] Ions that promote the dissolution of a compound in solution are called *salting-in ions*, while ions that exclude a solute from solution are called *salting-out ions*.[2−22] Despite the apparent simplicity of this theory, it still continues to puzzle scientists to this day.[23,24] The importance of this complicated solvation science is becoming ever more apparent as the study of interfacial phenomena and solvent structure on a molecular level is the key to understanding many areas of chemistry.[22−33] Due to their strongly ionic character, ionic liquids (ILs) have received particular attention lately in this area of solvation science.[34] Under the influence of salts, some water-miscible ILs can form IL-based aqueous biphasic systems (ABS).[34−49] More importantly, the properties of biphasic IL/water systems formed by water-immiscible ILs are also greatly affected by the addition of metals and mineral acids.[50−56] These water-immiscible ILs have shown great promise as organic phase in solvent extraction studies. The ILs can be used as diluents for extractants, or task-specific ILs can be prepared in which a functional (extracting) group is incorporated in the structure of the IL.[57] Due to the infinite number of possible anion and cation combinations, ILs are often considered designer or task-specific solvents.[58] A well-known example is the carboxyl-functionalized IL betainium bis(trifluorosulfonyl)imide [Hbet][Tf_2N], which can be used for the extraction of a range of metal ions.[59−64] In traditional solvent extraction, which uses apolar solvents such as toluene or kerosene as organic phase, the effect of metal salts is mostly visible in the mutual solubility of the organic phase and aqueous phase.[65] The solubility of uncharged hydrophobic molecules such as benzene or toluene in the aqueous phase can be increased by the adsorption of ions which counters the van der Waals attraction between the hydrophobic solutes.[10,66] Both anions and cations are effective at increasing the surface charge and improving their solubility by countering the van der Waals attraction. The effect of ions is therefore only related to their hydrophobicity since this will determine if they can adsorb on the hydrophobic surface and contribute to its surface charge. The charge density of an ion determines its level of hydration and therefore also its hydrophobicity (Figure 1). It was shown experimentally that the rank order of effectiveness of the anions in salting-out benzene is indeed SO_4^{2-} > Cl^- > Br^- > NO_3^- > I^-, and the rank order of the cations is Ca^{2+} > Na^+ > K^+ > NH_4^+ > Cs^+, which is in agreement with the series in Figure 1.[2,10,66] This corresponds to the Hofmeister series with a reversed

Received: March 28, 2015
Revised: May 13, 2015
Published: May 15, 2015

DOI: 10.1021/acs.jpcb.5b02980
J. Phys. Chem. B 2015, 119, 6747−6757

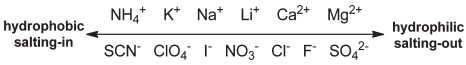

Figure 1. Salting-in/salting-out series for uncharged molecular solvents and ionic liquids. This ranking of anions and cations follows the hydrophobicity which is a consequence of the charge density and the resulting size of their hydration mantle.

cation series because the Hofmeister series was established for the negatively charged hydrophobic protein ovalbumin. Therefore, adsorbed cations diminish the surface charge of the protein and lower its solubility. Schwiertz et al., used this to predict the order of the salting-in/salting-out series depending on the surface charge and the hydrophobicity of a protein or colloid surface.[5,6]

The same order also applies to the solubility of ionic liquids in the water phase.[47,50−54,67,68] However, ILs are more complicated than the above-mentioned organic solvents in the sense that they consist of ions themselves. Therefore, salts can also cause other effects such as anion exchange, which can negatively affect the ionic liquid. This paper gives and overview of all the effects of metal salts and mineral acids on a selection of biphasic IL/water systems, relevant to solvent extraction. These effects include anion exchange, changes in mutual solubility and effects on the cloud point temperature of thermomorphic systems. The countless different combinations of anions and cations to form ILs, increases the need for a general prediction model that is applicable for all ILs, regardless of the structural characteristics of their anions and cations. Rationalizations and prediction models are therefore provided, which are generally applicable to all water-immiscible ILs. Understanding these aspects is important for the design of stable solvent extraction systems and to minimize the loss of IL to the water phase.[37,46,61,69−77] Particular emphasis was placed on water-immiscible ILs used as organic phase in solvent extraction of metal ions, such as the alkylated ammonium and phosphonium ILs and the functionalized ILs like [Hbet][Tf_2N].[59−62,73,76,78,79]

EXPERIMENTAL SECTION

Chemicals. $MgCl_2{\cdot}6H_2O$ (98%), NaCl (98%), $NaClO_4{\cdot}H_2O$ (98%), NaF (99%), $Mg(NO_3)_2{\cdot}6H_2O$, KSCN (99%), $LiNO_3$ (99%) and D_2O (99.9 atom % D) were obtained from Sigma-Aldrich (Diegem, Belgium). $CaCl_2{\cdot}2H_2O$ (99.5%), $NaNO_3$ (99%), Na_2SO_4 (99%), $Ca(NO_3)_2{\cdot}4H_2O$ (99%), KNO_3 (99%), NH_4NO_3 (99%) and HNO_3 (65%) were purchased from Chem-Lab (Zedelgem, Belgium). KCl (99.5%) and NaI (99.5%) were purchased from AppliChem (Darmstadt, Germany) and LiCl (99%) from Fisher Chemical (Loughborough, UK). CsCl (99%), NaBr (99.5%), NH_4Cl (99.5%), H_2SO_4 (96%), $HClO_4$ (70%), HCl (37%) and 1,4-dioxane (99.9%) were obtained from Acros Organics (Geel, Belgium). The silicone solution in isopropanol was purchased from SERVA Electrophoresis GmbH (Heidelberg, Germany). All chemicals were used as received without further purification.

Ionic Liquids. Table 1 shows the ILs used in this work. An overview of the chemical structure of all the ILs is provided in the Supporting Information (Figure S2). The ILs [N_{4111}][Tf_2N] (99%), [S_{222}][Tf_2N] (99%), [Chol][Tf_2N] (99%), [emim][Tf_2N] (99%) and [mppip][Tf_2N] (99%) were purchased from IoLiTec (HeilBronn, Germany). The ILs [P_{8444}][Cl] (Cyphos 253), [P_{66614}][Cl] (Cyphos 101) and [P_{66614}][Br] (Cyphos 102) were purchased from Cytec (Vlaardingen, Netherlands), and [N_{8881}][Cl] (Aliquat 336) was obtained from Sigma-Aldrich (Diegem, Belgium). The commercially available ILs were used as received without further purification. For the synthesized ILs, a detailed overview of the synthesis procedures and required chemicals is given in the Supporting Information.

Table 1. Overview of the Ionic Liquids Used in This Work

formula	full name	origin
[P_{8444}][Cl]	tributyl(octyl)phosphonium chloride	purchased
[P_{8444}][Br]	tributyl(octyl)phosphonium bromide	synthesized
[P_{8444}][NO_3]	tributyl(octyl)phosphonium nitrate	synthesized
[P_{8444}][ClO_4]	tributyl(octyl)phosphonium perchlorate	synthesized
[P_{8444}][Tf_2N]	tributyl(octyl)phosphonium bistriflimide[a]	synthesized
[P_{66614}][Cl]	trihexyl(tetradecyl)phosphonium chloride	purchased
[P_{66614}][Br]	trihexyl(tetradecyl)phosphonium bromide	purchased
[P_{66614}][NO_3]	trihexyl(tetradecyl)phosphonium nitrate	synthesized
[P_{66614}][Tf_2N]	trihexyl(tetradecyl)phosphonium bistriflimide	synthesized
[N_{8881}][Cl]	trioctyl(methyl)ammonium chloride	purchased
[N_{4111}][Tf_2N]	trimethyl(butyl)ammonium bistriflimide	purchased
[S_{222}][Tf_2N]	triethylsulfonium bistriflimide	purchased
[Hbet][Tf_2N]	betainium bistriflimide	synthesized
[Chol][Tf_2N]	choline bistriflimide	purchased
[$P_{444}E_5$][DEHP]	tributyl(2-[2-(2-methoxyethoxy)ethoxy] ethyl) phosphonium bis(2-ethylhexyl) phosphate	synthesized
[P_{4441}COOH][Cl]	tributyl(carboxymethyl)phosphonium chloride	synthesized
[emim][Tf_2N]	1-ethyl-3-methylimidazolium bistriflimide	purchased
[mppip][Tf_2N]	1-methyl-1-propylpiperidinium bistriflimide	purchased

[a]bistriflimide = bis(trifluoromethylsulfonyl)imide.

Equipment and Characterization. ^1H and ^{13}C spectra were recorded on a Bruker Avance 300 spectrometer, operating at 300 MHz for ^1H and 75 MHz for ^{13}C. A TMS-200 thermoshaker (Nemus Life) was used to shake the samples and a Heraeus Megafuge 1.0 centrifuge was used to accelerate phase separation. Total reflection X-ray fluorescence (TXRF) analysis was performed with a Bruker S2 Picofox TXRF spectrometer equipped with a molybdenum source. For the sample preparation, plastic microtubes were filled with a small amount of IL sample (10−50 mg) and ethanol/water (700 μL). The microtubes were then vigorously shaken on a vibrating plate (IKA MS 3 basic). Finally, a 1 μL drop of this solution was put on a quartz glass plate, previously treated with a silicone/isopropanol solution (Serva) to avoid spreading of the sample droplet on the quartz glass plate. The quartz glass plates were then dried for 30 min at 60 °C prior to analysis. Each sample was measured for 5 min.

Determination of the IL Solubility in the Water Phase with Quantitative ^1H NMR. The IL (1 g) was contacted with a water phase (1 g) and shaken for 1 h (25 °C, 2000 rpm) to guarantee equilibrium. The samples were then centrifuged (5000 rpm, 10 min) to accelerate phase separation. A sample of the water phase was taken (100 mg) and mixed with a known amount of 1,4-dioxane (5 mg) and diluted with deuterated water (500 mg). This mixture was then shaken on a vibrating plate (IKA MS 3 basic) and measured with ^1H NMR. The integrated intensity of the 1,4-dioxane signal (δ = 3.6) was compared with the IL signals (and corrected for the amount of protons) in order to quantify the concentration of IL in the water phase. The water peak did not cause problematic interferences. This analytical technique was validated using

DOI: 10.1021/acs.jpcb.5b02980
J. Phys. Chem. B 2015, 119, 6747−6757

Table 2. Degree of Anion Exchange (%) after Contacting Several ILs with Salt-Containing Aqueous Solutions (2 equiv)[a]

	Tf_2N^-	SCN^-	ClO_4^-	I^-	NO_3^-	Br^-	Cl^-	SO_4^{2-}
$[P_{66614}][Tf_2N]$	[b]	[b]	2.9	0.4	0.1	0.04	0.01	<DL[c]
$[P_{66614}][NO_3]$	98.7	98.1	97.3	96.9	[b]	51.2	16.4	0.5
$[P_{66614}][Br]$	99.7	99.5	99.4	99.1	84	[b]	27.1	1.8
$[P_{66614}][Cl]$	100	100	[b]	99.9	97.6	96.1	[b]	2.5

[a]Sodium salts were used except for $LiTf_2N$ and KSCN. The mixtures were shaken (2000 rpm) for 1 h at 50 °C. The anion exchange was quantified by TXRF. [b]Not quantifiable because the same element is present after exchange. [c]Below the detection limit for TXRF (1 ppm).

known amounts of betaine in solution (Figure S1) and has an average uncertainty of ±0.1 wt %.

Determination of the Cloud Point Temperature. The cloud point temperature (T_{CP}) of thermomorphic IL/water systems was determined visually. An oil bath setup was used to control the temperature of the IL-containing vial (4 mL) and a temperature probe was present in the mixture. The IL−water solvent mixtures were prepared in a 1:1 wt/wt ratio. The temperature of the sample was gradually increased or decreased (in steps of 0.1 °C) and allowed to equilibrate at every step until phase separation was observed. At every step the sample was shortly agitated (1 s) to overcome a possible metastable state. The determination of the cloud point temperature was repeated three times to guarantee its accuracy.

Studying Anion Exchange with TXRF Analysis. ILs of the type $[P_{66614}][X_A]$ (X_A = different anion) (1 g) were contacted with aqueous solutions (1 g) containing 2 equiv of sodium salts with the desired anion X_B. The mixtures were shaken (2000 rpm) at 50 °C for 1 h. Then, the samples were centrifuged (5000 rpm) to accelerate phase separation. A sample of the IL phase was then taken to determine the degree of anion exchange. This was quantified by measuring the P/X (phosphor/anion) ratio before and after the exchange, using total reflection X-ray fluorescence (TXRF). These relative measurements did not require an internal standard.

RESULTS AND DISCUSSION

1. Ionic Liquid Anion Exchange. When a hydrophobic (water-immiscible) IL is contacted with a water phase, a biphasic system is created. If salts are present in the aqueous phase, the salt anions can exchange with the anions of the IL depending on their affinity for the water phase and the IL phase. In some cases anion exchange is intended, for example, to synthesize an IL with a different anion than the anion present in the commercial IL.[73] In other cases, anion exchange can be an unwanted effect, for example, in metal extraction processes with different anions in the IL phase and the water phase. In such processes anion exchange can significantly pollute the IL phase and change its properties. Fortunately, the occurrence of anion exchange can be predicted based on the Hofmeister series. Hydrophobic anions (with low charge density) such as Tf_2N^-, SCN^-, ClO_4^- and I^- prefer to be in the IL, while more hydrophilic anions such as Cl^- and SO_4^{2-} prefer to be in the water phase where they are better solvated (Figure 1). The exact order of anion exchange was tested using trihexyl(tetradecyl)phosphonium ILs with the formula $[P_{66614}][X]$ (X = Tf_2N^-, NO_3^-, Br^-, and Cl^-). This IL has been used successfully for the extraction of various metal ions.[75,76,78−80] These very hydrophobic ILs were contacted with an aqueous phase (1:1 ratio wt/wt) containing 2 equiv of a salt ($LiTf_2N$, NaSCN, $NaClO_4$, NaI, $NaNO_3$, NaBr, NaCl, Na_2SO_4). The mixtures were shaken (2000 rpm) for 1 h at 50 °C. The P/X ratio (phosphor/anion) in the IL phase was analyzed by TXRF and compared with the initial P/X ratio to obtain the degree of anion exchange (%) (Table 2). The aim was not to obtain full equilibrium, but to measure the relative tendency of salt anions to exchange with IL anions.

Anion exchange is increasingly efficient from right to left (Table 2): $SO_4^{2-} < Cl^- < Br^- < NO_3^- < I^- < ClO_4^- < SCN^- < Tf_2N^-$, which corresponds to a decrease in charge density (Figure 1). Ions with a lower charge density are less well hydrated and have a higher affinity for the IL phase. The efficiency of anion exchange is also dependent on the IL anion (in the opposite direction). ILs containing Tf_2N^- anions are very difficult to exchange, while chloride ILs are very easy to exchange (Table 2). This is summarized in a graphical overview (Figure 2). The anions considered in this work are derived from strong acids and are therefore fully deprotonated at neutral pH. Note, however, that for anions derived from weak acids, their speciation will be pH dependent. This has to be taken into account as it will also influence their tendency for anion exchange.

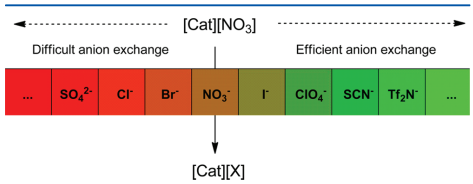

Figure 2. Prediction tool for the occurrence of anion exchange when a hydrophobic IL is contacted with a salt-containing water phase. The tendency of an IL $[Cat][X_A]$ toward anion exchange with a salt MX_B is shown. For example for an IL $[Cat][NO_3]$, the exchange will be efficient with the anions to the right, and difficult with the anions to the left of the position of NO_3^- in the series. This should be considered when designing IL synthesis routes and extraction systems.

This scheme can be used as a prediction tool for anion exchange, which is relevant both for the synthesis of ILs and the design of stable IL/water extraction systems. It is, for instance, possible to synthesize $[P_{66614}][Tf_2N]$ in one step starting from $[P_{66614}][Cl]$ and contacting it with an aqueous $LiTf_2N$ solution. The anion exchange reaction is fast and complete. On the other hand, the synthesis of $[P_{66614}][NO_3]$ starting from $[P_{66614}][Cl]$ requires three steps to obtain more than 99.9% purity.[73] For extraction experiments, this is also important when a different anion is present in the water phase and the organic or IL phase.[59,61,62,81,82] For example, Vander Hoogerstraete et al. and Onghena et al. have reported on metal extraction systems from chloride aqueous solutions using the IL $[Hbet][Tf_2N]$.[60−62] No chloride ions were detected in the IL since the exchange of Tf_2N^- by Cl^- ions does not occur (Table 2).[59] However, other extraction systems such as the extraction of metal ions from an aqueous phase with $[P_{66614}][Cl]$ must be done from chloride

DOI: 10.1021/acs.jpcb.5b02980
J. Phys. Chem. B 2015, 119, 6747−6757

solutions to avoid contamination of the IL.[78] Many more examples could be cited, but the conclusion is that due to the endless variety of ILs it is most important to understand the trends in anion exchange (Figure 2), so that an appropriate and stable extraction system can be designed for any given IL. Cation exchange is not observed since small inorganic cations do not form ILs and are always more hydrophilic than the bulky organic IL cations.

2. Water-Miscibility of Ionic Liquids: Structure Dependence. An important parameter in solvent extraction is the solubility of the organic phase in the aqueous phase. This can cause pollution of the water and loss of (valuable) organic solvent. In the case of IL/water extraction systems, this is particularly important due to their high cost. Recovery of ILs from water with physical methods such as nanofiltration or electrodialysis is still relatively cumbersome.[83−86] Therefore, it is more practical to limit the loss of IL to the aqueous phase in the first place by altering the structure of the IL or by the addition of metal salts to the aqueous phase.[69] The inherent solubility of the IL in the aqueous phase can vary a lot depending on the IL structure and the polarity of its anions and cations.[87] The long-chain tetraalkylphosphonium IL $[P_{66614}][Cl]$ for example, has a very low water solubility of 20−80 ppm (0.002−0.008 wt %), while the carboxyl-functionalized IL $[Hbet][Tf_2N]$ has a water solubility of 14 wt %.[59,80] A straightforward way to alter the water-miscibility of a certain IL, is by changing the IL cation or IL anion. The effect of the anion (X) on the water solubility is shown for the IL $[P_{8444}][X]$ (Table 3) and the effect of cation (Cat) is shown for the IL $[Cat][Tf_2N]$ (Table 4). The trends can be of interest when choosing an IL for solvent extraction.

Table 3. Solubility of the IL $[P_{8444}][X]$ in the Water Phase at 25 °C, for Increasingly Hydrophobic Anions X. A 1:1 Ratio (w/w) of IL/Water Was Used

	ionic liquid content in the water phase (wt %)[a]
$[P_{8444}][Cl]$	Homogeneous system
$[P_{8444}][Br]$	2.14
$[P_{8444}][NO_3]$	0.91
$[P_{8444}][ClO_4]$	0.04
$[P_{8444}][Tf_2N]$	<DL[b]

[a]All IL/water systems were biphasic, except for $[P_{8444}][Cl]$. $[P_{8444}][Br]$ has thermomorphic behavior with a LCST (24 °C) but is biphasic at 25 °C.[88] [b]Below detection limit using quantitative ^1H NMR.

Table 4. Solubility (25 °C) of the ILs $[Cat][Tf_2N]$ in the Water Phase for Increasingly Hydrophobic Cations (Cat) and 1:1 IL/Water Ratio (wt/wt)

	ionic liquid content in the water phase (wt %)[a]
$[Hbet][Tf_2N]$	14.0
$[Chol][Tf_2N]$	10.7
$[N_{4111}][Tf_2N]$	1.1
$[S_{222}][Tf_2N]$	0.81
$[emim][Tf_2N]$	0.72
$[mppip][Tf_2N]$	0.14
$[N_{8881}][Tf_2N]$	< DL[b]
$[P_{66614}][Tf_2N]$	< DL[b] (literature value: 0.002−0.008 wt %)[80]

[a]All IL/water systems were biphasic at 25 °C. [b]Below detection limit using quantitative ^1H NMR.

For the IL anions (Table 3), the hydrophobicity of the ILs follows the charge density series (Figure 1). Anions can alter the hydrophobicity of the IL very much: $[P_{8444}][Cl]$ is water-soluble, while $[P_{8444}][Br]$ forms a biphasic system with only around 2 wt % of IL in the aqueous phase. These large differences can be used to change the properties of known ILs by simply exchanging the IL anion (Figure 2). For cations, the differences are smaller between structurally similar aliphatic cations. However, when functional groups are incorporated in the cation (e.g., $[Hbet]^+$ or $[Chol]^+$), significantly higher solubilities are observed due to the formation of hydrogen bonds (Table 4). Water can also dissolve in the IL phase, but this is not problematic since it does not pollute the system nor cause loss of valuable reagents. Note, however, that for very hydrophobic ILs such as $[C_8mim][Tf_2N]$ or $[P_{66614}][Tf_2N]$, the solubility of water in the IL is significant, while the solubility of IL in the aqueous phase is almost negligible.[67,80]

3. Effect of Metal Salts on the Mutual Solubility if Biphasic IL/Water Systems. Instead of changing the structure of the IL to influence its water solubility, it is also possible to add metal salts to the aqueous phase. Salts can influence the solubility ILs in the aqueous phase and improve the process design and recovery of IL in solvent extraction processes.[69] It is therefore important to understand the effect that the presence of metal salts in aqueous phase can have on the solubility of ILs. The effect of metal salts has been studied for some specific ILs such as $[C_4mim][CF_3SO_3]$ and $[C_4mim][Tf_2N]$, but there is no general prediction model.[47,50−54,67,68] An intuitive model is therefore proposed here to rationalize the effect of metal salts on the solubility of any hydrophobic IL. In the liquid-precipitate model (Figure 3),

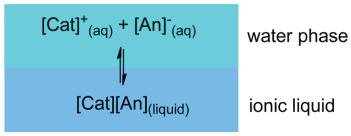

Figure 3. Schematic overview of the liquid-precipitate model described in this work. The model is based on the assumption that when a hydrophobic IL is contacted with water it behaves like a liquid-precipitate that is in equilibrium with an amount of dissolved IL in the water phase, just like salt precipitates.

biphasic IL/water systems are thought of as liquid organic salts (the IL) precipitating out of solution, while maintaining a certain equilibrium concentration in the aqueous phase, similar to the behavior of solid salt precipitates. Note that nano-aggregates of IL can exist in the aqueous phase, but this does not change the conclusions derived from this model.

As a consequence, the solubility of the hydrophobic IL is governed by the ability of the aqueous phase to solvate the IL cations and anions and counter the electrostatic attraction between the IL cations and anions. More polar IL anions and cations result in a better solvation by water molecules and therefore a higher water solubility. In the presence of salts, charge-neutralizing ion pairs can be formed between the IL ions and salt counterions.[31] Salts ions that are more effective at neutralizing the IL ion charge than water molecules, decrease the IL solubility (salting-out). Salt ions that are less effective at neutralizing the IL ions charge than water molecules, increase the IL solubility (salting-in). Therefore, the effect of salts on the

DOI: 10.1021/acs.jpcb.5b02980
J. Phys. Chem. B 2015, 119, 6747−6757

solubility of ILs follows the charge-density series (Figure 1) because a higher charge density results in stronger charge-neutralizing ion pairs.[31] This salting-out series based on the charge density (Figure 1) is valid for every IL regardless of its structure, but its best visible for hydrophobic ILs with a large water solubility (e.g., [Chol][Tf_2N] and [Hbet][Tf_2N]). The ILs were contacted with water to form biphasic systems and a range of inorganic salts was then added to the water to reveal the effect of salt cations (Figure 4) and anions (Figure 5) on

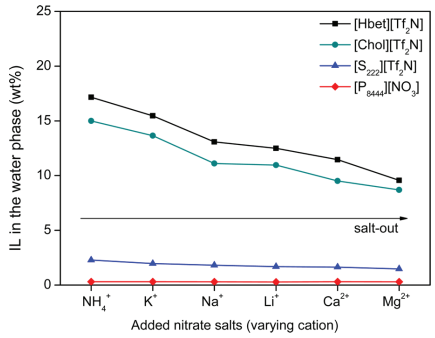

Figure 4. Influence of salt cations (added as nitrate salts, 0.5 mol.kg^{-1}) on the solubility of different ILs in the water phase (1:1 wt/wt ratio of IL/H_2O).

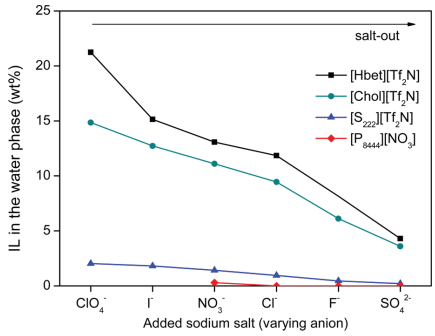

Figure 5. Influence of salt anions (added as sodium salts, 0.5 mol.kg^{-1}) on the solubility of different ILs in the water phase (1:1 ratio wt/wt of IL/H_2O). For [P_{8444}][NO_3], the anions I^- and ClO_4^- could not be tested due to anion exchange.

the solubility of these different ILs. The IL content in the water phase was determined by quantitative ^{1}H NMR. The results are in agreement with previously published results for ILs such as [C_4mim][CF_3SO_3] and [C_4mim][Tf_2N].[47,51] Note that this salting-out series for ILs (Figure 1) is different from the behavior of proteins, colloidal surfaces and polymers, where the effect of salts on the solubility is determined by the ability of adsorbed ions to increase the surface charge and improve the solubility by countering the van der Waals interactions.[5−8]

The influence of the salt concentration on the salting-in and salting-out effect was also investigated. A higher salt concentration simply reinforces the above-mentioned effects on the IL solubility, by increasing the salting-in or salting-out effects compared to pure water. This concentration effect was observed for all investigated ILs but is shown here for [Hbet][Tf_2N] (Figure 6 and 7). The reason that some data

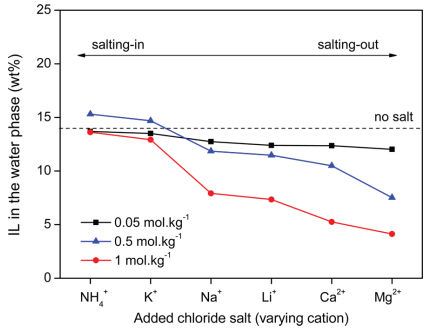

Figure 6. [Hbet][Tf_2N] content (wt %) in the water phase when adding different chloride salts and concentrations. A 1:1 wt/wt ratio of IL/H_2O was used.

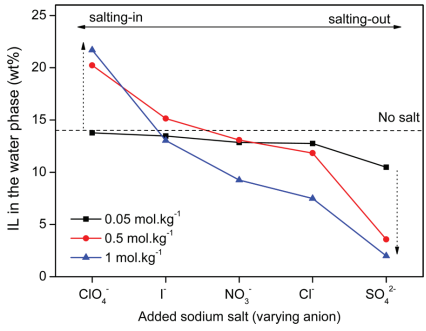

Figure 7. [Hbet][Tf_2N] content (wt %) in the water phase when adding different sodium salts and concentrations. A 1:1 wt/wt ratio of IL/H_2O was used.

points seem illogical is that the effect of the counterion has to be taken into account. For example for NH_4^+ ions (Figure 6), the salting-in effect does increase with the concentration at first, but the increasing Cl^- concentration counters this effects at high salt concentrations, due to its salting-out effect (Figure 5). The dominant salting-out effect of salts at high concentrations is a direct consequence of the above-mentioned model. At high salt concentrations the charge neutralizing effect of the salt ions on the IL ions will become more predominant, even for the ions with low charge densities, resulting in a lower IL solubility. This predominant salting-out effect at high salt concentrations was previously also observed by Freire et al.[51] Strong salting-out agents have been used previously to successfully recover spent IL from aqueous waste streams.[69,89] For example, [Hbet][Tf_2N] can be recovered efficiently by addition of Na_2SO_4 to the IL-containing aqueous phase. A concentration of 3 M Na_2SO_4 can reduce the [Hbet][Tf_2N] content in the

DOI: 10.1021/acs.jpcb.5b02980
J. Phys. Chem. B 2015, 119, 6747−6757

aqeuous phase to less than 0.15 wt %, compared to 14 wt % without salts.[59,89]

4. Effect of Mineral Acids on the Mutual Solubility of Biphasic IL/Water Systems. Extraction systems with acidic extractants require acids to strip the extracted metals. For ILs this is the case when the extracting IL is functionalized with an acidic group such as the carboxyl-functionalized [Hbet][Tf_2N] or when the IL is used as a diluent for an acidic extractant such as the [Chol][Tf_2N]/[Chol][hfac] extraction system (Figure 8).[59−62] In both cases, stripping with acids is required to

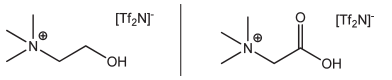

Figure 8. Structure of choline bis(trifluoromethylsulfonyl)imide [Chol][Tf_2N] (left) and betainium bis(trifluoromethylsulfonyl)imide [Hbet][Tf_2N] (right).

remove the metals from the IL phase after extraction.[59−62] The addition of concentrated mineral acids can significantly affect the solubility of the IL in the water phase, which can be an issue due to unwanted loss of IL.

The ILs were contacted with an aqueous phase containing different mineral acids to investigate the effect on the IL solubility (Figure 9). The results are compared with the effect

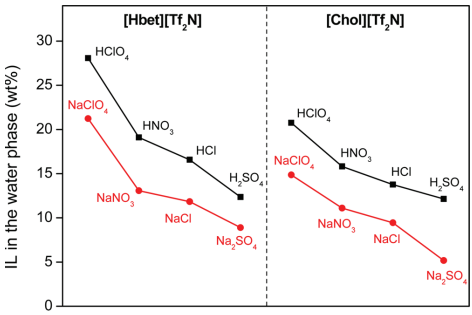

Figure 9. IL solubility (wt %) in the aqueous phase (1:1 wt/wt phase ratio) when adding mineral acids (1 N) or sodium salts (1 M). Without additives, [Hbet][Tf_2N] has a solubility of 14 wt %, and [Chol][Tf_2N] 10.7 wt %.

of equivalent sodium salts. It is clear that mineral acids follow the same salting-out trend (H_2SO_4 > HCl > HNO_3 > $HClO_4$) as their salt analogues. However, protons appear to be stronger salting-in agents than expected based on their charge density. This anomaly has been reported previously by Freire et al. for other ILs such as [C_4mim][Tf_2N] and was attributed to the basic character of the Tf_2N^- anion.[51] The fact that no significant difference was observed between the Brønsted acid functionalized [Hbet][Tf_2N] and the alcohol functionalized [Chol][Tf_2N] (Figure 9), supports that hypothesis. Although, the exact origin of the salting-in by acidic protons may not be fully understood yet, it is important to know that it exists because it influences the loss of IL during the stripping process.

5. Effect of Metal Salts and Mineral Acids on the Cloud Point Temperature of Thermomorphic IL/Water Systems. A lot of research has been done on the design of ILs with thermomorphic properties.[55,68,88,90−96] Thermomorphic systems change between a homogeneous system and a biphasic system by crossing the cloud point temperature (T_{CP}). This can be useful for biphasic extraction systems since a homogeneous phase guarantees very fast extraction equilibrium by removing the phase boundary.[60−62] This is especially true for ILs due to their high viscosity and relatively slow extraction kinetics.[60−62] Two types of thermomorphic systems can be distinguished based on the shape of the phase diagram (Figure 10): systems

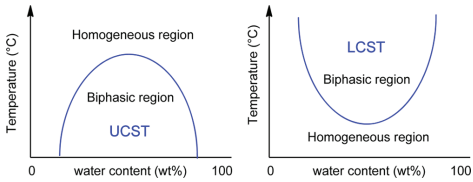

Figure 10. Schematic overview of the phase diagram of IL/water systems with a UCST and LCST.

with an upper critical solution temperature (UCST) and systems with a lower critical solution temperature (LCST). For UCST systems, the mixture is biphasic below the cloud point temperature ($T < T_{CP}$) and homogeneous above the cloud point temperature ($T > T_{CP}$), and for LCST systems the opposite is observed. The cloud point temperature and thermomorphic properties of an IL/water system can be controlled by altering the composition of the two phases (e.g., add salts) or by changing the phase ratio (Figure 10).[55]

It is well-known that for thermomorphic behavior to occur in IL/water systems, the IL must have the right balance between hydrophobic and hydrophilic character.[55,68,88,90−96] However, to the best of our knowledge, no general rules exist to predict whether the IL will have UCST or LCST behavior. Some guidelines are introduced here for the rational design of ILs with UCST or LCST behavior, based on the choice of IL anion. Thermodynamically, mixing of two components occurs when the Gibbs free energy of mixing is negative (eq 1).

$$\Delta G_{mix} = \Delta H_{mix} - T\Delta S_{mix} \quad (1)$$

For thermomorphic systems this means that UCST behavior is observed when the entropy of mixing (ΔS_{mix}) is positive and LCST behavior when ΔS_{mix} is negative. UCST behavior is more common since mixing two components is most likely to increase the entropy of the system ($\Delta S_{mix} > 0$).[68] LCST is less common than UCST but can occur when ΔS_{mix} is negative. Despite the large variety of anions and cations in ILs, some trends can be observed. Using lists of known thermomorphic IL/water systems such as the one provided by Kohno et al.,[88] we derived a general guideline for the rational design of systems with UCST or LCST behavior. It is our observation that generally ILs with weakly hydrated (low charge density) anions (e.g., Tf_2N^-, BF_4^-, I^-) show UCST behavior, while ILs with more strongly hydrated (high charge density) anions (e.g., Cl^-, Br^-, CF_3COO^-) show LCST behavior.[88] This is in agreement with the currently known thermomorphic IL/water systems.[68,88,90−95] The explanation is that ions with a higher charge density, structure a lot of water molecules around them to solvate their charge when dissolved in water. This reduces the entropy of mixing, which can become negative, resulting in LCST behavior. Low charge density ions on the other hand, do

DOI: 10.1021/acs.jpcb.5b02980
J. Phys. Chem. B 2015, 119, 6747−6757

not structure much water molecules around them which is why the entropy of mixing is generally positive (UCST behavior). Note how this is again related to the charge density (Hofmeister) series (Figure 1). A striking example is the contrast between the IL $[P_{4444}][maleate]$ (LCST) and $[P_{4444}][fumarate]$ (UCST).[91] Fumaric and maleic acid have the same molecular formula but due to their conformation, maleic acid is a hundred times more soluble in water than fumaric acid. This means the hydration of maleic acid is much stronger, which explains the LCST behavior according to the above-mentioned hypothesis. For biphasic systems consisting of ILs and apolar organic solvents, the affinity of the solvent for the IL anions is opposite to the situation for water. This results in a reversal of the above-mentioned rules, because the hydrophobic anions now have a higher affinity for the apolar solvent then hydrophilic anions. An interesting example is the fact that $[C_4mim][PF_6]$ and $[C_4mim][Tf_2N]$ have UCST behavior in polar solvents and LCST behavior in apolar solvents.[88] An overview of the above-mentioned rules for the rational design of ILs with UCST or LCST behavior is shown in Figure 11.

	weakly-hydrated IL anion (e.g. Tf_2N^-, PF_6^-, BF_4^-)	highly-hydrated IL anion (e.g. Cl^-, Br^-, CF_3COO^-)
polar solvent	UCST	LCST
apolar solvent	LCST	UCST

Figure 11. Prediction model for the rational design of ILs with UCST or LCST behavior. The UCST or LCST behavior of a biphasic IL/solvent system is determined by the charge density (hydration) of the IL anion (Figure 1).

It can be useful to tune the cloud point temperature of a thermomorphic IL/water system, so that the phase transition occurs at the desired temperature. The cloud point temperature is influenced by the IL/water ratio (Figure 10) and by the addition of metal salts.[55,96] The effect of metal salts on the cloud point temperature is different for UCST and LCST systems, but can be rationalized by linking it to the solubility of the IL in the aqueous phase. The addition of salting-in salts improves the mutual solubility of both phases and therefore favors the mixed (homogeneous) state. For UCST systems this means a decrease in the cloud point temperature while for LCST systems this means an increase in the cloud point temperature (Figure 10). Salting-out salts on the other hand, decrease the mutual solubility and therefore promote demixing of the phases which results in an increase of the cloud point temperature for UCST systems and a decrease for LCST systems.[55,97] This is shown here for the LCST system $[P_{444}E_3][DEHP]-H_2O$ and the UCST system $[Hbet][Tf_2N]-H_2O$. Both ILs are very relevant for solvent extraction.[60,98,99] These systems have a T_{CP} of 55 and 51 °C respectively, when no salts are added. This opposite effect on the cloud point temperature is clearly visible by comparing the effect of metal salts on the solubility of these two ILs in the water phase (Figure 12), with the change in cloud point temperature (Figure 13) caused by these same salts. It is evident that salt anions have a larger effect than salt cations. This is in agreement with previous observations (Figure 4 and 5) and is due to the poorer solvation of anions in water compared to cations.[100]

Finally, the impact of some mineral acids on the cloud point temperature of $[Hbet][Tf_2N]-H_2O$ is shown (Table 5). For acidic extractants such as $[Hbet][Tf_2N]$, acids are required to strip extracted metal ions back to the water phase. It is therefore useful to understand the impact of acids on the cloud

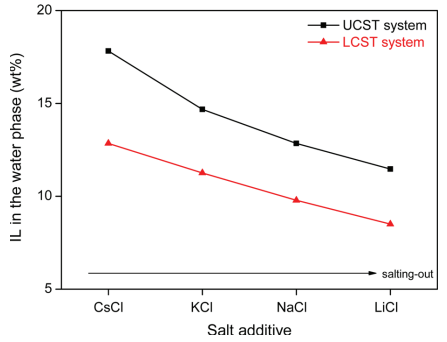

Figure 12. Effect of metal salts on the solubility of IL (wt %) in the water phase of the UCST system $[Hbet][Tf_2N]-H_2O$ (1:1 wt/wt) and the LCST system $[P_{444}E_3][DEHP]-H_2O$ (1:1 wt/wt). The salt concentration was 0.5 mol·kg^{-1} for the UCST system and 0.1 mol·kg^{-1} for the LCST system.

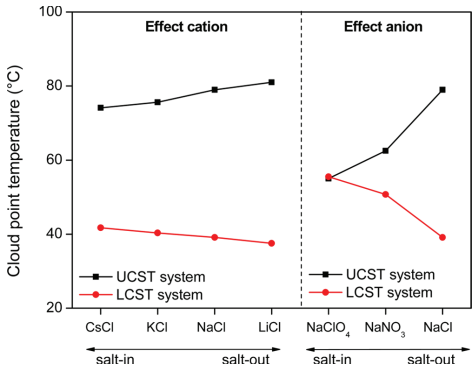

Figure 13. Effect of metal salts on the cloud point temperature of thermomorphic IL/water systems (1:1 wt/wt) with an UCST ($[Hbet][Tf_2N]-H_2O$) and an LCST ($[P_{444}E3][DEHP]-H_2O$). A salt concentration of 0.5 mol·kg^{-1} was used for the UCST system and 0.1 mol·kg^{-1} for the LCST system. Without salt, the UCST system has a cloud point of 55 °C and the LCST system of 51 °C.

Table 5. Cloud Point Temperature of a $[Hbet][Tf_2N]-H_2O$ System (1:1 wt/wt) When Adding Different Mineral Acids (1 N)

	cloud point temperature (°C)
$HClO_4$	24.2
HNO_3	49.4
No acid	55.0
HCl	67.5
H_2SO_4	66.5[a]

[a]The cloud point for H_2SO_4 (1 N) is lower than for HCl (1 N) because the concentration of sulfate ions is only half that of chloride ions.

DOI: 10.1021/acs.jpcb.5b02980
J. Phys. Chem. B 2015, 119, 6747−6757

point temperature of the system. The trend in TCP is in agreement with the effect of the various acids on the solubility of IL in the water phase (Figure 9).

6. Effect of Metal Salts on Water-Soluble ILs. So far we have discussed hydrophobic (water immiscible) ionic liquids that form biphasic IL/water systems. However, certain hydrophilic (water miscible) ILs can also form biphasic IL/water systems in the presence of large amounts of salt. These so-called Aqueous Biphasic Systems (ABS) are salt-induced biphasic systems that consist of two components (a hydrophilic IL and water) that are fully miscible in the absence of salts.[34−49] This field has grown very rapidly and is not discussed here in detail as it has been reviewed previously by Freire et al.[34] It is, however, interesting to note that the salting-out effect follows the same trend as the previously discussed IL/water systems and is often even more pronounced due to the large salt concentrations and high water solubility of the ILs used in ABS. We will restrict the discussion to a new carboxyl-functionalized ABS system with LCST behavior that was recently developed in our lab: $[P_{444}C_1COOH][Cl]$. This ionic liquid is very relevant due to its ability to extract metal ions. As mentioned before, carboxyl-functionalized ILs have been used successfully for metal ion extractions.[59−62] Note that the LCST behavior of this ABS system is also in agreement with our rational design model, which predicts LCST behavior for thermomorphic ILs with chloride anions. The large effect of salts on the cloud point temperature of this thermomorphic IL is shown in Figure 14.

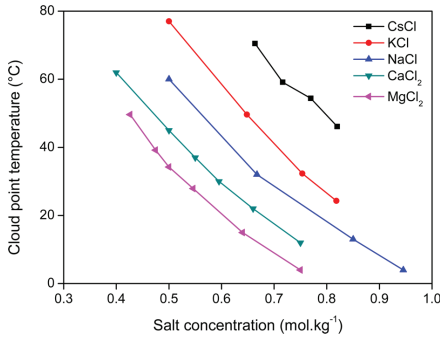

Figure 14. Effect of salt concentration on the cloud point temperature (LCST) of the aqueous biphasic system $[P_{444}C_1COOH][Cl]-H_2O$ (1:1 ratio wt/wt).

CONCLUSIONS

Biphasic IL/water systems show a lot of potential for solvent extraction. However, the presence of metal salts can affect these systems in many different ways such as (un)wanted anion exchange, changes in mutual solubility and changes in cloud point temperature in the case of thermomorphic. Due to the endless variety of ILs, it is important to find general trends instead of relying on case-by-case reports. Here, an overview is given of all the effects and intuitive guidelines and models are introduced to predict the effects of metal salts on any given IL/water system. Anion exchange was investigated and translated into guidelines for stable solvent extraction systems and synthetic strategies for ILs. The salting-in/salting-out effect of salts on the miscibility of ILs in water was also discussed and rationalized based on the charge density series (Hofmeister series). Salting-out salts can be used to recover lost IL in the aqueous phase and thus avoid pollution of the water. The effect of metal salts on the cloud point temperature of thermomorphic systems was also investigated. Thermomorphic systems with an upper critical solution temperature (UCST) are affected differently by salts than systems with a lower critical solution temperature (LCST). Finally, new insights were introduced for the rational design of thermomorphic ILs with UCST or LCST behavior. This paper is intended as a tool for the rational design of ILs and (thermomorphic) IL/water extraction systems as well as an overview of the general rules to find the most suitable salt additives. These insights will hopefully give an additional boost to this promising field of IL solvent extraction systems.

ASSOCIATED CONTENT

Supporting Information

Overview of the synthesis procedures, characterization, chemicals and equipment for the synthesized ionic liquids. Chemical structures of all ionic liquids discussed in this paper. Validation of quantitative ^1H NMR as analytical technique. The Supporting Information is available free of charge on the ACS Publications website at DOI: 10.1021/acs.jpcb.5b02980.

AUTHOR INFORMATION

Corresponding Author

*E-mail: Koen.Binnemans@chem.kuleuven.be.

Notes

The authors declare no competing financial interest.

ACKNOWLEDGMENTS

The authors wish to thank the KU Leuven (projects GOA/13/008 and IOF-KP RARE^3), the FWO Flanders (Ph.D. fellowship to David Dupont) and the IWT Flanders (Ph.D. fellowship to Daphne Depuydt) for financial support. The authors would like to thank Karel Duerinckx for NMR analysis.

REFERENCES

(1) Hofmeister, F. Zur Lehre von der Wirkung der Salze. *Arch. Exp. Pathol. Pharmacol.* **1888**, *24*, 247−260.
(2) Baldwin, R. L. How Hofmeister Ion Interactions Affect Protein Stability. *Biophys. J.* **1996**, *71*, 2056−2063.
(3) Carbonnaux, C.; Ries-Kautt, M.; Ducruix, A. Relative Effectiveness of Various Anions on the Solubility of Acidic Hypoderma Lineatum Collagenase at pH 7.2. *Protein Sci.* **1995**, *4*, 2123−2128.
(4) Salis, A.; Cugia, F.; Parsons, D. F.; Ninham, B. W.; Monduzzi, M. Hofmeister Series Reversal for Lysozyme by Change in pH and Salt Concentration: Insights from Electrophoretic Mobility Measurements. *Phys. Chem. Chem. Phys.* **2012**, *14*, 4343−4346.
(5) Schwierz, N.; Horinek, D.; Netz, R. R. Reversed Anionic Hofmeister Series: The Interplay of Surface Charge and Surface Polarity. *Langmuir* **2010**, *26*, 7370−7379.
(6) Schwierz, N.; Horinek, D.; Netz, R. R. Anionic and Cationic Hofmeister Effects on Hydrophobic and Hydrophilic Surfaces. *Langmuir* **2013**, *29*, 2602−2614.
(7) Zhang, Y.; Cremer, P. S. Interactions Between Macromolecules and Ions: The Hofmeister Series. *Curr. Opin. Chem. Biol.* **2006**, *10*, 658−663.
(8) Zhang, Y.; Cremer, P. S. The Inverse and Direct Hofmeister Series for Lysozyme. *Proc. Natl. Acad. Sci. U. S. A.* **2009**, *106*, 15249−15253.
(9) Lo Nostro, P.; Ninham, B. W. Hofmeister Phenomena: An Update on Ion Specificity in Biology. *Chem. Rev.* **2012**, *112*, 2286−2322.

DOI: 10.1021/acs.jpcb.5b02980
J. Phys. Chem. B 2015, 119, 6747−6757

(10) Pegram, L. M.; Record, M. T. Thermodynamic Origin of Hofmeister Ion Effects. *J. Phys. Chem. B* **2008**, *112*, 9428−9436.
(11) Kim, H.; Lee, H.; Lee, G.; Kim, H.; Cho, M. Hofmeister Anionic Effects on Hydration Electric Fields Around Water and Peptide. *J. Chem. Phys.* **2012**, *136*, 124501.
(12) Schwartz, C. P.; Uejio, J. S.; Duffin, A. M.; England, A. H.; Kelly, D. N.; Prendergast, D.; Saykally, R. J. Investigation of Protein Conformation and Interactions with Salts via X-ray Absorption Spectroscopy. *Proc. Natl. Acad. Sci. U. S. A.* **2010**, *107*, 14008−14013.
(13) Prevysh, V. A.; Wang, B. C.; Spontak, R. J. Effect of Added Salt on the Stability of Hydrogen-Bonded Interpolymer Complexes. *Colloid Polym. Sci.* **1996**, *274*, 532−539.
(14) Tomé, L. I. N.; Pinho, S. P.; Jorge, M.; Gomes, J. R. B.; Coutinho, J. A. P. Salting-in with a Salting-out Agent: Explaining the Cation Specific Effects on the Aqueous Solubility of Amino Acids. *J. Phys. Chem. B* **2013**, *117*, 6116−6128.
(15) Thormann, E. On Understanding of the Hofmeister Effect: How Addition of Salt Alters the Stability of Temperature Responsive Polymers in Aqueous Solutions. *RSC Adv.* **2012**, *2*, 8297−8305.
(16) Wang, J.; Satoh, M. Novel PVA-Based Polymers Showing an Anti-Hofmeister Series Property. *Polymer* **2009**, *50*, 3680−3685.
(17) Guo, Y.; Li, S.; Li, W.; Moosa, B.; Khashab, N. M. The Hofmeister Effect on Nanodiamonds: How Addition of Ions Provides Superior Drug Loading Platforms. *Biomater. Sci.* **2014**, *2*, 84−88.
(18) Bae, S.; Son, H.; Kim, Y.-G.; Hohng, S. Z-DNA Stabilization is Dominated by the Hofmeister Effect. *Phys. Chem. Chem. Phys.* **2013**, *15*, 15829−15832.
(19) Blachechen, L.; Silva, J.; Barbosa, L. S.; Itri, R.; Petri, D. S. Hofmeister Effects on the Colloidal Stability of Poly(ethylene glycol)-Decorated Nanoparticles. *Colloid Polym. Sci.* **2012**, *290*, 1537−1546.
(20) Zhang, F.; Skoda, M. W. A.; Jacobs, R. M. J.; Dressen, D. G.; Martin, R. A.; Martin, C. M.; Clark, G. F.; Lamkemeyer, T.; Schreiber, F. Gold Nanoparticles Decorated with Oligo(ethylene glycol) Thiols: Enhanced Hofmeister Effects in Colloid−Protein Mixtures. *J. Phys. Chem. C* **2009**, *113*, 4839−4847.
(21) López-León, T.; Santander-Ortega, M. J.; Ortega-Vinuesa, J. L.; Bastos-González, D. Hofmeister Effects in Colloidal Systems: Influence of the Surface Nature. *J. Phys. Chem. C* **2008**, *112*, 16060−16069.
(22) Salis, A.; Ninham, B. W. Models and Mechanisms of Hofmeister Effects in Electrolyte Solutions, and Colloid and Protein Systems Revisited. *Chem. Soc. Rev.* **2014**, *43*, 7358−7377.
(23) Wilson, E. K. Hofmeister Still Mystifies. *Chem. Eng. News* **2012**, *90*, 42−43.
(24) Kunz, W.; Henle, J.; Ninham, B. W. 'Zur Lehre von der Wirkung der Salze' (About the Science of the Effect of Salts): Franz Hofmeister's Historical Papers. *Curr. Opin. Colloid Interface Sci.* **2004**, *9*, 19−37.
(25) Jungwirth, P.; Cremer, P. S. Beyond Hofmeister. *Nat. Chem.* **2014**, *6*, 261−263.
(26) Leberman, R.; Soper, A. K. Effect of High Salt Concentrations on Water Structure. *Nature* **1995**, *378*, 364−366.
(27) Collins, K. D.; Washabaugh, M. W. The Hofmeister Effect and the Behaviour of Water at Interfaces. *Q. Rev. Biophys.* **1985**, *18*, 323−422.
(28) Cacace, M. G.; Landau, E. M.; Ramsden, J. J. The Hofmeister Series: Salt and Solvent Effects on Interfacial Phenomena. *Q. Rev. Biophys.* **1997**, *30*, 241−277.
(29) Kunz, W.; Lo Nostro, P.; Ninham, B. W. The Present State of Affairs with Hofmeister Effects. *Curr. Opin. Colloid Interface Sci.* **2004**, *9*, 1−18.
(30) Gurau, M. C.; Lim, S.-M.; Castellana, E. T.; Albertorio, F.; Kataoka, S.; Cremer, P. S. On the Mechanism of the Hofmeister Effect. *J. Am. Chem. Soc.* **2004**, *126*, 10522−10523.
(31) Lyklema, J. Simple Hofmeister series. *Chem. Phys. Lett.* **2009**, *467*, 217−222.
(32) Nucci, N. V.; Vanderkooi, J. M. Effects of Salts of the Hofmeister Series on the Hydrogen Bond Network of Water. *J. Mol. Liq.* **2008**, *143*, 160−170.
(33) Galamba, N. Mapping Structural Perturbations of Water in Ionic Solutions. *J. Phys. Chem. B* **2012**, *116*, 5242−5250.
(34) Freire, M. G.; Claudio, A. F. M.; Araujo, J. M. M.; Coutinho, J. A. P.; Marrucho, I. M.; Lopes, J. N. C.; Rebelo, L. P. N. Aqueous Biphasic Systems: A Boost Brought About by Using Ionic Liquids. *Chem. Soc. Rev.* **2012**, *41*, 4966−4995.
(35) Bridges, N. J.; Rogers, R. D. Can Kosmotropic Salt/Chaotropic Ionic Liquid (Salt/Salt Aqueous Biphasic Systems) be Used to Remove Pertechnetate From Complex Salt Waste? *Sep. Sci. Technol.* **2008**, *43*, 1083−1090.
(36) Pereira, J. F. B.; Rebelo, L. P. N.; Rogers, R. D.; Coutinho, J. A. P.; Freire, M. G. Combining Ionic Liquids and Polyethylene Glycols to Boost the Hydrophobic−Hydrophilic Range of Aqueous Biphasic Systems. *Phys. Chem. Chem. Phys.* **2013**, *15*, 19580−19583.
(37) Gutowski, K. E.; Broker, G. A.; Willauer, H. D.; Huddleston, J. G.; Swatloski, R. P.; Holbrey, J. D.; Rogers, R. D. Controlling the Aqueous Miscibility of Ionic Liquids: Aqueous Biphasic Systems of Water-Miscible Ionic Liquids and Water-Structuring Salts for Recycle, Metathesis, and Separations. *J. Am. Chem. Soc.* **2003**, *125*, 6632−6633.
(38) Ventura, S. P. M.; Neves, C. M. S. S.; Freire, M. G.; Marrucho, I. M.; Oliveira, J.; Coutinho, J. A. P. Evaluation of Anion Influence on the Formation and Extraction Capacity of Ionic-Liquid-Based Aqueous Biphasic Systems. *J. Phys. Chem. B* **2009**, *113*, 9304−9310.
(39) Neves, C. M. S. S.; Ventura, S. P. M.; Freire, M. G.; Marrucho, I. M.; Coutinho, J. A. P. Evaluation of Cation Influence on the Formation and Extraction Capability of Ionic-Liquid-Based Aqueous Biphasic Systems. *J. Phys. Chem. B* **2009**, *113*, 5194−5199.
(40) Tomé, L. I. N.; Pereira, J. F. B.; Rogers, R. D.; Freire, M. G.; Gomes, J. R. B.; Coutinho, J. A. P. Evidence for the Interactions Occurring Between Ionic Liquids and Tetraethylene Glycol in Binary Mixtures and Aqueous Biphasic Systems. *J. Phys. Chem. B* **2014**, *118*, 4615−4629.
(41) Freire, M. G.; Pereira, J. F. B.; Francisco, M.; Rodríguez, H.; Rebelo, L. P. N.; Rogers, R. D.; Coutinho, J. A. P. Insight into the Interactions That Control the Phase Behaviour of New Aqueous Biphasic Systems Composed of Polyethylene Glycol Polymers and Ionic Liquids. *Chem.—Eur. J.* **2012**, *18*, 1831−1839.
(42) Bridges, N. J.; Gutowski, K. E.; Rogers, R. D. Investigation of Aqueous Biphasic Systems Formed from Solutions of Chaotropic Salts with Kosmotropic Salts (Salt−Salt ABS). *Green Chem.* **2007**, *9*, 177−183.
(43) Ventura, S. P. M.; Sousa, S. G.; Serafim, L. S.; Lima, Á. S.; Freire, M. G.; Coutinho, J. A. P. Ionic Liquid Based Aqueous Biphasic Systems with Controlled pH: The Ionic Liquid Cation Effect. *J. Chem. Eng. Data* **2011**, *56*, 4253−4260.
(44) Pereira, J. F. B.; Lima, A. S.; Freire, M. G.; Coutinho, J. A. P. Ionic Liquids as Adjuvants for the Tailored Extraction of Biomolecules in Aqueous Biphasic Systems. *Green Chem.* **2010**, *12*, 1661−1669.
(45) Pei, Y.; Wang, J.; Liu, L.; Wu, K.; Zhao, Y. Liquid−Liquid Equilibria of Aqueous Biphasic Systems Containing Selected Imidazolium Ionic Liquids and Salts. *J. Chem. Eng. Data* **2007**, *52*, 2026−2031.
(46) Freire, M. G.; Teles, A. R. R.; Canongia Lopes, J. N.; Rebelo, L. P. N.; Marrucho, I. M.; Coutinho, J. A. P. Partition Coefficients of Alkaloids in Biphasic Ionic-Liquid-Aqueous Systems and their Dependence on the Hofmeister Series. *Sep. Sci. Technol.* **2011**, *47*, 284−291.
(47) Shahriari, S.; Neves, C. M. S. S.; Freire, M. G.; Coutinho, J. A. P. Role of the Hofmeister Series in the Formation of Ionic-Liquid-Based Aqueous Biphasic Systems. *J. Phys. Chem. B* **2012**, *116*, 7252−7258.
(48) Najdanovic-Visak, V.; Lopes, J.; Visak, Z.; Trindade, J.; Rebelo, L. Salting-out in Aqueous Solutions of Ionic Liquids and K_3PO_4: Aqueous Biphasic Systems and Salt Precipitation. *Int. J. Mol. Sci.* **2007**, *8*, 736−748.
(49) Abraham, M. H.; Zissimos, A. M.; Huddleston, J. G.; Willauer, H. D.; Rogers, R. D.; Acree, W. E. Some Novel Liquid Partitioning Systems: Water−Ionic Liquids and Aqueous Biphasic Systems. *Ind. Eng. Chem. Res.* **2003**, *42*, 413−418.

DOI: 10.1021/acs.jpcb.5b02980
J. Phys. Chem. B 2015, 119, 6747−6757

(50) Peng, X.-M.; Hu, Y.-F.; Jin, C.-W. Solubilities of Imidazolium-Based Ionic Liquids in Aqueous Salt Solutions at 298.15 K. *J. Chem. Thermodyn.* **2011**, *43*, 1174−1177.
(51) Freire, M. G.; Carvalho, P. J.; Silva, A. M. S.; Santos, L. M. N. B. F.; Rebelo, L. P. N.; Marrucho, I. M.; Coutinho, J. A. P. Ion Specific Effects on the Mutual Solubilities of Water and Hydrophobic Ionic Liquids. *J. Phys. Chem. B* **2009**, *113*, 202−211.
(52) Freire, M. G.; Neves, C. M. S. S.; Carvalho, P. J.; Gardas, R. L.; Fernandes, A. M.; Marrucho, I. M.; Santos, L. M. N. B. F.; Coutinho, J. A. P. Mutual Solubilities of Water and Hydrophobic Ionic Liquids. *J. Phys. Chem. B* **2007**, *111*, 13082−13089.
(53) Tomé, L. I. N.; Varanda, F. R.; Freire, M. G.; Marrucho, I. M.; Coutinho, J. A. P. Towards an Understanding of the Mutual Solubilities of Water and Hydrophobic Ionic Liquids in the Presence of Salts: The Anion Effect. *J. Phys. Chem. B* **2009**, *113*, 2815−2825.
(54) Freire, M. G.; Santos, L. M. N. B. F.; Fernandes, A. M.; Coutinho, J. A. P.; Marrucho, I. M. An Overview of the Mutual Solubilities of Water−Imidazolium-Based Ionic Liquids Systems. *Fluid Phase Equilib.* **2007**, *261*, 449−454.
(55) Trindade, J. R.; Visak, Z. P.; Blesic, M.; Marrucho, I. M.; Coutinho, J. A. P.; Canongia Lopes, J. N.; Rebelo, L. P. N. Salting-Out Effects in Aqueous Ionic Liquid Solutions: Cloud-Point Temperature Shifts. *J. Phys. Chem. B* **2007**, *111*, 4737−4741.
(56) Sadeghi, R.; Mostafa, B.; Parsi, E.; Shahebrahimi, Y. Toward an Understanding of the Salting-Out Effects in Aqueous Ionic Liquid Solutions: Vapor−Liquid Equilibria, Liquid−Liquid Equilibria, Volumetric, Compressibility, and Conductivity Behavior. *J. Phys. Chem. B* **2010**, *114*, 16528−16541.
(57) Zhao, D. Design, Synthesis and Applications of Functionalized Ionic Liquids. PhD Thesis, EPFL, Lausanne, Switersland, 2007.
(58) Plechkova, N. V.; Seddon, K. R. Applications of Ionic Liquids in the Chemical Industry. *Chem. Soc. Rev.* **2008**, *37*, 123−150.
(59) Onghena, B.; Binnemans, K. Recovery of Scandium(III) from Aqueous Solutions by Solvent Extraction with the Functionalized Ionic Liquid Betainium Bis(trifluoromethylsulfonyl)imide. *Ind. Eng. Chem. Res.* **2015**, *54*, 1887−1898.
(60) Onghena, B.; Jacobs, J.; Van Meervelt, L.; Binnemans, K. Homogeneous Liquid-Liquid Extraction of Neodymium(III) by Choline Hexafluoroacetylacetonate in the Ionic Liquid Choline Bis(trifluoromethylsulfonyl)imide. *Dalton Trans.* **2014**, *43*, 11566−11578.
(61) Vander Hoogerstraete, T.; Onghena, B.; Binnemans, K. Homogeneous Liquid−Liquid Extraction of Metal Ions with a Functionalized Ionic Liquid. *J. Phys. Chem. Lett.* **2013**, *4*, 1659−1663.
(62) Vander Hoogerstraete, T.; Onghena, B.; Binnemans, K. Homogeneous Liquid−Liquid Extraction of Rare Earths with the Betaine—Betainium Bis(trifluoromethylsulfonyl)imide Ionic Liquid System. *Int. J. Mol. Sci.* **2013**, *14*, 21353−21377.
(63) Sasaki, K.; Takao, K.; Suzuki, T.; Mori, T.; Arai, T.; Ikeda, Y. Extraction of Pd(II), Rh(III) and Ru(III) from HNO_3 Aqueous Solution to Betainium Bis(trifluoromethanesulfonyl)imide Ionic Liquid. *Dalton Trans.* **2014**, *43*, 5648−5651.
(64) Sasaki, K.; Suzuki, T.; Mori, T.; Arai, T.; Takao, K.; Ikeda, Y. Selective Liquid-Liquid Extraction of Uranyl Species Using Task-specific Ionic Liquid, Betainium Bis(trifluoromethylsulfonyl)imide. *Chem. Lett.* **2014**, *43*, 775−777.
(65) Lo, T. C.; Baird, M. H. I.; Hanson, C. *Handbook of Solvent Extraction*. Wiley-Interscience: New York, 1983.
(66) Ganguly, P.; Hajari, T.; van der Vegt, N. F. A. Molecular Simulation Study on Hofmeister Cations and the Aqueous Solubility of Benzene. *J. Phys. Chem. B* **2014**, *118*, 5331−5339.
(67) Freire, M. G.; Carvalho, P. J.; Gardas, R. L.; Marrucho, I. M.; Santos, L. M. N. B. F.; Coutinho, J. A. P. Mutual Solubilities of Water and the $[C_nmim][Tf_2N]$ Hydrophobic Ionic Liquids. *J. Phys. Chem. B* **2008**, *112*, 1604−1610.
(68) Kohno, Y.; Ohno, H. Ionic Liquid/Water Mixtures: From Hostility to Conciliation. *Chem. Commun.* **2012**, *48*, 7119−7130.
(69) Neves, C. M. S. S.; Freire, M. G.; Coutinho, J. A. P. Improved Recovery of Ionic Liquids from Contaminated Aqueous Streams Using Aluminium-Based Salts. *RSC Adv.* **2012**, *2*, 10882−10890.
(70) Li, Z.; Pei, Y.; Wang, H.; Fan, J.; Wang, J. Ionic Liquid-Based Aqueous Two-Phase Systems and Their Applications in Green Separation Processes. *Trends Anal. Chem.* **2010**, *29*, 1336−1346.
(71) Pei, Y.; Wang, J.; Wu, K.; Xuan, X.; Lu, X. Ionic Liquid-Based Aqueous Two-Phase Extraction of Selected Proteins. *Sep. Purif. Technol.* **2009**, *64*, 288−295.
(72) Rogers, R. D.; Seddon, K. R. Ionic Liquids—Solvents of the Future? *Science* **2003**, *302*, 792−793.
(73) Vander Hoogerstraete, T.; Binnemans, K. Highly Efficient Separation of Rare Earths from Nickel and Cobalt by Solvent Extraction with the Ionic Liquid Trihexyl(tetradecyl)phosphonium Nitrate: A Process Relevant to the Recycling of Rare Earths from Permanent Magnets and Nickel Metal Hydride Batteries. *Green Chem.* **2014**, *16*, 1594−1606.
(74) Visser, A. E.; Swatloski, R. P.; Reichert, W. M.; Mayton, R.; Sheff, S.; Wierzbicki, A.; Davis, J. J. H.; Rogers, R. D. Task-Specific Ionic Liquids for the Extraction of Metal Ions from Aqueous Solutions. *Chem. Commun.* **2001**, 135−136.
(75) Wellens, S.; Goovaerts, R.; Möller, C.; Luyten, J.; Thijs, B.; Binnemans, K. A Continuous Ionic Liquid Extraction Process for the Separation of Cobalt from Nickel. *Green Chem.* **2013**, *15*, 3160−3164.
(76) Wellens, S.; Thijs, B.; Möller, C.; Binnemans, K. Separation of Cobalt and Nickel by Solvent Extraction with Two Mutually Immiscible Ionic Liquids. *Phys. Chem. Chem. Phys.* **2013**, *15*, 9663−9669.
(77) Zhang, Q.; Zhang, S.; Deng, Y. Recent Advances in Ionic Liquid Catalysis. *Green Chem.* **2011**, *13*, 2619−2637.
(78) Vander Hoogerstraete, T.; Wellens, S.; Verachtert, K.; Binnemans, K. Removal of Transition Metals from Rare Earths by Solvent Extraction with an Undiluted Phosphonium Ionic Liquid: Separations Relevant to Rare-Earth Magnet Recycling. *Green Chem.* **2013**, *15*, 919−927.
(79) Wellens, S.; Thijs, B.; Binnemans, K. An Environmentally Friendlier Approach to Hydrometallurgy: Highly Selective Separation of Cobalt from Nickel by Solvent Extraction with Undiluted Phosphonium Ionic Liquids. *Green Chem.* **2012**, *14*, 1657−1665.
(80) Wellens, S.; Vander Hoogerstraete, T.; Möller, C.; Thijs, B.; Luyten, J.; Binnemans, K. Dissolution of Metal Oxides in an Acid-Saturated Ionic Liquid Solution and Investigation of the Back-Extraction Behaviour to the Aqueous Phase. *Hydrometallurgy* **2014**, *144*−*145*, 27−33.
(81) Fowler, C. J.; Haverlock, T. J.; Moyer, B. A.; Shriver, J. A.; Gross, D. E.; Marquez, M.; Sessler, J. L.; Hossain, M. A.; Bowman-James, K. Enhanced Anion Exchange for Selective Sulfate Extraction: Overcoming the Hofmeister Bias. *J. Am. Chem. Soc.* **2008**, *130*, 14386−14387.
(82) Patil, S. K.; Sharma, H. D. Ion Exchange and Solvent Extraction Equilibria in Mixed Electrolytes. *Can. J. Chem.* **1969**, *47*, 3851−3858.
(83) Bai, L.; Wang, X.; Nie, Y.; Dong, H.; Zhang, X.; Zhang, S. Study on the Recovery of Ionic Liquids from Dilute Effluent by Electrodialysis Method and the Fouling of Cation-Exchange Membrane. *Sci. China: Chem.* **2013**, *56*, 1811−1816.
(84) Abels, C.; Redepenning, C.; Moll, A.; Melin, T.; Wessling, M. Simple Purification of Ionic Liquid Solvents by Nanofiltration in Biorefining of Lignocellulosic Substrates. *J. Membr. Sci.* **2012**, *405*−*406*, 1−10.
(85) Fernández, J. F.; Waterkamp, D.; Thöming, J. Recovery of Ionic Liquids from Wastewater: Aggregation Control for Intensified Membrane Filtration. *Desalination* **2008**, *224*, 52−56.
(86) Lemus, J.; Palomar, J.; Heras, F.; Gilarranz, M. A.; Rodriguez, J. J. Developing Criteria for the Recovery of Ionic Liquids from Aqueous Phase by Adsorption with Activated Carbon. *Sep. Purif. Technol.* **2012**, *97*, 11−19.
(87) Chiappe, C.; Pomelli, C. S.; Rajamani, S. Influence of Structural Variations in Cationic and Anionic Moieties on the Polarity of Ionic Liquids. *J. Phys. Chem. B* **2011**, *115*, 9653−9661.

DOI: 10.1021/acs.jpcb.5b02980
J. Phys. Chem. B 2015, 119, 6747−6757

(88) Kohno, Y.; Saita, S.; Men, Y.; Yuan, J.; Ohno, H. Thermoresponsive Polyelectrolytes Derived from Ionic Liquids. *Polym. Chem.* **2015**, *6*, 2163−2178.
(89) Dupont, D.; Binnemans, K. Rare-Earth Recycling Using a Functionalized Ionic Liquid for the Selective Dissolution and Revalorization of Y_2O_3:Eu^{3+} from Lamp Phosphor Waste. *Green Chem.* **2015**, *17*, 856−868.
(90) Annat, G.; Forsyth, M.; MacFarlane, D. R. Ionic Liquid Mixtures—Variations in Physical Properties and Their Origins in Molecular Structure. *J. Phys. Chem. B* **2012**, *116*, 8251−8258.
(91) Fukaya, Y.; Sekikawa, K.; Murata, K.; Nakamura, N.; Ohno, H. Miscibility and Phase Behavior of Water-Dicarboxylic Acid Type Ionic Liquid Mixed Systems. *Chem. Commun.* **2007**, *29*, 3089−3091.
(92) Fukumoto, K.; Ohno, H. LCST-Type Phase Changes of a Mixture of Water and Ionic Liquids Derived from Amino Acids. *Angew. Chem., Int. Ed.* **2007**, *46*, 1852−1855.
(93) Kohno, Y.; Arai, H.; Saita, S.; Ohno, H. Material Design of Ionic Liquids to Show Temperature-Sensitive LCST-type Phase Transition after Mixing with Water. *Aust. J. Chem.* **2011**, *64*, 1560−1567.
(94) Kohno, Y.; Ohno, H. Temperature-Responsive Ionic Liquid/Water Interfaces: Relation Between Hydrophilicity of Ions and Dynamic Phase Change. *Phys. Chem. Chem. Phys.* **2012**, *14*, 5063−5070.
(95) Saita, S.; Mieno, Y.; Kohno, Y.; Ohno, H. Ammonium Based Zwitterions Showing Both LCST- and UCST-type Phase Transitions After Mixing with Water in a Very Narrow Temperature Range. *Chem. Commun.* **2014**, *50*, 15450−15452.
(96) Visak, Z. P.; Canongia Lopes, J. N.; Rebelo, L. P. N. Ionic Liquids in Polyethylene Glycol Aqueous Solutions: Salting-in and Salting-out Effects. *Monatsh. Chem.* **2007**, *138*, 1153−1157.
(97) Il'in, K. K.; Cherkasov, D. G. Phase Equilibria and Salting-out Effects in a Cesium Nitrate-Triethylamine-Water System at 5−25 °C. *Russ. J. Phys. Chem. A* **2013**, *87*, 598−602.
(98) Nockemann, P.; Thijs, B.; Parac-Vogt, T. N.; Van Hecke, K.; Van Meervelt, L.; Tinant, B.; Hartenbach, I.; Schleid, T.; Ngan, V. T.; Nguyen, M. T.; Binnemans, K. Carboxyl-Functionalized Task-Specific Ionic Liquids for Solubilizing Metal Oxides. *Inorg. Chem.* **2008**, *47*, 9987−9999.
(99) Fagnant, D. P.; Goff, G. S.; Scott, B. L.; Runde, W.; Brennecke, J. F. Switchable Phase Behavior of [HBet][Tf_2N]−H_2O upon Neodymium Loading: Implications for Lanthanide Separations. *Inorg. Chem.* **2013**, *52*, 549−551.
(100) Yang, Z. Hofmeister Effects: An Explanation for the Impact of Ionic Liquids on Biocatalysis. *J. Biotechnol.* **2009**, *144*, 12−22.

DOI: 10.1021/acs.jpcb.5b02980
J. Phys. Chem. B 2015, 119, 6747−6757

Paper 8: Functionalized magnetic nanoparticles to retrieve REEs

Title:

Selective Uptake of Rare Earths from Aqueous Solutions by EDTA-functionalized Magnetic and Non-magnetic Nanoparticles

Type: Full paper
Journal: ACS Applied Materials & Interfaces (IF 6.72)
Publisher: American Chemical Society (ACS)
Publication date: 18/03/2014

Electronic Supplementary Information (ESI) available: http://pubs.acs.org.

Graphical abstract

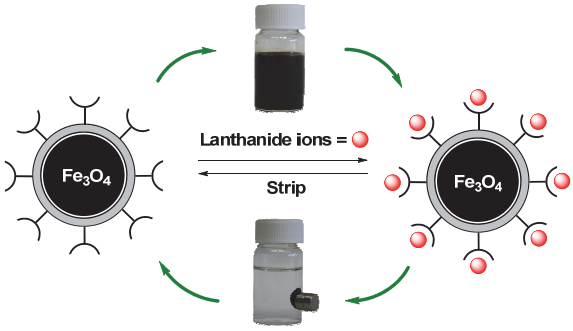

Nanoparticles functionalized with TMS-EDTA were used for the adsorption and separation of rare-earth ions from aqueous solutions. The separation of pairs of rare-earth ions was found to be dependent on the density of EDTA groups on the surface of the nanoparticles.

ACS APPLIED MATERIALS & INTERFACES

Research Article

www.acsami.org

Selective Uptake of Rare Earths from Aqueous Solutions by EDTA-Functionalized Magnetic and Nonmagnetic Nanoparticles

David Dupont,[†] Ward Brullot,[‡] Maarten Bloemen,[‡] Thierry Verbiest,[‡] and Koen Binnemans*[,†]

[†]Molecular Design and Synthesis, Department of Chemistry, KU Leuven, Celestijnenlaan 200F, P.O. Box 2404, B-3001 Heverlee, Belgium

[‡]Molecular Imaging and Photonics, Department of Chemistry, KU Leuven, Celestijnenlaan 200D, P.O. Box 2425, B-3001 Heverlee, Belgium

Supporting Information

ABSTRACT: Magnetic (Fe_3O_4) and nonmagnetic (SiO_2 and TiO_2) nanoparticles were decorated on their surface with *N*-[(3-trimethoxysilyl)propyl]ethylenediamine triacetic acid (TMS-EDTA). The aim was to investigate the influence of the substrate on the behavior of these immobilized metal coordinating groups. The nanoparticles functionalized with TMS-EDTA were used for the adsorption and separation of trivalent rare-earth ions from aqueous solutions. The general adsorption capacity of the nanoparticles was very high (100 to 400 mg/g) due to their large surface area. The heavy rare-earth ions are known to have a higher affinity for the coordinating groups than the light rare-earth ions but an additional difference in selectivity was observed between the different nanoparticles. The separation of pairs of rare-earth ions was found to be dependent on the substrate, namely the density of EDTA groups on the surface. The observation that sterical hindrance (or crowding) of immobilized ligands influences the selectivity could provide a new tool for the fine-tuning of the coordination ability of traditional chelating ligands.

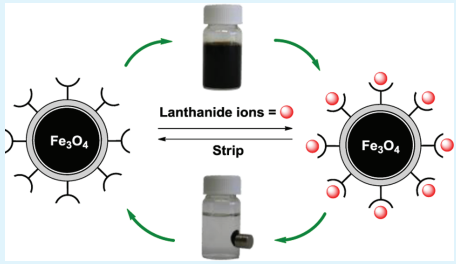

KEYWORDS: *EDTA, lanthanides, magnetic nanoparticles, magnetite, metal recovery, rare earths*

1. INTRODUCTION

Magnetic nanoparticles are very popular advanced materials.[1,2] The possibility to guide these particles magnetically to recover them from solution by a magnet and to functionalize their surface with a large variety of functional groups has led to their application in biomedicine, homogeneous catalysis, wastewater processing and many other technological fields.[3−14] Biomedical applications include targeted drug delivery, biosensors and dual imaging by lanthanide ions attached to magnetic nanoparticles.[3−5] Functionalized magnetic nanoparticles are also excellent candidates for the selective extraction of metal traces from wastewater streams or industrial effluents.[6−15] These sophisticated adsorbents can act toward metal ions as a kind of "nanosponges" and they can easily be retrieved from solution with a magnet (Figure 1). After the adsorbed ions are stripped, the nanoparticles can be reused, making this a promising sustainable and green technology. The recovery of heavy metals and precious metals with functionalized nanoparticles has been studied extensively,[6−14] but the recovery of rare earths by nanoparticles has received far less attention.[16] Core−shell nanoparticles with magnetic (Fe_3O_4) cores and SiO_2 or TiO_2 shells are also excellent candidates for this type of applications.[8,9,15,17] These SiO_2 or TiO_2 shells can be functionalized with metal coordinating groups and they would greatly benefit from a better insight into the influence of the substrate on the behavior of the metal coordinating groups on their surface. This paper reports on the differences in adsorption and separation of lanthanide ions by *N*-[(3-trimethoxysilyl)propyl]ethylenediamine triacetic acid (TMS-EDTA) attached to Fe_3O_4, SiO_2 or TiO_2 surfaces.

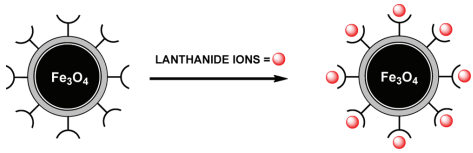

Figure 1. Schematic representation of the capture of lanthanide ions by functionalized magnetic nanoparticles.

Silane chemistry is a powerful tool to anchor functional groups on the surface of nanoparticles.[18−22] The large number of commercially available trialkoxysilanes with functional groups offers unique possibilities for the surface-modification of oxide nanoparticles.[15,18−22] The silane groups form strong

Received: December 29, 2013
Accepted: March 17, 2014
Published: March 18, 2014

covalent bonds with the hydroxyl groups on the surface of oxide nanoparticles and increase their stability in solution.[21] TMS-EDTA allows functionalization of oxide nanoparticles with EDTA functional groups for coordination of metal ions. The covalently bonded TMS-EDTA yields nanoparticles with a much better long-term stability and resistance to acidic conditions than nanoparticles where EDTA is directly bonded to the surface by weak electrostatic interactions.[7,10] Although the selectivity of traditional complexing agents such as EDTA and DTPA toward different metal ions is well understood in aqueous solutions, this is not the case for the behavior of their analogues attached to a surface. The density of immobilized coordination groups on a surface can be high and the steric hindrance (crowding) can alter the selectivity of the coordination groups, which creates new opportunities for the fine-tuning of the ligand selectivity. This possibility of fine-tuning of the ligand selectivity is of importance for the difficult separation of rare-earth ions. Most extractants (e.g., tributyl phosphate (TBP) and di-(2-ethylhexyl)phosphoric acid (DEHPA)) and chelating agents (e.g., EDTA and diethylene triamine pentaacetic acid (DTPA)) have an increased affinity for the heavier rare-earth ions, due to the smaller ionic radii and higher charge densities of the heavy rare-earth ions.[23,24] Unfortunately, the difference in ionic radius between neighboring rare-earth elements is small, making an efficient sized-based separation very challenging.[23] Progress has been made in the development of more selective extractants for liquid/liquid extraction of rare earths, but the separation is still inefficient.[23,25]

In this paper, a new approach is proposed to tune the selectivity of existing ligands and extractants. The selectivity is achieved by combining the inherent selectivity of EDTA groups with the steric hindrance of coordinating groups on the surface of oxide nanoparticles. Magnetic (Fe_3O_4) and nonmagnetic (TiO_2 and SiO_2) nanoparticles were functionalized with TMS-EDTA. These oxides were selected because they have different densities of OH groups on their surfaces. The OH density increases in the order Fe_3O_4 < TiO_2 < SiO_2.[26−29] Higher densities of OH groups should result in higher densities of EDTA groups on the nanoparticles, because the silanes react with these hydroxyl groups. The functionalized nanoparticles were characterized extensively and their behavior in solution was investigated both for the adsorption and the separation of rare-earth ions by selective uptake.

2. EXPERIMENTAL SECTION

Chemicals. Anhydrous $FeCl_3$ (97%), SiO_2 nanoparticles (12 nm, 99.5%), TiO_2 nanoparticles (21 nm, 99.5%), $Y(NO_3)_3{\cdot}6H_2O$ (99.9%) and $Lu(NO_3)_3{\cdot}5H_2O$ (99.9%) were purchased from Sigma-Aldrich. *N*-[(3-Trimethoxysilyl)propyl]ethylenediamine triacetic acid trisodium salt (TMS-EDTA) (45 wt %) was purchased from ABCR chemicals, HCl (32 wt %), methanol (HPLC grade) and NaOH (97%) were purchased from VWR. $Sm(NO_3)_3{\cdot}6H_2O$ (99.9%), $Gd(NO_3)_3{\cdot}6H_2O$ (99.9%), $Er(NO_3)_3{\cdot}5H_2O$ (99.9%) and *n*-octylamine (NOA) (99.9%) were purchased from Acros Chemicals. $La(NO_3)_3{\cdot}6H_2O$ (99.9%) and $Pr(NO_3)_3{\cdot}6H_2O$ (99.9%) were purchased from Chempur. $Nd(NO_3)_3{\cdot}6H_2O$ (99.9%), $Tb(NO_3)_3{\cdot}5H_2O$ (99.9%), $Dy(NO_3)_3{\cdot}5H_2O$ (99.9%), $Ho(NO_3)_3{\cdot}5H_2O$ (99.9%) and $Yb(NO_3)_3{\cdot}5H_2O$ (99.9%) were purchased from Alfa Aesar. All chemical were used as received without further purification.

Equipment and Characterization. A Branson 5510 (10 L) and a Branson 2510 MTH (3 L) sonicator bath were used to disperse nanoparticles in a solvent. A mechanical shaker (IKA KS 130 basic with universal attachment) was employed during adsorption experiments and a vibrating plate (IKA MS 3 basic) was used in the sample preparation for TXRF analysis. Finally, a centrifuge (Heraeus labofuge 200) was used to separate the nonmagnetic nanoparticles from solution. Transmission Electron Microscopy (TEM) was carried out on a JEOL JEM2100 apparatus using an acceleration voltage of 80 or 200 kV. The size determination was done using ImageJ software. Magnetization data were obtained from vibrating sample magnetometry (VSM) experiments performed on a VSM Maglab setup from Oxford Instruments at 300 K. Fourier Transform Infrared (FTIR) spectra were measured between 5000 and 400 cm^{-1} on a Bruker Vertex 70 spectrometer, with a Platinum ATR module. Thermogravimetric analysis (TGA) was performed with a TA Instruments Q600 thermogravimeter, measuring from 25 to 1300 °C (10 °C per minute, argon atmosphere). Finally, the carbon, hydrogen and nitrogen contents of the functionalized nanoparticles were determined by CHN elemental analysis with a CE Instruments EA-1110 elemental analyzer. The hydrodynamic properties and of the nanoparticles were probed by dynamic light scattering (DLS) and ζ-potential measurements using a Brookhaven 90Plus particle analyzer with the scattering angle set at 90°. The acidity of the EDTA groups was investigated with a Mettler-Toledo T90 automatic titrator using HCl (0.01 M) and NaOH (0.01 M) as the titrant. Total reflection X-ray fluorescence (TXRF) analysis was used to measure the rare-earth concentrations. A benchtop Bruker S2 PICOFOX TXRF spectrometer equipped with a molybdenum X-ray source was used. Rare-earth concentrations were measured directly on the nanoparticle dispersion, which is a major advantage of TXRF compared to inductively coupled plasma mass spectrometry analysis where nanoparticles have to be disintegrated in acid prior to analysis. For the sample preparation, Eppendorf microtubes were filled with an amount of sample solution and a similar concentration (10 to 100 mg/L) of Ga^{3+} as internal standard (1000 ppm gallium dissolved in 2−3% HNO_3, Merck). Gallium was chosen because this element has a high sensitivity and does not interfere with the lanthanide signals. Finally, a 5 μL drop of this solution was put on a quartz plate, previously treated with a silicone/isopropanol solution (Serva) and dried for 15 min at 60 °C prior to analysis. Each sample was measured for 200 s.

Synthesis of Precursor Magnetite Nanoparticles. A well-described in-house synthesis procedure was followed for the synthesis of the magnetite nanoparticles.[30] First, ethylene glycol (37.5 mL) and *n*-octylamine (NOA) (25 mL) were poured into a flask and heated to 150 °C. At the same time, $FeCl_3$ (2.4 g) was dissolved in a beaker containing ethylene glycol (10 mL) and Milli-Q water (3.5 mL). Once $FeCl_3$ was totally dissolved, the iron(III)-containing solution was slowly added to the flask with ethylene glycol and *n*-octylamine and further heated to reflux at 180 °C for 24 h. After reaction, the obtained particles were precipitated from the reaction mixture by a NdFeB magnet and washed three times with acetone. Finally, they were dried in vacuo at room temperature for 20 min to obtain a black powder of Fe_3O_4(NOA) nanoparticles with a typical yield of 1 g.

Silanization of Nanoparticles. Fe_3O_4(NOA), TiO_2 and SiO_2 nanoparticles were functionalized with TMS-EDTA. The Fe_3O_4(NOA) nanoparticles were used as such, but the TiO_2 and SiO_2 nanoparticles were dried at 50 °C in vacuo for 24 h. The silanization protocol started by dissolving 100 mg of nanoparticles in MeOH (100 mL). The beaker was placed in an ultrasonic bath for 2 h. TMS-EDTA (1 mmol) was then added together with a few drops of glacial acetic acid. The beaker was placed for another 2 h in the ultrasonic bath. The particles were precipitated from the reaction mixture by a small magnet or a centrifuge (5300 rpm, 15 min) and washed one time with water and two times with acetone. Finally, they were dried in vacuo at room temperature for 20 min, resulting in Fe_3O_4(TMS-EDTA), TiO_2(TMS-EDTA) and SiO_2(TMS-EDTA).

Procedure for Adsorption, Separation and Stripping Experiments. Functionalized nanoparticles (5 mg) were dissolved in Milli-Q water (10 mL) by placing the solution in an ultrasonic bath for 1 h. The vials were then taken out and the desired volume of equimolar, binary rare-earth solution (5×10^{-3} M) was added. These mixtures of rare earths pairs were prepared in advance by combining and diluting concentrated stock solutions of the individual rare-earth elements (0.05 M). All the concentrations were verified by total reflection X-ray fluorescence (TXRF). The pH was set using HCl (0.1 M) or NaOH

(0.1 M). The vials were then placed on a mechanical shaker for 24 h to ensure equilibrium was reached. The particles were settled using a small NdFeB magnet in the case of magnetic nanoparticles or a centrifuge (5300 rpm, 20 min) in the case of nonmagnetic nanoparticles. The solution was removed and the nanoparticles were washed two times with acetone in order not to influence the adsorption equilibrium. The rare-earth content on the nanoparticles was then analyzed with TXRF. The stripping of rare-earth ions from the nanoparticles was done by redispersing the washed nanoparticles in water and lowering the pH to 2.75 by an HCl solution (0.1 M). After 1 h, the nanoparticles were retrieved, washed and analyzed using TXRF.

3. RESULTS AND DISCUSSION

Magnetic Nanoparticles. The magnetite nanoparticles were synthesized using a forced hydrolysis method.[30] The nanoparticles were of high quality, in the sense that they had a high saturation magnetization (66 emu/g) and a relatively well-defined spherical shape (TEM) The *n*-octylamine layer on the precursor nanoparticles is weakly bonded and can be replaced by a covalently bonded layer of functional silanes. The silanes are first hydrolyzed to silanols, which react with the hydroxyl groups on the surface of the nanoparticles in a condensation reaction. The resulting product was a black powder with an excellent shelf life. Magnetite nanoparticles functionalized with EDTA-silane (Figure 2) will be referred to as Fe_3O_4(TMS-EDTA). Commercially available SiO_2 and TiO_2 nanoparticles were dried prior to use. Drying the particles before silanization and then redispersing them in water increases the surface coverage.[26] This procedure and the influence of the concentration surface hydroxyl groups on the silanization of SiO_2 were studied extensively by Dugas et al.[26] For magnetite (Fe_3O_4) nanoparticles, this step was not necessary because the precursor particles had a hydrophobic *n*-octylamine coating. The silanization was carried out in the same way as for the magnetite nanoparticles. The final products were white powders that will be referred to as SiO_2(TMS-EDTA) and TiO_2(TMS-EDTA).

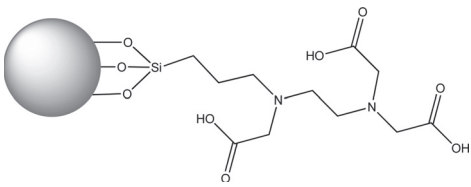

Figure 2. Nanoparticle functionalized with TMS-EDTA.

Characterization of the Nanoparticles. The TEM images (Figures S5–S7, Supporting Information) showed that the Fe_3O_4 particles had a relatively spherical shape and were monodisperse with an average core diameter of (10.5 ± 1.8) nm. The SiO_2 nanoparticles and TiO_2 were more polydisperse and had a diameter of (16.6 ± 5.8) nm and (17.9 ± 5.9) nm, respectively. Vibrating Sample Magnetometry (VSM) measurements (Figure S4, Supporting Information) showed that the magnetic nanoparticles had a saturation magnetization of 66 emu/g and negligible coercivity and remanent magnetization, indicating superparamagnetic behavior. This property allows for convenient retrieval of the nanoparticles from solution, using only a permanent magnet (Figure 3). Full retrieval (>99.9%) was possible in less than 10 s.

Figure 3. Fe_3O_4(TMS-EDTA) nanoparticles dispersed in water (left) and the retrieval using a permanent magnet (right).

The presence of EDTA on the nanoparticles was verified using FTIR spectroscopy (Figure S1–S3, Supporting Information). EDTA has two strong absorption bands between 1570–1610 cm^{-1} and 1350–1450 cm^{-1}.[19,21] These bands occur as a pair and can be assigned to asymmetrical and symmetrical COO^- stretching vibrations, respectively. Fe_3O_4(TMS-EDTA) has IR absorption bands at 1592 and 1401 cm^{-1}, TiO_2(TMS-EDTA) at 1594 and 1404 cm^{-1} and SiO_2(TMS-EDTA) at 1591 and 1408 cm^{-1}. Si–O–Si bands due to oligomerization of the silanes can be found between 1150 and 1000 cm^{-1} and the Si–O–M bonds (M = Fe, Si, Ti) bonds cause a strong band between 900 and 1000 cm^{-1}, depending on the metal.[19,21,31] For Fe_3O_4(TMS-EDTA), these bands were found at 1091 and 903 cm^{-1}, respectively, for TiO_2(TMS-EDTA) at 1090 and 919 cm^{-1} and for SiO_2(TMS-EDTA) only one band at 1062 cm^{-1} because M = S. The lattice vibration band of the core broadens and shifts, due to the formation of Si–O–M (M = Fe, Si, Ti) bonds in the silane surface layer and was found at 548 cm^{-1} for Fe_3O_4, 430 cm^{-1} for TiO_2 and 802 cm^{-1} for SiO_2. Other features include the weak asymmetric and symmetric CH2 stretchings at 2922–2931 and 2852–2856 cm^{-1}.[17,19]

The EDTA-silane groups and the free hydroxyl groups on the oxide surface of the nanoparticle core can form positively or negatively charged species, depending on the pH. Surface hydroxyl groups on Fe_3O_4, TiO_2 and SiO_2 show amphoteric behavior and have a point of zero charge around pH 7, pH 6.5 and pH 2.2, respectively.[32–34] These charges are negligible though, compared to the many charges of the TMS-EDTA groups. TMS-EDTA contains five sites with acid–base behavior: two tertiary amines and three carboxylic acid groups (Figure 4). The positively charged species are often omitted because these only occur at very low pH.

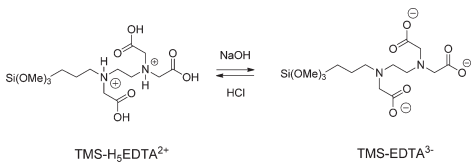

Figure 4. Structure of TMS-EDTA in its most positively and negatively charged state.

Knowing the pK_a values of TMS-EDTA is important because these determine the speciation of TMS-EDTA as function of pH. Because no pK_a values were found for TMS-EDTA in the literature, a titration was carried out to determine the pK_a values of TMS-EDTA on the nanoparticles. The pK_a of the pure silane cannot be determined because the silane would hydrolyze in water and react with the glass of the pH electrode.

The pK_a values for EDTA-silane (TMS-EDTA) attached to a Fe_3O_4 nanoparticle were found to be pK_{a1} = 4.17, pK_{a2} = 6.89, pK_{a3} = 10.00. The pK_a values of the positively charged species could not be determined because of the instability at pH ≤ 2.5; ζ-potential measurements (Figure S9, Supporting Information) for a dispersion of Fe_3O_4(TMS-EDTA) nanoparticles showed that the negative charge on the particles increases with pH because the carboxylic acid groups are gradually deprotonated. The point of zero charge (PZC) is situated at pH 2.8, where all the carboxylic acid groups are fully protonated. If the ionic strength of the solution is raised too much, the absolute value of the ζ-potential diminishes, causing aggregation and/or sedimentation. The application of functionalized nanoparticles as sorbents is therefore limited to the adsorption of low or trace metal concentrations.[6−14] Dynamic light scattering (DLS) was carried out to measure the hydrodynamic radii and the polydispersity (aggregation) of the nanoparticles at different pH values (Table S1, Supporting Information). The increase in hydrodynamic radius with pH confirmed that the solvation shell increases with increasing surface charge or ζ-potential. The low polydispersity index confirmed the absence of aggregation in solution at the relevant pH values.

Density of EDTA Groups. The amount of EDTA-silane groups on the surface of the nanoparticles was determined by CHN elemental analysis and TGA measurements (Table 1).

Table 1. Surface Group Fraction (FSG) for the Different Nanoparticles Measured by CHN Analysis and TGA

	CHN F_{SG}[a] (wt %)	TGA F_{SG} (wt %)	average (wt %)
Fe_3O_4(NOA)	6 ± 0.6	11	8.5 ± 0.6
Fe_3O_4(TMS-EDTA)	15 ± 2	17	16 ± 2
TiO_2(TMS-EDTA)	36 ± 3	42	39 ± 3
SiO_2(TMS-EDTA)	61 ± 5	50	55.5 ± 5

[a]F_{SG} = surface group fraction.

The weight loss during TGA measurements is a gradual process at first, due to interdigitation (entanglement) of the ligands, but around 400 °C a sudden drop in weight is observed, after which most of the TMS-EDTA is removed (Figure S8, Supporting Information). This observed weight loss can be directly translated into the surface group fraction (F_{SG}), which is the weight fraction of TMS-EDTA in the nanoparticle. Furthermore, the carbon and nitrogen weight fraction measured by CHN elemental analysis was also used to calculate the surface group fraction F_{SG}. Both methods (CHN and TGA) have their advantages, but each method induced a small error. The best approximation is to use the average of both measurements.

One of the aims of the research described in this paper was to investigate the influence of the sterical crowding of the immobilized ligand on the selectivity. Silane molecules can bind to the hydroxyl groups on the surface of the nanoparticles. This means that the density of TMS-EDTA groups on the nanoparticle is related to the initial density of hydroxyl groups on that oxide.[19,26,35] Three different oxides were selected with an increased affinity for silanes in the order Fe_3O_4 < TiO_2 < SiO_2.[36] The exact hydroxyl group density depends on several factors, including synthesis conditions, particle morphology and the nature of the crystalline phase.[26] This makes it difficult to give exact values, but approximate literature values can be used to get an idea of the relative abundance of hydroxyl groups on the surface of the different oxides.[19,26,29,35] The commercially available SiO_2 nanoparticles had the appearance of a very fine, flake-like powder. This type of silica is known to have a high hydroxyl group density on its surface especially in aqueous solution (6.0 − 8.0 μmol/m^2).[26] The commercially available TiO_2 nanoparticles consisted of type P25 TiO_2 (produced by Evonik Degussa) with a 80:20 anatase:rutile ratio and have an intermediate hydroxyl group density on their surface (4.6 μmol/m^2).[27] The Fe_3O_4 nanoparticles were covered with *n*-octylamine and are known to contain fewer OH groups on their surface (1.0−1.5 μmol/m^2).[28] The surface density (SD) of TMS-EDTA was approximated using eq 1:

$$\mathrm{SD}(\mu\mathrm{mol/m^2}) = \frac{\left(\frac{F_{SG}}{100}\right) r\rho}{3M_{SG}} \times 10^6 \quad (1)$$

where F_{SG} is the surface group fraction (wt %) (Table 1), M_{SG} is the molar mass of the surface group (345 g/mol), r is the particle radius (m) obtained by TEM measurements, and ρ the density (g/m^3) of the core material. For Fe_3O_4, SiO_2 and TiO_2, the densities are 5.1, 2.6 and 3.9 g/cm^3, respectively.[37] The diameters are 10.5 nm, 16.6 and 17.9 nm (TEM). From this data, the specific surface was calculated assuming spherical nanoparticles and the surface density of EDTA-silane groups indeed increases in the order Fe_3O_4 < TiO_2 < SiO_2 (Table 2).

Table 2. Calculated Specific Surface and Density of Functional Silanes on the Surface of the Different Nanoparticles Compared to the Initial Hydroxyl Group Density

	specific surface of the core (m^2/g)	OH[a] (μmol/m^2)	TMS-EDTA[b] (μmol/m^2)
Fe_3O_4	115	1.0−1.5	4.1
TiO_2	86	4.6	11.6
SiO_2	139	6.0−8.0	13.1

[a]Approximate hydroxyl group densities found in literature.[26−28] [b]Calculated surface density (SD) of TMS-EDTA, using eq 1.

The footprint of a silane molecule is about 0.32−0.38 nm^2.[38] This means that a perfect silane monolayer has an approximate surface density of 3 molecules/nm^2 (5 μmol/m^2). The higher surface density found for TiO_2(TMS-EDTA) and SiO_2(TMS-EDTA) (Table 2) means that there is a larger degree of oligomerization and multilayer formation. These are unavoidable phenomena when trialkylsilanes are used, even on surface of the less reactive Fe_3O_4 nanoparticles.[19,20,38]

Adsorption of Rare Earths. The adsorption of rare-earth ions from solution was investigated. The TMS-EDTA groups form the largest number of binding sites for metal ions, but metal ions can also bind nonspecifically to the deprotonated hydroxyl end groups on the hydrolyzed silanes or on the surface of the nanoparticle (Figure 5).[39] This is supported by the fact that the observed uptake of Gd^{3+} ions by TMS-EDTA functionalized nanoparticles is higher than the TMS-EDTA content on these nanoparticles (Table 3). The adsorption capacity is also pH dependent because both the EDTA carboxylic acid groups and hydroxyl groups are deprotonated at higher pH values.[39]

The influence of pH on the adsorption of Gd^{3+} was investigated (Figure 6). Gd^{3+} was chosen because it is located in the middle of the lanthanide series, which makes it a good model ion. An 8 mL solution containing 5 mg of nanoparticles and 3.75 × 10^{-3} M of Gd^{3+} was used (6 μmol/mg) to

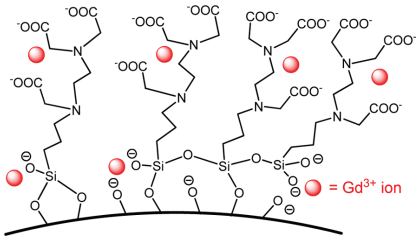

Figure 5. Schematic representation of the possible binding sites for metal ions (e.g., Gd^{3+}) on the surface of TMS-EDTA functionalized nanoparticles.

Table 3. Maximal Adsorption Capacity of the Fe_3O_4(TMS-EDTA), TiO_2(TMS-EDTA) and SiO_2(TMS-EDTA) Nanoparticles Compared with the Unfunctionalized Analogues and with Other Functionalized Nanoparticles in the Literature

particle(ligand)	core size (nm)	surface group (wt %)	ion	ion uptake (mg/g)
Fe_3O_4	10.5		Gd^{3+}	14
SiO_2	17.9		Gd^{3+}	20
TiO_2	16.6		Gd^{3+}	41
Fe_3O_4(TMS-EDTA)	10.5 ± 1.8	16 ± 2	Gd^{3+}	113 ± 6
TiO_2(TMS-EDTA)	17.9 ± 5.9	39 ± 3	Gd^{3+}	263 ± 11
SiO_2(TMS-EDTA)	16.6 ± 5.8	55.5 ± 5	Gd^{3+}	395 ± 32
Fe_3O_4(humic acid)[16]	14	15.5	Eu^{3+}	10.6
Fe_3O_4(DEHPA)[15]	N/A	13.9	La^{3+}	55.9
Fe_3O_4(EDTA)[7]	312.3	7.8	Cu^{2+}	46.3
Fe_3O_4(chitosan)[41]	13.5	4.9	Cu^{2+}	21.5
Fe_3O_4(dien)[42]	11.6	N/A	Cu^{2+}	12.43
GO(TMS-EDTA)[a][39]	N/A	N/A	Pb^{2+}	479

[a]Graphene oxide (GO) consists of graphene nanosheets with surface OH and COOH groups (high toxicity).[39]

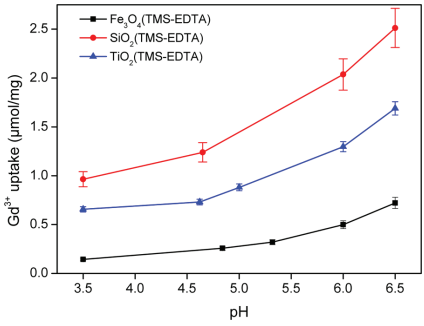

Figure 6. Uptake of Gd^{3+} ions by Fe_3O_4(TMS-EDTA), SiO_2(TMS-EDTA) and TiO_2(TMS-EDTA) nanoparticles as a function of pH.

guarantee an excess of rare-earth ions in order to obtain the maximal uptake capacity. The uptake of Gd^{3+} ions is the highest at pH 6.5 because of the increasingly deprotonated TMS-EDTA groups. Above pH 6.5, the solubility product of Gd^{3+} is exceeded (K_{SP} = 10^{-24}) and the Gd^{3+} ions in solution precipitate as $Gd(OH)_{3(s)}$ (Figure S10, Supporting Information).[40] The average uptake of rare-earth ions clearly increases in the order: SiO_2(TMS-EDTA) > TiO_2(TMS-EDTA) > Fe_3O_4(TMS-EDTA) due to the increasing amounts of EDTA-silane on the surface of these nanoparticle. The adsorption characteristics of several elements of the lanthanide series by Fe_3O_4(TMS-EDTA), SiO_2(TMS-EDTA) and TiO_2(TMS-EDTA) are shown in Figure 7. Single element solutions were

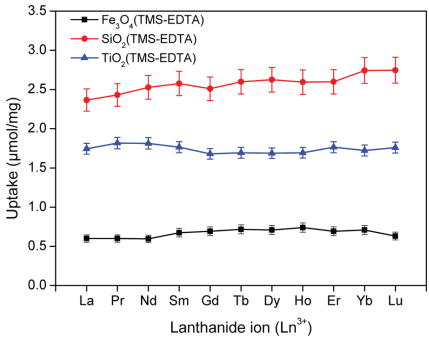

Figure 7. Uptake of rare-earth ions from single-element solutions by Fe_3O_4(TMS-EDTA), SiO_2(TMS-EDTA) and TiO_2(TMS-EDTA) nanoparticles at pH 6.3.

used with a large excess of rare-earth ion (6 μmol/mg) at pH 6.3 to obtain the highest possible uptake without precipitation. In the absence of competition between different ions, the uptake of the different lanthanide ions is quite similar (Figure 7). Furthermore, the stripping of rare-earth ions from Fe_3O_4(TMS-EDTA) nanoparticles was investigated. Complete stripping was observed after less than 5 min (Figure S13, Supporting Information) and a plateau value was reached at pH 3 with 98% stripping efficiency (Figure 8)). This is in good agreement with the fact that the carboxylic acid groups are fully protonated below pH 3 (ζ-potential > 0).

The stability of the different TMS-EDTA modified nanoparticles in acidic and alkaline solutions was tested. Nano-

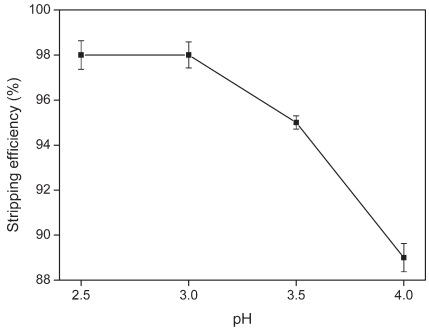

Figure 8. Stripping of Gd^{3+} from Fe_3O_4(TMS-EDTA) nanoparticles previously saturated with an excess of Gd^{3+} ions.

particles (10 mg) were dispersed in Milli-Q water (5 mL) and the pH was adjusted with a HCl (1 M) or NaOH (1 M) solution. The dispersion was then shaken for 24 h. The particles were removed from solution and the remaining metal content (Fe, Si or Ti) in the water was determined by TXRF analysis. Polypropylene sample carriers were used to determine the silicon content instead of the quartz sample carriers. The results show that the nanoparticles are stable between pH 2.5 and pH 10 (Figure 9). This wide pH window permits complex

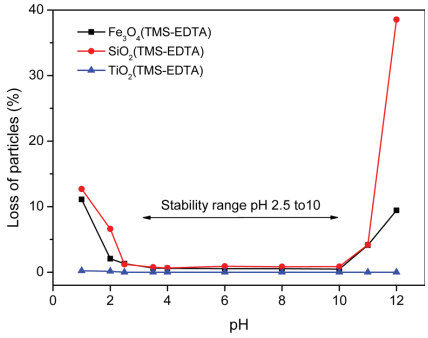

Figure 9. Nanoparticle stability in solutions with different pH values. The loss of particles after 24 h is shown as a function of pH.

formation and stripping of metal ions from the nanoparticles without damaging the nanoparticles, making this system reusable. Repeated adsorption (pH 6.5) and stripping (pH 2.75) cycles showed a negligible decrease in adsorption capacity after three cycles.

The adsorption capacity was compared with different functionalized nanoparticles reported in the literature (Table 3).[7,15,39,41−43] The functionalization of the nanoparticles with TMS-EDTA drastically increased the adsorption capacity. The lanthanide adsorption capacities (mg/g) are high compared to literature reports, this can be explained by the high surface group content and specific surface of these small nanoparticles and the low degree of aggregation, which keeps all the TMS-EDTA groups available.[7,15] Lighter materials (TiO_2 and SiO_2) with a higher EDTA density have even larger adsorption capacities (mg/g). This is why Madadrang et al. showed record adsorption capacities of 479 mg/g for Pb^{2+} on the very light graphene-oxide sheets functionalized with TMS-EDTA.[39] Few nanoparticle sorbents have been used for the adsorption of lanthanide ions, so the results were compared with the ion showing a maximal adsorption capacity for each system.

Separation of Rare Earths. The selectivity was reported using the enrichment factor (EF), which compares the molar ratio of two elements A and B before and after separation, according to eq 2. B was always chosen to be the heavier of the two rare earths because this results in an enrichment factor >1, which is easier to work with. The ratio B/A after separation was determined directly on the nanoparticles using TXRF. Because the metal ions can be full striped from the nanoparticles, the ratio on the nanoparticles is the same ratio that can be found when measuring the stripping solution.

$$\mathrm{EF} = \frac{(B/A)_{\text{after separation}}}{(B/A)_{\text{before separation}}} = \frac{(B/A)_{\text{on the nanoparticles}}}{(B/A)_{\text{feed solution}}} \quad (2)$$

The working conditions were optimized for the separation experiments. Tests showed that the rare-earth ions had to be added in excess compared to the amount of EDTA groups on the nanoparticles in solution (Figure S11, Supporting Information). Without an excess of rare-earth ions in solution, the EDTA groups captured every ion in solution without much selectivity. The influence of the counterion (nitrate or chloride salts) was negligible (Figure S12, Supporting Information). The influence of pH is illustrated in Figure 10. The separation of

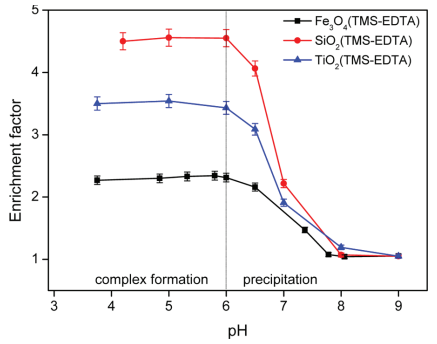

Figure 10. Separation of La^{3+} and Er^{3+} by different EDTA-functionalized nanoparticles at different pH values.

La^{3+}/Er^{3+} was chosen because the large difference in selectivity helps visualizing a possible trend. The solution contained 3 μmol of each rare earth per mg of nanoparticles (a large excess, see Figure 7). The selectivity of the system does not change much in the range between pH 4 and 6. A high pH is desirable to increase the adsorption of rare-earth ions (Figure 6), so the separation of rare-earth ions is therefore best carried out between pH 6 and 6.5, to ensure a maximal uptake of rare-earth ions with high selectivity. Beyond pH 6.5, precipitation of rare-earth hydroxides occurred.

Influence of Sterical Crowding on the Selectivity. It is well-known that EDTA and other metal chelating compounds have an inherent selectivity.[24,44,45] However, because the EDTA groups on the nanoparticles are, in principle identical, one would not expect additional differences in selectivity, depending on which substrate the TMS-EDTA is attached to. The difference in selectivity between the different nanoparticles is therefore definitely the most remarkable observation to be made (Figure 10). It is assumed that this effect originates from the fact that Fe_3O_4, TiO_2 and SiO_2 nanoparticles have increasingly high densities of TMS-EDTA on their surface (Table 2). The denser the EDTA coating, the more the selectivity increases toward the smaller Er^{3+} ion and decreases toward the larger La^{3+} ion. This could originate from the fact that a dense EDTA-silane (multi)layer is more impenetrable for larger ions or from the fact that the size of the EDTA cage is reduced due to sterical crowding caused by the high density of EDTA groups on the surface of the nanoparticle. Thermodynamic models exist to describe the complex interactions between neighboring metal ions in polynuclear complexes.[46−52]

However, determining the exact structure and speciation of the dense EDTA-silane layer on the surface of the nanoparticles is not as straightforward as for chelating complexes in solution. Quantifying the interactions between rare-earth ions within the dense EDTA-silane layer is therefore too complex to attempt here. Instead, experimental evidence is proposed to support this theory of a size-based selectivity related to the density of ligands on the surface of the nanoparticles.

This effect was further investigated by looking at the separation of La^{3+} ions from other trivalent lanthanide ions (Ln^{3+}) (Figure 11). As expected, the enrichment factors

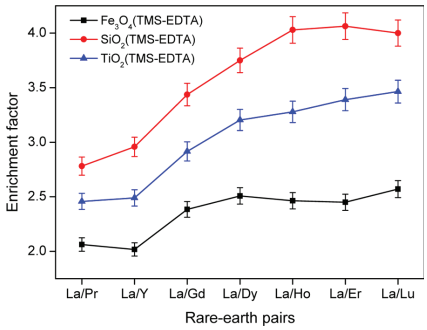

Figure 11. Separation of La^{3+}/Ln^{3+} rare-earth pairs (pH 6.5) with increasingly different ionic radii from left to right.

increased with increasing difference in ionic radius, but it is also evident that TiO_2(TMS-EDTA) and SiO_2(TMS-EDTA) have a higher selectivity toward smaller (heavier) ions than Fe_3O_4(TMS-EDTA). In addition, SiO_2(TMS-EDTA) shows the steepest increase in enrichment factor over the series, which can be explained by the fact that it has the largest density of TMS-EDTA on its surface. TiO_2(TMS-EDTA) and Fe_3O_4(TMS-EDTA) show a less steep increase in enrichment factor because their EDTA-coating is less dense and therefore less capable of size-based selectivity due to sterical crowding.

Large differences in enrichment factors (EF) for different nanoparticles were only found for rare-earth pairs containing lanthanum (Figure 11), possibly because La^{3+} is the only ion that is large enough to trigger the selectivity due to the density of EDTA groups on the surface. Note that EDTA has an inherent selectivity toward the heavier (smaller) lanthanide ions, so that any selectivity arising from the difference in surface density is only observable if it is large enough compared to the inherent selectivity of EDTA. For the other rare-earth ions, the difference was much smaller. The Lu^{3+}/Ln^{3+} series (Figure S15, Supporting Information) and Pr^{3+}/Ln^{3+} series (Figure S16, Supporting Information), for example, both showed some difference in selectivity, but the effect was not as large as that for La^{3+}/Ln^{3+} (Figure 11). The position of yttrium in the separation series was elucidated by looking at the yttrium separation series (Figure S14, Supporting Information). It is evident that Y^{3+} behaves like Pr^{3+} or Nd^{3+} in our system (EF = 1), even though the ionic radius of Y^{3+} is closer to that of Ho^{3+}.[53] This is in agreement with previous reports on the complex formation of lanthanide ions with EDTA and HEDTA in solution.[24] The "itinerant" behavior of Y^{3+} is a phenomenon that describes the fact that Y^{3+} can move across the lanthanide series, depending on the extraction system.[44]

4. CONCLUSION

Magnetic (Fe_3O_4) and nonmagnetic (TiO_2 and SiO_2) nanoparticles were coated with EDTA-silane and their adsorption capacity and selectivity toward rare-earth ions was investigated. The covalently bonded TMS-EDTA protects the surface of the nanoparticles from oxidation and provides surface charges to prevent aggregation. The high adsorption capacities (100 to 400 mg/g) of these nanoparticles is due to their small diameter (10 to 20 nm) and high surface area (85 to 140 m^2/g), combined with a large coverage of TMS-EDTA. It was found that the selectivity toward smaller rare-earth ions increased in the same order as the density of the EDTA-silane on the surface, namely Fe_3O_4(TMS-EDTA) < TiO_2(TMS-EDTA) < SiO_2(TMS-EDTA). This observation could be used to tune the selectivity of other existing extractants and further research will be directed to explore this phenomenon of selectivity enhancement by steric crowding. The main advantage of magnetic nanoparticles is the fact that they can be easily retrieved from solution using a small magnet. On the other hand, SiO_2 and TiO_2 nanoparticles can hold larger quantities of TMS-EDTA on their surface and can therefore adsorb more rare-earth ions, but their removal from solution is more tedious. This knowledge about the differences in adsorption capacity and selectivity of TMS-EDTA attached to these different oxides could prove valuable for the future design of Fe_3O_4@SiO_2 or Fe_3O_4@TiO_2 core–shell nanoparticles. These hybrid materials with a magnetic Fe_3O_4 core and a nonmagnetic shell could combine the convenience of magnetic retrieval with the high adsorption capacity and selectivity of SiO_2-based nanoparticles.

■ ASSOCIATED CONTENT

Supporting Information

DLS, VSM, TGA measurements, FTIR spectra, and TEM pictures. Graphs showing the precipitation threshold for adsorption experiments, the effect of counterion on separation efficiency, the influence of the rare-earth/EDTA ratio on the selectivity, the influence of stripping time, and some additional graphs showing the separation of various rare-earths pairs. This material is available free of charge via the Internet at http://pubs.acs.org.

■ AUTHOR INFORMATION

Corresponding Author

*K. Binnemans. E-mail: Koen.Binnemans@chem.kuleuven.be.

Notes

The authors declare no competing financial interest.

■ ACKNOWLEDGMENTS

The authors thank the KU Leuven (projects GOA/13/008 and IOF-KP RARE^3) and the FWO Flanders (Ph.D. fellowship to D.D. and research project G.0618.11 N) for financial support. CHN analyses were performed by Dirk Henot, DLS and ζ-potential measurements by Dr. Naveen K. Reddy and TGA measurements by Danny Winant and Dr. Stijn Schaltin.

■ REFERENCES

(1) Hao, R.; Xing, R.; Xu, Z.; Hou, Y.; Gao, S.; Sun, S. Synthesis, Functionalization, and Biomedical Applications of Multifunctional Magnetic Nanoparticles. *Adv. Mater.* **2010**, *22*, 2729–2742.

(2) Lu, A.-H.; Salabas, E. L.; Schüth, F. Magnetic Nanoparticles: Synthesis, Protection, Functionalization, and Application. *Angew. Chem., Int. Ed.* **2007**, *46*, 1222−1244.
(3) Liu, Z.; Li, B.; Wang, B.; Yang, Z.; Wang, Q.; Li, T.; Qin, D.; Li, Y.; Wang, M.; Yan, M. Magnetic Nanoparticles Modified with DTPA-AMC-Rare Earth for Fluorescent and Magnetic Resonance Dual Mode Imaging. *Dalton Trans.* **2012**, *41*, 8723−8728.
(4) Wang, B.; Hai, J.; Wang, Q.; Li, T.; Yang, Z. Coupling of Luminescent Terbium Complexes to Fe_3O_4 Nanoparticles for Imaging Applications. *Angew. Chem., Int. Ed.* **2011**, *50*, 3063−3066.
(5) Xi, P.; Cheng, K.; Sun, X.; Zeng, Z.; Sun, S. Magnetic Fe_3O_4 Nanoparticles Coupled with a Fluorescent Eu Complex for Dual Imaging Applications. *Chem. Commun.* **2012**, *48*, 2952−2954.
(6) Goon, I. Y.; Zhang, C.; Lim, M.; Gooding, J. J.; Amal, R. Controlled Fabrication of Polyethylenimine-Functionalized Magnetic Nanoparticles for the Sequestration and Quantification of Free Cu^{2+}. *Langmuir* **2010**, *26*, 12247−12252.
(7) Liu, Y.; Chen, M.; Yongmei, H. Study on the Adsorption of Cu(II) by EDTA Functionalized Fe_3O_4 Magnetic Nano-Particles. *Chem. Eng. J.* **2013**, *218*, 46−54.
(8) Ren, Y.; Abbood, H. A.; He, F.; Peng, H.; Huang, K. Magnetic EDTA-modified Chitosan/SiO_2/Fe_3O_4 Adsorbent: Preparation, Characterization, and Application in Heavy Metal Adsorption. *Chem. Eng. J.* **2013**, *226*, 300−311.
(9) Sun, L.; Li, Y.; Sun, M.; Wang, H.; Xu, S.; Zhang, C.; Yang, Q. Porphyrin-Functionalized Fe_3O_4@SiO_2 Core/Shell Magnetic Colorimetric Material for Detection, Adsorption and Removal of Hg^{2+} in Aqueous Solution. *New J. Chem.* **2011**, *35*, 2697−2704.
(10) Warner, C. L.; Addleman, R. S.; Cinson, A. D.; Droubay, T. C.; Engelhard, M. H.; Nash, M. A.; Yantasee, W.; Warner, M. G. High-Performance, Superparamagnetic, Nanoparticle-Based Heavy Metal Sorbents for Removal of Contaminants from Natural Waters. *ChemSusChem* **2010**, *3*, 749−757.
(11) Rossier, M.; Koehler, F. M.; Athanassiou, E. K.; Grass, R. N.; Aeschlimann, B.; Gunther, D.; Stark, W. J. Gold Adsorption on the Carbon Surface of C/Co Nanoparticles Allows Magnetic Extraction from Extremely Diluted Aqueous Solutions. *J. Mater. Chem.* **2009**, *19*, 8239−8243.
(12) Rossier, M.; Koehler, F. M.; Athanassiou, E. K.; Grass, R. N.; Waelle, M.; Birbaum, K.; Günther, D.; Stark, W. J. Energy-Efficient Noble Metal Recovery by the Use of Acid-stable Nanomagnets. *Ind. Eng. Chem. Res.* **2010**, *49*, 9355−9362.
(13) Yantasee, W.; Warner, C. L.; Sangvanich, T.; Addleman, R. S.; Carter, T. G.; Wiacek, R. J.; Fryxell, G. E.; Timchalk, C.; Warner, M. G. Removal of Heavy Metals from Aqueous Systems with Thiol Functionalized Superparamagnetic Nanoparticles. *Environ. Sci. Technol.* **2007**, *41*, 5114−5119.
(14) Hao, Y.-M.; Man, C.; Hu, Z.-B. Effective Removal of Cu (II) Ions from Aqueous Solution by Amino-functionalized Magnetic Nanoparticles. *J. Hazard. Mater.* **2010**, *184*, 392−399.
(15) Wu, D.; Sun, Y.; Wang, Q. Adsorption of Lanthanum (III) from Aqueous Solution Using 2-ethylhexyl Phosphonic Acid Mono-2-ethylhexyl Ester-Grafted Magnetic Silica Nanocomposites. *J. Hazard. Mater.* **2013**, *260*, 409−419.
(16) Yang, S.; Zong, P.; Ren, X.; Wang, Q.; Wang, X. Rapid and Highly Efficient Preconcentration of Eu(III) by Core−Shell Structured Fe_3O_4@Humic Acid Magnetic Nanoparticles. *ACS Appl. Mater. Interfaces* **2012**, *4*, 6891−6900.
(17) Li, Y.; Wu, J.; Qi, D.; Xu, X.; Deng, C.; Yang, P.; Zhang, X. Novel Approach for the Synthesis of Fe_3O_4@TiO_2 Core-Shell Microspheres and their Application to the Highly Specific Capture of Phosphopeptides for MALDI-TOF MS Analysis. *Chem. Commun.* **2008**, 564−566.
(18) Tucker-Schwartz, A. K.; Farrell, R. A.; Garrell, R. L. Thiol−ene Click Reaction as a General Route to Functional Trialkoxysilanes for Surface Coating Applications. *J. Am. Chem. Soc.* **2011**, *133*, 11026−11029.
(19) De Palma, R.; Peeters, S.; Van Bael, M. J.; Van den Rul, H.; Bonroy, K.; Laureyn, W.; Mullens, J.; Borghs, G.; Maes, G. Silane Ligand Exchange to Make Hydrophobic Superparamagnetic Nanoparticles Water-Dispersible. *Chem. Mater.* **2007**, *19*, 1821−1831.
(20) Larsen, B. A.; Hurst, K. M.; Ashurst, W. R.; Serkova, N. J.; Stoldt, C. R. Mono and Dialkoxysilane Surface Modification of Superparamagnetic Iron Oxide Nanoparticles for Application as Magnetic Resonance Imaging Contrast Agents. *J. Mater. Res.* **2012**, *27*, 1846−1852.
(21) Bloemen, M.; Brullot, W.; Luong, T. T.; Geukens, N.; Gils, A.; Verbiest, T. Improved Functionalization of Oleic Acid-Coated Iron Oxide Nanoparticles for Biomedical Applications. *J. Nanopart. Res.* **2012**, *14*, 1100−1010.
(22) Hermanson, G. T. In *Bioconjugate Techniques*, 2nd ed.; Hermanson, G. T., Ed.; Academic Press: New York, 2008; pp 562−581.
(23) Xie, F.; Zhang, T. A.; Dreisinger, D.; Doyle, F. A critical review on solvent extraction of rare earths from aqueous solutions. *Miner. Eng.* **2014**, *56*, 10−28.
(24) Choppin, G. R.; Goedken, M. P.; Gritmon, T. F. The Complexation of Lanthanides by Aminocarboxylate Ligands - II. *J. Inorg. Nucl. Chem.* **1977**, *39*, 2025−2030.
(25) Vander Hoogerstraete, T.; Onghena, B.; Binnemans, K. Homogeneous Liquid−Liquid Extraction of Rare Earths with the Betaine−Betainium Bis(trifluoromethylsulfonyl)imide Ionic Liquid System. *Int. J. Mol. Sci.* **2013**, *14*, 21353−21377.
(26) Dugas, V.; Chevalier, Y. Surface Hydroxylation and Silane Grafting on Fumed and Thermal Silica. *J. Colloid Interface Sci.* **2003**, *264*, 354−361.
(27) Mueller, R.; Kammler, H. K.; Wegner, K.; Pratsinis, S. E. OH Surface Density of SiO_2 and TiO_2 by Thermogravimetric Analysis. *Langmuir* **2002**, *19*, 160−165.
(28) Cornell, R. M.; Schwertmann, U. *The Iron Oxides: Structure, Properties, Reactions, Occurrences and Uses*, 2nd ed.; Wiley-VCH: Weinheim, 2003; Chapter 10, pp 221−235.
(29) Zhao, J.; Milanova, M.; Warmoeskerken, M. M. C. G.; Dutschk, V. Surface Modification of TiO_2 Nanoparticles with Silane Coupling Agents. *Colloids Surf., A* **2012**, *413*, 273−279.
(30) Brullot, W.; Reddy, N. K.; Wouters, J.; Valev, V. K.; Goderis, B.; Vermant, J.; Verbiest, T. Versatile Ferrofluids Based on Polyethylene Glycol Coated Iron Oxide Nanoparticles. *J. Magn. Magn. Mater.* **2012**, *324*, 1919−1925.
(31) Anderson, D. R. In *Analysis of Silicones*; Smith, A. L., Ed.; Wiley-Interscience: New York, 1974; p 10.
(32) Kosmulski, M. pH-Dependent Surface Charging and Points of Zero Charge. II. Update. *J. Colloid Interface Sci.* **2004**, *275*, 214−224.
(33) Kosmulski, M. pH-Dependent Surface Charging and Points of Zero Charge. III. Update. *J. Colloid Interface Sci.* **2006**, *298*, 730−741.
(34) Kosmulski, M. *Surface Charging and Point of Zero Charge*; CRC Press: Boca Raton, FL, 2009.
(35) Huang, X.; Schmucker, A.; Dyke, J.; Hall, S. M.; Retrum, J.; Stein, B.; Remmes, N.; Baxter, D. V.; Dragnea, B.; Bronstein, L. M. Magnetic Nanoparticles with Functional Silanes: Evolution of Well-Defined Shells from Anhydride Containing Silane. *J. Mater. Chem.* **2009**, *19*, 4231−4239.
(36) Witucki, G. L. A Silane Primer - Chemistry and Applications of Alkoxy Silanes. *J. Coat. Technol.* **1993**, *65*, 57−60.
(37) Harrison, R. D.; Ellis, H. *Book of Data*; Longman: Edinburgh Gate, U.K., 1984; p 166.
(38) Fadeev, A. Y.; McCarthy, T. J. Self-Assembly Is Not the Only Reaction Possible Between Alkyltrichlorosilanes and Surfaces: Monomolecular and Oligomeric Covalently Attached Layers of Dichloro- and Trichloroalkylsilanes on Silicon. *Langmuir* **2000**, *16*, 7268−7274.
(39) Madadrang, C. J.; Kim, H. Y.; Gao, G.; Wang, N.; Zhu, J.; Feng, H.; Gorring, M.; Kasner, M. L.; Hou, S. Adsorption Behavior of EDTA-Graphene Oxide for Pb (II) Removal. *ACS Appl. Mater. Interfaces* **2012**, *4*, 1186−1193.
(40) Diakonov, I. I.; Ragnarsdottir, K. V.; Tagirov, B. R. Standard Thermodynamic Properties and Heat Capacity Equations of Rare Earth Hydroxides:: II. Ce(III)-, Pr-, Sm-, Eu(III)-, Gd-, Tb-, Dy-, Ho-,

Er-, Tm-, Yb-, and Y-Hydroxides. Comparison of Thermochemical and Solubility Data. *Chem. Geol.* **1998**, *151*, 327−347.
(41) Chang, Y.-C.; Chen, D.-H. Preparation and Adsorption Properties of Monodisperse Chitosan-Bound Fe_3O_4 Magnetic Nanoparticles for Removal of Cu(II) Ions. *J. Colloid Interface Sci.* **2005**, *283*, 446−451.
(42) Huang, S.-H.; Chen, D.-H. Rapid Removal of Heavy Metal Cations and Anions from Aqueous Solutions by an Amino-functionalized Magnetic Nano-Adsorbent. *J. Hazard. Mater.* **2009**, *163*, 174−179.
(43) Liu, J.-f.; Zhao, Z.-s.; Jiang, G.-b. Coating Fe_3O_4 Magnetic Nanoparticles with Humic Acid for High Efficient Removal of Heavy Metals in Water. *Environ. Sci. Technol.* **2008**, *42*, 6949−6954.
(44) Collier, D. C. The Itinerant Position of Yttrium as Evidenced by Carboxylic Acid Extraction. Ph.D. thesis, University of Tennessee, Knoxville, TN, 2012.
(45) Huang, C.-H. *Rare Earth Coordination Chemistry: Fundamentals and Applications*; Wiley: Singapore, 2010.
(46) Arago, J.; Bencini, A.; Bianchi, A.; Garcia-Espana, E.; Micheloni, M.; Paoletti, P.; Ramirez, J. A.; Paoli, P. Interaction of "Long" Open-Chain Polyazaalkanes with Hydrogen and Copper(II) Ions. *Inorg. Chem.* **1991**, *30*, 1843−1849.
(47) Koper, G. J. M.; van Duijvenbode, R. C.; Stam, D. D. P. W.; Steuerle, U.; Borkovec, M. Synthesis and Protonation Behavior of Comblike Poly(ethyleneimine). *Macromolecules* **2003**, *36*, 2500−2507.
(48) Borkovec, M.; Hamacek, J.; Piguet, C. Statistical Mechanical Approach to Competitive Binding of Metal Ions to Multi-Center Receptors. *Dalton Trans.* **2004**, 4096−4105.
(49) Dalla-Favera, N.; Hamacek, J.; Borkovec, M.; Jeannerat, D.; Ercolani, G.; Piguet, C. Tuneable Intramolecular Intermetallic Interactions as a New Tool for Programming Linear Heterometallic 4f−4f Complexes. *Inorg. Chem.* **2007**, *46*, 9312−9322.
(50) Riis-Johannessen, T.; Dalla Favera, N.; Todorova, T. K.; Huber, S. M.; Gagliardi, L.; Piguet, C. Understanding, Controlling and Programming Cooperativity in Self-Assembled Polynuclear Complexes in Solution. *Chem.—Eur. J.* **2009**, *15*, 12702−12718.
(51) Dalla Favera, N.; Kiehne, U.; Bunzen, J.; Hytteballe, S.; Lützen, A.; Piguet, C. Intermetallic Interactions Within Solvated Polynuclear Complexes: A Misunderstood Concept. *Angew. Chem., Int. Ed.* **2010**, *49*, 125−128.
(52) Zaim, A.; Favera, N. D.; Guenee, L.; Nozary, H.; Hoang, T. N. Y.; Eliseeva, S. V.; Petoud, S.; Piguet, C. Lanthanide Hexafluoroacetylacetonates vs. Nitrates for the Controlled Loading of Luminescent Polynuclear Single-Stranded Oligomers. *Chem. Sci.* **2013**, *4*, 1125−1136.
(53) Cotton, S. In *Lanthanide and Actinide Chemistry*; Woolins, D., Crabtree, B., Atwood, D., Meyer, G., Eds.; Wiley: Chichester, U.K., 2006; Chapter 4, pp 35−60.

Paper 9: Functionalized core-shell nanoparticles to retrieve REEs

Title:
Acid-Stable Magnetic Core–Shell Nanoparticles for the Separation of Rare Earths

Type: Full paper
Journal: Industrial & Engineering Chemistry Research (IF 2.59)
Publisher: American Chemical Society (ACS)
Publication date: 03/09/2014

[(a)]Experimental work carried out by Jakob Luyten under my supervision.

Electronic Supplementary Information (ESI) available: http://pubs.acs.org.

Graphical abstract

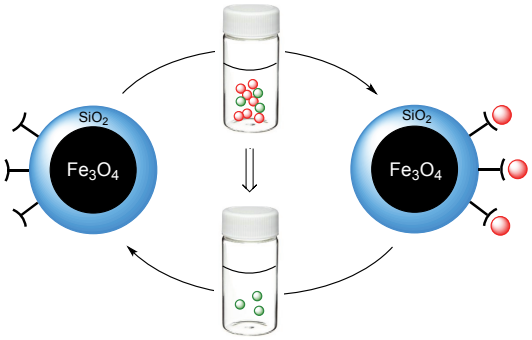

Magnetic Fe_3O_4 nanoparticles were coated with a SiO_2 shell and functionalized with EDTA to investigate the extraction and separation of rare-earth ions. The advantages of the SiO_2 shell include a larger grafting density and an improved resistance to acidic environments.

I&EC research
Industrial & Engineering Chemistry Research

Article

pubs.acs.org/IECR

Acid-Stable Magnetic Core−Shell Nanoparticles for the Separation of Rare Earths

David Dupont,[†] Jakob Luyten,[†] Maarten Bloemen,[‡] Thierry Verbiest,[‡] and Koen Binnemans*,[†]

[†]Molecular Design and Synthesis, Department of Chemistry, and [‡]Molecular Imaging and Photonics, Department of Chemistry, KU Leuven, B-3001 Heverlee, Belgium

Supporting Information

ABSTRACT: Core−shell Fe_3O_4@SiO_2 nanoparticles were prepared with a modified Stöber method and functionalized with *N*-[(3-trimethoxysilyl)propyl]ethylenediamine triacetic acid (TMS-EDTA). The synthesis was optimized to make core−shell nanoparticles with homogeneous and thin SiO_2 shells (4.8 ± 0.5 nm) around highly superparamagnetic Fe_3O_4 cores (14.5 ± 3.0 nm). The core−shell Fe_3O_4@SiO_2(TMS-EDTA) nanoparticles were then used for the extraction and separation of rare-earth ions. By comparing them with previously published results for Fe_3O_4(TMS-EDTA) and SiO_2(TMS-EDTA) nanoparticles, it was clear that the core−shell nanoparticles combine the advantage of magnetic retrieval observed for Fe_3O_4(TMS-EDTA) nanoparticles with the higher selectivity observed for SiO_2(TMS-EDTA). The advantages of the SiO_2 shell include a lower specific weight and a larger grafting density compared to Fe_3O_4 surfaces, but also the improved resistance to acidic environments required for the stripping of rare-earth ions.

1. INTRODUCTION

Magnetic nanoparticles are very interesting materials that can be recovered from solution with the use of a magnet.[1−3] Task-specific magnetic nanoparticles can be prepared by coating the surface with functional groups.[2,3] Applications are found in targeted drug delivery, biosensors, dual imaging compounds, recoverable catalysts, and selective recovery of metal ions or molecules.[3−15] Functionalized magnetic nanoparticles are well-suited for the selective extraction of metal traces from diluted wastewater streams or industrial effluents.[7−20] This is done by capturing metal ions in solution, retrieving the loaded nanoparticles with a magnet, and then stripping the metal ions from the nanoparticles. This is a sustainable process since the nanoparticles are reusable and no hazardous chemicals are involved. Most examples report on the recovery of transition metals, heavy metals, or precious metals.[7−25] On the other hand, the capture of rare-earth ions has been far less investigated.[16,21,26]

Core−shell nanoparticles are slightly more complex than conventional nanoparticles, but these hybrid materials can have significantly enhanced properties.[27−29] The core is usually a magnetic and vulnerable material such as magnetite or cobalt that is prone to oxidation or dissolution in acidic environments. These cores are capped with an inert shell of, e.g., SiO_2, TiO_2, ZrO_2, gold, graphene, or a polymer.[3,30−32] The shell protects the core from oxidation or attack by chemicals, and it can be further functionalized by attaching functional groups to its surface.[3,16,21−24] The advantage of layered materials can be the better stability or a synergy between different materials, which can result in unique chemical or physical properties.[27−29]

Functionalization of core−shell and regular nanoparticles can be achieved by covalent bonding, chemisorption, or electrostatic interactions of ligands onto their surface. Good results have been obtained with functionalized siloxanes, because these versatile compounds form strong covalent bonds with most oxide surfaces due to the presence of hydroxyl groups.[33−37] The large number of commercially available trialkoxysilanes with various functional groups offers unique possibilities for the task-specific surface modification of oxide nanoparticles.[16,35,38−41] The *N*-[(3-trimethoxysilyl)propyl]ethylenediamine triacetic acid (TMS-EDTA) used in this work is an EDTA derivative in which one of the carboxylate groups is replaced by an alkyl spacer with a reactive trialkoxysilane group for binding to the surface of the nanoparticle. EDTA has a good affinity for rare-earth ions and is also capable of separating them based on small differences in charge density.[42−44] TMS-EDTA was therefore the preferred ligand to decorate the surface of the nanoparticles. The covalently bonded TMS-EDTA also provides nanoparticles with a good resistance against the strongly acidic environments required for the stripping of rare-earth ions after coordination (pH <2).[26]

Recently, our group compared the adsorption capacity and selectivity of TMS-EDTA-functionalized Fe_3O_4, TiO_2, and SiO_2 nanoparticles to gain a better understanding of the influence of the substrate on the behavior of the surface group.[26] It was shown that TMS-EDTA-functionalized SiO_2 nanoparticles performed better than the analogous Fe_3O_4 or TiO_2 nanoparticles. This was attributed to the fact that SiO_2 contains the highest density of hydroxyl groups on its surface, resulting in a large grafting density of TMS-EDTA functional groups. This dense layer of TMS-EDTA groups is capable of binding high quantities of rare-earth ions, but it also exhibits a significant size-based selectivity. It was shown that a denser layer of TMS-EDTA results in a better separation between small and large rare-earth ions. However, both SiO_2 and TiO_2 nanoparticles are

Received: June 24, 2014
Revised: August 31, 2014
Accepted: September 3, 2014
Published: September 3, 2014

not magnetic, so their removal from solution is much more tedious than the fast magnetic retrieval that is possible for Fe_3O_4 nanoparticles. In this paper, core−shell nanoparticles were prepared consisting of magnetic Fe_3O_4 cores and a SiO_2 shell, which was subsequently functionalized with TMS-EDTA (Figure 1). The aim was to investigate whether these

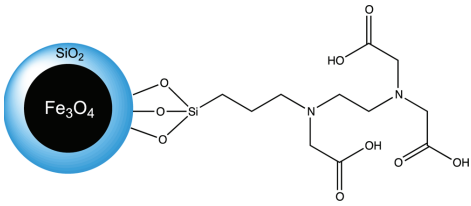

Figure 1. Core−shell Fe_3O_4@SiO_2 nanoparticle functionalized with TMS-EDTA.

functionalized core−shell nanoparticles could combine the advantage of magnetic retrieval, with the enhanced selectivity that was observed for TMS-EDTA attached to SiO_2 nanoparticles. The chemical stability and loss of efficiency of these core−shell nanoparticles were also investigated to evaluate their potential as high-performance, reusable sorbents for rare-earth ions.

2. EXPERIMENTAL SECTION

Chemicals. *N*-[(3-Trimethoxysilyl)propyl]ethylenediamine triacetic acid trisodium salt (TMS-EDTA) (45 wt %) was obtained from ABCR chemicals. Anhydrous $FeCl_3$ (97%) was purchased from Sigma-Aldrich. Ammonia (25 wt %) was obtained from Chem-Lab. Methanol (HPLC grade), absolute ethanol, glacial acetic acid, NaOH (97%), and HCl (37%) were purchased from VWR. $Sm(NO)_3{\cdot}6H_2O$ (99.9%), $Gd(NO_3)_3{\cdot}6H_2O$ (99.9%), $Er(NO_3)_3{\cdot}5H_2O$ (99.9%), *n*-octylamine (NOA) (99.9%), and tetraethyl orthosilicate (TEOS) (98%) were purchased from Acros Organics. $La(NO_3)_3{\cdot}6H_2O$ (99.9%) and $Pr(NO_3)_3{\cdot}6H_2O$ (99.9%) were supplied by Chempur. $Nd(NO_3)_3{\cdot}6H_2O$ (99.9%), $Tb(NO_3)_3{\cdot}5H_2O$ (99.9%), $Dy(NO_3)_3{\cdot}5H_2O$ (99.9%), and $Ho(NO_3)_3{\cdot}5H_2O$ (99.9%) were supplied by Alfa Aesar. All chemicals were used as received without further purification.

Equipment and Characterization. The nanoparticles were dispersed in a solvent using a Branson 5510 (10 L) and a Branson 2510 MTH (3 L) ultrasonic bath. The shaking during adsorption experiments was done with a mechanical shaker (IKA KS 130 basic). Particle imaging was done on a JEOL JEM2100 transmission electron microscope (TEM) using an acceleration voltage of 80 or 200 kV. ImageJ software was used for the size determination. The particles were dispersed in methanol (1 mg/mL) and deposited on a grid by solvent evaporation. Specific surface measurements were done by collecting nitrogen physisorption isotherms using a Micromeritics 3Flex surface characterization analyzer at 77 K. Prior to the measurement, the samples were outgassed at 353 K for 6 h under vacuum (Micromeritics VacPrep system). The BET method was applied in the 0.05−0.3 p/p_0 range using the 3Flex 3.00 software. Magnetization data were obtained with vibrating sample magnetometry (VSM) experiments performed on a VSM Maglab setup from Oxford Instruments at 300 K. Fourier transform infrared (FTIR) spectra were measured between 4000 and 400 cm^{-1} on a Bruker Vertex 70 spectrometer, with a platinum ATR module. Thermogravimetric analysis (TGA) was performed with a TA Instruments Q600 thermogravimeter, measuring from 25 to 1200 °C (10 °C/min, argon atmosphere). A CE Instruments EA-1110 elemental analyzer was used to measure the carbon, hydrogen, and nitrogen (CHN) content of the functionalized nanoparticles. The rare-earth concentrations were determined by total reflection X-ray fluorescence (TXRF) analysis on a benchtop Bruker S2 Picofox TXRF spectrometer equipped with a molybdenum X-ray source. This technique allows direct determination of the rare-earth content on the nanoparticles in dispersion. This is a major advantage of TXRF compared to inductively coupled plasma mass spectrometric (ICP-MS) analysis, where nanoparticles have to be digested in acid prior to analysis. For the sample preparation, Eppendorf microtubes were filled with an amount of sample solution (900 μL) and a similar concentration (10−100 ppm) of Ga^{3+} as internal standard (1000 ppm gallium dissolved in 2−3% HNO_3, Merck). Gallium was chosen because this element has a high sensitivity and does not interfere with the lanthanide signals. The microtubes were then vigorously shaken on a vibrating plate (IKA MS 3 basic). Finally, a 7 μL drop of this solution was put on a quartz plate, previously treated with a silicone/isopropyl alcohol solution (Serva) to avoid spreading of the sample droplet. The plates were then dried for 30 min at 60 °C prior to analysis. Each sample was measured for 30 min.

Synthesis of Fe_3O4@SiO_2 Nanoparticles. An in-house synthesis procedure was followed to prepare precursor Fe_3O_4 nanoparticles coated with *n*-octylamine.[45] Ethylene glycol (37.5 mL) and *n*-octylamine (NOA; 25 mL) were combined into a flask and heated to 150 °C. Anhydrous $FeCl_3$ (2.4 g) was dissolved in a beaker containing ethylene glycol (10 mL) and Milli-Q water (3.0 mL). The iron(III) solution was slowly added to the flask containing ethylene glycol and *n*-octylamine, and further heated to reflux at 180 °C for 24 h. The particles were precipitated from the reaction mixture by a small magnet and washed three times with acetone. Finally, they were dried in vacuo at room temperature for 20 min to obtain a black powder of Fe_3O_4(NOA) nanoparticles with a typical yield of 1 g. The silica shell was grown on these seeds using a modified and optimized Stöber method.[22,31] Fe_3O_4(NOA) nanoparticles (50 mg) were dispersed in ethanol (40 mL) by placing them in an ultrasonic bath for 1 h. Without removing the solution from the sonicator bath, NH_3 (25%; 2 mL) was added to the nanoparticle dispersion and TEOS (0.8 mL) was added dropwise over an hour. The solution was then left in the sonicator bath for another 5 h. The nanoparticles were settled using centrifugation (11 000 rpm, 15 min) and washed one time with water and two times with acetone. Finally, they were dried in vacuo (room temperature (RT)) for 30 min to obtain a grayish powder with a typical yield of 100 mg.

Functionalization Protocol. The Fe_3O_4@SiO_2 nanoparticles were functionalized with TMS-EDTA. The silanization procedure started by setting the pH at 4.5 with HCl (1 M) and then dispersing 100 mg of nanoparticles in MeOH/H_2O 85:15 (100 mL). The beaker was placed in an ultrasonic bath for 2 h. TMS-EDTA (1 mmol) was then added together with a few drops of glacial acetic acid. The beaker was placed for another 2 h in the ultrasonic bath. The particles were precipitated from the reaction mixture by a small magnet and washed one time with water and two times with acetone. Finally, they were dried

in vacuo at room temperature for 30 min, resulting in Fe_3O_4@SiO_2(TMS-EDTA) with a typical yield of 95−100 mg.

Procedure for Adsorption and Stripping Experiments. The TMS-EDTA functionalized core−shell nanoparticles were used to adsorb rare-earth ions from nitrate solutions and to separate rare-earth pairs. Adsorption and separation experiments started by dispersing 5 mg of nanoparticles in 5 mL of Milli-Q water using an ultrasonic bath (1 h). After a homogeneous dispersion of nanoparticles was obtained, single and binary rare-earth nitrate solutions were used to obtain the desired concentration of rare earths (1 mmol/L). This corresponds to 1 μmol of rare-earth ions per milligram of nanoparticles (an excess compared to the EDTA content). The pH was set using HCl (0.1 M) or NaOH (0.1 M), and the vials were placed on a mechanical shaker (240 rpm, 18 h). The particles were settled using a small NdFeB magnet. The solution was removed and the nanoparticles were washed two times with acetone to remove the remaining aqueous feed solution without influencing the adsorption equilibrium. The nanoparticles were then redispersed in 1 mL of Milli-Q water and the rare-earth content on the nanoparticles was analyzed with TXRF. The stripping of rare-earth ions from the nanoparticles was done by redispersing the washed nanoparticles in water (5 mL) and lowering the pH to 1.5 using an acidic HCl solution (1 M). The solution was then shaken for 2 h on a mechanical shaker (240 rpm).

3. RESULTS AND DISCUSSION

Optimizing the Synthesis of Fe_3O_4@SiO_2(TMS-EDTA) Nanoparticles. The magnetite nanoparticles were synthesized using a forced hydrolysis method.[26,45] The Fe_3O_4 nanoparticles are capped with *n*-octylamine to protect their surface and can be stored for months.[45] However, this weakly bound coating can be replaced by siloxane molecules in a later stage to allow further modification of the nanoparticle surface with functional groups or SiO_2 shells.[26,45] The synthesis of the SiO_2 shell and the functionalization with TMS-EDTA was investigated in detail and optimized for its use as nanosorbent. A modified Stöber method was used to grow SiO_2 shells around the Fe_3O_4 seeds with an average yield of 100 mg per batch. The thickness of the SiO_2 shell around the magnetite core could be tuned by varying the NH_3/TEOS ratio but was also influenced by other parameters such as the solvent/reagent ratio.[32] The thickness is related to the size of the Si−O−Si band in the infrared spectrum at 1091 cm^{-1} (Figure 2). Methods A and B yielded poor nanoparticles, with insufficient covering of silica. Method C, D, and E were much more successful and ensured a reproducible covering of the nanoparticles with a thin but homogeneous layer of silica. The synthesis method that was retained used the following ratio of reagents: ethanol (40 mL), 25% NH_3 (2 mL), and TEOS (0.8 mL) (method E). This method yields nanoparticles with a homogeneous 4.8 ± 0.5 nm thick SiO_2 shell (TEM). This thickness is the right compromise between a good protection of the nanoparticle core, without losing too much surface area.

The functionalization parameters have great influence on the quality of the functional coating. The functionalization reaction of Fe_3O_4@SiO_2 nanoparticles with TMS-EDTA is pH-dependent because the hydrolysis rate of the alkoxysilanes is pH-controlled.[33] Acidic conditions are required for the controlled silanization of the surface (pH 3−5) because an alkaline pH causes rapid polymerization of the silane chains.[33,34] The solvent composition is also important. Water increases the hydrolysis rate while methanol slows it down. Different methanol/water ratios were tested to optimize the degree of functionalization (Figure 3) The success of the functionalization was monitored by FTIR spectroscopy by looking at the intensity of the carboxylate bands.[7] The compiled FTIR spectra (Figure 3) show the intense asymmetrical stretch of the carboxylate groups around 1650 cm^{-1} accompanied by the symmetrical stretch around 1400 cm^{-1}. Pure methanol was not an ideal solvent for the hydrophilic TMS-EDTA and caused partial precipitation, whereas pure water caused a too fast hydrolysis of the silanes resulting in rapid polymerization and a bad functionalization. A methanol/water volume ratio of 85:15 was chosen because of the reproducibility and the high quality of the functional coating prepared under these conditions.

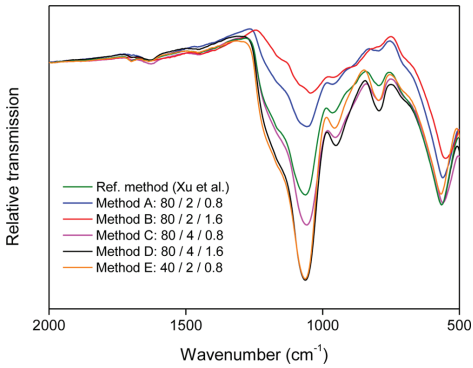

Figure 2. FTIR spectra of Fe_3O_4@SiO_2 samples from different synthesis methods. The influence of the reagent ratio on the Si−O peak at 1091 cm^{-1} is shown. The ratio of reagents is given as ethanol (mL)/25% NH_3 (mL)/TEOS (mL).

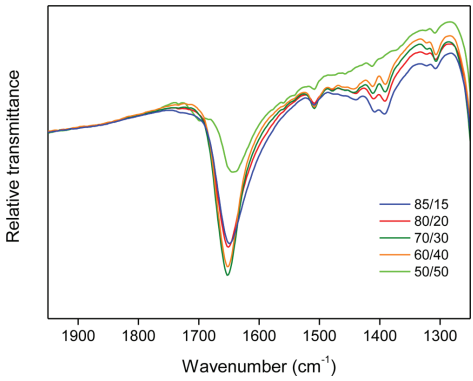

Figure 3. FTIR spectra of different Fe_3O_4@SiO_2(TMS-EDTA) samples. The influence of the solvent (MeOH/H_2O ratio) on the carboxylate peaks at 1650 and 1400 cm^{-1} is shown. This signal is related to the degree of TMS-EDTA functionalization.

Characterization of Nanoparticles. The core−shell Fe_3O_4@SiO_2(TMS-EDTA) nanoparticles were characterized

by FTIR, CHN, TGA, BET, and TEM analysis. All TGA curves for Fe_3O_4@SiO_2 and Fe_3O_4@SiO_2(TMS-EDTA) can be found in the Supporting Information (Figure S2). The average TMS-EDTA content obtained from CHN analysis was 4.2 ± 0.3 wt %, compared to 3.0 wt % determined by TGA analysis. The average of both analytical techniques was used, which indicates that the nanoparticles contain 0.12 μmol/mg TMS-EDTA. This value is useful for comparison with the adsorption experiments. Vibrating sample magnetometry showed that the superparamagnetic Fe_3O_4(NOA) seeds had a saturation magnetization of 66 emu/g (Supporting Information, Figure S1). TEM images showed that the functionalized core−shell Fe_3O_4@SiO_2(TMS-EDTA) nanoparticles had a diameter of 24.1 ± 4.0 nm (Figure 4B). The Fe_3O_4(NOA) seeds had a relatively well-

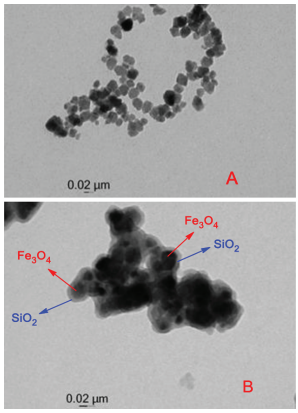

Figure 4. TEM images of (A) Fe_3O_4(NOA) seeds and (B) Fe_3O_4@SiO_2(TMS-EDTA) nanoparticles. The magnetic core and the thin homogeneous SiO_2 shell are indicated on image B.

defined spherical shape and an average diameter of 14.5 ± 3.0 nm (Figure 4A). The SiO_2 shell on the core−shell Fe_3O_4@SiO_2 nanoparticles had a thickness of 4.8 ± 0.5 nm (Figure 4B). The aggregation of the core−shell nanoparticles in Figure 4 is due to the TEM sample preparation. During the solvent evaporation the nanoparticles aggregate on the grid.

Since the SiO_2 shell is thin and homogeneous, this results in a relatively high specific surface area. The specific surface area of the nanoparticles was 44.1 m^2/g as determined by surface analysis using the BET method. This is an important characteristic for a sorbent nanoparticle. A thin SiO_2 shell is also important to maintain a high magnetic susceptibility, required for a fast magnetic removal of the nanoparticles from solution. The core−shell Fe_3O_4@SiO_2(TMS-EDTA) nanoparticles are quite hydrophilic due to the deprotonated carboxylate groups, thus forming very homogeneous and stable dispersions at pH 6 (used for adsorption experiments). Once they bind lanthanide ions, the surface charge diminishes and the nanoparticles can be removed from solution efficiently. Full retrieval (>99.9%) was possible within 10 s (Figure 5). Additionally, during stripping the carboxylate groups are protonated due to the acidic conditions (pH 1.5), making them less hydrophilic and therefore easy to retrieve. This greatly facilitates the adsorption/stripping process.

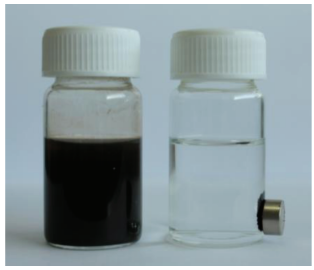

Figure 5. Magnetic retrieval of Fe_3O_4@SiO_2(TMS-EDTA) nanoparticles dispersed in water (1 mg/mL), before (left) and after 10 s (right).

Adsorption and Stripping of Rare Earths. The adsorption of rare earths is pH-dependent because TMS-EDTA contains three carboxylic acid groups that are gradually deprotonated at increasing pH values. An excess of rare-earth ions was used and the samples were shaken for 18 h to ensure that a maximal adsorption was reached. Nd^{3+} was chosen as a model system because of its industrial relevance. Complex formation was observed between pH 3 and 6 (Figure 6). The

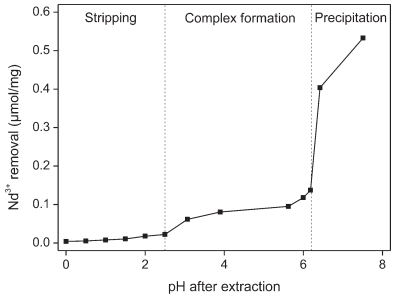

Figure 6. Nd^{3+} removal from solution by Fe_3O_4@SiO_2(TMS-EDTA) nanoparticles as a function of pH. Depending on the pH, different domains were identified where the Nd^{3+} could be adsorbed by the nanoparticles, precipitated, or stripped back from the nanoparticles.

excess of rare-earth ions helps to visualize the precipitation threshold. There is still complex formation at pH values higher than 6, but also hydrolysis and precipitation of the lanthanide ions. This pH range is therefore not convenient since the precipitation interferes with the complex formation. Below pH 2.5, the Nd^{3+} adsorption is quite low; therefore this lower pH range can be used to strip the lanthanide ions from the nanoparticles.

Adsorption of rare-earth ions is best performed at pH 6, resulting in an adsorption of 0.118 μmol/mg (17.0 mg/g) for Nd^{3+}. An excess of Nd^{3+} was used to obtain the maximal adsorption capacity. This value (0.118 μmol/mg) is in good agreement with the TMS-EDTA content on the surface of the nanoparticle (0.12 μmol/mg). If the adsorption capacity is compared with other nanoparticles described in the literature (Table 1), it is well within the range of most reported chelating nanoparticles. However, the main advantage of these nano-

Table 1. Literature Overview of Magnetic Chelating Nanoparticles with Their Maximal Adsorption Capacity, Compared with the Nanoparticles Described in This Work[8,16,20,21,26,46,47]

particle(ligand)	particle size (nm)	surf. group content (wt %)	ion	ion uptake (mg/g)
Fe_3O_4@SiO_2(TMS-EDTA)[a]	24.1	3.6	Nd^{3+}	17.0
Fe_3O_4(TMS-EDTA)[26]	10.5	16	Gd^{3+}	113
Fe_3O_4(humic acid)[21]	14	15.5	Eu^{3+}	10.6
Fe_3O_4@SiO_2(P507)[16]	500	13.9	La^{3+}	55.9
Fe_3O_4(PEI)(DTPA)[20]	50	6.4	Cu^{2+}	12.1
Fe_3O_4(EDTA)[8]	312.3	7.8	Cu^{2+}	46.3
Fe_3O_4(chitosan)[47]	13.5	4.9	Cu^{2+}	21.5
Fe_3O_4(dien)[46]	11.6	N/A	Cu^{2+}	12.43

[a]This is the core−shell nanoparticle described in this paper.

particles is not their adsorption capacity, but their selectivity and ability to separate rare-earth ions from each other.

The adsorption kinetics were also investigated by contacting the nanoparticles with an excess of Nd^{3+} ions at pH 6.0 for increasing periods of time (mechanical shaker, 240 rpm). The results show a saturation of the nanoparticles with Nd^{3+}ions after 6 h (Figure 7). However, during most adsorption

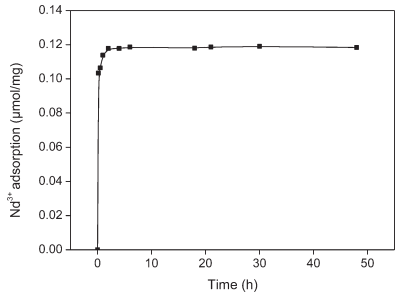

Figure 7. Adsorption kinetics for Nd^{3+} ions with Fe_3O_4@SiO_2(TMS-EDTA) nanoparticles.

experiments the samples were shaken overnight (18 h) for convenience. The relatively long equilibrium times are attributed to the dense layer of EDTA on the surface, which is also responsible for the better than expected size-based selectivity that was observed (see Separation of Rare Earths).

The stripping efficiency as a function of pH was tested, together with the stability of the core−shell nanoparticles. After the nanoparticles were fully loaded with a solution containing an excess of Nd^{3+} ions, the nanoparticles were isolated. The nanoparticles were then contacted with an acidic solution to protonate the carboxylate groups and release the Nd^{3+} ions back in solution. For this stripping step, the pH was set using HCl (1 M) and the solutions were shaken for 2 h (same result as for 24 h). The damage to the nanoparticles was measured by analyzing the iron content in the stripping solution with TXRF, after 24 h of shaking. This iron content was then translated into a particle loss (percent). Stripping is best performed at pH 1.5 in order to have the right compromise between a high stripping efficiency (94%) and little damage to the nanoparticles (<0.5% particle loss) (Figure 8).

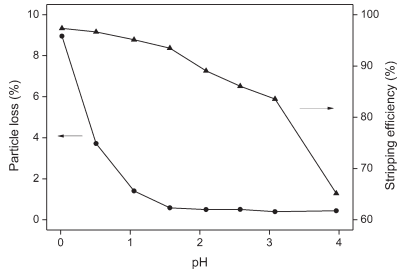

Figure 8. Stripping efficiency and particle loss (determined by TXRF) as a function of pH for core−shell nanoparticles, fully loaded with Nd^{3+} ions.

By comparing the stability of the core−shell nanoparticles with the simple (core) magnetite nanoparticles, it is clear that the SiO_2 shell significantly increased the resistance of magnetite nanoparticles to acidic solutions (Figure 9). The SiO_2 shell is

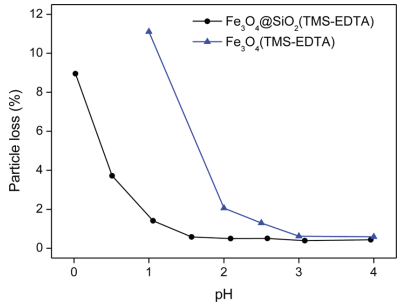

Figure 9. Stability of functionalized magnetite nanoparticles compared with the stability of functionalized core−shell nanoparticles after shaking for 24 h in an acidic solution. The pH was set with an HCl solution.

only 4.8 nm thick, but it drastically increases the stability of the nanoparticles. SiO_2 is much less sensitive to degradation by HCl than Fe_3O_4 that is easily dissolved as $FeCl_3$. The increased stability of core−shell nanoparticles in acidic solutions is particularly useful for metal binding surface groups that require harsher stripping conditions.

This increased stability is also translated into a good reusability. A sequence of five adsorption (pH 6.0) and stripping (pH 1.5) cycles with an excess of Nd^{3+} ions shows the evolution of the adsorption capacity of the core−shell nanoparticles (Figure 10). The experiments were done three times to reduce the experimental error. During the first cycle, a loss of adsorption capacity was observed from 0.118 to 0.092 μmol/mg. This is due to the release of some of the less well bonded TMS-EDTA groups or some irreversible adsorption. During the functionalization, some of the TMS-EDTA groups are weakly bound to other TMS-EDTA groups through one Si−O−Si linker. This partial oligomerization is an unavoidable phenomenon for trialkoxysilanes; however, most TMS-EDTA groups are firmly attached to the SiO_2 surface with three Si−O−Si bonds.[36] After this initial drop in adsorption capacity, the

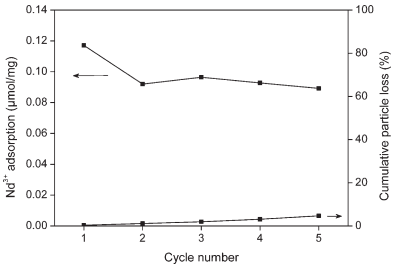

Figure 10. Evolution of adsorption capacity and particle loss over five adsorption/stripping cycles of Nd^{3+} ions with Fe_3O_4@SiO_2(TMS-EDTA) nanoparticles.

adsorption capacity then stabilized and remained practically unchanged over the next four adsorption/stripping cycles. The initial drop in adsorption capacity can be avoided by washing the synthesized nanoparticles one time with a pH 1.5 HCl solution, before using them in adsorption experiments. The particle loss in each cycle increased slightly from 0.3% in cycle 1 to 1.6% in cycle 5, resulting in a cumulated particle loss of 4.7%. Furthermore, it should be mentioned that no particle degradation was observed visually. The supernatant remained completely colorless (Figure 5). This indicates that the particle loss is very limited and is most likely also due to process steps. The particles have to be transferred multiple times in different flasks, inevitably leading to some loss of particles along the way. Small quantities of nanoparticles were used (10 mg); therefore the percent particle loss seems higher even though only 0.47 mg of particles was lost after five adsorption/stripping cycles. The average stripping efficiency over the five cycles was 93%, which is in agreement with previously mentioned results (Figure 8).

Separation of Rare Earths. The separation of rare earths as a group from other elements is usually relatively efficient, and based on differences in oxidation state or chemical behavior.[48] However, the mutual separation of a mixture of rare-earth ions is a challenge because of their common +III oxidation state and very similar chemical behavior. Most current techniques are based on the small differences in ionic radii.[42] The selectivity of the functionalized core−shell nanoparticles was investigated and reported using enrichment factors (EFs). The enrichment factor compares the molar ratio of elements A and B before and after separation, according to eq 1. B was chosen to be the heavier (smaller) of the two rare-earth ions because this results in an enrichment factor of >1.

$$\mathrm{EF} = \frac{\left(\frac{\mathrm{B}}{\mathrm{A}}\right)_{\text{on nanoparticles}}}{\left(\frac{\mathrm{B}}{\mathrm{A}}\right)_{\text{feed solution}}} \quad (1)$$

The separation of Er^{3+}/La^{3+} was chosen as a model to investigate the influence of the pH on the selectivity. The relatively large difference in ionic radius results in a high enrichment factor which helps to visualize a possible trend. An excess of rare-earth ions was used compared to the amount of TMS-EDTA groups and the rare-earth pairs were present in a 1:1 molar ratio. The core−shell Fe_3O_4@SiO_2(TMS-EDTA) nanoparticles display the highest selectivity around pH 6 (Figure 11). At this pH, TMS-EDTA also has a high adsorption capacity and selectivity. Higher pH values cause hydrolysis and precipitation of lanthanide ions (Figure 6).

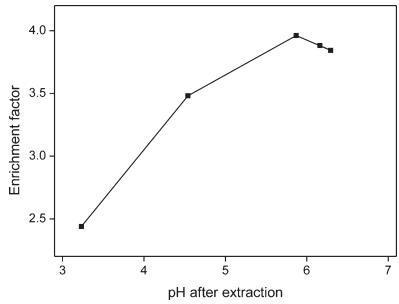

Figure 11. Influence of pH on separation of Er^{3+}/La^{3+} by core−shell Fe_3O_4@SiO_2(TMS-EDTA) nanoparticles.

Furthermore, the selectivity of the core−shell Fe_3O_4@SiO_2(TMS-EDTA) nanoparticles toward different pairs of lanthanide ions was investigated and compared with previously published results for Fe_3O_4(TMS-EDTA) and SiO_2(TMS-EDTA).[26] Ln^{3+}/La^{3+} separations showed that the core−shell nanoparticles behaved similarly to SiO_2(TMS-EDTA) (Figure 12).

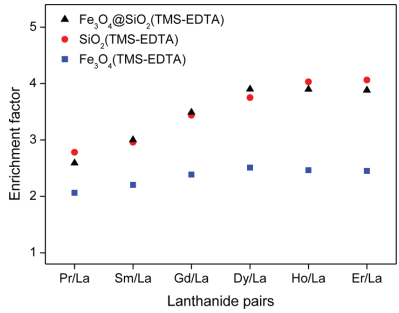

Figure 12. Separation of Ln^{3+}/La^{3+} rare-earth pairs (pH 6.0) with increasingly different ionic radii from left to right. The results for Fe_3O_4@SiO_2(TMS-EDTA) particles are compared with previously published data for Fe_3O_4(TMS-EDTA) and SiO_2(TMS-EDTA) nanoparticles.[26]

One can notice that the enhanced selectivity of TMS-EDTA on SiO_2 substrates was also observed for the core−shell nanoparticles.[26] This further supports the hypothesis that the higher density of TMS-EDTA groups on SiO_2 surfaces is responsible for this enhanced size-based selectivity.[26] It must be noted that the enrichment factor increases rapidly at the beginning of the Ln^{3+}/La^{3+} separation series and stagnates for the heaviest lanthanides. This is a well-known trend for solvent extraction and aminocarboxylate ligands.[42,43] Another explanation for this can be that the heavier (smaller) lanthanide ions are able to penetrate the dense TMS-EDTA surface layer more easily, making the size-based selectivity less efficient.

4. CONCLUSIONS

Core−shell Fe_3O_4@SiO_2 nanoparticles were synthesized and functionalized with metal-coordinating TMS-EDTA groups. The idea was that this type of hybrid nanoparticles could combine the advantage of magnetic retrieval (Fe_3O_4 core) with the higher selectivity that had been observed when TMS-EDTA was attached to SiO_2 compared to Fe_3O_4 nanoparticles.[26] Thin and homogeneous SiO_2 shells (4.8 ± 0.5 nm thick) were grown around Fe_3O_4 cores (14.5 ± 3.0 nm diameter), using a modified and optimized Stöber method. This synthesis protocol allowed synthesizing high-quality Fe_3O_4@SiO_2(TMS-EDTA) nanoparticles. It was also shown that the functionalized SiO_2 shell offers a good size-based separation of rare-earth ions similar to the selectivity that had been previously observed for SiO_2(TMS-EDTA) nanoparticles, but with the added advantage of magnetic retrieval.[26] The fact that these core−shell nanoparticles combine the advantages of both the possibility of magnetic retrieval and a high selectivity for the metal sorption makes this a very interesting sorbent for the selective recovery of rare-earth ions from dilute aqueous solutions. The nanoparticles showed a good chemical stability even in strongly acidic environments thanks to the SiO_2 shell. The reusability of the nanoparticles was also satisfactory with the adsorption capacity remaining stable after the first adsorption/stripping cycle.

■ ASSOCIATED CONTENT

Ⓢ Supporting Information

VSM measurement of the magnetite seed particles Fe_3O_4(NOA) and TGA measurements for Fe_3O_4@SiO_2 and Fe_3O_4@SiO_2(TMS-EDTA). Infrared spectra of Fe_3O_4, Fe_3O_4@SiO_2, and Fe_3O_4@SiO_2(TMS-EDTA) nanoparticles. This material is available free of charge via the Internet at http://pubs.acs.org.

■ AUTHOR INFORMATION

Corresponding Author

*E-mail: Koen.Binnemans@chem.kuleuven.be.

Notes

The authors declare no competing financial interest.

■ ACKNOWLEDGMENTS

The authors thank the KU Leuven (Projects GOA/13/008 and IOF-KP RARE^3) and the FWO Flanders (Ph.D. fellowship to D.D.) for financial support. CHN analyses were performed by Dirk Henot, and TGA measurements were performed by Danny Winant and Dr. Stijn Schaltin. VSM was measured by Ward Brullot, and the BET surface analysis was performed by Ivo Stassen.

■ REFERENCES

(1) Hao, R.; Xing, R.; Xu, Z.; Hou, Y.; Gao, S.; Sun, S. Synthesis, Functionalization, and Biomedical Applications of Multifunctional Magnetic Nanoparticles. *Adv. Mater.* **2010**, *22*, 2729.

(2) Lu, A.-H.; Salabas, E. L.; Schüth, F. Magnetic Nanoparticles: Synthesis, Protection, Functionalization, and Application. *Angew. Chem., Int. Ed.* **2007**, *46*, 1222.

(3) Grass, R. N.; Athanassiou, E. K.; Stark, W. J. Covalently Functionalized Cobalt Nanoparticles as a Platform for Magnetic Separations in Organic Synthesis. *Angew. Chem., Int. Ed.* **2007**, *46*, 4909.

(4) Liu, Z.; Li, B.; Wang, B.; Yang, Z.; Wang, Q.; Li, T.; Qin, D.; Li, Y.; Wang, M.; Yan, M. Magnetic Nanoparticles Modified with DTPA-AMC-Rare Earth for Fluorescent and Magnetic Resonance Dual Mode Imaging. *Dalton Trans.* **2012**, *41*, 8723.

(5) Wang, B.; Hai, J.; Wang, Q.; Li, T.; Yang, Z. Coupling of Luminescent Terbium Complexes to Fe_3O_4 Nanoparticles for Imaging Applications. *Angew. Chem., Int. Ed.* **2011**, *50*, 3063.

(6) Xi, P.; Cheng, K.; Sun, X.; Zeng, Z.; Sun, S. Magnetic Fe_3O_4 Nanoparticles Coupled with a Fluorescent Eu Complex for Dual Imaging Applications. *Chem. Commun.* **2012**, *48*, 2952.

(7) Goon, I. Y.; Zhang, C.; Lim, M.; Gooding, J. J.; Amal, R. Controlled Fabrication of Polyethylenimine-Functionalized Magnetic Nanoparticles for the Sequestration and Quantification of Free Cu^{2+}. *Langmuir* **2010**, *26*, 12247.

(8) Liu, Y.; Chen, M.; Yongmei, H. Study on the Adsorption of Cu(II) by EDTA Functionalized Fe_3O_4 Magnetic Nano-Particles. *Chem. Eng. J.* **2013**, *218*, 46.

(9) Ren, Y.; Abbood, H. A.; He, F.; Peng, H.; Huang, K. Magnetic EDTA-modified Chitosan/SiO_2/Fe_3O_4 Adsorbent: Preparation, Characterization, and Application in Heavy Metal Adsorption. *Chem. Eng. J.* **2013**, *226*, 300.

(10) Sun, L.; Li, Y.; Sun, M.; Wang, H.; Xu, S.; Zhang, C.; Yang, Q. Porphyrin-Functionalized Fe_3O_4@SiO_2 Core/Shell Magnetic Colorimetric Material for Detection, Adsorption and Removal of Hg^{2+} in Aqueous Solution. *New J. Chem.* **2011**, *35*, 2697.

(11) Warner, C. L.; Addleman, R. S.; Cinson, A. D.; Droubay, T. C.; Engelhard, M. H.; Nash, M. A.; Yantasee, W.; Warner, M. G. High-Performance, Superparamagnetic, Nanoparticle-Based Heavy Metal Sorbents for Removal of Contaminants from Natural Waters. *ChemSusChem* **2010**, *3*, 749.

(12) Rossier, M.; Koehler, F. M.; Athanassiou, E. K.; Grass, R. N.; Aeschlimann, B.; Gunther, D.; Stark, W. J. Gold Adsorption on the Carbon Surface of C/Co Nanoparticles Allows Magnetic Extraction from Extremely Diluted Aqueous Solutions. *J. Mater. Chem.* **2009**, *19*, 8239.

(13) Rossier, M.; Koehler, F. M.; Athanassiou, E. K.; Grass, R. N.; Waelle, M.; Birbaum, K.; Günther, D.; Stark, W. J. Energy-Efficient Noble Metal Recovery by the Use of Acid-stable Nanomagnets. *Ind. Eng. Chem. Res.* **2010**, *49*, 9355.

(14) Yantasee, W.; Warner, C. L.; Sangvanich, T.; Addleman, R. S.; Carter, T. G.; Wiacek, R. J.; Fryxell, G. E.; Timchalk, C.; Warner, M. G. Removal of Heavy Metals from Aqueous Systems with Thiol Functionalized Superparamagnetic Nanoparticles. *Environ. Sci. Technol.* **2007**, *41*, 5114.

(15) Hao, Y.-M.; Man, C.; Hu, Z.-B. Effective Removal of Cu (II) Ions from Aqueous Solution by Amino-functionalized Magnetic Nanoparticles. *J. Hazard. Mater.* **2010**, *184*, 392.

(16) Wu, D.; Sun, Y.; Wang, Q. Adsorption of Lanthanum (III) from Aqueous Solution Using 2-ethylhexyl Phosphonic Acid Mono-2-ethylhexyl Ester-Grafted Magnetic Silica Nanocomposites. *J. Hazard. Mater.* **2013**, *260*, 409.

(17) Saiz, J.; Bringas, E.; Ortiz, I. New Functionalized Magnetic Materials for As^{5+} Removal: Adsorbent Regeneration and Reuse. *Ind. Eng. Chem. Res.* **2014**, DOI: 10.1021/ie500912k.

(18) Zargoosh, K.; Abedini, H.; Abdolmaleki, A.; Molavian, M. R. Effective Removal of Heavy Metal Ions from Industrial Wastes Using Thiosalicylhydrazide-Modified Magnetic Nanoparticles. *Ind. Eng. Chem. Res.* **2013**, *52*, 14944.

(19) Zhang, F.; Shi, Y.; Zhao, Z.; Ma, B.; Wei, L.; Lu, L. Amino-functionalized Fe_3O_4/SiO_2 Magnetic Submicron Composites and In^{3+} Ion Adsorption Properties. *J. Mater. Sci.* **2014**, *49*, 3478.

(20) Koehler, F. M.; Rossier, M.; Waelle, M.; Athanassiou, E. K.; Limbach, L. K.; Grass, R. N.; Gunther, D.; Stark, W. J. Magnetic EDTA: coupling heavy metal chelators to metal nanomagnets for rapid removal of cadmium, lead and copper from contaminated water. *Chem. Commun.* **2009**, 4862.

(21) Yang, S.; Zong, P.; Ren, X.; Wang, Q.; Wang, X. Rapid and Highly Efficient Preconcentration of Eu(III) by Core−Shell Structured Fe_3O_4@Humic Acid Magnetic Nanoparticles. *ACS Appl. Mater. Interfaces* **2012**, *4*, 6891.

(22) Xu, Y.; Zhou, Y.; Ma, W.; Wang, S.; Li, S. Functionalized Magnetic Core−shell Fe_3O_4@SiO_2 Nanoparticles for Sensitive Detection and Removal of Hg^{2+}. *J. Nanopart. Res.* **2013**, *15*, 1.
(23) Li, Y.; Wu, J.; Qi, D.; Xu, X.; Deng, C.; Yang, P.; Zhang, X. Novel Approach for the Synthesis of Fe_3O_4@TiO_2 Core-Shell Microspheres and their Application to the Highly Specific Capture of Phosphopeptides for MALDI-TOF MS Analysis. *Chem. Commun.* **2008**, *5*, 564.
(24) Huang, C.; Hu, B. Silica-coated Magnetic Nanoparticles Modified with γ-Mercaptopropyltrimethoxysilane for Fast and Selective Solid Phase Extraction of Trace Amounts of Cd, Cu, Hg, and Pb in Environmental and Biological Samples Prior to their Determination by Inductively Coupled Plasma Mass Spectrometry. *Spectrochim. Acta, Part B* **2008**, *63*, 437.
(25) Saman, N.; Johari, K.; Mat, H. Adsorption Characteristics of Sulfur-Functionalized Silica Microspheres with Respect to the Removal of Hg(II) from Aqueous Solutions. *Ind. Eng. Chem. Res.* **2014**, *53*, 1225.
(26) Dupont, D.; Brullot, W.; Bloemen, M.; Verbiest, T.; Binnemans, K. Selective Uptake of Rare Earths from Aqueous Solutions by EDTA-functionalized Magnetic and Non-magnetic Nanoparticles. *ACS Appl. Mater. Interfaces* **2014**, *6*, 4980.
(27) Wei, S.; Wang, Q.; Zhu, J.; Sun, L.; Lin, H.; Guo, Z. Multifunctional Composite Core-Shell Nanoparticles. *Nanoscale* **2011**, *3*, 4474.
(28) Schartl, W. Current Directions in Core-shell Nanoparticle Design. *Nanoscale* **2010**, *2*, 829.
(29) Ghosh Chaudhuri, R.; Paria, S. Core/Shell Nanoparticles: Classes, Properties, Synthesis Mechanisms, Characterization, and Applications. *Chem. Rev.* **2011**, *112*, 2373.
(30) Morel, A.-L.; Nikitenko, S. I.; Gionnet, K.; Wattiaux, A.; Lai-Kee-Him, J.; Labrugere, C.; Chevalier, B.; Deleris, G.; Petibois, C.; Brisson, A.; Simonoff, M. Sonochemical Approach to the Synthesis of Fe_3O_4@SiO_2 Core−Shell Nanoparticles with Tunable Properties. *ACS Nano* **2008**, *2*, 847.
(31) Hui, C.; Shen, C.; Tian, J.; Bao, L.; Ding, H.; Li, C.; Tian, Y.; Shi, X.; Gao, H.-J. Core-shell Fe_3O_4@SiO_2 Nanoparticles Synthesized with Well-dispersed Hydrophilic Fe_3O_4 Seeds. *Nanoscale* **2011**, *3*, 701.
(32) Ding, H. L.; Zhang, Y. X.; Wang, S.; Xu, J. M.; Xu, S. C.; Li, G. H. Fe_3O_4@SiO_2 Core/Shell Nanoparticles: The Silica Coating Regulations with a Single Core for Different Core Sizes and Shell Thicknesses. *Chem. Mater.* **2012**, *24*, 4572.
(33) Witucki, G. L. A Silane Primer—Chemistry and Applications of Alkoxy Silanes. *J. Coat. Technol.* **1993**, *65*, 57.
(34) Hermanson, G. T. In *Bioconjugate Techniques*, 2nd ed.; Hermanson, G. T., Ed.; Academic Press: New York, 2008; pp 562−581.
(35) De Palma, R.; Peeters, S.; Van Bael, M. J.; Van den Rul, H.; Bonroy, K.; Laureyn, W.; Mullens, J.; Borghs, G.; Maes, G. Silane Ligand Exchange to Make Hydrophobic Superparamagnetic Nanoparticles Water-Dispersible. *Chem. Mater.* **2007**, *19*, 1821.
(36) Fadeev, A. Y.; McCarthy, T. J. Self-Assembly Is Not the Only Reaction Possible Between Alkyltrichlorosilanes and Surfaces: Monomolecular and Oligomeric Covalently Attached Layers of Dichloro- and Trichloroalkylsilanes on Silicon. *Langmuir* **2000**, *16*, 7268.
(37) Onclin, S.; Ravoo, B. J.; Reinhoudt, D. N. Engineering Silicon Oxide Surfaces Using Self-Assembled Monolayers. *Angew. Chem., Int. Ed.* **2005**, *44*, 6282.
(38) Tucker-Schwartz, A. K.; Farrell, R. A.; Garrell, R. L. Thiol−ene Click Reaction as a General Route to Functional Trialkoxysilanes for Surface Coating Applications. *J. Am. Chem. Soc.* **2011**, *133*, 11026.
(39) Larsen, B. A.; Hurst, K. M.; Ashurst, W. R.; Serkova, N. J.; Stoldt, C. R. Mono and Dialkoxysilane Surface Modification of Superparamagnetic Iron Oxide Nanoparticles for Application as Magnetic Resonance Imaging Contrast Agents. *J. Mater. Res.* **2012**, *27*, 1846.
(40) Bloemen, M.; Brullot, W.; Luong, T. T.; Geukens, N.; Gils, A.; Verbiest, T. Improved Functionalization of Oleic Acid-Coated Iron Oxide Nanoparticles for Biomedical Applications. *J. Nanopart. Res.* **2012**, *14*, 1100.
(41) Wu, W.; He, Q. G.; Jiang, C. Z. Magnetic Iron Oxide Nanoparticles: Synthesis and Surface Functionalization Strategies. *Nanoscale Res. Lett.* **2008**, *3*, 397.
(42) Xie, F.; Zhang, T. A.; Dreisinger, D.; Doyle, F. A Critical Review on Solvent Extraction of Rare Earths from Aqueous Solutions. *Miner. Eng.* **2014**, *56*, 10.
(43) Choppin, G. R.; Goedken, M. P.; Gritmon, T. F. The Complexation of Lanthanides by Aminocarboxylate Ligands—II. *J. Inorg. Nucl. Chem.* **1977**, *39*, 2025.
(44) Cotton, S. In *Lanthanide and Actinide Chemistry*; Wiley: Chichester, U.K., 2006; Chapter 4, pp 35−60.
(45) Brullot, W.; Reddy, N. K.; Wouters, J.; Valev, V. K.; Goderis, B.; Vermant, J.; Verbiest, T. Versatile Ferrofluids Based on Polyethylene Glycol Coated Iron Oxide Nanoparticles. *J. Magn. Magn. Mater.* **2012**, *324*, 1919.
(46) Huang, S.-H.; Chen, D.-H. Rapid Removal of Heavy Metal Cations and Anions from Aqueous Solutions by an Amino-functionalized Magnetic Nano-Adsorbent. *J. Hazard. Mater.* **2009**, *163*, 174.
(47) Chang, Y.-C.; Chen, D.-H. Preparation and Adsorption Properties of Monodisperse Chitosan-Bound Fe_3O_4 Magnetic Nanoparticles for Removal of Cu(II) Ions. *J. Colloid Interface Sci.* **2005**, *283*, 446.
(48) Vander Hoogerstraete, T.; Wellens, S.; Verachtert, K.; Binnemans, K. Removal of Transition Metals from Rare earths by Solvent Extraction with an Undiluted Phosphonium Ionic Liquid: Separations Relevant to Rare-earth Magnet Recycling. *Green Chem.* **2013**, *15*, 919.

4 Science communication to a broad audience

Besides scientific publications, I also published several articles intended as science communication for a broader audience.

Article 1: Recycling International (October 2015)

RESEARCH

Leuven lab discovers selective recycling process

As the name implies, rare earths are not as abundant as some commonly-used elements. And yet many of them are vital components in a range of modern technologies; hence the constant debate in recent years surrounding supply threats. Recycling is therefore an important consideration where rare earths are concerned, and this article examines a more sustainable and energy-efficient alternative for the recycling of lamp phosphor waste. To date, the process only applies to laboratory conditions.

Figure 2: Urban mining efforts such as the recycling of fluorescent lamps can help guarantee a sustainable supply of critical elements.

The rare earths are a group of metals that are essential to modern-day technologies such as hard disk drives, wind turbines, electric cars, energy-saving light bulbs and speakers. The two main markets for rare earths are strong permanent magnets and fluorescent lamp phosphors, together accounting for 70% of the value of the rare-earth market. Other applications such as polishing powders attract very large volumes of rare earths but have a lower added value.

Today, over 90% of the world's production of rare earths is situated in China, thus raising fears of market distortion and supply constraints. The price of these metals continues to be highly volatile even though worldwide efforts are being undertaken to restart old mines and explore new deposits outside of China. While primary mining is certainly important, it has two major drawbacks:

- The environmental burden and disposal of radioactive elements (thorium) associated with the processing of the rare-earth-containing ores. The processing and purification of these ores requires large amounts of acids and organic solvents.
- The large mismatch between supply and demand for the different rare earths. This phenomenon, called the 'balance problem', is very pronounced for rare earths owing to the fact that these elements are always present as a group in the ores but only some of them have a sizeable market. These critical rare earths are neodymium and dysprosium for strong permanent magnets and europium, terbium and yttrium for the lamp phosphors used in fluorescent lamps. Enough ore has to be mined every year to satisfy the demand for these five elements, creating very large overproduction of other, more common rare earths such as lanthanum and cerium. A large amount of energy also goes into the difficult separation of the individual rare earths.

Collection and recycling technology

This is where recycling comes in. Recycling of end-of-life consumer products could help in closing the loop for these critical rare earths by recovering them in the same ratio that is needed for the manufacturing of new products. Recycling could also help shift the production of rare earths to Europe and the USA given that most consumer products con-

taining rare earths are made for these markets. Two aspects of recycling must be addressed: collection and also recycling technology. For most products, collection is the biggest bottleneck. The reuse of industrial manufacturing scrap is therefore one of the first matters to be considered but about which very little is known because company production secrets may be involved.

Recycling from end-of-life consumer products requires a more elaborate collection effort. Some car and air-conditioning manufacturers are considering the recovery of valuable neodymium-iron-boron magnets from their end-of-life products, but the best collection rate at present is observed for fluorescent lamps. In most Western countries, collection of these lamps is mandatory and organised by the government owing to the presence of trace amounts of mercury. Most of the time, however, the lamps are simply dismantled to safely dispose of the mercury and sometimes also recycle the glass, but nothing is done with the rare-earth-containing phosphor powders.

Critical and less critical

These phosphor powders convert the ultraviolet light generated by the mercury in the lamp into green, red and blue visible light, which together are perceived as white light by the human eye. These phosphors contain significant amounts of the critical rare earths yttrium, terbium and europium, as well as the less critical lanthanum and cerium. Unfortunately, the lamp phosphor waste also contains large amounts of less valuable products such as the broadband white halophosphate phosphor 'HALO', alumina and glass particles.

An overview of the phosphor powder composition is given in the table accompanying this feature. The most valuable component by far is the red phosphor YOX, which holds 80% of the rare earths and 70% of the value in the lamp phosphor powder.

Waste and energy challenges

In 2012, Solvay launched a recycling operation at La Rochelle in France for the annual treatment of around 2000 tons of phosphor waste. The company's patented process is based on the total dissolution of the lamp phosphor waste using a variety of acidic, alkaline and high-temperature attacks. All the elements are then separated by multiple-stage solvent extraction to produce pure rare earths. This process is very effective but is relative long and therefore requires significant amounts of chemicals and energy. Researchers worldwide are therefore looking at innovative ways to process this waste more efficiently. There are two main technical challenges associated with the treatment of lamp phosphor waste. The first is the unwanted dissolution of the non-valuable HALO: this phosphor is very easily dissolved in diluted acidic solutions, and since it can make up almost 50% by weight of the waste, it leads to substantial acid consumption and pollutes the solution with unwanted elements, which in turn generates waste.

OVERVIEW OF THE APPROXIMATE LAMP PHOSPHOR WASTE COMPOSITION

Name	Formula	Waste fraction [a] (wt%)	Value
HALO	$(Sr,Ca)_{10}(PO_4)_6(Cl,F)^2 : Sb^{3+}, Mn^{2+}$	50	Low
YOX	$Y_2O_3 : Eu^{3+}$ (red)	20	High
BAM	$BaMgAl_{10}O_{17} : Eu^{2+}$ (blue)	5	Low
LAP	$LaPO_4 : Ce^{3+},Tb^{3+}$ (green)	5	High
CAT	$CeMgAl_{11}O_{19} : Tb^{3+}$ (green)	5	High

[a] Approximate fraction found in lamp phosphor waste; the remaining consists of SiO_2 and Al_2O_3.
* The full paper can be consulted for free: D. Dupont, K. Binnemans, Green Chemistry, 2015, 17, 856-868

The second challenge concerns the processing of the very inert phosphors LAP, BAM and CAT. These are currently subjected to a high-temperature process called alkaline fusion: a source of oxygen such as Na_2O, NaOH or Na_2CO_3 is mixed with the phosphor powder and then heated at 700-1000 °C to convert all the elements into oxides, which can then be dissolved in nitric acid. This process is quite energy-intensive and researchers are therefore also looking at ways of significantly reducing the required temperature.

Achieving selectivity

Recently, we published a front-cover article in the 'Green Chemistry' journal* outlining a new, patented recycling process that addresses the unwanted dissolution of HALO. In this process, the most valuable component in the lamp phosphor powders, namely YOX, is dissolved selectively and the phosphor can be regenerated at the end of this three-step process.

To achieve this selectivity, we used an acid-functionalised ionic liquid called betainium bistriflimide. Ionic liquids are organic solvents which consist entirely of ions and which are liquid below 100 °C. The fact that they consist entirely of ions gives them some unique properties such as negligible vapour pressure (no evaporation), low flammability and relatively low toxicity, especially compared to other organic solvents. Ionic liquids are also often considered designer solvents owing to the endless different combinations of anions and cations to form ionic liquids.

A specialised, task-specific ionic liquid can therefore be designed for each particular application in order to meet its requirements in the best possible manner. The ionic liquid used in our process contains betaine as cation and a bistriflimide anion: betaine is used worldwide as a food additive for animals and bistriflimide anions are used as electrolyte in lithium-ion batteries. The wide availability of both components and the convenient one-step synthesis of this ionic liquid render it relatively affordable to make, despite

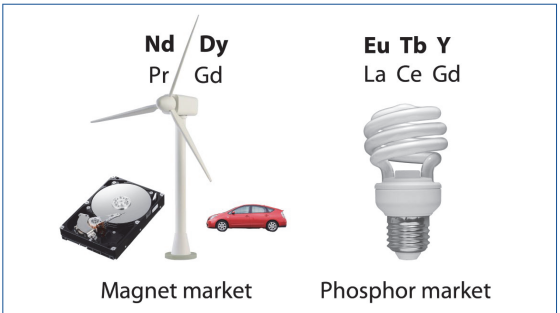

Figure 1: The main markets (by value) for rare-earth elements are the NdFeB magnets used in electronics, hybrid cars and wind turbines and the lamp phosphors used in fluorescent lamp tubes and compact fluorescent lamps.

its seemingly complex structure. The acidic group on the betaine cation (indicated in red on the figure) makes this ionic liquid very suitable for the dissolution of metal oxides. In particular, we saw that we could dissolve the red phosphor YOX without dissolving the other components. This cannot be achieved in water with traditional acids because the non-valuable HALO will always go in solution prior to the YOX. As mentioned, this consumes large amounts of acids and pollutes the water with unwanted elements, which then requires many additional process steps to recover the pure rare earths.

The reason behind this selectivity would lead us too far for this feature, but it suffices to say that the ionic liquid has a particular affinity for the dissolution of metal oxides. Other commonly-known water-soluble compounds such as table salt do not dissolve in this ionic liquid. The selective dissolution of the red phosphor YOX also means that no purification (solvent extraction) steps are necessary. The dissolved yttrium and europium can be removed from the ionic liquid by precipitating with solid oxalic acid – a common process in the rare-earth industry because it is very efficient and selective. The mixed yttrium/europium oxalate is a solid, which is used as precursor for the synthesis of new YOX phosphor. By calcining this material in an oven, the oxalate is transformed into YOX and CO_2.

Fully regenerated

On testing the resulting red phosphor, it was found to have approximately the same quality and luminescence as the commercially-available product. By optimising the calcination step, a high quality YOX could be prepared which would meet industry standards. It is also important to stress that the ionic liquid is fully regenerated during the precipitation step and that it can therefore be reused as such. The reusability of the ionic liquid is important considering that it is a relatively expensive solvent. This process thus recovers 70 % of the value in the phosphor waste by selectively recovering the most valuable component, YOX. The remaining value is held in the green phosphors, which require much harsher conditions (700–1000 °C) to be processed. However, the terbium content in this residue justifies further attempts to try and find a method to process these phosphors at lower temperatures. We are currently working on different ideas to recover these phosphors too, at temperatures below 200 °C. A schematic overview of the recycling process for YOX is given in this feature:

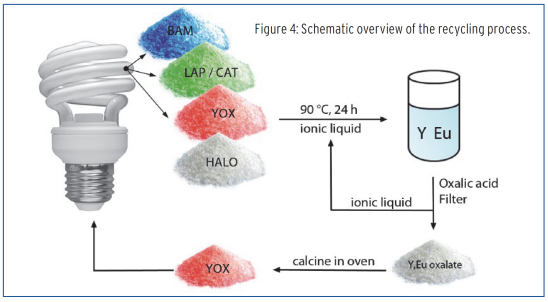

Figure 4: Schematic overview of the recycling process.

The process consists of three main steps:

1. The phosphor waste powder is stirred in the ionic liquid for 24 hours at 90 °C to selectively dissolve the red phosphor YOX.
2. The yttrium and europium dissolved in the ionic liquid are removed with solid oxalic acid. Oxalic acid precipitates the yttrium and europium as a mixed oxalate and regenerates the ionic liquid.
3. The oxalate precipitate can be calcined in an oven at high temperature to obtain the pure red phosphor, which can be used again for the manufacturing of new fluorescent lamps.

Economic advantage

The main economic advantage of this process is that it avoids the use of complex solvent extraction plants, which require very large investment. The separation of individual rare earths with solvent extraction requires hundreds of consecutive counter-current mixer settlers to obtain sufficient purity. By avoiding the contamination in the first place through our selective leaching procedure, we eliminated entirely the need for solvent extraction. The apparent simplicity of this process should allow it to be built on-site close to recyclers.

A second important advantage is that no wastewater is generated because the dissolution of HALO is avoided. The dissolved YOX is reused in the end to make new YOX in a process that only produces CO_2 and no side products.

Using a selective dissolution of the most valuable component in lamp phosphor waste powder, we can recover 70 % of the value without generating any extra waste. The ionic liquid, required for this process, is also entirely reusable. Therefore, we hope the resulting recycling process offers a more sustainable and energy-efficient alternative for the recycling of lamp phosphor waste.

The patent for this process is currently held by the KU Leuven university in Belgium, but we are working in close collaboration with interested industrial partners with a view to perhaps bringing this technology to the market. Our different research consortia such as RARE3 (www.rare3.eu) are aiming to bridge the gap between academia and industry in an attempt to find breakthrough solutions for rare-earth recycling and technology.

By David Dupont

The Authors:
Drs. David Dupont:
david.dupont@chem.kuleuven.be
Phone +32(0)479457025

Prof. Koen Binnemans:
koen.binnemans@chem.kuleuven.be
Phone +32(0)16327446

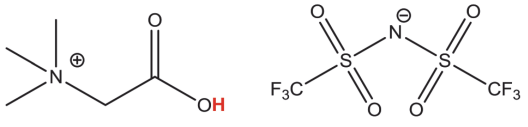

Figure 3: Chemical structure of the ionic liquid "betainium bistriflimide".

The authors wish to thank the KU Leuven (projects GOA/13/008 and IOF-KP RARE3) and the FWO Flanders (PhD fellowship to David Dupont) for financial support.

Article 2: IUPAC Chemistry International (July 2014)

Youth Views on Sustainability

Let's Not Waste Our e-waste

By David Dupont

Waste. Most people will associate this word with something they want to get rid of, something without value. But electronic waste or so-called e-waste still contains vast amounts of scarce metals and valuable elements.

E-waste is the most rapidly growing type of waste all over the world, as the first generations of mobile phones and computers are reaching the recyclers. In 2012, 14.2 kg of e-waste was discarded on average by every person on earth.[1] The potential of this type of waste as a sustainable resource for scarce elements is enormous, because e-waste is already a concentrate of gold, palladium, silver, rare-earths, etc. For example, a mobile phone contains about 305 mg of silver and 30 mg of gold which is 40 to 50 times more concentrated than in the ores from primary mining.[2,4]

In addition, the recycling of e-waste also regenerates the required metals in the ratios needed to manufacture these devices again. The amount of useless side products is therefore reduced to a minimum compared to ordinary mining.

Closed Loop Production

The biggest bottleneck at this moment is the efficient collection of this type of waste. Surveys show that every American consumer holds two unused cell phones on average at home, because 60% cannot be bothered to turn in their old devices—even though the recycling value of modern smartphones can easily reach a hundred dollars.[3] It is estimated that US consumers are sitting on $33.8 billion in used mobile phones.[3] More effective marketing and financial incentives could motivate people to bring their unused electronic equipment to collection points.

Your FORMULA
Fresh ideas for a sustainable future

YourFormula.eu is an online platform and multimedia magazine, powered by Cefic (The European Chemical Industry Council) where young chemistry enthusiasts blog about chemistry's role in a sustainable world. In addition to inspiring articles, YourFormula collects videos, news and events, sharing the great innovations taking place in Europe and pointing to a more sustainable future.

This online platform also covers major international scientific discussions, such as the Young Observers World Leadership Meeting 2013, during the IUPAC General Assembly, in Istanbul. IUPAC also wants to support and highlight the views of younger generations on sustainability matters, and will be featuring some blog posts from the YourFormula community in upcoming issues of *Chemistry International* Magazine.

www.yourformula.eu

Several encouraging examples exist like shops offering discounts for a new mobile phone when an old one is handed in.

Fluorescent lights and batteries have an advance compared to other electronic equipment because they contain toxic elements that have to be dealt with accordingly, to avoid them ending up in the wrong places. Governments therefore put in place efficient collection methods and urged the public to bring in their used batteries and energy-saving lightbulbs, using advertising campaigns to raise public awareness about this issue.

These strategies were initially put in place to deal with the toxic elements they contained, but very soon different companies started to develop recycling schemes to retrieve the valuable elements from this new type of feedstock. Several successful examples exist like the recycling of computer circuits, rechargeable batteries, mobile phones, high-end magnets and energy-saving light bulbs by chemical companies such as Umicore and Solvay.[4] These companies have developed a profitable business around this idea of urban mining, where waste is no longer considered a problem but a solution!

With over $21 billion worth of gold and silver used in electronic gadgets every year, and only 15-20% of that being recycled, it is not surprising that green tech was the most rapidly growing industry of 2013.[5]

The rapidly growing amount of e-waste is therefore receiving increasing attention as the feedstock of the future. The European Commission and the United Nations have identified the recycling of e-waste as a top priority for the development of a sustainable high-tech industry and the safeguarding of scarce resources.[6,7] Reusing the valuable elements trapped inside these devices is the key to a "closed loop" sustainable manufacturing of the electronic gadgets we are all so keen on.

The burden on the environment often associated with primary mining would become too large if the upcoming economies started consuming high-tech products as we do. But in a closed-loop system, very few of these rare elements are lost and a completely new innovative industry can even emerge to try and retrieve them as efficiently as possible – transforming piles of mobile phones into fresh new bars of gold, silver, palladium, cobalt and all the other elements needed to manufacture these amazing devices that connect us to the world. The way we think about waste is changing rapidly!

References

1. www.step-initiative.org/index.php/WorldMap.html
2. M. Buchert et al., Recycling critical raw materials from waste electronic equipment, Oeko-institut, Darmstadt 2012.
3. www.prweb.com/releases/2013/2/prweb10432797.htm
4. K. Binnemans et al., Recycling of rare earths: a critical review. *Journal of Cleaner Production,* **2013**, *51*, 1-22.
5. http://thediplomat.com/2013/11/the-potential-of-urban-mining/
6. http://ec.europa.eu/enterprise/policies/sustainable-business/sustainable-industry/forums/index_en.htm
7. www.unep.org/pdf/Recycling_From_e-waste_to_resources.pdf

David Dupont is a PhD student in chemistry at the University of Leuven, Belgium. His research focuses on the recycling of rare earths and valuable metals. He is interested in moving towards (R&D) management or policymaking in the chemical industry or in a European institution. This would combine his interest in chemistry and sustainable resources with his aptitude to think global and change the way we think about resources.

Check out www.yourformula.eu and read more articles. Comment and share this, other blog posts and other material from the platform via social media. Follow us on Facebook, Twitter and Pinterest!

Article 3: Chemistry in Australia (December 2014)

This is a republishing of the article that appeared in IUPAC Chemistry International

sustainability

Let's not waste our e-waste


iStockphoto/bakalusha

Waste. Most people will associate this word with something they want to get rid of, something without value. But electronic waste, or so-called e-waste, still contains vast amounts of scarce metals and valuable elements.

E-waste is the most rapidly growing type of waste all over the world, as the first generations of mobile phones and computers are reaching the recyclers. In 2012, 14.2 kilograms of e-waste was discarded on average by every person on Earth (www.step-initiative.org/index.php/WorldMap.html). The potential of this type of waste as a sustainable resource for scarce elements is enormous because e-waste is already a concentrate of gold, palladium, silver, rare earths etc. For example, a mobile phone contains about 305 milligrams of silver and 30 milligrams of gold which is 40–50 times more concentrated than in the ores from primary mining (www.oeko.de/oekodoc/1375/2012-010-en.pdf; K. Binnemans et al. *J. Clean. Prod.* 2013, vol. 51, pp. 1–22).

In addition, the recycling of e-waste also regenerates the required metals in the ratios needed to manufacture these devices again. The amount of useless side products is therefore reduced to a minimum compared to ordinary mining.

Closed loop production

The biggest bottleneck at this moment is the efficient collection of this type of waste. Surveys show that every American consumer holds two unused cell phones on average at home, because 60% cannot be bothered to turn in their old devices – even though the recycling value of modern smartphones can easily reach $100 (www.prweb.com/releases/2013/2/prweb10432797.htm). It is estimated that US consumers are sitting on $33.8 billion in used mobile phones. More effective marketing and financial incentives could motivate people to bring their unused electronic equipment to collection points.

Several encouraging examples exist, such as shops offering discounts for a new mobile phone when an old one is handed in.

Fluorescent lights and batteries have an advance compared to other electronic equipment because they contain toxic elements that have to be dealt with accordingly, to avoid them ending up in the wrong places. Governments therefore put in place efficient collection methods and urged the public to bring in their used batteries and energy-saving lightbulbs, using advertising campaigns to raise public awareness about this issue.

These strategies were initially put in place to deal with the toxic elements they contained, but very soon different companies started to develop recycling schemes to retrieve the valuable elements from this new type of feedstock. Several successful examples exist such as the recycling of computer circuits, rechargeable batteries, mobile phones, high-end magnets and energy-saving light bulbs by chemical companies such as Umicore and Solvay (K. Binnemans et al. op cit.) These companies have developed a profitable business around this idea of urban mining, where waste is no longer considered a problem but a solution!

With over $21 billion worth of gold and silver used in electronic gadgets every year, and only 15–20% of that being recycled, it is not surprising that green tech was the most rapidly growing industry of 2013 (http://thediplomat.com/2013/11/the-potential-of-urbanmining).

The rapidly growing amount of e-waste is therefore receiving increasing attention as the feedstock of the future. The European Commission and the United Nations have identified the recycling of e-waste as a top priority for the development of a sustainable high-tech industry and the safeguarding of scarce resources (http://ec.europa.eu/enterprise/policies/sustainablebusiness/sustainable-industry/forums/index_en.htm; www.unep.org/pdf/Recycling_From_e-waste_to_resources.pdf). Reusing the valuable elements trapped inside these devices is the key to a 'closed loop' sustainable manufacturing of the electronic gadgets we are all so keen on.

The burden on the environment often associated with primary mining would become too large if the upcoming economies started consuming high-tech products as we do. But in a closed-loop system, very few of these rare elements are lost and a completely new innovative industry can even emerge to try and retrieve them as efficiently as possible – transforming piles of mobile phones into fresh new bars of gold, silver, palladium, cobalt and all the other elements needed to manufacture these amazing devices that connect us to the world. The way we think about waste is changing rapidly!

David Dupont is a PhD student in chemistry at the University of Leuven, Belgium. His research focuses on the recycling of rare earths and valuable metals. YourFormula.eu is an online platform and multimedia magazine, powered by Cefic (The European Chemical Industry Council), where young chemistry enthusiasts blog about chemistry's role in a sustainable world.

First published at www.yourformula.eu and reproduced in *Chemistry International*, 2014, vol. 36(4). pp. 10–11.

5 Conclusions and outlook

The main conclusion of this PhD thesis is that ionic liquids (ILs) could provide greener solutions to metal processing than classic hydrometallurgy. Not because ionic liquids are inherently greener, which they are not, but because the intelligent use of ionic liquids can sometimes provide more efficient processes, which use less chemicals and produce less waste. The key here is to understand the properties that make certain ionic liquids unique and to use these properties to resolve issues encountered in classic hydrometallurgy or solvent extraction.

The first part of this PhD focused on the recovery of critical metals from end-of-life products. We showed how the ionic liquid betaine bistriflimide [Hbet][Tf_2N] can be used to recover rare earths from lamp phosphor waste and NdFeB permanent magnets in a series of innovative processes. The reusability of the ionic liquid is key here, since it is too expensive to dispose of. The selectivity and unique properties such as the thermomorphic behavior of this ionic liquid allowed us to design new processes which cannot be mimicked in aqueous solutions. In the case of the lamp phosphors we managed to selectively remove the most valuable component, the red phosphor Y_2O_3:Eu^{3+}, which cannot be achieved in aqueous solutions. This drastically improves the efficiency of the process and minimizes the amount of waste created during the recycling process. For NdFeB magnets the innovative angle was to take advantage of the thermomorphic properties of the IL/water system [Hbet][Tf_2N]/H_2O, in order to first dissolve the REE oxides in a homogeneous system (> 60 °C) and then, upon cooling, obtain phase separation which automatically separates the valuable elements (REEs and cobalt) from the less valuable iron. This combined leaching/extraction process has the potential to drastically reduce the amounts of steps required during the processing of complex ores or waste products. Finally, the general observation that acidic ionic liquids can be used to selectively dissolve metal oxides over salts, is very useful to recover valuable metals from oxidized slags or end-of-life waste.

During the design of these recycling processes, a key aspect was to ensure that the process would results in a low or even zero waste valorization scheme. This was also at the core of our work on antimony recycling from lamp phosphor waste. The antimony content in the powder is low, so in order to make it feasible the process should consume as little energy as possible and not produce additional waste. This was achieved using a HCl/NaOH process in combination with an IL extraction step. The process allows the treatment of the halophosphate fraction of the lamp phosphor waste, and the recovery of antimony and a valuable fertilizer precursor. The process produces only clean salt water (NaCl) as waste, which can be discharged in the sea.

In the second part of this PhD we focused on the design of new ionic liquids, in particular very acidic ionic liquids. The idea was to expand the applicability of IL-based recycling processes to other (more inert) types of materials. The idea for the design of these new ionic liquids also resulted from the observation that certain extractants cannot be used in classic solvent extraction due to their detergent properties (e.g. alkylsulfates or sulfonates) or due to their pungent odor (e.g. thiols). By incorporating these metal-extracting groups in an IL, it is possible to overcome these problems and thus develop successful solvent extraction systems based on these acidic extractants. Using this principle we designed a range of sulfonic acid functionalized ILs ($pK_a \approx -2$) and we demonstrated the dissolution of metal oxides in these ILs. The absence of toxic fumes makes these strongly acidic ionic liquids very safe to handle compared to mineral acids such as HCl or HNO_3. Furthermore, for the first time, water-immiscible sulfonic acid ILs were prepared which opened up the possibility of solvent extraction. Starting from choline chloride (a cheap and green precursor) and chlorosulfonic acid, we were also able to synthesize other strongly acidic ionic liquids functionalized with alkylsulfuric acid groups ($pK_a \approx -3.5$). These ILs are more hydrophobic and have improved physical properties compared to sulfonic acid ILs. We therefore hope that this work will instigate other researchers to further explore this interesting new class of ionic liquids.

It was also very important for us to understand the underlying fundamentals behind the sometimes strange behavior of ionic liquids towards metal ions. Only by understanding what makes an ionic liquid perform the way it does, can we optimize this phenomenon and apply it in future processes. Concretely, we studied the effect of metal salts and mineral acids on the properties of IL/water systems. Salts and acids can drastically affect the mutual solubility of IL and water, but also the thermomorphic properties and even the structure of the IL through anion exchange reactions. The result was a series of general prediction models and theories to describe this behavior and predict the influence of salts and acids on the properties IL/water systems. This toolbox can be applied to the synthesis of ionic liquids as well as the rational design of IL-based solvent extraction processes.

Finally, in a separate part of this PhD, we also introduced EDTA-functionalized magnetic nanoparticle as a way to recover rare earths from dilute waste streams. These magnetic nanoparticles are simple to retrieve and reuse. Such nanosorbents complement solvent extraction which is more targeted towards the recovery from concentrated solutions. The key observation was that it was possible to improve the selectivity of chelating extractants through “surface crowding”. In other words, we observed that the density of chelating extractants grafted on the surface of these nanoparticles, affected the selectivity with which the rare earths could be separated from each other. This hypothesis was later confirmed by other researchers.

Outlook

Future work could use the toolbox of ideas and processes developed in this PhD thesis, to recycle critical metals from other products, waste streams or industrial residues. The processes described in this PhD thesis were performed on lab scale and should be further optimized and upscaled in order to test the robustness of the processes. The flexibility of the processes should also be tested using waste from different origins and quality. During the upscaling, systems must be devised to efficiently separate and reuse the IL, which is key to the success of the process.

New ionic liquids can also be designed with affinity for other types of critical metals (e.g. indium, gallium). The introduction of other functional groups (e.g. thiols, thioethers, sulfonyls, sulfonic acids) will allow the (selective) extraction of different metals and therefore the treatment of new types of waste such as spent catalysts, slags, ores, tailings, end-of-life products, etc. An interesting area of research is also the synthesis of ionic liquids with equivalent behavior as the ones used in this PhD thesis but with better properties such as a lower viscosity, a lower cloud point temperature or a greener (fluoride-free) structure. Many possibilities exist to make biodegradable ionic liquids or ionic liquids from renewable feedstock. It is also a challenge to find ionic liquids with the same efficacy but a lower price or simpler synthesis. A good example has been shown for the synthesis of alkylsulfuric acid functionalized ILs, using choline chloride as a feedstock. This cheap animal feed additive is an ideal precursor to many functionalized ionic liquids. Using choline chloride or the chlorocholine chloride derivate as starting material, a wide range of functionalized ionic liquids are accessible. We already showed how to synthesize alkylsulfuric acid ILs from choline chloride using chlorosulfonic acid, but additional research could focus on chlorocholine chloride as precursor. A thiourea/NaOH reaction can be used to synthesize a thiol functionalized IL starting from chlorocholine chloride. These thiol ionic liquids can then be used to obtain thioether or sulfonyl functionalized ILs. A lot of these ionic liquids have not been synthesized yet and should have very interesting properties.

Another interesting research area is the design of base-stable ionics. These would open up the possibility of alkaline metal processing, including alkaline leaching and solvent extraction from alkaline solutions. Alkaline processing is particularly interesting for amphoteric and acidic oxides such as BeO, ZnO, Al_2O_3, Cr_2O_3, Ga_2O_3, In_2O_3, As_2O_3, SnO_2, PbO_2, GeO_2, V_2O_5, As_2O_5, Sb_2O_5, Bi_2O_5 and MoO_3, many of which are considered highly critical elements. In alkaline media these elements can form negatively charged hydroxyl complexes or oxoanions, which can be selectively extracted by anion exchange extractants such as quaternary ammonium ionic liquids with branched alkyl chains to block the Hofmann elimination. This research area is still underexplored.

Generally, the use of ionic liquids in metal processing is still in an early stage but its potential is very clear. However, ionic liquids should only be considered if they offer a clear and undeniable advantage which cannot be achieved in aqueous solutions. This requires creativity and a good understanding of the possibilities of ionic liquids. The enormous variety of possible ionic liquids, which has been estimated to be in the billions, offers unprecedented opportunities to design and optimize an ionic liquid with the appropriate properties for a certain process. Trial-and-error is clearly not the right approach here, which is why we put a lot of time and effort in understanding the ionic liquid behavior in metal recovery and solvent extraction processes.

The urgent need for a more circular economy and the constantly increasing demand for critical metals will continue to drive this field in the future and it is up to researchers to find clever answers which can be implemented in reality and which are economically feasible.

Safety aspects

The experimental work performed during this PhD thesis was executed in compliance with the code of practice for safety in the lab (http://chem.kuleuven.be/en/hse/procedures/liab1.htm) and the Introduction Safety Guidelines of the Department of Chemistry (http://chem.kuleuven.be/veiligheid/documenten/safety-brochure.pdf).

The following safety precautions were taken:

- Risk assessments were approved before each experiment and are available: https://www.groupware.kuleuven.be/sites/depchemrisico/Risk%20Assessments/Forms/per%20division.aspx

- For unsupervised experiments, additional risk assessments were prepared and approved by the necessary people according to the procedure: http://chem.kuleuven.be/en/hse/procedures/Unattended_Lab_Experiments

- The chemicals used in this PhD project did not represent an unusual safety risk and did therefore not require additional safety measures beyond the ones described above: working under a fumehood, and wearing the appropriate gloves, safety goggles and labcoat.

Additional remarks:

- Direct exposure to toxic metal salts (e.g. antimony, chromium), corrosive chemicals (acids/bases) and hazardous organic compounds was minimized using the abovementioned protection measures. The corresponding waste was also discarded according to lab regulations.

- Particular care was taken during the handling of antimony oxide powder and nanopowders in general (SiO_2, TiO_2). These fine powders can be harmful to the respiratory system and are potential carcinogenic compounds.

- The strongly acidic ionic liquids were handled with care and direct skin contact was avoided using gloves. However, the absence of toxic fumes makes these acidic ionic liquids relatively safe compared to mineral acids (i.e. HCl, HNO_3).

Safety trainings:

- Introductory safety course about safety guidelines (start of PhD)
- Radiation protection, 15/10/2013
- Safety in the lab, 6/11/2013

Awards

The following awards were obtained during the course of this PhD:

1. **KU Leuven Science & Innovation Award 2015** (December, 2015)
The Science and Innovation Award is awarded every 2 years and aims at acknowledging the relevance to society of fundamental scientific research as a necessary and essential ingredient in the innovation chain. It awards innovative and knowledge driven research with a connection to the corporate world.

2. **Umicore Materials Technology MSc Award** (March, 2014)
On the initiative of Umicore nv, the FWO awards two annual prizes in recognition of an outstanding Master's thesis that makes an original contribution in the field of sustainable materials & technologies.

Media coverage

Following the publication of the breakthrough process for lamp phosphor recycling (Dupont *et al.*, Green Chem., 2015, 17, 856-868) a KU Leuven press release was organized. This resulted in the following coverage in the national and international media (only a selection is shown here):

1. KU Leuven Nieuws (March 10, 2015)

- http://nieuws.kuleuven.be/node/14874
- http://www.kuleuven.be/onderzoek/news/binnemans.html

Chemici vinden nieuwe manier om zeldzame aarden uit lampen te recycleren

10 Mrt 2015
Binnemans Dupont chemie duurzaamheid Onderzoek recyclage

Chemici van de KU Leuven hebben een nieuwe methode ontwikkeld om uit ingezamelde tl- en spaarlampen de metalen europium en yttrium te recycleren. Ze gebruikten een ionische vloeistof die heel wat voordelen heeft tegenover de klassieke oplosmiddelen: ze lost enkel de metalen op en is zelf herbruikbaar. De metalen zijn ook meteen bruikbaar in nieuwe lampen.

Met de nieuwe methode vergt de recyclage van europium (Eu) en yttrium (Y) uit tl- en spaarlampen minder chemicaliën en energie.

Voor heel wat moderne elektronica en schone technologieën wordt gebruik gemaakt van zeldzame aarden, een groep metalen. In tegenstelling tot wat de naam doet vermoeden, zijn die elementen niet echt zeldzaam. Ze zijn wel moeilijk te ontginnen en te zuiveren. Omdat de meeste mijnen zich in China bevinden, is de bevoorrading bovendien onderhevig aan geopolitieke spanningen. Er bestaat wereldwijd dan ook interesse om zeldzame aarden te recycleren uit afvalstromen in plaats van ze te ontginnen.

Twee van die zeldzame aarden, europium en yttrium, worden gebruikt in rode lampfosfor. Dat is een vaste stof die ultraviolet licht omzet naar rood licht. Ze wordt bijvoorbeeld al meer dan veertig jaar gebruikt in kleurenschermen voor tv-apparaten en in de buizen van fluorescentielampen. "Omdat ze zeer moeilijk te vervangen is door verbindingen zonder zeldzame aarden, loont het de moeite om te kijken of de rode fosfor uit die lampen kan worden gerecupereerd. Afgedankte tl- en spaarlampen worden al verplicht ingezameld, maar tot nu toe was de recyclage er vooral op gericht om het giftige kwik uit het afval te halen. Omdat het recupereren van europium en yttrium met de klassieke solventen technisch complex was, werd het poeder dat de twee zeldzame aarden bevat meestal niet hergebruikt", vertelt professor Koen Binnemans.

Voor dat laatste probleem vonden de Leuvense chemici een oplossing, legt David Dupont uit. "In plaats van een zuur gebruiken wij een ionische vloeistof als solvent: dat is een organisch oplosmiddel dat volledig bestaat uit ionen of elektrisch geladen deeltjes. Het verdampt niet, is niet brandbaar en het werkt heel selectief: we kunnen het zo maken dat het enkel de rode lampfosfor oplost. Het europium en yttrium dat ermee gerecupereerd wordt, kan onmiddellijk opnieuw gebruikt worden. Bovendien is de ionische vloeistof zelf ook herbruikbaar." Met deze nieuwe methode vergt de recyclage dus minder chemicaliën en energie, zegt professor Binnemans: "Het is dus zowel technisch als ecologisch een interessant alternatief voor de klassieke oplosmiddelen."

Onderzoek van David Dupont en Koen Binnemans leidt tot een doorbraak op het gebied van recycleren van zeldzame aarden uit oude fluorescentielampen.

De afvalfractie aan lampfosforpoeders die ontstaat bij het recycleren van oude fluorescentielampen en spaarlampen bevat aanzienlijke hoeveelheden aan kritieke metalen zoals europium, yttrium en terbium, allen elementen uit de reeks van de zeldzame aarden (rare earths). De zeldzame aarden zijn echter niet gelijkmatig verdeeld in deze afvalfractie, maar geconcentreerd in slechts 10 tot 20% van de totale afvalfractie (de rest bestaat uit glaspoeder, aluminiumoxide en lampfosforen die geen zeldzame aarden bevatten). De meest waardevolle component is de rode lampfosfor europiumhoudend yttriumoxide, vaak afgekort tot kortweg YOX. In de state-of-the-art processen voor het recycleren van zeldzame aarden uit deze lampfosforpoeders was een grote hoeveelheid sterke zuren vereist, omdat eerst de economisch waardeloze lampfosforen zonder zeldzame aarden moesten worden opgelost vooraleer men toegang kreeg tot de YOX fosfor. Het nieuwe proces dat we aan de KU Leuven hebben ontwikkeld, maakt gebruikt van een ionische vloeistof (een organisch oplosmiddel dat enkel uit ionen bestaat) om selectief de YOX fosfor uit de afvalfractie van lamppoeders op te lossen, zonder eerst de niet-gewenste componenten te moeten oplossen. Na het in oplossing brengen van de YOX kunnen de zeldzame aarden uit de ionische vloeistof worden verwijderd en verder worden omgezet in nieuwe YOX fosfor die qua performantie niet van de nieuwe commerciële YOX te onderscheiden is. De ionische vloeistof kan worden gerecycleerd en opnieuw worden ingezet voor het verder oplossen van YOX.

Het onderzoek kadert in het doctoraatsonderzoek van David Dupont. Het behoort tot de onderzoeksactiviteiten van het kennisplatform RARE3 rond het recycleren van zeldzame aarden en andere kritieke metalen (http://www.kuleuven.rare3.eu/). KU Leuven LRD heeft een octrooiaanvraag voor dit proces ingediend.

2. KU Leuven News (March 10, 2015)

- https://chem.kuleuven.be/en/news/research-by-david-dupont-and-koen-binnemans-triggers-a-breakthrough-in-the-recycling-of-rare-earths-from-end-of-life-fluorescence-lamps
- http://www.kuleuven.be/english/news/2015/recycling-of-rare-earth-elements-from-fluorescent-and-energy-saving-lamps

Research by David Dupont and Koen Binnemans triggers a breakthrough in the recycling of rare-earths from End-of-Life fluorescence lamps

During the recycling of End-of-Life fluorescence and energy saving lamps a lamp phosphor waste fraction is obtained. This waste fraction contains a considerable amount of critical metals such as europium, yttrium and terbium, which are three particular (critical) rare-earth elements. However, the rare earths are not distributed uniformly in this waste fraction. In reality the valuable rare-earth fraction only represents 10 to 20% of the overall waste fraction, as the remaining 80 to 90% is glass powder, aluminium oxide and other lamp phosphors which do not contain rare earths. The most valuable component is the red lamp phosphor: europium containing yttrium oxide, commonly known as YOX. In the state-of the art processes for the recycling of rare earths from these lamp phosphor powders a large amount of acids is required, corresponding with the requirement to first dissolve the economically invaluable lamp phosphors before one gets access to the valuable YOX phosphor. The newly developed KU Leuven process makes use of an ionic liquid (an organic solvent which only consists of ions) that is able to selectively dissolve the YOX fraction from the mixed lamp phosphor waste powder, without first having to dissolve the non-desired components. After the YOX is dissolved, it is possible to recover the rare earths from the ionic liquid and to produce fresh YOX phosphor. In terms of performance, the recycled YOX phosphor cannot be distinguished from newly produced, commercial YOX. Furthermore, the ionic liquid can be recycled as well so that it can be reused for subsequent YOX dissolution.

Recycling of rare-earth elements from fluorescent and energy saving lamps

(c) Shutterstock

10 March 2015

KU Leuven Chemists have developed an innovative process, based on ionic liquid technology, for the recycling of the metals europium and yttrium from collected fluorescent and energy saving lamps. The metals are directly reusable in new lamps. Compared to traditional solvents, the ionic liquid has a multitude of advantages, including its selectivity for metal dissolution and its reusability.

For many modern electronic and cleantech applications rare-earth elements are indispensable. Although rare earths are not per se “rare”, they are difficult to mine and to purify. Furthermore, because the majority of the operational mines are located in China, the supply is subject to geopolitical tensions. Worldwide there is an increased interest to recycle rare earths from waste streams to mitigate the supply risk.

Two critical rare earths, europium and yttrium, are used in red lamp phosphor, a substance which transforms ultraviolet light into red light. This phosphor has been used for more than 40 years in the colour screens of televisions and in the tubes of fluorescent lamps. “Because it is very difficult to replace the red phosphor with a rare-earth free mixture, attention goes out the recyclability of the red phosphor fraction from fluorescent lamps. Although it is already obligatory to collect end-of-life fluorescent and energy saving lamps, the involved recycling is strongly focused on the safe removal of mercury from the waste. Because of the technical complexity to recuperate europium and yttrium using traditional solvents, the powder containing these two critical metals is typically not reused”, explains Professor Koen Binnemans.

To tackle this problem, KU Leuven chemists developed an alternative method. David Dupont: “Instead of employing an acid as the solvent, we use an ionic liquid: this is an organic dissolving agent that consists entirely of ions or electrically loaded particles. It does not evaporate, it is inflammable and it works very selectively: we can design it in such a way that it only dissolves the red lamp phosphor. The recycled europium and yttrium can be directly reused. Furthermore, the ionic liquid is also reusable for a next cycle.” With this new method the recycling requires less chemicals and energy, adds Koen Binnemans: “Both from a technical and environmental perspective, this approach is a very interesting alternative for traditional solvents.”

3. De Standaard (March 12, 2015)

Chemici recycleren zeldzame metalen uit tl en spaarlampen – *by Pieter Van Dooren*

http://www.standaard.be/cnt/dmf20150311_01574881

SCHEIKUNDE

Chemici recycleren zeldzame metalen uit tl- en spaarlampen

12 MAART 2015 | Van onze redacteur Pieter Van Dooren

Scheikundigen van de KU Leuven hebben een nieuwe methode ontwikkeld om kostbare metalen terug te winnen uit tl- en spaarlampen.

Leuk voor een lichtfestival, maar wat doe je er nadien mee? fvv

Leuvense onderzoekers bedachten een nieuw oplosmiddel – een 'ionische vloeistof' – om exotische metalen terug te winnen uit tl-lampen en hun meer geavanceerde neefjes, de spaarlampen. Het gaat vooral om de gegeerde metalen europium en yttrium.

Die twee stoffen vormen met vijftien andere zware metalen een scheikundige groep met de wat bizarre naam 'zeldzame aardmetalen'. Begin negentiende eeuw, toen de naam gegeven werd, waren er inderdaad maar heel weinig chemici die ooit zo'n metaal onder ogen hadden gehad, maar intussen weten we dat ze helemaal niet zo zeldzaam zijn. Het zeldzaamste lid van de groep komt nog steeds vaker voor dan goud.

Maar moeilijk te winnen en te zuiveren zijn ze wel, omdat hun chemische eigenschappen zo dicht bij elkaar liggen. Bovendien komt bijna de hele wereldproductie uit China, wat hen politiek gevoelig maakt. Ze zijn dus misschien niet zeldzaam, maar op de markt wel schaars. Zeker nu smartphones, en andere elektronische apparaten waarin ze onmisbaar zijn, zo populair zijn. Yttrium is ook onmisbaar in krachtige lasers, en in keramische supergeleiders. Europeum wordt, behalve in spaarlampen, ook gebruikt in kwikdamplampen en in MRI-scanners. Beide metalen zijn nodig voor de rode beeldpunten in tv-schermen.

Kleurpoeder

Ze worden ook gebruikt in de 'rode fosfor' in fluorescentielampen, zoals tl- en spaarlampen. Dat soort lampen produceert eigenlijk ultraviolet licht. Poeders op het glas van die lampen zetten dat UV-licht vervolgens om in zichtbaar licht. Een van die fluorescerende poeders produceert rood licht, en dat poeder bevat europium en yttrium. Er is, ondanks hard zoeken, nooit een goed alternatief voor gevonden. Gezien de prijs van europium en yttrium, zou het dus een goed idee zijn om het lamppoeder te recycleren. Maar dat is er nooit echt van gekomen, wegens technisch te moeilijk.

Spaar- en tl-lampen worden nochtans al verplicht ingezameld. Maar dat is om het giftige kwik eruit te halen. De poeders laat men meestal maar zo. Al recycleert Solvay sedert 2012 tweeduizend ton poeder per jaar, met een techniek die herhaalde aanvallen met zuren en loog vergt, waarvan één stap bij duizend graden.

David Dupont vond bij zijn doctoraatsonderzoek een oplossing, meldt hij met zijn promotor Koen Binnemans in *Green Chemistry*, een vakblad van de Britse Royal Society of Chemistry. Hij ontwikkelde een 'ionische vloeistof', een organische vloeistof die zich gedraagt zoals water: ze lost stoffen op die normaal net niet oplossen in organische oplosmiddelen. Het oplosmiddel bestaat uit elektrisch geladen deeltjes, ionen, en is daarmee een buitenbeentje in de organische chemie, waar de stoffen zelden als ionen voorkomen.

Het oplosmiddel (voor de fijnproevers: betainium bis(trifluoromethylsulfonyl)imide) is zo samengesteld dat het specifiek het rode lamppoeder oplost. Omdat geen verstorende rotzooi meekomt, zijn de twee metalen er vervolgens heel eenvoudig uit te recupereren. Het oplosmiddel zelf is ook herbruikbaar. 'Een zeer groen en efficiënt alternatief' noemen de vorsers het in hun publicatie.

4. Knack (February 2015)

Afval bevat waardevolle metalen – *by Dirk Draulans*

http://www.kuleuven.rare3.eu/wp-content/uploads/2015/02/Knack_25_FEB_2015_BINNEMANS.pdf

Afval bevat waardevolle metalen

Uit oude fluorescentielampen kunnen zeldzame metalen gewonnen worden.

Onze industrie draait voor een deel op zeldzame aarden: metalen die dikwijls maar op een paar plaatsen in de wereld gewonnen worden. Wetenschappers slagen er almaar beter in om zulke kritische metalen te winnen uit oude producten. Recyclage wordt dus een alternatief voor aankoop van moeilijk te krijgen elementen uit vaak moeilijke regio's als China.

David Dupont en Koen Binnemans van het Departement Scheikunde aan de KU Leuven presenteren in het vakblad *Green Chemistry* een doorbraak in de recyclage van zeldzame aarden uit oude fluorescentielampen en spaarlampen. Die bevatten kritieke metalen zoals europium, yttrium en terbium, die echter niet evenredig over de afvalfractie verdeeld zijn, maar geconcentreerd zitten in 10 tot 20 procent van het afval.

De meest waardevolle component is het yttriumoxide uit rodelampfosfor dat europium bevat. Vroeger was een grote hoeveelheid sterke zuren vereist om de stof los te maken, waarbij eerst alle economisch waardeloze producten verwijderd moesten worden. Met het nieuwe proces kan dat veel eenvoudiger, door toepassing van een organisch oplosmiddel dat enkel uit ionen bestaat. De gewenste stof kan daarna uit de oplossing gehaald worden voor hergebruik. Er is geen enkel verschil met de kwaliteit van het origineel. Zelfs het oplosmiddel kan worden gerecycleerd en hergebruikt.

De universiteit heeft een octrooi op het procedé aangevraagd.

OUDE FLUORESCENTIELAMP: interessant voor de industrie.

iStock

WWW.KNACK.BE

5. Frankfurter Allgemeine Zeitung (26/06/2015)

Ein Schatz schlummert in alten Energiesparlampen – *by Antonia Rötger*

http://www.faz.net/aktuell/wissen/physik-chemie/umweltschonendes-recycling-ein-schatz-schlummert-in-alten-energiesparlampen-13662703.html

Ein Schatz schlummert in alten Energiesparlampen

Energiesparlampen enthalten neben Quecksilber auch Seltene Erden. Mit einem schonenden Verfahren will man die begehrten Metalle nun recyceln.

Von Antonia Rötger

Energiesparlampen haben die klassischen Glühbirnen mittlerweile fast überall abgelöst. Sie erzeugen Licht wesentlich effizienter als die althergebrachten Leuchtmittel mit ihren Drahtwendeln, und zwar durch Anregung von Quecksilberatomen, die daraufhin ultraviolettes Licht aussenden. Eine auf der Innenseite aufgebrachte Schicht aus verschiedenen Leuchtstoffen wandelt die energiereiche Strahlung in sichtbares Licht um. Etwa 20 Prozent dieser Leuchtstoffmischung besteht aus sogenanntem YOX, einer Yttriumoxid-Verbindung, die mit Europium dotiert ist und für die warmen, roten Farbtöne des ausgesandten Lichts sorgt. Yttrium und Europium gehören zu den Seltenen Erden, die in Smartphones, Handys und anderen Hightech-Geräten stecken. Diese Elemente sind äußerst wertvoll, weil sie nicht allzu häufig vorkommen, schwer abzubauen und aufzubereiten sind. Außerdem liegen in China die weltweit größten Lagerstätten. Deshalb sucht man nach Wegen, die YOX-Verbindungen aus alten Energiesparlampen zu recyceln, was jedoch mit großem Aufwand verbunden ist. Chemiker von der Katholischen Universität in Löwen haben nun ein vielversprechendes umweltfreundliches Verfahren entwickelt, mit denen sich der rote Leuchtstoff einfacher aus dem Abfall abtrennen und daraus Yttrium und Europium wiedergewinnen lässt.

Alte Energiesparlampen werden üblicherweise in Glas, Kunststoffe und Metallreste getrennt, wobei man das Quecksilber entsorgt oder wiedergewinnt. Das Leuchtstoffgemisch wird jedoch in der Regel nicht aufbereitet, sondern allenfalls in Spezialdeponien gelagert. Denn das Gemisch setzt sich aus billigen halogenhaltigen Phosphaten, wertvollem Yttriumoxid und weiteren Verbindungen zusammen, die nur schwer voneinander separiert werden können. Ein Vorreiter beim Recycling der wertvollen YOX-Verbindung aus Leuchtstoffen ist die belgische Firma Solvay, die seit dem Jahr 2012 in einem Pilotprojekt das Leuchtstoffgemisch auftrennt – allerdings sind dazu große Mengen an Säuren und an Energie erforderlich.

Einen anderen Ansatz haben kürzlich Chemiker um Koen Binnemans von der Katholischen Universität Leuven in Belgien entwickelt: „Wir lösen die Beschichtung nicht mit Säuren ab, sondern verwenden eine funktionalisierte ionische Flüssigkeit, die nur den roten Leuchtstoff aus der Leuchtstoffmischung herauslöst", sagt David Dupont aus der Arbeitsgruppe von Binnemans. Ionische Flüssigkeiten bestehen aus großen organischen Molekülen, deren elektrische Ladungen sich wie die Ionen eines Salzes gegenseitig anziehen. Anders als anorganische Salze ordnen sie sich aber nicht zu einem festen Kristallgitter an, sondern bleiben flüssig. Diese flüssigen Salze können deshalb auch nicht verdampfen oder brennen. „Ionische Flüssigkeiten sind eine Art Designer-Lösemittel, die man gezielt auf bestimmte Anwendungen zuschneiden kann", erklärt Dupont. Gibt man eine Leuchtstoffmischung in eine bestimmte ionische Flüssigkeit, so löst sich ausschließlich das YOX darin auf, während die anderen Bestandteile nicht in Lösung gehen. „Wir waren selbst überrascht, wie selektiv das YOX aus der Mischung herausgelöst wird", erklärt Dupont.

Mit diesem Verfahren benötigt man deutlich weniger Chemikalien, insbesondere Säuren und Energie, um Europium und Yttrium zurückzugewinnen. Das gelöste YOX wird mit einem weiteren Schritt schließlich aus der ionischen Flüssigkeit herausgefiltert und liegt anschließend mit einem Reinheitsgrad von 99,9 Prozent vor. Das reiche aus, um die YOX-Verbindung wieder als hochwertigen Leuchtstoff verwenden zu können, schreiben die belgischen Forscher in der Zeitschrift „Green Chemistry" (Bd. 17, S. 856). Auch die ionische Flüssigkeit kann weiter genutzt werden. „Zurzeit arbeiten wir nur mit einigen Gramm Leuchtstoffen im Labormaßstab", erklärt Dupont. „Wir erwarten aber keine größeren Schwierigkeiten, wenn wir das Verfahren auf Kilogramm- oder Tonnen-Mengen hochskalieren." Die belgischen Wissenschaftler forschen im Rahmen eines europaweiten Projekts zur Rückgewinnung von Seltenen Erden (www.rare3.eu), an dem auch 30 industrielle Partner beteiligt sind. Nach ihrer Schätzung könnten aus dem gebrauchten Leuchtstoffpulver, das bis zum Jahr 2020 anfällt, rund 25 000 Tonnen an Seltenen Erden wiedergewonnen werden.

Allerdings hapert es noch beim allerersten Schritt in der Wiederverwertungskette: der korrekten Abgabe gebrauchter Energiesparlampen. Gerade für die privaten Haushalte ist der Aufwand bei der richtigen Entsorgung offenbar noch immer zu hoch: Manche Verbraucher wissen nicht, wo sie ihre Energiesparlampen abgeben können, viele sind zu bequem, um den nächsten Recyclinghof aufzusuchen. Nicht alle Händler sind verpflichtet, Energiesparlampen zurückzunehmen. Und so, schätzt die Deutsche Umwelthilfe, werden in Deutschland nur etwa 20 bis 30 Prozent der alten Lampen aus Privathaushalten getrennt gesammelt, der Rest dürfte im Keller oder sogar im Hausmüll landen.

6. EOS Wetenschap (10/03/2015)

Zeldzame grondstoffen uit tl-lamp – *by Dieter De Cleene*

http://eoswetenschap.eu/artikel/zeldzame-grondstoffen-uit-tl-lamp

Zeldzame grondstoffen uit tl-lamp

ARTIKEL | 10 MAART, 2015 - 13:09 | DOOR DIETER DE CLEENE

Het fosforpoeder in tl-lampen bevat zeldzame aarden.

Spaar- en tl-lampen bevatten waardevolle metalen zoals yttrium en europium, zogenoemde 'zeldzame aarden'. Wetenschappers aan de KU Leuven hebben een proces ontwikkeld om die terug te winnen.

De zeldzame aarden zijn een groep van 17 moeilijk te winnen chemische elementen die vaak worden gebruikt in elektronica. Je vindt ze ook in fluorescentielampen zoals tl- en spaarlampen. Die bevatten fosforen, chemische stoffen die in staat zijn licht met een bepaalde golflengte om te zetten in licht met een andere golflengte – in dit geval uv-licht in zichtbaar licht. In het laagje fosforpoeder in de lamp – dat verwarrend genoeg niets te maken heeft met het chemisch element fosfor – zitten exotische zeldzame aarden zoals yttrium en europium.

Omdat de lampen ook kwik bevatten, worden ze sinds 2005 ingezameld om te vermijden dat dat kwik in het milieu terecht komt – in 2013 werd ruim 1.200 ton lampen verzameld. De lampen worden vermalen, metalen, glas en plastic worden gerecycled, en uit het resterende poeder kunnen we de zeldzame aarden terugwinnen.

David Dupont en Koen Binnemans, verbonden aan het onderzoeksplatform RARE3 van de KU Leuven, ontdekten een middel dat in staat is de waardevolle materialen selectief op te lossen. Met een zogenoemde ionische vloeistof, die uit geladen moleculen of ionen bestaat, slaagden ze erin yttrium en europium uit het afval te isoleren. Door aan de oplossing vervolgens oxaalzuur toe te voegen, slaan de zeldzame aarden neer. Verhitting levert vervolgens een fosforpoeder op dat we opnieuw in lampen kunnen gebruiken.

Mijnbouw in België

De oude methodes om zeldzame aarden te recupereren, doen net het omgekeerde: door zuren toe te voegen lossen alle waardeloze stoffen eerst op en blijven yttrium en europium over. Maar aangezien die slechts twintig procent van de totale massa vertegenwoordigen, is dat niet efficiënt.

De onderzoekers willen nu proberen het nieuwe proces op grotere schaal toe te passen, in samenwerking met geïnteresseerde bedrijven. Of die zich zullen aandienen, zal onder meer afhangen van de prijs van zeldzame aarden op de wereldmarkt.

Een groot deel van de bekende voorraden zeldzame aarden bevindt zich in China, dat de handel domineert en in 2013 goed was voor meer dan negentig procent van het aanbod op de wereldmarkt. Toen China in 2010 zijn exportquota verscherpte, schoten de prijzen de hoogte in. De Europese Commissie bestempelde zeldzame aarden als 'kritieke grondstoffen', van fundamenteel belang voor de economie, maar met een onzekere aanvoer.

Net als de prijzen steeg ook de interesse in alternatieve bronnen, zoals mijnen buiten China en recycling. 'Het fosforpoeder in tl- en spaarlampen kan je vergelijken met een erts dat zeldzame aarden bevat', zegt Binnemans. 'Maar de concentratie is veel hoger dan in eender welke mijn.'

Nadat het land op de vingers werd getikt door de Wereldhandelsorganisatie schafte China de exportquota begin dit jaar af, waardoor de prijzen weer daalden. 'Daardoor krijgen bedrijven die hebben geïnvesteerd in alternatieve bronnen van zeldzame aarden het moeilijk', zegt Binnemans. 'Door de prijzen te laten fluctueren blijft China controle uitoefenen en smoort het alternatieven in de kiem.'

6. Chemistry World (26/03/2015)

Ionic liquid a perfect fit for rare earth recycling – *by Jonathan Midgley*

http://www.rsc.org/chemistryworld/2015/03/ionic-liquid-rare-earth-recycling

chemistryworld

Ionic liquid a perfect fit for rare earth recycling

26 March 2015 **Jonathan Midgley**

Chemists in Belgium have shown how an intriguing ionic liquid they developed 10 years ago can recover valuable rare earth metals from stockpiles of used **fluorescent lamps** and **magnets**.

Rare earth metals are important in high tech applications, but China controls most of the world's dwindling supply, periodically setting export quotas and driving up prices. They occur naturally elsewhere, but new production is time consuming and costly to establish.

It is estimated that by 2020 stockpiled lamp phosphor waste will contain around 25,000 tons of rare earths

However, significant quantities of these metals exist in sources much closer to home: neodymium rich magnets, which are crucial components of electric motors and dynamos, and fluorescent light bulbs. Recycling is not widespread as current methods are expensive and polluting, using a large amount of solvent to dissolve mostly unwanted material. The valuable rare earth content – in the form of red phosphor, $Y_2O_2:Eu^{3+}$ – is not often recovered from old household light bulbs, the main focus being safe mercury disposal with the rest going to landfill.

Koen Binnemans and **David Dupont** at the University of Leuven realised an ionic liquid, [Hbet][Tf_2N], they developed in 2006 could be the answer due to its ability to selectively dissolve certain metal oxides. 'It was a strange coincidence … we had largely forgotten for several years, until quite recently we realised that red phosphor is in fact an oxide … we thought, OK, let's give it a try, and let's hope that the other compounds do not go into solution,' recounts Binnemans. Their foresight was rewarded – results showed that 100% of the red phosphor, and nothing else, dissolved. Then, they took advantage of the fact that [Hbet][Tf_2N] is thermomorphic – meaning that on mixing with water it separates from one into two phases as it cools below 80 °C – to firstly dissolve, and then separate, metal oxides from pre-roasted NdFeB magnets. Upon cooling, iron oxides move into the ionic liquid phase and all the valuable metal oxides are found in the water.

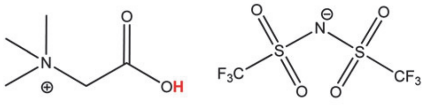

Structure of the ionic liquid with the acidic proton of the betaine group highlighted in red

'It's some kind of magic ionic liquid, with many applications,' says Binnemanns. But what causes these highly selective phenomena? 'It's the special combination of having a positive charge on the cation close to the carboxylic acid group that gives the ionic liquid special properties, in combination with the anion that makes the ionic liquid non-miscible in water.'

After dissolution it is simple to precipitate out the metals using oxalic axid, which also automatically rejuvenates the ionic liquid, a significant economic and environmental advantage. 'It is clear that these methods are very selective in separating the targeted rare earths and that there are many advantages compared to conventional solvent extraction routes, for example that the ionic liquid can be regenerated easily,' comments rare earth magnet expert, **Allan Walton**, from the University of Birmingham, UK.

The group are keen for their processes to be scaled up in collaboration with chemical engineers and industry, but the economics of this are dependent on the volatile price of rare earth metals. Meanwhile their next target is the much tougher dissolution of green lamp phosphor ($LaPO_4:Ce^{3+}$), and although preliminary results are promising, the structure of the ionic liquid used cannot yet been revealed.

7. Chemistry World (02/10/2015)

Antimony recovery lights up lamp waste recycling – *by Tom Wilson*

http://www.rsc.org/chemistryworld/2015/10/antimony-recovery-lamp-phosphor-waste-recycling-fertiliser

chemistryworld

Antimony recovery lights up lamp waste recycling

2 October 2015 **Tom Wilson**

Researchers in Belgium have developed **a method to extract antimony from lamp phosphor waste** and convert residues from the process into fertiliser. This approach is completely non-toxic with the only byproduct being sodium chloride – table salt – which is easily discarded.

A recent report by the European Commission identified antimony as one of the most critical elements with a supply risk. At present, 90% of world production is in China. With mines in Europe unlikely to reopen, a secondary production source of antimony is needed to satisfy demand.

Koen Binnemans and co-workers at the University of Leuven are no strangers to recycling scarce metals, having previously **recovered rare earth metals using ionic liquids**. David Dupont, who worked with Binnemans on this latest project, says the chemistry involved is not actually that complicated; rather it connects ideas together to produce useful materials and non-toxic byproducts. Indeed, the process has to be simple and use readily available materials to be feasible on a larger scale.

By dissolving lamp phosphor waste in hydrochloric acid, an antimony-containing compound which produces white light, called halophosphate, which makes up 50 percent by weight of the powder, can be extracted with a reusable ionic liquid. The remaining aqueous solution is treated with sodium hydroxide, which precipitates calcium phosphate – a useful material for fertilisers and other applications. Indeed, Dupont explains this is a cleaner way to obtain fertilisers than extracting the material from rock. 'Phosphate rock is problematic as it contains toxic radioactive metals such as uranium, so these metals need removing and lead to toxic products; our method is much more pure as the lamps need high purity products.'

Srecko Stopic, an expert in metal processing and recycling at RWTH Aachen University, Germany, believes the Leuven study will significantly influence and impact waste recovery, and also be important for European countries seeking to produce antimony at room temperature with minimal energy and chemical consumption. 'This idea to recover antimony can be a driving force to use a similar principle for other waste materials, for example ceramic waste materials,' he says.

Dupont agrees, saying there are many other metal-rich industrial waste processes. Furthermore, antimony is not the only scarce metal in demand. Dupont says the group is now developing methods to recover other critical metals, such as gallium and indium, from industrial waste streams.

8. C2W + Mens & Molecule (02/10/2015)

TL-Buis als antimoonbron – *by Arjen Dijkgraaf*

http://www.c2w.nl/tl-buis-als-antimoonbron.412564.lynkx

TL-BUIS ALS ANTIMOONBRON

Leuvens extractieproces verkleint lampenafvalberg nog verder.

Met zuur en een ionische vloeistof kun je antimoon en fosfaten terugwinnen uit afval van oude tl-buizen. Daarmee is de oplossing van dit milieuprobleem zo'n beetje rond, schrijven Koen Binnemans en David Dupont in het tijdschrift *Green Chemistry*.

Eerder (zie *Mens & Molecule* 3) kwamen deze Leuvense onderzoekers al met een proces om zeldzame aarden terug te winnen uit fluorescentiepoeders in recente spaarlampen. Die moderne 'fosforen' bevatten geen antimoon, en trouwens ook niet veel fosfor. In oudere buizen zitten echter witte halofosfaatfosforen (HALO), uitgevonden in 1942, die deze twee elementen wél bevatten en juist geen zeldzame aarden. Ooit is daar zó veel van geproduceerd dat de helft van de tl-afvalberg nog altijd uit HALO bestaat. Financieel was antimoon terugwinnen nooit de moeite waard. Maar inmiddels staat het hoog op de lijst van elementen die schaars dreigen te worden, vooral omdat 90 % van de huidige productie uit China komt.

Binnemans en Dupont willen nu gebruikmaken van het feit dat HALO (voluit $(Sr,Ca)_5(PO_4)_3(Cl, F):Sb^{3+}, Mn^{2+}$) de enige fosfor in de afvalberg is die gemakkelijk oplost in verdund zoutzuur. Vervolgens kun je het antimoon selectief uit de vloeistof extraheren met trioctylmethylammoniumchloride, een ionische vloeistof die wordt verkocht onder de naam Aliquat 336. Met een NaOH-oplossing extraheer je vervolgens het antimoon uit de ionische vloeistof, waarbij het neerslaat als Sb_2O_3. Vergeleken met de huidige extractie van antimoon uit erts, is dit terugwinningsproces behoorlijk 'schoon'.

Door met nog meer NaOH het zuur te neutraliseren, laat je de fosforresten neerslaan als apatiet, oftewel calciumfosfaat, dat je als grondstof kunt verkopen aan de kunstmestindustrie. Er zitten wel wat restjes van andere elementen doorheen, maar vergeleken met ruw fosfaaterts is het heilig. Het wachten is nu op een bedrijf dat het op grotere schaal durft te proberen.

(AD) |

9. Flanders Today (11/03/2015)

KU Leuven chemists retrieve rare earth metals from lamps – *by Andy Furniere*

http://www.flanderstoday.eu/innovation/ku-leuven-chemists-retrieve-rare-earth-metals-lamps

11 Mar '15

KU Leuven chemists retrieve rare earth metals from lamps

Chemists from the University of Leuven have developed a new method to retrieve the metals europium and yttrium from discarded fluorescent and energy-saving lamps. They used an ionic fluid that offers many advantages over traditional solvents, according to the research team.

The rare earth elements are used in red lamp phosphor, a substance that transforms ultraviolet light into red light. It is used, for example, in TV screens and in fluorescent lamps. Until now, recycling processes mostly focused on removing the poisonous mercury from discarded fluorescent and energy saving lamps because the recuperation of europium and yttrium was such a complex and expensive process.

Instead of using an acid, the researchers worked with an organic solvent that consists of ions, or electrically charged particles. The solvent works very selectively: It can dissolve the red lamp phosphor only. The recuperated rare earth metals are immediately reusable and the ionic fluid itself can also be used again.

"With this method, recycling requires a lot less chemicals and energy," explained professor Koen Binnemans. "It is a better alternative, both technically and ecologically, for traditional solvents."

10. C2W (10/03/2015)
Oplossing voor spaarlampen – *by Arjen Dijkgraaf*
http://www.c2w.nl/oplossing-voor-spaarlampen.400846.lynkx

11. Recycling Portal (11/03/2015)
Europium and Yttrium: Recycled from energy saving lamps for direct reuse
http://recyclingportal.eu/Archive/12038

12. Regiopunt (10/03/2015)
Chemici KU Leuven recycleren zeldzame aarden uit TL- en spaarlampen – *by Elisabeth Pyck*
http://regiopunt.be/pagina/leesBericht.php?id=1799

13. Recycling Magazine (11/03/2015)
Recycling of rare-earth elements from fluorescent and energy saving lamps
http://www.recyclingmagazin.de/rmeng/news_en_detail.asp?ID=20840&NS=1

14. Waste Management World (10/03/2015)
Chemists Crack Rare Earth Recycling from Waste Lamps at Belgian University− *by Ben Messenger*
http://www.waste-management-world.com/articles/2015/03/chemists-crack-rare-earth-recycling-from-waste-lamps-at-belgian-university.html

15. Energy News (25/03/2015)
A material from fluorescent and low consumption lamps that is rare in nature can be recycled
http://www.energynews.es/english/a-material-from-fluorescent-and-low-consumption-lamps-that-is-rare-in-nature-can-be-recycled/

16. Engineers Online (14/03/2015)
Chemici vinden nieuwe manier om zeldzame aarden uit lampen terug te winnen
http://www.engineersonline.nl/nieuws/id24956-chemici-vinden-nieuwe-manier-om-zeldzame-aarden-uit-lampen-terug-te-winnen.html

---

Further information and an overview of the media coverage of KU Leuven research on rare-earth recycling can be found on the website: www.kuleuven.rare3.eu

Chronological list of first-author publications

1. Full paper (March 2014)

Dupont, D.; Brullot, W.; Bloemen, M.; Verbiest, T.; Binnemans, K. Selective Uptake of Rare Earths from Aqueous Solutions by EDTA-functionalized Magnetic and Non-magnetic Nanoparticles. *ACS Applied Materials & Interfaces* **2014**, 6, 4980-4988. (IF 2015: 6.72)

2. Full paper (September 2014)

Dupont, D.; Luyten, J.; Bloemen, M.; Verbiest, T.; Binnemans, K. Acid-Stable Magnetic Core–Shell Nanoparticles for the Separation of Rare Earths. *Industrial Engineering & Chemistry Research* **2014**, 53, 15222-15229. (IF 2015: 2.59)

3. Full paper + Front cover (November 2014)

Dupont, D.; Binnemans, K. Rare-earth recycling using a functionalized ionic liquid for the selective dissolution and revalorization of Y_2O_3:Eu^{3+} from lamp phosphor waste. *Green Chemistry* **2015**, 17, 856-868. (IF 2015: 8.02)

4. Full paper + Inside front cover (March 2015)

Dupont, D.; Binnemans, K. Recycling of rare earths from NdFeB magnets using a combined leaching/extraction system based on the acidity and thermomorphism of the ionic liquid [Hbet][Tf_2N]. *Green Chemistry* **2015**, 17, 2150-2163. (IF 2015: 8.02)

5. Communication (April 2015)

Dupont, D.; Raiguel, S.; Binnemans, K. Sulfonic acid functionalized ionic liquids for dissolution of metal oxides and solvent extraction of metal ions. *Chemical Communications* **2015**, 51, 9006-9009 (IF 2015: 6.83)

6. Full paper (May 2015)

Dupont, D.; Depuydt, D.; Binnemans, K.; Overview of the Effect of Salts on Biphasic Ionic Liquid/Water Solvent Extraction Systems: Anion Exchange, Mutual Solubility, and Thermomorphic Properties. *Journal of Physical Chemistry B* **2015**, 119, 6747−6757 (IF 2015: 3.30)

7. Full paper (September 2015)

Dupont, D.; Binnemans, K.; Antimony recovery from the halophosphate fraction in lamp phosphor waste: a zero-waste approach. *Green Chemistry* **2016**, 18, 176-185. (IF 2015: 8.02)

8. Review (January 2016)

Dupont, D.; Arnout, S.; Jones, P. T.; Binnemans, K.; Antimony recovery from end-of-life products and industrial process residues: a critical review. *Journal of Sustainable Metallurgy* **2016**, 2, 79-103.

9. Communication (February 2016)

Dupont, D.; Renders, E.; Binnemans, K.; Alkylsulfuric acid ionic liquids: a promising class of strongly acidic room-temperature ionic liquids. *Chemical Communications* **2016**, DOI: 10.1039/C6CC00094K (IF 2015: 6.83)

Attended conferences, trainings and teaching assignments

Attended conferences

1. Oral presentation
1st European Rare Earth Resources Conference (ERES 2014), Milos (Greece), 4−7 September 2014.
Title: Extraction and separation of rare earths with functionalized magnetic nanoparticles.

2. Oral presentation
3rd international Symposium on Green Chemistry (ISGC) Conference, La Rochelle (France), 3−7 May 2015
Title: Rare-earth recycling using a functionalized ionic liquid for the selective dissolution and revalorization of Y_2O_3:Eu^{3+} from lamp phosphor waste.

3. Invited talk
4th International Conference on Rare Earth Materials (REMAT), Wroclaw (Poland), 25-28 October 2015
Title: Recycling of rare earths using ionic liquid technology

Presentations at RARE^3 events and seminars

1. Oral presentation
2nd Industrial User Committee meeting of RARE³ (Research platform for the Advanced Recycling and Reuse of Rare Earths), Leuven (Belgium), 16 Sept 2013.
Title: Separation of rare earths with functionalised magnetic nanoparticles**.**

2. Lecture
KU Leuven master course: Lanthanide & Actinides, Leuven (Belgium), 24 Nov 2014.
Title: Introduction to rare-earth economics, challenges and recycling.

3. Oral presentation
4th Industrial User Committee meeting of RARE³ (Research platform for the Advanced Recycling and Reuse of Rare Earths), Leuven (Belgium), 30 March 2015.
Title: Recycling of REEs from lamp phosphor waste using functionalized ionic liquids.

Mentoring

2013−2014: Master thesis student (Jakob Luyten)
Topic: *Extraction and separation of rare earths using EDTA-functionalized magnetic core-shell nanoparticles*

2014-2015: Internship student (Stijn Raiguel)
Topic: *Dissolution of metal oxides in ionic liquids relevant to rare-earth recycling*

2015−2016: Master thesis student (Evelien Renders)
Topic: *Synthesis of strongly acidic ionic liquids for the processing of metal oxides and metal-containing waste.*

Attended courses, seminars, workshops and summer schools

• Radiation protection, 15/10/2013 (1/6 ECTS)
• Safety in the lab, 6/11/2013 (1/6 ECTS)
• Assistant training, 13/02/2014 (1/2 ECTS)
• Managing my PhD, 10/03/2014 (2 ECTS)
• Scientific integrity for starting PhD's, 15/04/2014 (1/6 ECTS)
• EREAN summer school on Rare Earths, 18-21/08/2014 (1 ECTS)
• Introduction to leadership, 17/12/2014 (1/6 ECTS)
• BASF International Summer Course, 2-8 August 2015 (2 ECTS)

References

1. D. Dupont, W. Brullot, M. Bloemen, T. Verbiest and K. Binnemans, *ACS Appl. Mater. Interfaces*, 2014, **6**, 4980-4988.
2. D. Dupont, J. Luyten, M. Bloemen, T. Verbiest and K. Binnemans, *Ind. Eng. Chem. Res.*, 2014, **53**, 15222-15229.
3. R. A. Kerr, *Science*, 2014, **343**, 722-724.
4. *Report on Critical raw materials for the EU*, European Commission, DG Enterprise & Industry, Brussels, 2014.
5. K. Binnemans, P. T. Jones, K. Acker, B. Blanpain, B. Mishra and D. Apelian, *JOM*, 2013, **65**, 846-848.
6. M. A. Reuter, U. M. J. Boin, S. A, E. Verhoef, K. Heiskanen, Y. Yang and G. Georgalli, *The Metrics of Material and Metal Ecology: Harmonizing the resource, technology and environmental cycles*, Elsevier Science, Amsterdam, 2005.
7. U.S. Department of Energy, Critical Materials Strategy, USA, 2011
8. K. Binnemans, P. T. Jones, B. Blanpain, T. Van Gerven, Y. Yang, A. Walton and M. Buchert, *J. Clean. Prod.*, 2013, **51**, 1-22.
9. K. Binnemans, P. T. Jones, B. Blanpain, T. Van Gerven and Y. Pontikes, *J. Clean. Prod.*, 2015, **99**, 17-38.
10. K. Binnemans, Y. Pontikes, P. T. Jones, T. Van Gerven and B. Blanpain, Recovery of Rare Earths from Industrial Waste Residues: a Concise Review, Proceedings of the Third International Slag Valorisation Symposium, Leuven, Belgium.
11. M. Buchert, A. Manhart, D. Bleher and D. Pingel, *Recycling critical raw materials from waste electronic equipment*, Öko-Institut, Darmstadt, Germany, 2012.
12. D. Schüler, M. Buchert, R. Liu, G. S. Dittrich and C. Merz, *Study on rare earths and their recycling*, Öko-Institut, Darmstadt, 2011.
13. T. E. Graedel, J. Allwood, J.-P. Birat, B. K. Reck, S. F. Sibley, G. Sonnemann, M. Buchert and C. Hagelüken, *Recycling Rates of Metals*, United Nations Environmental Programme (UNEP), 2011.
14. J. Kooroshy, G. Tiess, A. Tukker and A. Walton, *Strenghtening the European rare earths supply chain: Challenges and policy options*, ERECON, 2015.
http://ec.europa.eu/growth/sectors/raw-materials/specific-interest/erecon/index_en.htm
15. J. Gambogi, U.S. Geological survey, Department of the interior, Rare Earths statistics and information, USA, 2013
16. A. Golev, M. Scott, P. D. Erskine, S. H. Ali and G. R. Ballantyne, *Resources Policy*, 2014, **41**, 52-59.
17. S. Massari and M. Ruberti, *Resources Policy*, 2013, **38**, 36-43.
18. N. Krishnamurthy and C. K. Gupta, *Extractive Metallurgy of Rare Earths*, CRC Press, Boca Raton, FL, 2004.
19. K. Binnemans and P. T. Jones, *J. Rare Earths*, 2014, **32**, 195-200.
20. C. Helling and J. Strube, *Chem. Ing. Tech.*, 2013, **85**, 1272-1281.
21. C. Sonic-Mullion, *Rare Earth Elements: A review of production, processing, recycling and assiociated environmental issues*, Environmental Protection Agency (EPA), Cincinnati, OH (USA), 2012.
22. M. Tanaka, T. Oki, K. Koyama, H. Narita and T. Oishi, in *Handbook on the Physics and Chemistry of Rare Earths*, eds. J.-C. G. Bünzli and V. K. Pecharsky, Elsevier, Amsterdam, 2013, vol. 43, ch. 255, pp. 159-212.
23. Y. Wu, X. Yin, Q. Zhang, W. Wang and X. Mu, *Resour. Conserv. Recy.*, 2014, **88**, 21-31.
24. D. Dupont and K. Binnemans, *Green Chem.*, 2015, **17**, 856-868.
25. D. Dupont and K. Binnemans, *Green Chem.*, 2016, **18**, 176-185.
26. M. Jang, S. M. Hong and J. K. Park, *Waste Manage.*, 2005, **25**, 5-14.
27. W. A. Durão Jr, C. A. de Castro and C. C. Windmöller, *Waste Manage.*, 2008, **28**, 2311-2319.

28. C. Raposo, C. C. Windmöller and W. A. Durão Júnior, *Waste Manage.*, 2003, **23**, 879-886.
29. C. Tunsu, C. Ekberg and T. Retegan, *Hydrometallurgy*, 2014, **144–145**, 91-98.
30. C. Tunsu, C. Ekberg, M. Foreman and T. Retegan, *Waste Manage.*, 2015, **36**, 289-296.
31. V. Innocenzi, I. De Michelis, B. Kopacek and F. Vegliò, *Waste Manage.*, 2014, **34**, 1237-1250.
32. T. Hirajima, A. Bissombolo, K. Sasaki, K. Nakayama, H. Hirai and M. Tsunekawa, *Int. J. Miner. Process.*, 2005, **77**, 187-198.
33. T. Hirajima, K. Sasaki, A. Bissombolo, H. Hirai, M. Hamada and M. Tsunekawa, *Sep. Purif. Technol.*, 2005, **44**, 197-204.
34. I. Urniezaite, G. Denafas and D. Jankunaite, *Waste Manage. Res.*, 2009, **28**, 606-614.
35. T. Horikawa and K. Machida, *Mater. Integr.* , 2011, **24**, 37-43.
36. G. Mei, P. Rao, M. Mitsuaki and F. Toyohisa, *Journal of Wuhan University*, 2009, **24**, 418-423.
37. F. Yang, F. Kubota, Y. Baba, N. Kamiya and M. Goto, *J. Hazard. Mater.*, 2013, **254-255**, 79-88.
38. T.-C. Chang, S.-F. Wang, S.-J. You and A. Cheng, *J. Environ. Eng. Manage.*, 2007, 435-439.
39. R. Otto and A. Wojtalewicz, *Method for the Recovery of Rare Earths From Fluorescent Lamps,* US patent 2012/0027651 A1.
40. H. L. Yang, W. Wang, H. M. Cui, D. L. Zhang, Y. Liu and J. Chen, *J. Chem. Technol. Biotechnol.*, 2012, **87**, 198-205.
41. J. J. Braconnier and A. Rollat, *Method for recovering rare-earth elements from a solid mixture containing a halophosphate and a compound of one or more rare-earth elements, Solvay, European Patent,* EP 2419377 A1, 2012.
42. M. A. Rabah, *Waste Manage.*, 2008, **28**, 318-325.
43. I. De Michelis, F. Ferella, E. F. Varelli and F. Vegliò, *Waste Manage.*, 2011, **31**, 2559-2568.
44. V. Innocenzi, I. De Michelis, F. Ferella, F. Beolchini, B. Kopacek and F. Vegliò, *Waste Manage.*, 2013, **33**, 2364-2371.
45. H. Liu, S. Zhang, D. Pan, J. Tian, M. Yang, M. Wu and A. A. Volinsky, *J. Hazard. Mater.*, 2014, **272**, 96-101.
46. E. Alonso, A. M. Sherman, T. J. Wallington, M. P. Everson, F. R. Field, R. Roth and R. E. Kirchain, *Environ. Sci. Technol.*, 2012, **46**, 3406-3414.
47. R. S. Sheridan, A. J. Williams, I. R. Harris and A. Walton, *J. Magn. Magn. Mater.*, 2014, **350**, 114-118.
48. A. Walton, H. Yi, N. A. Rowson, J. D. Speight, V. S. J. Mann, R. S. Sheridan, A. Bradshaw, I. R. Harris and A. J. Williams, *J. Clean. Prod.*, 2015, **104**, 236-241.
49. W. Lai, M. Liu, C. Li, H. Suo and M. Yue, *Hydrometallurgy*, 2014, **150**, 27-33.
50. S. Riano and K. Binnemans, *Green Chem.*, 2015, **17**, 2931-2942.
51. T. Vander Hoogerstraete, B. Blanpain, T. Van Gerven and K. Binnemans, *RSC Adv.*, 2014, **4**, 64099-64111.
52. T. Itakura, R. Sasai and H. Itoh, *J. Alloys Compd.*, 2006, **408–412**, 1382-1385.
53. C.-H. Lee, Y.-J. Chen, C.-H. Liao, S. Popuri, S.-L. Tsai and C.-E. Hung, *Metallurgical and Materials Transactions A*, 2013, **44**, 5825-5833.
54. K. Koyama, A. Kitajima and M. Tanaka, *Kidorui*, 2009, **54**, 36-37.
55. T. Vander Hoogerstraete and K. Binnemans, *Green Chem.*, 2014, **16**, 1594-1606.
56. T. Vander Hoogerstraete, S. Wellens, K. Verachtert and K. Binnemans, *Green Chem.*, 2013, **15**, 919-927.
57. D. Dupont and K. Binnemans, *Green Chem.*, 2015, **17**, 2150-2163.
58. J. W. Lyman and G. R. Palmer, *Scrap treatment method for rare earth transition metal alloys, US Patent,* 5,129,945, 1992.
59. P. T. Anastas and J. C. Warner, *Green Chemistry: theory and practice*, Oxford University Press, Oxford, 1998.

60. M. Poliakoff and P. Licence, *Nature*, 2007, **450**, 810-812.
61. J. H. Clark, *Green Chem.*, 1999, **1**, 1-8.
62. N. V. Plechkova and K. R. Seddon, *Chem. Soc. Rev.*, 2008, **37**, 123-150.
63. R. D. Rogers and K. R. Seddon, *Science*, 2003, **302**, 792-793.
64. R. P. Swatloski, S. K. Spear, J. D. Holbrey and R. D. Rogers, *J. Am. Chem. Soc.*, 2002, **124**, 4974-4975.
65. A. P. Abbott and K. J. McKenzie, *Phys. Chem. Chem. Phys.*, 2006, **8**, 4265-4279.
66. S. Zhang, X. Lu, Q. Zhou, X. Li, X. Zhang and S. Li, *Ionic Liquids: Physicochemical Properties*, Elsevier Science, Oxford, UK, 2009.
67. C. M. Gordon, M. J. Muldoon, M. Wagner, C. Hilgers, J. H. Davis and P. Wasserscheid, in *Ionic Liquids in Synthesis*, Wiley-VCH, Weinheim, Germany, 2008, pp. 7-55.
68. C. J. Bradaric, A. Downard, C. Kennedy, A. J. Robertson and Y. Zhou, *Green Chem.*, 2003, **5**, 143-152.
69. D. Dupont, D. Depuydt and K. Binnemans, *J. Phys. Chem. B*, 2015, **119**, 6747-6757.
70. E. Alcalde, I. Dinarès, A. Ibáñez and N. Mesquida, *Molecules*, 2012, **17**, 4007.
71. C. Yue, D. Fang, L. Liu and T.-F. Yi, *J. Mol. Liq.*, 2011, **163**, 99-121.
72. D. Zhao, PhD Thesis, EPFL, 2007.
73. P. Nockemann, B. Thijs, T. N. Parac-Vogt, K. Van Hecke, L. Van Meervelt, B. Tinant, I. Hartenbach, T. Schleid, V. T. Ngan, M. T. Nguyen and K. Binnemans, *Inorg. Chem.*, 2008, **47**, 9987-9999.
74. P. Nockemann, B. Thijs, S. Pittois, J. Thoen, C. Glorieux, K. Van Hecke, L. Van Meervelt, B. Kirchner and K. Binnemans, *J. Phys. Chem. B*, 2006, **110**, 20978-20992.
75. A. Laschewsky, *Polymers*, 2014, **6**, 1544.
76. P. Wasserscheid, Drie, R. van Hal, H. C. Steffens and J. Zimmermann, *Chem. Commun.*, 2003, 2038-2039.
77. T. A. Wielema and J. B. F. N. Engberts, *Eur. Polym. J.*, 1987, **23**, 947-950.
78. S. Wellens, B. Thijs and K. Binnemans, *Green Chem.*, 2012, **14**, 1657-1665.
79. T. Vander Hoogerstraete, B. Onghena and K. Binnemans, *J. Phys. Chem. Lett.*, 2013, **4**, 1659-1663.
80. W. L. Hough, M. Smiglak, H. Rodriguez, R. P. Swatloski, S. K. Spear, D. T. Daly, J. Pernak, J. E. Grisel, R. D. Carliss, M. D. Soutullo, J. J. H. Davis and R. D. Rogers, *New J. Chem.*, 2007, **31**, 1429-1436.
81. D. R. MacFarlane, N. Tachikawa, M. Forsyth, J. M. Pringle, P. C. Howlett, G. D. Elliott, J. H. Davis, M. Watanabe, P. Simon and C. A. Angell, *Energ. Environ. Sci.*, 2014, **7**, 232-250.
82. M. Smiglak, A. Metlen and R. D. Rogers, *Acc. Chem. Res.*, 2007, **40**, 1182-1192.
83. T. Torimoto, T. Tsuda, K.-i. Okazaki and S. Kuwabata, *Adv. Mater.*, 2010, **22**, 1196-1221.
84. T. Welton, *Green Chem.*, 2011, **13**, 225-225.
85. Y. Fukaya, Y. Iizuka, K. Sekikawa and H. Ohno, *Green Chem.*, 2007, **9**, 1155-1157.
86. D. Nageshwar, D. M. Rao and P. V. R. Acharyulu, *Synth. Commun.*, 2009, **39**, 3357-3368.
87. B. Yang, Q. Zhang, Y. Fei, F. Zhou, P. Wang and Y. Deng, *Green Chem.*, 2015, **17**, 3798-3805.
88. G.-h. Tao, L. He, W.-s. Liu, L. Xu, W. Xiong, T. Wang and Y. Kou, *Green Chem.*, 2006, **8**, 639-646.
89. H. Ohno and K. Fukumoto, *Acc. Chem. Res.*, 2007, **40**, 1122-1129.
90. K. D. Weaver, H. J. Kim, J. Sun, D. R. MacFarlane and G. D. Elliott, *Green Chem.*, 2010, **12**, 507-513.
91. M. T. Garcia, N. Gathergood and P. J. Scammells, *Green Chem.*, 2005, **7**, 9-14.
92. N. Gathergood, M. T. Garcia and P. J. Scammells, *Green Chem.*, 2004, **6**, 166-175.
93. N. Ferlin, M. Courty, S. Gatard, M. Spulak, B. Quilty, I. Beadham, M. Ghavre, A. Haiß, K. Kümmerer, N. Gathergood and S. Bouquillon, *Tetrahedron*, 2013, **69**, 6150-6161.
94. L. Poletti, C. Chiappe, L. Lay, D. Pieraccini, L. Polito and G. Russo, *Green Chem.*, 2007, **9**, 337-341.
95. A. C. Cole, J. L. Jensen, I. Ntai, K. L. T. Tran, K. J. Weaver, D. C. Forbes and J. H. Davis, *J. Am. Chem. Soc.*, 2002, **124**, 5962-5963.

96. Q. Zhang, S. Zhang and Y. Deng, *Green Chem.*, 2011, **13**, 2619-2637.
97. J. Gui, X. Cong, D. Liu, X. Zhang, Z. Hu and Z. Sun, *Catal. Commun.*, 2004, **5**, 473-477.
98. D. Dupont, S. Raiguel and K. Binnemans, *Chem. Commun.*, 2015, **51**, 9006-9009.
99. Z. Fei, D. Zhao, T. J. Geldbach, R. Scopelliti and P. J. Dyson, *Chem-Eur. J.*, 2004, **10**, 4886-4893.
100. P. N. Muskawar, S. Senthil Kumar and P. R. Bhagat, *J. Mol. Catal. A: Chem.*, 2013, **380**, 112-117.
101. G. M. Blackburn and H. L. H. Dodds, *J. Chem. Soc., Perkin Trans. 2*, 1974, **47**, 377-382.
102. D. Fang, X.-L. Zhou, Z.-W. Ye and Z.-L. Liu, *Ind. Eng. Chem. Res.*, 2006, **45**, 7982-7984.
103. D.-J. Tao, J. Wu, Z.-Z. Wang, Z.-H. Lu, Z. Yang and X.-S. Chen, *RSC Adv.*, 2014, **4**, 1-7.
104. A. Zare, F. Abi, A. R. Moosavi-Zare, M. H. Beyzavi and M. A. Zolfigol, *J. Mol. Liq.*, 2013, **178**, 113-121.
105. B. Soberats, M. Yoshio, T. Ichikawa, S. Taguchi, H. Ohno and T. Kato, *J. Am. Chem. Soc.*, 2013, **135**, 15286-15289.
106. S. Ueda, J. Kagimoto, T. Ichikawa, T. Kato and H. Ohno, *Adv. Mater.*, 2011, **23**, 3071-3074.
107. G. A. Benson and W. J. Spillane, *Chem. Rev.*, 1980, **80**, 151-186.
108. R. J. W. Cremlyn, *Chlorosulfonic Acid*, Royal Society of Chemistry, Cambridge, UK, 2002.
109. R. D. Long, N. P. Hilliard, Jr., S. A. Chhatre, T. V. Timofeeva, A. A. Yakovenko, D. K. Dei and E. A. Mensah, *Beilstein J. Org. Chem.*, 2010, **6**, 31.
110. F. Shirini and N. G. Khaligh, *Phosphorus Sulfur Silicon Relat. Elem.*, 2011, **186**, 2156-2165.
111. F. Shirini and N. G. Khaligh, *Dyes Pigm.*, 2012, **95**, 789-794.
112. A. Zare, A. R. Moosavi-Zare, M. Merajoddin, M. A. Zolfigol, T. Hekmat-Zadeh, A. Hasaninejad, A. Khazaei, M. Mokhlesi, V. Khakyzadeh, F. Derakhshan-Panah, M. H. Beyzavi, E. Rostami, A. Arghoon and R. Roohandeh, *J. Mol. Liq.*, 2012, **167**, 69-77.
113. K. Weisenberger, D. Mayer and S. R. Sandler, in *Ullmann's Encyclopedia of Industrial Chemistry*, Wiley-VCH, Weinheim, Germany, 2000.
114. A. Wibbertmann, I. Mangelsdorf, K. Gamon and R. Sedlak, *Ecotoxicol. Environ. Saf.*, 2011, **74**, 1089-1106.
115. E. E. Gilbert, *Chem. Rev.*, 1962, **62**, 549-589.
116. J. Jacquemin, P. Goodrich, W. Jiang, D. W. Rooney and C. Hardacre, *J. Phys. Chem. B*, 2013, **117**, 1938-1949.
117. A. P. Abbott, D. Boothby, G. Capper, D. L. Davies and R. K. Rasheed, *J. Am. Chem. Soc.*, 2004, **126**, 9142-9147.
118. A. P. Abbott, G. Capper, D. L. Davies, K. J. McKenzie and S. U. Obi, *J. Chem. Eng. Data*, 2006, **51**, 1280-1282.
119. A. P. Abbott, G. Frisch, S. J. Gurman, A. R. Hillman, J. Hartley, F. Holyoak and K. S. Ryder, *Chem. Commun.*, 2011, **47**, 10031-10033.
120. A. P. Abbott, G. Frisch, J. Hartley and K. S. Ryder, *Green Chem.*, 2011, **13**, 471-481.
121. J. Sniekers, N. R. Brooks, S. Schaltin, L. Van Meervelt, J. Fransaer and K. Binnemans, *Dalton Trans.*, 2014, **43**, 1589-1598.
122. H. D. Pratt Iii, A. J. Rose, C. L. Staiger, D. Ingersoll and T. M. Anderson, *Dalton Trans.*, 2011, **40**, 11396-11401.
123. I. J. B. Lin and C. S. Vasam, *J. Organomet. Chem.*, 2005, **690**, 3498-3512.
124. P. Nockemann, B. Thijs, N. Postelmans, K. Van Hecke, L. Van Meervelt and K. Binnemans, *J. Am. Chem. Soc.*, 2006, **128**, 13658-13659.
125. S. K. Panja and S. Saha, *RSC Adv.*, 2013, **3**, 14495-14500.
126. B. Mallick, B. Balke, C. Felser and A.-V. Mudring, *Angew. Chem. Int. Ed.*, 2008, **47**, 7635-7638.
127. J. A. Whitehead, G. A. Lawrance and A. McCluskey, *Green Chem.*, 2004, **6**, 313-315.

128. A. Kilicarslan, M. Saridede, S. Stopic and B. Friedrich, *Int. J. Min. Met. Mater.*, 2014, **21**, 138-143.
129. A. Mohammad, *Green Solvents II: Properties and Applications of Ionic Liquids*, Springer Dordrecht, Netherlands, 2012.
130. P. Nockemann, B. Thijs, K. Lunstroot, T. N. Parac-Vogt, C. Görller-Walrand, K. Binnemans, K. Van Hecke, L. Van Meervelt, S. Nikitenko, J. Daniels, C. Hennig and R. Van Deun, *Chem-Eur. J.*, 2009, **15**, 1449-1461.
131. J. Rydberg, *Solvent Extraction Principles and Practice, Revised and Expanded*, Marcel Dekker, New York, USA, 2004.
132. T. Sekine and Y. Hasegawa, *Solvent extraction chemistry: fundamentals and applications*, Marcel Dekker, New York, USA, 1977.
133. T. C. Lo, M. H. I. Baird and C. Hanson, *Handbook of Solvent Extraction*, Wiley-Interscience, New York, 1983.
134. Y. Marcus and A. S. Kertes, *Ion exchange and solvent extraction of metal complexes*, Wiley-Interscience, New York, USA, 1969.
135. A. M. Wilson, P. J. Bailey, P. A. Tasker, J. R. Turkington, R. A. Grant and J. B. Love, *Chem. Soc. Rev.*, 2014, **43**, 123-134.
136. A. P. De Los Rios and F. J. H. Fernandez, *Ionic Liquids in Separation Technology*, Elsevier Science, Oxford, UK, 2014.
137. H. Zhao, S. Xia and P. Ma, *J. Chem. Technol. Biotechnol.*, 2005, **80**, 1089-1096.
138. M. L. Dietz, *Sep. Sci. Technol.*, 2006, **41**, 2047-2063.
139. X. Sun and K. E. Waters, *ACS Sustain. Chem. Eng.*, 2014, **2**, 1910-1917.
140. B. Onghena and K. Binnemans, *Ind. Eng. Chem. Res.*, 2015, **54**, 1887-1898.
141. K. Sasaki, T. Suzuki, T. Mori, T. Arai, K. Takao and Y. Ikeda, *Chem. Lett.*, 2014, **43**, 775-777.
142. K. Sasaki, K. Takao, T. Suzuki, T. Mori, T. Arai and Y. Ikeda, *Dalton Trans.*, 2014, **43**, 5648-5651.
143. N. Li, G. Fang, B. Liu, J. Zhang, L. Zhao and S. Wang, *Anal. Sci.*, 2010, **26**, 455-459.
144. A. E. Visser, R. P. Swatloski, W. M. Reichert, R. Mayton, S. Sheff, A. Wierzbicki, J. J. H. Davis and R. D. Rogers, *Chem. Commun.*, 2001, 135-136.
145. G. Y. Markovits and G. R. Choppin, in *Ion Exch. Solvent Extr.*, eds. J. A. Marinsky and Y. Marcus, Marcel Dekker, New York, USA, 1973, vol. 3, pp. 51-81.
146. S. Wellens, R. Goovaerts, C. Moller, J. Luyten, B. Thijs and K. Binnemans, *Green Chem.*, 2013, **15**, 3160-3164.
147. J. C. Godfrey and J. Slater, *Liquid-Liquid Extraction Equipment*, Wiley, New York, USA, 1995.
148. N. V. Thakur, *Miner. Process. Extr. M.*, 2000, **21**, 277-306.
149. F. Xie, T. A. Zhang, D. Dreisinger and F. Doyle, *Miner. Eng.*, 2014, **56**, 10-28.
150. Y. Kohno, H. Arai, S. Saita and H. Ohno, *Aust. J. Chem.*, 2011, **64**, 1560-1567.
151. Y. Kohno and H. Ohno, *Chem. Commun.*, 2012, **48**, 7119-7130.
152. Y. Kohno and H. Ohno, *Phys. Chem. Chem. Phys.*, 2012, **14**, 5063-5070.
153. Y. Kohno, S. Saita, Y. Men, J. Yuan and H. Ohno, *Polym. Chem.*, 2015, **6**, 2163-2178.
154. Y. Fukaya, K. Sekikawa, K. Murata, N. Nakamura and H. Ohno, *Chem. Commun.*, 2007, **29**, 3089-3091.
155. K. Fukumoto and H. Ohno, *Angew. Chem. Int. Ed.*, 2007, **46**, 1852-1855.
156. Y. Fukaya and H. Ohno, *Phys. Chem. Chem. Phys.*, 2013, **15**, 4066-4072.
157. J. E. L. Dullius, P. A. Z. Suarez, S. Einloft, R. F. de Souza, J. Dupont, J. Fischer and A. De Cian, *Organometallics*, 1998, **17**, 815-819.
158. B. Onghena, J. Jacobs, L. Van Meervelt and K. Binnemans, *Dalton Trans.*, 2014, **43**, 11566-11578.
159. U. Domańska and K. Paduszyński, *J. Phys. Chem. B*, 2008, **112**, 11054-11059.
160. D. Depuydt, L. Liu, C. Glorieux, W. Dehaen and K. Binnemans, *Chem. Commun.*, 2015, **51**, 14183-14186.
161. H. R. Dittmar and W. H. Schröer, *J. Phys. Chem. B*, 2009, **113**, 1249-1252.

162. T. Vander Hoogerstraete, B. Onghena and K. Binnemans, *Int. J. Mol. Sci.*, 2013, **14**, 21353-21377.
163. F. Hofmeister, *Arch. Exp. Pathol. Pharmacol.*, 1888, **24**, 247-260.
164. R. L. Baldwin, *Biophys. J.*, 1996, **71**, 2056-2063.
165. A. Salis, F. Cugia, D. F. Parsons, B. W. Ninham and M. Monduzzi, *Phys. Chem. Chem. Phys.*, 2012, **14**, 4343-4346.
166. A. Salis and B. W. Ninham, *Chem. Soc. Rev.*, 2014, **43**, 7358-7377.
167. N. Schwierz, D. Horinek and R. R. Netz, *Langmuir*, 2010, **26**, 7370-7379.
168. N. Schwierz, D. Horinek and R. R. Netz, *Langmuir*, 2013, **29**, 2602-2614.
169. M. C. Gurau, S.-M. Lim, E. T. Castellana, F. Albertorio, S. Kataoka and P. S. Cremer, *J. Am. Chem. Soc.*, 2004, **126**, 10522-10523.
170. W. Kunz, P. Lo Nostro and B. W. Ninham, *Curr. Opin. Colloid Interface Sci.*, 2004, **9**, 1-18.
171. M. G. Cacace, E. M. Landau and J. J. Ramsden, *Q. Rev. Biophys.*, 1997, **30**, 241-277.
172. L. M. Pegram and M. T. Record, *J. Phys. Chem. B*, 2008, **112**, 9428-9436.
173. E. Thormann, *RSC Adv.*, 2012, **2**, 8297-8305.
174. Z. Yang, *J. Biotechnol.*, 2009, **144**, 12-22.
175. P. Jungwirth and P. S. Cremer, *Nature Chem.*, 2014, **6**, 261-263.
176. E. K. Wilson, *Chem. Eng. News*, 2012, **90**, 42-43.
177. M. G. Freire, P. J. Carvalho, R. L. Gardas, I. M. Marrucho, L. M. N. B. F. Santos and J. A. P. Coutinho, *J. Phys. Chem. B*, 2008, **112**, 1604-1610.
178. M. G. Freire, P. J. Carvalho, A. M. S. Silva, L. M. N. B. F. Santos, L. P. N. Rebelo, I. M. Marrucho and J. A. P. Coutinho, *J. Phys. Chem. B*, 2009, **113**, 202-211.
179. M. G. Freire, C. M. S. S. Neves, P. J. Carvalho, R. L. Gardas, A. M. Fernandes, I. M. Marrucho, L. M. N. B. F. Santos and J. A. P. Coutinho, *J. Phys. Chem. B*, 2007, **111**, 13082-13089.
180. M. G. Freire, L. M. N. B. F. Santos, A. M. Fernandes, J. A. P. Coutinho and I. M. Marrucho, *Fluid Phase Equilib.*, 2007, **261**, 449-454.
181. L. I. N. Tomé, F. R. Varanda, M. G. Freire, I. M. Marrucho and J. A. P. Coutinho, *J. Phys. Chem. B*, 2009, **113**, 2815-2825.
182. C. J. Fowler, T. J. Haverlock, B. A. Moyer, J. A. Shriver, D. E. Gross, M. Marquez, J. L. Sessler, M. A. Hossain and K. Bowman-James, *J. Am. Chem. Soc.*, 2008, **130**, 14386-14387.
183. K. Larsson and K. Binnemans, *Hydrometallurgy*, 2015, **156**, 206-214.